ProQuest LLC.
789 East Eisenhower Parkway
P.O. Box 1346
Ann Arbor, MI 48106 – 1346

A STUDY OF RESIDUAL STRESSES IN LOW ALLOY STEEL THETA RING CASTINGS

BY

R. A. AKHTAR

A THESIS SUBMITTED TO THE COUNCIL FOR NATIONAL ACADEMIC AWARDS IN PARTIAL FULFILMENT FOR THE DEGREE OF

DOCTOR OF PHILOSOPHY

IN INDUSTRIAL METALLURGY

COLLABORATING ESTABLISHMENTS:-

David Brown Gear Industries Ltd., Foundries Division, Penistone, Sheffield.

Steel Casting Research & Trade Assoc. Sheffield.

SPONSORING ESTABLISHMENT:-

Department of Metallurgy, Sheffield City Polytechnic,

March 1981.

PREFACE

All the work reported in this thesis was carried out during the period for which the candidate was registered for a higher degree.

In accordance with the regulations for PhD in Industrial Metallurgy, a full course in Metallurgical Process and Management was successfully completed. The details of the course are given below:

MODULE - 1

Process Metallurgy

Mechanical Metallurgy

Advanced Thermodynamics

MODULE - 2

Accountancy

Micro-Economics and Financial Control

Computational Methods and Operational Research

MODULE - 3

Oxygen Steel making

Metals and Competitive Materials

Electric Arc Furance Steel making

Heat Treatment and Transformations

Quality Control

Tool Materials

MODULE - 4

Industrial Case Studies

One of the case studies, which is related to the current research work, is attached with the thesis, as Appendix.

The Candidate's performance during the above mentioned courses was assessed by means of written examinations and continuous assessment of specific assignments.

A STUDY OF RESIDUAL STRESSES IN LOW ALLOY STEEL THETA RING CASTINGS

R. A. AKHTAR

ABSTRACT

Residual stresses generated during the casting and heat treatment of a low alloy steel, BW2 have been studied using a theta ring so that temperature differentials could be varied using different tie bar sizes. Residual stresses have been measured using centre hole drilling and tie bar sectioning techniques. Centre hole drilling was shown to be sensitive to surface preparation methods. Stresses induced by drilling were accounted for in measured stresses and drilling stresses were found to be greater in cast than annealed samples.

Cast theta rings have been shown to have compressive residual stresses, becoming less compressive or tensile as the tie bar width was reduced. Tie bar sectioning produced expansion which increased with increasing tie bar width, although there was no direct correlation between tie bar stress and width. Results from both techniques have been explained using factors contributing to residual stress formation. The S-shaped runner contained residual stresses and its removal altered residual stress levels.

Heat treatments have been found to produce different amounts of stress relief according to the geometry and thermal cycle imposed. In a uniform section theta ring normalising and tempering relieved stresses in the tie bar but not in the outer ring, and the tie bar contained no stresses after sectioning. For the non-uniform section theta ring annealing made stresses more compressive whilst normalising and tempering generated stresses due to differential cooling, and the tie bar contained compressive stresses after sectioning. Maximum Von Mises equivalent in the cast theta ring was shown to be 25% of the yield strength and reduced further after heat treatment.

A computational model based on finite difference has been used to simulate solidification of a tie bar across the width. Temperature gradients computed along this bar axis were shown to be small and are believed not to significantly contribute to residual stresses.

ACKNOWLEDGEMENTS

The author is heavily indebted to Dr. R.P. Stratton, Mr. A.B. Barnsley and Dr. M.S. Found for their continuous support, encouragement and advice throughout the duration of the work.

Grateful appreciation is also expressed to the Technical Staff of the Department of Metallurgy whose services were invaluable. Thanks are also due to the Department of Mechanical Engineering for use of their facilities.

The author would also like to express his gratitude to Dr. A.W.D. Hills, Head of Department of Metallurgy, and his staff, particularly Dr. A.J. Fletcher, for their encouragement, advice and the provision of facilities for the work.

David Brown Gear Industries Limited and Steel Casting Research and Trade Association, Sheffield, are thanked for their initial encouragement of this work.

Grateful thanks must also be expressed to the people of Pakistan for their sacrifices in terms of their financial support.

Thanks are due to friends, and colleagues at Sheffield City Polytechnic without whose encouragement it would not be possible to complete this work.

Mrs. J. Harper is also to be thanked for her patience and excellent typing.

Finally, the support, the encouragement and sheer endurance of my Wife and Family deserve greater acknowledgements than words can express.

NOMENCLATURE

For Solidification Model

Bi	Biot number
Cp	Specific heat, J/kg ^{o}C
FDA	Finite difference approximation
Fo	Fourier number
h	heat transfer coefficient, W/m^2 ^{o}C
i	Grid-point subscript
k	thermal conductivity, W/m ^{o}C
PDE	Partial differential equation
p_o	subscript for pouring
m	subscript for metal
m_o	subscript for molten metal
q	Heat flux per unit area, W/m^2
s	subscript for sand
t	time, secs
T	temperature, ^{o}C
T_{liq}	Liquidus temperature of metal, ^{o}C
T_s	Solidus temperature of metal, ^{o}C
x	distance co-ordinate, m
α	thermal diffusitivity, m^2/sec
Δt	time increment, sec
Δx	grid spacings, m
ΔtT	Abbreviation for a finite difference approximation to $\partial T/\partial t$
ΔH_{fusion}	Latent heat of fusion, J/kg
$\delta^2 xT$	Abbreviations for finite difference approximation to $\partial^2 T/\partial x^2$
ρ	density, kg/m^3
x_o	Interface position
T_i	Interface temperature, ^{o}C

NOMENCLATURE

For the Stress section:

A	Crossectional area of the arm, m^2
B	Crossectional area of the ring, m^2
e	Distance from neutral axis to surface, m
E	Young's modulus, N/m^2
l	Length of arm (distance between points), m
Δl	Displacement after sectioning, m
K1, K2	Constants
R	Radius of curvature of neutral axis, m
α	Angle between gauge 1 and principal stress direction, degrees
$\epsilon_1, \epsilon_2, \epsilon_3$	Relaxed strains, $\mu\epsilon$
$\epsilon_a, \epsilon_b, \epsilon_c$	Axial and transverse strains on semiaxially loaded beam,
$\epsilon'_a, \epsilon'_b, \epsilon'_c$	Axial and transverse relaxed strains on uniaxially loaded beam,
χ	Crossectional coefficient of Ring, m
ν	Poisson's ratio
$\mu\epsilon$	Microstrains
$\sigma_{max,\ min}$	Maximum and minimum principal stresses, N/m^2
σ_T	Residual stress in the tie bar, N/m^2

CONTENTS

1.0 INTRODUCTION

The interest in residual stresses usually arises from distortion and inferior mechanical properties which may lead to premature failures. Residual stresses have been observed in a wide range of industrial products such as Castings, Forgings and Gears.[1,2]

Identification of the origin and subsequent control of these stresses gives considerable potential for improving the product quality. This is particularly important for an industrial problem accentuated by residual stress formation in the case of premature failure caused by fatigue. Generally, the presence of residual stress is considered undesirable although there are circumstances where the presence of particular residual stress levels may be advantageous.[3]

This particular study arises from unfavourable residual stresses in commercially produced cast and heat treated low alloy steel industrial gears which may be a cause of premature fatigue service failure. Residual stresses are also responsible for distortion problems, and although these difficulties have largely been overcome by machining methods,[4] it is potentially useful to minimise the stresses which create the distortion and necessity for elaborate machining.

In the past, design engineers had little reliable residual stress data but, being conscious of their presence, were obliged to use an excessively high design factor. The

practice was, for many years unchallenged in the absence of a simple method of determining, and predicting the magnitude and distribution of residual stresses. However, the demand for more precise and improved cost effectiveness in the use of materials creates the need for more understanding of the residual stress contribution to failure mechanisms. The absence of residual stress data is clearly unsatisfactory for modern designing attitudes where 'scientific feasibility' and 'economic feasibility'[5] dominated material selection are important and sometimes conflicting. Therefore, the determination and prediction of residual stress levels will yield information concerning their control by altering manufacturing processes. If the manufacturing processes cannot be altered then the designer must include measured or predicted values in design calculations. This study of residual stresses was undertaken in the light of these objectives.

The size and intricate shape of commercial gears makes a fundamental experimental determination, and theoretical prediction of residual stresses too complex. A more realistic approach will be adopted in this study by using a simulative model based upon a circular ring connected diametrically by a tie bar and referred to as a Theta ring. This model will assist the basic understanding of the casting and thermal processes in the manufacture of gears and will demonstrate their contribution to overall residual stress patterns. The experimental approach will be to use Theta rings with variable tie bar dimensions which allow changes in residual stress levels due to

critical parameter such as temperature differentials to be varied. These stresses will be measured and correlated with these variables. A preliminary investigation will be made to identify the crucial dimensions responsible for the occurrence of residual stresses employing computational techniques involving Finite differences. Dimensions of theta rings will also provide data for the computational model. It is anticipated that the theoretical quantitative prediction of residual stress is too complex for full agreement with experimental measurements but the data will form a useful basis for the future work of predicting precise stress levels in theta rings and with the ultimate objective of applying this approach to large commercial gears.

Details will be presented of the background fundamental aspects relating to the origin of residual stresses. This will be followed by review of experimental techniques used, established and developed for measuring stresses together with the theoretical models used for prediction of residual stresses. In order to establish further link with the industrial heat treatment specifications the theta rings will be subjected to processes such as annealing, normalizing and tempering with thermal history of the theta ring during casting and heat-treatment being presented. Details of results of experimental determination of residual stresses, their occurrence in relation to thermal history and their significance will also be discussed in the context of the objectives previously referred to.

2.1 DEFINITION OF RESIDUAL STRESSES

Several different terms have been used to describe residual stresses, these include 'Thermal stresses'[6,7] and 'Internal stresses'.[8,9] The term 'thermal stresses' indicates those stresses in a body which originate due to external restraints which prevent its expansion and contraction. This term also refers to stresses resulting from thermal gradients in a material whilst the term 'internal stress' refer to those stresses existing in bodies upon which no external forces are acting. The latter term may be regarded as a misnomer since all stresses, acting as well as potential, are always internal.[1] These stresses are also referred to as 'locked up' stresses.[10]

The term 'residual stress' is best defined as stress resulting from non uniform temperatures and other internal raisers which arise during manufacture of a component.

2.2 CLASSIFICATION OF STRESSES

Residual stresses occurring over different distances are distinguished by the reference to the terms macrostresses and microstresses.

Macrostresses arise over much larger distances than microstresses and affect long range properties and external dimensions. They arise when external factors such as non uniform stress or temperature affect individual parts of a component in different ways even if the body of material is quite homogeneous. These stresses are also referred to as 'body stresses'. In contrast, microstresses are stresses

extending over short, microscopic distances and occur at microstructural inhomogenities in the material even if the external factor is homogeneous. These stresses are present within individual grains and may be randomly distributed. They are also known as 'tessellated stresses'[11] or 'textural stresses'.[9] The word 'tessellation' means chequering and this does not apply to many types of stresses in this group.[9] Deviations from the perfect lattice determine the 'texture' of the material and therefore the term 'textural stresses' should be preferred to the term 'tessellated stresses'. Macrostresses are also known as First order residual stresses, and microstresses as Second and Third order residual stresses.

The Iron and Steel Technical committee of Society of Automotive Engineers (Division 4)[12] has developed the following definitions for the two categories of residual stresses, macro and microstresses.

a) Macrostress is the mean stress over the gauge length of measurement and is measurable by both mechanical and Xray diffraction techniques.

b) Microstresses are the stresses being averaged by the macro-measurement, and they exist within the gauge length of macro-measurement. Variation in microstresses cause Xray line broadening and hence can only be measured by Xray techniques. The size of gauge length is of no consequence although both macro and microstresses have been defined in terms of gauge length.

Strictly speaking the terms macro and micro stress are misnomers. The residual stress in microscopically small volumes, e.g. a tiny crack, is 'macrostress' whereas, over large volumes, internal stress due to two very large grains is 'micro stress'.

A further classification[13] of stresses is shown in Figure 1 where there are two broad branches of Body and textural stresses and both of these can be further sub-divided into 'contingent stresses' and 'residual stresses'. Contingent stresses are those which are contingent in the sense that they depend upon the source from which they are derived. They also include elastic stresses produced by external loads when acting on a body, these being stresses usually dealt with in design of components. Except for these elastic stresses they can be called 'contingent residual stresses'. 'Residual stresses' may be present without and are not contingent upon the co-existence of the source e.g. thermal gradients, from which they are derived.

The present work on [redacted] steel castings will principally be concerned with macrostresses and these will be referred to as 'residual stresses' in this work.

2.3 CAUSES OF RESIDUAL STRESSES

Macro or micro residual stresses arise to varying degrees in a range of industrial products due to the following causes:[10,14-17]

1. Plastic deformation introduced by processes such as rolling, drawing, extruding, bending, forming, machining, grinding and shot peening.

2. Welding processes.

3. Heat treatment processes such as direct quenching, precipitation, transformation, carburisation, nitriding or other surface hardening treatments.

4. Casting processes.

5. Electro-deposition.

6. Forced alignment of components during assembly.

A convenient summary of these causes is shown in Figure 2.[18]

Macro stress may result from a non unifrom expansion, contraction or shear distortion of mechanical, chemical or thermal origin. Large temperature gradients exist at start of cooling but these gradually diminish as thermal equilibrium is established. The thermal gradients produced due to differential cooling rates are responsible for volume changes which produce residual stresses. Steels are subjected to thermal contraction on quenching from austenizing temperature down to Ms, followed by transformation of austenite to martensite with continuing decrease in temperature,[19] transformation being accompanied by a volume expansion of 4.3%. This effect is illustrated by the cooling of a steel cylinder which will produce compressive stresses at the surface and tensile stresses at core due to thermal contractions caused by the thermal gradient. Volume changes also result from phase transformations and their effect is generally opposite to the changes of thermal origin. Transformation stresses produced in solid cyliinder are tensile in the surface and

compressive in the core. A more complex stress distribution is produced when different parts of a body cool at different rates and thus exhibit volume changes due to phase transformation at different times.

Shrinkage of metal is a volume reduction accompanying the temperature drop from the pouring temperature to room temperature. Cast metals undergo 'liquid contraction' as they cool from the pouring temperature to the solidification temperature producing 'solidification contraction' as they freeze and solid contraction as the solid contracts whilst the solid casting cools to room temperature. Shrinkage defects arise from failure to compensate for liquid during solidification contraction. Hot tears are produced by shrinkage during casting solidification if parts of the casting are still above the solidus temperature and liquid feeding is insufficient to counter the shrinkage. Dimensional change due to solid contraction begins as soon as coherent solid mass is formed. In practice, however, the mould resists this contraction and metal needs to develop sufficient cohesive strength to overcome this resistance. Macrostresses are also produced from differential cooling below the solidus temperature and stresses can thus arise either from external restraint or from thermal conditions alone. Microstresses arise from microstructural inhomogenities such as grain structure, inclusions and deformation heterogenities. These stresses may be anistropic and are caused by thermal expansion, stresses around dislocations or transformation stresses. Dislocations are associated

with localised heterogeneous deformation whilst martensitic transformation may also induce transformation stresses.

2.3.1 ORIGIN OF 'CASTING STRESSES'

The term 'Casting Stresses' is used to describe those stresses which remain in a casting after removal from the mould. They arise during the solidification and subsequent cooling and do not depend on any external source of stresses, apart from the mould restraints.

The quantitative determination of casting stresses was first reported by Heyn in 1907[20]. This work was followed by several investigators[21-25] involving tests on strain grids similar to those used by Heyn and they provided an initial explanation of stress development. This was subsequently extended to heavy and light castings.

The later workers who have examined the casting stresses include Dodd[26], Parkins and Cowans[27], Subcommittee TS 32 of the Institute of British Foundrymen[28], Konstantinov[29] and very recently Chijiiwa et al[30-32], Othahal[33], Medek[34] and Havelicek[35]. These investigations will be referred to in more detail later.

More recent experiences confirm that the basic principles of casting stress development is the same irrespective of the size or section of the castings. Variations of stress-strain relationship as a function of temperature are particularly significant to the development of casting stresses. This can be partially understood by considering the stress during the solidification of an

aluminium alloy bar under tension. As the metal cools from above liquidus temperature the following discrete stages are observed, as shown in Figure 3.[36,37]

1. Liquid stage: In this stage no stress is created because the liquid metal follows the end plates so that tears do not develop.

2. Liquid-solid stage: This stage is significant in alloys where solidification occurs over a temperature range and sufficient liquid is present to compensate for contraction. No long range cohesion exists and metal has negligible strength but infinite ductility.

3. Solid-liquid stage: In this stage solidification has advanced so that a network of solid crystals emerges which has some strength because of coherency created but development of full cohesion is delayed due to the presence of small amounts of residual liquid. Contraction is all due entirely to solidification but the overall metal is weak and ductility is almost negligible. The structure may rupture at low applied stresses because of indendritic liquid film and tears occur if liquid does not fill them. This is also known as the 'coherent brittle' stage and occurs when the metal is 50-90% solid. Hot tearing may occur in this stage.[38]

Hot tearing is characterised by an irregular form with partial or complete fracture following an intergranular path. It normally occurs over the temperature range in which alloy possesses a certain cohesion, yet

freezing range of the alloy, since cohesion is attained at some critical proportion of solid to residual liquid. Alloys with very short freezing ranges show little tearing tendency wheareas alloys with long freezing range and small amounts of eutectic are prone to tearing. Tears may also occur just below the theoretical solidus due to presence of liquid resulting from impurities which decrease the actual solidus temperature e.g. effect of Sulphur in steels. Probability of tearing is increased by the presence of longitudinal temperature differentials which produce hot spots during cooling. In case of a confined and intense hot spot, the tearing tendency increases because strain resulting from the hindered contraction of the whole member is then concentrated within a narrow zone of weakness, where it must be accommodated by relatively few films of residual liquid[37].

4. Solid: High temperature stage; Metal develops limited strength, high ductility and a capacity for plastic deformation without strain hardening. Metal grains contract on cooling unless they are restrained, when plastic flow occurs accompanied by recrystallization. Creep is also an important feature of this stage.

5. Solid: Low temperature stage; The plastic to elastic behaviour transition (of stage 4) generally occurs over a temperature range and a metal with a lower temperature has high strength and exhibits elastic behaviour.

The stress-strain curves for different temperature ranges are summarized in figure 4[36] for Aluminium alloys

(referred to in figure 3). Because the alloy in stages (1) and (2) is predominantly liquid, curves (i) and (ii) show no appreciable stress and strain is infinite when metal becomes coherent. Fracture occurs with little deformation and at low stress, as indicated by curve (iii). Curve (iv) shows marked plastic behaviour at low stress, and curve (v) exhibits elastic deformation. The residual stress primarily develop in stage (5) due to plastic deformation in stage (4).

2.3.2 EFFECT OF CASTING VARIABLES

Residual stresses in castings arise due to inhomogeneous plastic deformations. Whilst cooling to room temperature, elastic strains corresponding to residual stresses develop in order to enable the parts of casting to fit together. The main casting variables which produce non uniform deformations are:[27,28,39]

A) Temperature differentials

B) Mould effects

C) Transformations

Residual stresses may also be produced by temperature gradients from the surface to centre of casting. In this case, stresses are related to the overall rate of cooling. The stresses arising due to this cause only attain significant proportions under conditions of rapid cooling. Compositional and structural heterogeniety can also cause stresses.

The relative contributions of the above three factors

to the final residual stress level depend on the shape and material of the casting, together with other foundry variables. Phase transformations and mould hindrance only cause appreciable amounts of stress if a large temperature difference exists between parts of the casting during cooling.

MECHANISM OF RESIDUAL STRESS FORMATION

Residual stresses in castings arise from different cooling rates in sections with varying size, especially in grid castings of the type shown in figure 5a.[27] When the molten metal is poured into the mould the thinner outer sections solidify and cool faster than the thicker section in the middle. This means that the thinner sections will have contracted more than the middle thicker section in the same time interval. The greater contraction of thinner sections thus compress the thick middle section. This produces tensile stresses in thinner and outer section and compressive stresses in thick section. As previously mentioned, the mechanical strength is a temperature dependent property, and the more rapidly cooling thin outer sections are first to enter the range where they take up elastic strains. When the thin sections enter this range, the thick section is still in the plastic range where it cannot support elastic strains. The thin sections therefore compress and plastically deform the thick section. As cooling progresses, the thin section attains temperatures where the rate of cooling decreases and consequent contractions become smaller. Up to this stage the outer sections are in tensile stress. After a certain time, the

cooling rate of the thick section equals and afterwards exceeds that of the thin section. When the thick section cools into the elastic zone, where it can take up elastic strains, a process of reversal takes place as shown in figure 5b.[40] Firstly, the tensile stress in thin sections decreases and then becomes compressive. The thick section then tries to contract but it is restrained by the rigid outer frame. The effort by thick section to contract and thereby to pull together the stiff outer members is resisted and this leads to tensile stresses in thick centre section. Cracking can occur if tensile stress thus produced exceeds the tensile strength at those temperatures, and buckling may occur if the compressive stresses are high in thin outer sections. Alternatively, the casting may be left in a balanced state of stress.

The local plastic deformation of one part of a casting is an essential feature in the mechanism for the formation of residual stresses. If the different cooling rates in different parts of a casting induced only elastic deformation all parts of the casting would ultimately contract by the same amount and there would be no residual stresses. It is the local plastic deformation which leads to differences in the ultimate amount of contraction in different parts of the casting, and so to the formation of Casting stresses.[28] These stresses will only reach an appreciable magnitude at low temperatures because stresses imposed on the casting when it is well above the recrystallization temperature will be removed by plastic deformation as soon as they form.

TEMPERATURE DIFFERENTIALS

Temperature differences within a casting during cooling are a principal cause of casting stresses. This applies to all metals and all shapes of casting which give rise to internal temperature gradients. Parkins and Cowans[27] conducted a series of experiments to study the mechanism of residual stress formation in sand castings. The rectangular frame work castings shown in figure 5a were heated and cooled under conditions which would have existed in a sand mould. Some members were lagged with asbestos rope in order to achieve appreciable temperature differences between the member during the subsequent cooling in air. The temperature of centre and outside bars were being monitored during cooling down from different temperatures. They were able to establish as shown in figure 6[27] a linear relationship between final residual stress and maximum temperature difference for non-ferrous alloys and cast iron.

Oki et al[41] confirmed that temperature differences cause residual stresses in castings of cylindrical shape because of their dependence on creep rate and temperature. In another study Chijiiwa et al[30] confirmed that, if cooling rate of castings are remarkably different, then residual stress is increased and is proportional to the rate of casting shrinkage.

If the mechanism of differential cooling is operative then the casting stresses can be increased by increasing temperature differences of various casting sections by

increasing the difference in section thicknesses. However, the increase in stress cannot continue indefinitely because after a certain value of cross sectional ratio, large stresses produced in the thin outer members, cannot cause much plastic deformation in the centre member owing to its large area of cross section. This results in lower residual stress in the centre section compared with a lower ratio of cross sectional area. This is clearly demonstrated by experiments of Dodd[26] for Aluminium alloy castings in sand moulds as shown in figure 7. TS 32[40] investigated the residual stress in triangular grey iron grids with a series of varying sectional thicknesses in the centre limb of the grid and showed tensile residual stresses in the heavier section. When cross sectional area of centre member was lower than that of the outer members, compressive residual stress was observed in the centre member. As thickness of centre limb was increased, the compressive stress decreased and finally became tensile, after passing through zero. The higher residual stresses were found when the difference in sectional thickness was greater. Chijiiwa et al[31] showed that if there are identical cooling ratios throughout the casting, the residual stress is the same irrespective of its overall size.

MOULD EFFECTS

Mould effects contribute significantly to residual stress development because, when a casting contracts in the mould, its contraction may be hindered by the sand mould surrounding the casting. Steel castings are prone to hot

tearing if the mould is too hard to crush under the pressure of the casting contracting on to it. Cracks are formed as hot tears which will generally widen at further contraction on subsequent cooling and may relieve existing casting stresses. However, casting stresses may remain if hindrance to contraction leads to local plastic deformation of the casting.

Dodd[26] from his investigation on an Al alloy in sand moulds concluded that residual stress was independent of mould hardness and that no variation in residual stress was found with changes in dry mould strength. Medek[34] suggests that castings made in machine made green compressed moulds will have higher residual stress levels compared with manually made moulds because of their higher tensile strength and modulus of elasticity. TS 32, using triangular grid castings reports the effect of mould strength on residual stress. There was no consistent variation of stress with strength of mould but although no residual stress was observed in the case of flanged bars, the casting in the hard rammed mould had contracted more than casting in medium rammed mould after it had been removed from the mould. This suggests that, provided sufficient temperature differential exists, the casting in a high density mould can lead to higher residual stresses. Parkins and Cowans[42] also investigated the effect of mould resistance on residual stress in sand castings, and concluded that hindrance to the contraction of a casting is governed by the strength characteristics of

moulding sand. The plastic deformation which results from this hindrance to contraction is cummulative over a high temperature range and hence would not be expected to show a simple relationship to the room temperature sand strength. It will depend upon both the high temperature sand strength and ability of sand remote from the casting to prevent yielding of hot sand. Thus, in castings subjected to casting stresses, the hot strength of the sand and the extent to which heat is passed on to adjacent sand will determine the contribution of the sand hindrance to the total stress. This stress may be small in castings where the principal source of stress is temperature difference but, in other cases, its contribution may be significant.

Chijiiwa et al[30] investigating residual stresses in Theta rings of cast steel found that casting stresses in CO_2 mould are higher than those in green sand and dry sand moulds.

Other foundry variables which have been investigated in relation to casting stresses include

1) Pouring temperature; Angus and Tonk[2] using grey cast iron observed that low pouring temperatures give rise to slag and blow hole defects. These defects, particularly in light castings can provide stress raisers and initiate cracks. Relatively high pouring temperatures were reported to reduce temperature differentials and retard the overall cooling rate. However, Dodd[26] observed a slight increase in residual stress with increase

in pouring temperature in Al alloy casting. This was also confirmed by TS 32[28] in their investigation with Al alloy and steel. Girschovish et al[43] in his investigation of T section cast iron castings observed an increased in deflection of castings with increase in pouring temperature. Medek[34] referred to the investigations of various workers into the effect of pouring temperature on residual stresses, where it was suggested (by some workers) that increase of pouring temperature is conducive to a reduction of casting stresses, the explanation being that higher casting temperature produces a heating through of the mould whilst some reported the opposite effect. Medek apportions these discrepancies to the different shapes of the castings used in these investigations and suggests that pouring temperature is only a secondary factor, in the formation of residual stresses, temperature differential being the primary factor.

2) Moisture Content of mould; Dodd[26] and TS 32[40] (using Al alloy and steel), found that residual stresses increased linearly with water content in the mould. Kasch and Mikelonis[44] observed slightly higher residual stress values whilst casting in dry moulds than those cast in green sand moulds. Medek[34] suggested that heating up the mould will reduce temperature difference between mould and casting thereby reducing cooling rate of casting and residual stress. An alternative proposal was that is heating up of the mould with molten metal in the zone of gating system will slow down the casting cooling rate so that

temperature differentials will reduce and hence the residual stress will decrease. Another improvement[37] suggested was to charge the casting immediately into a hot furnace where cooling can be controlled and equalised throughout the critical period. TS 32[40] also found that casting into the hot moulds substantially reduced residual stress level.

3) Stripping temperature of casting; Dodd (Al alloy),[26] TS 18 (grey cast iron),[46] TS 32(Al alloy and steel),[40] and Otahal (grey cast iron)[33] observed increase in residual stress with stripping time. The explanation proposed is that the temperature differentials in castings comes down when they are knocked out early, producing a drastic reduction of residual stress level. TS 18[46] also indicated that castings stripped from mould while still at a high temperature above the A_3 critical point were of higher tensile strength and hardness. Reduction in distortion and residual stress level in castings containing widely spaced limbs were also reported. The distortion however, was greater in castings with closer limbs and very similar sections. TS 18[46] does not however investigate partial stripping of castings i.e. exposing different sections to different cooling rates. Another approach to equalisation of cooling rates and reducing of residual stress is that described by Longden[45] in which ducted air was used for selective cooling within mould.

Kasch and Mikelonis[44] observed, however, in case of

increasing stripping time. Crowe[47] presenting his method of calculating the cooling rate of iron castings concludes that the knock out influences the metal structure, premature knockout leading to problems of porosity and cracking.

TS 32 also investigated the influence of runner dimensions on residual stress levels. They observed an increase in residual stress with increase in the diameter of the runner but no explanation was proposed for this increase.

Balasingh et al[39] reviewed various investigations on the effect of compositional variables, such as Carbon, Phosphorus, Sulphur and Manganese on the residual stress levels. Middleton and Protheroe[48] and Ellis[49] reported the influence of compositional variables upon the resistance to hot tearing of steel. Middleton and Protheroe[48] found that hot tearing tendency and severity increases with increasing casting temperature. Carbon content was found to have considerable influence on hot tearing. Silicon addition is found to be beneficial although its effect is dependent on the Sulphur and Carbon content, Sulphur additions lowering the resistance to tearing.

TS 32[40] also observed a relationship between the structure of metal and residual stresses in triangular grid iron casting. In general, the castings usually cracked in the mould when side members of the grid showed

a heavy chill structure. However, the castings did not crack when the side members were grey.

PHASE TRANSFORMATIONS

Metals and alloys frequently undergo solid state transformations during cooling in the mould and transformations are accompanied by volume changes. These volume changes may occur non uniformly in a casting and at different times. Figure 6b for residual stress/max temperature differences relationship for cast iron framework shows a sharp increase in residual stress at 180°C. This discontinuity is associated with Ar_1 transformations and the experiments[27] accentuated the fact that transformation occurred in another location in the casting where the temperature was higher. When samples were cooled from 730°C or below, the transformation in all members took place under cooling conditions which are similar, and consequently had no effect on the final value of residual stress. However, while cooling from higher temperatures, the deformations associated with higher temperature are not completely reversed and this adds to the final value of the stress.

Transformation stresses are more pronounced when they are accompanied by large volume increases. The largest volume changes are associated with the austenitic/martensitic transformation, lesser ones with transformation to non martensitic transformation products, e.g. Bainite and pearlite[50]. The phenomena occurring during quenching

cooled surface. The extent of transformation depending on actual temperature of transformation. The formation of martensite involves a volume expansion occurring at a freely cooling surface enclosing a hotter and plastic interior. On further cooling the interior undergoes transformation and expands and it has compressive stresses imposed by the rigid martensitic envelope. The stresses may be of sufficient magnitude to inhibit or even suppress further transformation[16] or may crack the martensitic shell.

The precipitation of second phase particles in a single phase matrix is another typical transformation leading to a non uniform volume change producing very localised microstresses. If this reaction proceeds non uniformly through a section there may be significant differences in chemical composition or rate of heat transfer so that variations in micro stress distribution will produce macrostress. Nitriding processes for example, produce microstresses distributed around nitride particles, whilst carburisation processes involves carbon diffusion into the component surface and then quenching to produce a martensitic shell. These processes are diffusion controlled reactions and can occur only on a surface with consequent non uniform volume increase in this region. Thus, a macro compressive residual stress at the surface is balanced by the tensile residual stress in the interior.

In iron castings, Balasingh et al[39] suggests that the magnitude of transformation stresses remaining at

with associated volume changes, occur at high temperatures where the stresses are continuously reduced by plastic deformation or whether the phase changes take place at a temperature when the material can take up higher elastic strains. He also refers to observations of Patterson and Dietzel[51] that any alloying element which influences the rate of transition of elastic plastic behaviour during deformation also alters the residual stresses.

Parkins and Cowans[27] conclude that in materials which are accompanied by transformation, such as cast iron, the contribution to residual stress levels due to phase transformation and sand hindrance may be of the same order as that due to the temperature differentials.

It can be concluded that, in certain heat treatments, the contribution of phase transformations to the residual stresses may be higher than in solidification processes.

The magnitude and distribution of residual stresses arising during casting can be influenced, to a certain degree, by reducing temperature differentials within a casting and controlling the cooling rate. However, it is frequently desirable to further reduce the intensity of residual stresses by means of stress relief. It is commercially viable to reduce residual stresses to very low levels by these methods, which also may form part of an overall objective, that includes dimensional control and dimensional stabilisation.

Stress relief treatments have been classified into two categories[51,52] thermal treatments and mechanical treatments

THERMAL TREATMENTS:

Thermal treatments involve heating to a certain stress relieving temperature followed by holding and cooling at a suitable rate.

Stress relief annealing is an extensively used and effective method for reducing residual stresses. The relief of stresses during the treatment is due to two effects. Firstly, the residual stress level is reduced because heating decreases the yield stress value with consequent plastic flow since residual stresses cannot exceed the yield stress. Secondly, further stress relief is due to the creep process where there is a time dependent stress relaxation. Residual stress levels just below the yield stress at room temperature are reduced by the decrease

temperature. Stress relaxation processes are important when residual stresses must be reduced to low values but are less effective with increased heat treatment time. They are most effective in reducing residual stresses to particularly low levels at very high temperature, but also play an important role when possible deterioration in properties forces the use of lower temperatures and extended times of annealing.

Stewart[53], Rominski and Taylor[54], Jeim and Herris[55] and many workers[3,39,44,56,57] have investigated and reported many aspects of stress relief.

The choice of temperature for stress relief annealing is partly governed by the final properties required in the material. Full annealing carried out at above the recrystallisation temperature followed by slow and uniform cooling, is primarily carried out to soften the structure. However, this treatment is also accompanied by full stress relief. The temperature given by Beeley[37] for rapid stress relief lies in the region of 0.3-0.4 Tm where Tm is the melting temperature of the metal expressed in Kelvin. The temperature for stress relief is also determined by composition of the metal.

Rominski and Taylor[54] devised a method for the determination of rates of relief of stress as a function of temperature. They were able to calculate the time required at any temperature to reduce the stress from any

ation data obtained for plain carbon steel at various stress relieving temperatures. They also pointed out that removing stresses at the furnace temperature does not necessarily assume a stress free condition because conditions of cooling may re-establish stresses of a high order. Jelm and Herres,[55] in their investigation, found temperature to be the main variable governing rate of relief of stress and, as shown in Figure 8, increased treatment times were not very advantageous. They also found that after a given thermal stress relief treatment, higher original residual stress level increased the final stress levels.

A thermal stress relief treatment will only be effective if the heating rate, temperature at which treatment is carried out, holding time at that temperature and subsequent cooling rates are carefully controlled. Saunders,[57] referring to these four important variables in thermal stress relief treatments presented stress relieving requirements, shown in Figure 9, for C-Mn steels in two national codes. He did not explain the discrepancy in the holding times recommended by these two codes.

Stress relief heat treatment may also effect material properties, some adversely.[53] Higher temperatures, for example, will reduce stresses to extremely low levels in short times but may also cause loss of strength and hardness. It is generally possible to arrange a compromise,

where the levels of residual stresses are substantially reduced without detirimental effect. Fully quenched martensitic steel is generally very brittle, has high residual stress and possesses low toughness and ductility. Stress relief tempering carried out at low temperatures will reduce residual stress level and brittleness of this steel while still maintaining high degree of hardness and strength.

Residual stresses resulting from compositional and structural heterogenity in castings are not removed by annealing.[58]

Thermal shock is another form of thermal treatment reported by Balasingh[39] in his review of residual stresses in iron castings. The method uses combinations of repeated rapid heating or cooling, and is reported to lower residual stress level whilst considerably raising stress relaxation resistance so that subsequent machining does not cause any renewed distortion. Rapid heating causes permanent elongation of castings with thicker sections and contractions of those elements with thinner sections. Rapid cooling causes deformation in the opposite direction and also reduces the time necessary for repeating the process.[39] TS 32[40] also reported the effectiveness of thermal shock treatment for aluminium alloys, the possible explanation of the underlying mechanism behind the stress relief was by repeated expansion and contraction of castings over a wide range of temperature. However, this method is reported to carry

risk of failure during treatment.

Scaling or discolouration are the problems associated with thermal treatments, but these can be overcome by carrying out treatments in a controlled atmosphere or prior to finish machining.

MECHANICAL TREATMENTS:

A wide variety of mechanical stress relief treatments exist such as Stretching,[59] Reverse bending,[3] Shot peening,[51] Vibratory Stress Relieving[60,61] and Static overloading.[37]

Vibratory stress relieving(VSR) involves inducing a metal structure into one or more resonant or sub-resonant vibrating states using portable high exciters, causing the structure to undergo overall elastic distortion. Although nominal applied strains are elastic, any regions of residual stress or points of stress concentration give rise to local plasticity, where the sum of internal and vibrating induced strains exceeds the yield point of the material concerned. This plasticity then allows a redistribution and accompanied reduction in the residual stresses. VSR achieves a balanced stress redistribution in the stressed state whereas thermal stress relieving achieves a balanced stress reduction in the unstressed condition.[60] Size, Weight and stiffness of the component to be treated are important considerations in the selection of the VSR treatment.

Kotsyubinskii et al[61] found that VSR could reduce residual stress by 25% and in their investigation with Cast iron found that the amount of stress relief was directly proportional to the amplitude of vibration. However, amplitude cannot be increased infinitely since fatigue failure can start above a critical level. The bulk of stress reduction takes place during the first hour and, extending the time, leads to further reduction but the amount of stress relieved is small. They carried out their tests at frequencies between 7600 and 1200 cycles/minutes at approximately constant amplitudes of $\pm$2.8-3.5 kg/mm^2, the vibration time in all cases was constant at 6 hours.

VSR is reported to use less than 1% of the potential fatigue life of the component. The advantages of VSR treatment are that it does not alter metallurgical condition, there is no scaling or discoloration, it is a low cost process with little distortion.

TS 32[62] in their third report on the effect of vibration on stress relief of castings, concluded that no useful stress relief was achieved by any form of vibration treatments applied under any conditions, though there was an indication of a very small relief of stress by vibration at high levels of residual stress. VSR is to be avoided in situations where cold cracking phenomena or brittle fracture are a serious risk.[61]

Static overloading involves loading the component in the static condition with the direction of load same as the residual stress. Kotsyubinskii et al[58] compared the static overloading and vibration techniques and found that, for the same overload, the percentage of stress reduced by vibration is higher than that obtained by static overloading. However, the same degree of stress relief can be obtained by increasing the magnitude of the additional imposed static load.

The advantage of this method over the vibration technique is that there is no possibility of crossing the fatigue limit, it is however necessary that the sum of residual stress and static load should be within the static strength of material. This static overloading method is not suitable for stress relieving a casting of complex shape.

Natural ageing or Weathering is another method of stress relieving. This treatment slightly increases resistance to stress relaxation and a certain dimensional stability is obtained. Balasingh et al[39] confirmed several reports that natural ageing relieves stress by about 10-15% in Cast iron castings.

Novichkov[63] summarised the achievements of the different treatments and concluded that the main parameters to be considered of stress relief process are residual stress level and stress relaxation resistances, as shown in Table 1.

2.5 SIGNIFICANCE OF RESIDUAL STRESSES

In steel castings, residual stresses may give rise to cracking and distortion during the production process whilst they may cause dimensional instability, distortion and cracking in service. Depending on their magnitude and direction, however, some residual stresses are beneficial to service requirements.

Compressive residual stresses at the surface of a casting are generally beneficial and tensile residual stresses are detrimental because a compressive stress increases the fatigue strength while a tensile stress reduces it.[4,52,64] The principle involved is that initial cracks leading to failure originate in the surface zone as a result of the tensile part of cyclic straining. If the component originally possesses residual surface stresses which are compressive, these are subtracted from the tensile stresses imposed by the applied load and the maximum tensile stress actually attained is thereby reduced. Residual compressive stresses of sufficient magnitude and depth prevent a macrocrack opening and, so, either retard its growth or cause it to remain inactive until the stress level is raised. Alternatively, tensile residual stresses will open a crack and make its subsequent propagation easier in situations where there is a subsequent increase in tensile stress range. Compressive residual stresses will, for a given stress range, increase the change-over length between the microcrack and macrocrack growth stages.[65] Therefore, if fatigue cracks are initiated in either plain or notched samples

or notch root respectively, then the crack must grow an appreciable distance as a microcrack in order to penetrate the volume of material under the influence of residual stress. The cracks will finally grow as a macrocrack normal to the loading direction.(65)

The relationship between fatigue strength and the residual stresses induced by mechanical working processes, such as surface rolling or shot peening, has been widely studied because the processes induce biaxial compressive residual stresses in all free surfaces. This is unlike bending and restraightening techniques which induce tensile and compressive residual stresses in opposite faces, the bending technique tending to decrease the fatigue limit. Surface compressive residual stresses induced by shot blasting usually increase the fatigue resistance of a casting. Accelerated stress corrosion cracking may also occur if these residual stresses exist in steel castings used for chemical or other process plant.(65)

For castings subjected to torsion, residual stresses are not as significant because torsional fatigue strength is less affected by a static torque.(66) It is generally difficult to assess the effectof residual stress on fatigue strength because residual stresses are difficult to measure and may alter in magnitude as a result of further stressing. Also, the various methods used to produce residual stress will influence the intrinsic fatigue of the steel. However, providing the residual

stresses can be measured or calculated from theory, it should be possible to assess component life and monitor casting performance in service.[66]

A fracture mechanics approach can be used to design steel castings with knowledge of magnitude and direction of residual stresses and this will allow the calculation of component life and critical defect size. The significance of residual stresses on calculation of critical defect sizes was presented by Found[65] as shown in Table 2 for a relatively tough steel containing $1\frac{1}{2}$% Mn and a brittle 1%Cr-0.5C steel. In the calculations it has been assumed that the casting contains a through thickness crack. Critical defect sizes have been determined for three residual stress conditions, (a) zero residual stresses (b) a residual stress level of 80 N/mm^2, which is a realistic level for most steel castings, and (c) a residual stress equal to yield stress of the steel. The data in this table shows that residual stress levels significantly effect critical defect sizes, and hence indicate the defect sizes that can be tolerated in castings designed on a fracture mechanics basis.

Timofeev and Shumov,[67] using multilink shrinkage framework, 'Squirrel cage', investigated the effect of initial casting stresses on mechanical properties of steel. They concluded that the properties of steel subjected to casting stresses and subsequently relieved of them were lower than the properties of steel not subjected to stresses.

There was a larger decrease of 25-30% in the impact strength and they finally concluded that residual stresses had a detrimental effect on the reliability of castings.

2.6 RESIDUAL STRESS MEASUREMENT TECHNIQUES

Residual stresses cannot be measured directly, in the manner that applied stresses are measured. Residual stresses, in contrast, are measured indirectly by measuring strains existing within a metal that is residually stressed.[68] These strains are generally measured by various methods and corresponding stresses calculated from elastic theory formulae. The various methods of measuring residual stress have been reviewed extensively[3, 10,13,18,39,59,69,70-72] but reference will be made to some of the industrially significant techniques.

Residual stress measurement techniques are classified as mechanical and Xray types, although an alternative is to classify them according to their destructive nature as shown in Table 3.

2.6.1 MECHANICAL METHODS

The mechanical method of determining residual stresses is based on the property of stresses being purely elastic, even if they result from plastic deformation. The residual stress may be released by operations which release the elastic deformations, with consequent dissipation of the elastic potential energy stored in the material. These operations may be accompanied by plastic

deformation and the formation of additional residual stresses. The mechanical methods involve cutting, boring or removal of surface layers, so that there is a dimensional change due to relaxation of the material because of the readjustment of residual stresses, dimensional changes being measured directly or with strain gauges. These methods generally depend on the assumption that the removal or cutting process does not alter the stresses in the remainder of the component, with the implication that very great care is needed in carrying out the techniques. Computation of the relaxed stress from either deflection or strain is based on the assumption that the dimensional changes caused by relaxation are purely elastic. It follows that mechanical methods only measure relaxed strains and not actual strains produced by the existing residual stress.

Mechanical methods usually measure stresses that are balanced over areas of component which are large compared with the microstructure, microstresses being well balanced over these areas.[13] Hence, as a rule, mechanical methods measure only macrostresses.

Various special devices have been devised for the determination of the strain, these include high precision calipers with large gauge lengths (10-20mm) that have been defined by small balls peened in to the surface as shown in Figure 10, or by indentations on the surface, as shown in Figure 11. These devices suffer from the long gauge lengths required, which make them unsuitable for regions

of high stress gradient and represent an average over substantial depth of material. A superior approach is the adoption of short gauge length bonded electrical resistant strain gauges.[71]

Most mechanical methods are destructive to a certain extent. Numerous mechanical methods of measuring residual stress exist and some of the important ones are reviewed;

a) Boring and Turning method:[10,39,68-70,72-74]

This is a specialised layer removal method that may be used only on a circular cylindrical member. The tangential, radial and longitudinal stress distribution along a radius may be determined by removing layers from the bore or the outer surface, and measuring the longitudinal and tangential strain changes.

The two assumptions made in the measurement are:

i) The stresses are symmetrical about the central axis and constant along its length.

ii) The removal of the layer produces a constant change in the longitudinal stress at all points in the specimen.

The strains are measured on the side opposite to the one on which the layers are removed, and are a measure of the stresses released in the removed layer. If the complete stress distribution is desired, or if the stresses at bore or the outer surface are to be determined with greatest possible precision, then primary and secondary layer removal may be used.

An example,[39] of required measurement of stresses at the surface of a solid shaft, in this case, the shaft is bored first (primary cuts) which reduces the stiffness so that secondary cuts at the surface produce significant strain changes. Similarly, in the case of a thick walled tube, if the stresses at the bore are required with the greatest precision, primary cuts are made at the outer surface and secondary cuts at the bore, combination of boring and turning being necessary to reduce the error.

The precision of the boring and turning method is largely determined by the accuracy of the measurement of dimensional changes and the care taken in the layer removal techniques. The inherent stiffness of a cylindrical member causes only small changes in strain for a given thickness of layer removal and therefore requires extremely precise measurements of the thickness to be removed and strain changes to be obtained. It is also important to eliminate temperature gradients in the specimen and to maintain a constant temperature each time the strain readings are obtained. The length of specimen should be more than twice its diameter otherwise end corrections are necessary.

b) Parting out method;[10,39,73,74]

This method can be used as a first stage in a detailed residual stress determination, complemented by other methods, or as a method complete in itself. The

method requires removal of a layer with the shape of a flat plate, or with either a straight or curved beam. Strain and/or curvature produced in the parted out layer are measured to compute the stresses.

Residual stresses in the parent part may be determined if the distribution of the stresses through the thickness of the layer is known or can be reasonably assumed. The type of layer to be parted out depends on the state of stress to be measured and on other factors such as parent part geometry. Plate or beam layers may be used to measure either biaxial or uniaxial residual stresses. Plates must be used if the residual stresses have completely unknown principal directions, only one beam being needed, when the stresses are uniaxial but two beams being generally needed if the stresses are biaxial. The method is ideally suited to determine average stresses in large parts.

c) Cutting-deflection methods;[10,69]

This method measures a change in diameter of a slit tube or the change in the curvature of a plate. Changes in dimensions are greater than those obtained in the boring method for an equivalent amount of layer removal. Layer removal techniques are often dictated in cutting-deflection methods by shape of the specimen, Figure 12 showing cutting deflection methods for different shapes. A knowledge of the relationships between the stress and deflection of the specimen are required. The methods are carried out rapidly, and are convenient to operate, but they are not highly accurate.

d) Layer removal method;

This method is useful for measuring residual stresses in flat plates or beams in which the stress varies with the thickness, especially when stress gradient is steep. The stress in a layer is determined by removing the layer and measuring the strain and curvature change in the remaining part. However, some investigators[74-76] measure the strain and curvature in the layer, the probably discrepancy arising due to size of the layer removed relative to the remainder of the part. Longitudinal stresses were measured in these examples, transverse stresses being negligible.

Strain gauges and mechanical extensometers have been used for strain measurements. The residual stresses may be measured by either a beam or a plate layer, and either specimen type may be used to measure uniaxial or biaxial stress systems. Plates must be used if the principal stress directions are unknown. Two beams parted out in the principal directions are used to measure biaxial stresses, whereas only one beam is needed for the determination of uniaxial stress. The thickness of layer removed depends on the extent of stress measurement required, size of the parent part, precision of the measurement required and steepness of the stress gradient.

Care must be taken to induce minimum machining stresses, temperature control is essential, but it is relatively complex for thick curved beams.

e) Sectioning Method;

This method was developed to specifically determine residual stresses in cast Theta rings. The tie bar is cut across, as shown in Figure 13, and the change in length recorded using standard formulas to calculate residual stresses in tie bars. Significant errors may arise in this method due to temperature changes, and therefore measurements need to be taken where the temperature is uniform, or the same before and after sectioning.

f) Indentation Methods;[69,75,77-79]

Several methods exist for determination of residual stresses which are based on the principle that the hardness of the metal parts depends on the stresses acting on those parts. Investigations conducted on steel indicate a linear relationship between stress and change of hardness, provided stresses are within a linear range, hardness changes being greater for tensile rather than compressive stresses. Accuracy is also reported to be lower for the latter and a limitation of these methods is the calibration requirements for each initial hardness. Other sources of error may be scatter of hardness, support of specimen, and specimen texture.

g) Brittle Lacquer method;[69,74,75,80]

This is a convenient method to initially detect the direction of stress with only indication of its intensity. The surface is coated with a lacquer, dried, and hole drilled to bring about relaxation of residual stresses. The crack pattern, as shown in Figure 14, is characteristic

provide sufficient sensitivity to detect residual stresses great enough to have a bearing on fatigue life. The main feature of this method is its simplicity but it gives only a qualitative assessment of residual stresses. Difficulties may arise because the coating is sensitive to changes in temperature and humidity.

h) Centre Hole drilling technique;[39,71,73,75,81-91]

This method involves the change in stresses and the measurement of the corresponding strain changes that are produced when a hole is drilled into the surface of a member containing a uniform or non-uniform residual stress field. The drilling of the hole in the stress field redistributes the equilibrium of stresses, resulting in measurable deformations on the surface adjacent to the hole.

Mathar[81] described a technique of drilling the hole and measuring displacements between two points across the hole using mechanical extensometers. Main criticisms of his work was the limitation to cases where stresses are uniform through the thickness and the precision of the experimental technique. Later, Soete and Van Crombrugge[13] proposed that relaxed strains might be experimentally obtained as functions of hole depth so that residual stresses at any depth below the surface might be computed. Kelsey[82] investigated the hole drilling technique using four gauge rosette placed 90^{o} to each other, and used sharp fluted end mills for the drilling of the holes. Initial

tests investigated the feasibility of using the drilling method for measuring non-uniform residual stresses, whilst subsequent tests evaluated the effect of hole diameter and the type of strain gauge arrangement on the sensitivity of the method. It was established that the surface strains increased with hole depth to about one diameter and do not change appreciably for greater hole depth, the depth to which non-uniform residual stresses can be accurately measured being about one-half the hole diameter. The depth to which residual stresses could be measured was increased by doubling the hole diameter, gauge length and distance of the gauge from the hole.

Calibration constants K1 and K2, obtained from uniaxial tests, were established to be valid when calculating stresses in a biaxial stress field. The calibration constants are necessary in the analysis because the incremental surface strain in the hole drilling method is not a direct measure of the average residual stress in a given increment of the hole depth, and therefore a proportionality factor K must be introduced. Gauge layouts consisting of 4 or 8 strain gauges are placed at 90° or 45° to each other and surrounding the potential hole site, were found to be satisfactory arrangements. The directions of the principal residual stresses are determined using the stresses in any three directions, whilst the stresses in the remaining direction can be used as a check.

Later, Rendler and Vigness also developed equations, as previously developed by others,[13,82] relating the relaxed strains measured by three element rosette to the initial stress fields. Rendler and Vigness[82] and Bathgate[83] also confirmed that the maximum relaxation is obtained at the surface for a depth equal to the hole diameter. It was also demonstrated that, in principle, the technique can be used to measure stress gradients between the surface and the bottom of the drilled hole.

The most pertinent and recent critical evaluation of the centre hole drilling technique is by Beaney and Procter,[88] the major difference between their technique and that by Kelsey[82] being that they calibrated a separate value for stresses induced by machining the hole, the latter including the machining stresses in the calibration constants K1 and K2. Since the amount of strain induced during machining depends on the value of Young's modulus for the material concerned, it is advantageous to separate machining stresses from the calibration constants. The constants therefore became independent of Young's modulus of elaticity, and it can be assumed that the result will suffice for any elastic isotropic material.

Tests were carried out involving several operators to determine the induced strain using 1.5875mm(0.0625 inch) milling cutters on mild steel specimens. The average value obtained for induced strain was $-40\mu\epsilon$, the maximum scatter being $\pm 10\mu\epsilon$. From these results it was concluded that

residual stresses can be determined by the centre hole drilling technique with an accuracy of better than ± 10%, assuming there is no additional stress from the machining operation and that the hole is accurately located within elements of the rosettes.

The hole was considered as a potential stress raiser and, if the stress is very high, localised plasticity could occur round the hole. As shown in Figure 15, this leads to additional errors in the predicted stresses for a uniaxial loaded bar. Fortunately, at stress value less than half the yield value, the errors are considered to be negligible, but at full yield stress, errors may rise to 10%. Large errors in the predicted directions of principal stresses also result from small errors in the measured strains, and, therefore, incorrectly predicted angles between stress directions do not necessarily reflect on the reliability of the predicted stresses. Values for one of the constants, K1, was highly sensitive to the hole diameter and a relationship between the constant and the hole diameter, as shown in Figure 16, was presented.

Account was taken of the fact that a large hole will give greater sensitivity and accuracy and a small hole will minimise strains. These strains increase substantially in stainless steel or high strength steels so that the stress measurements will be unreliable. Beaney[89] also developed an abrasive hole forming technique. This machining system allows successful residual stress measurements to be made in all types of steel and reduces the induced machining

was re-established between the constant used in equations for this improved hole drilling technique. The overall measurement accuracy is reported to be $\pm$ 8%, except when residual stresses are greater than 50% of the yield stress. Above this level, the errors increase due to plasticity local to the hole. Depending on stress field and material behaviour, the error was found to increase by up to 16% on a residual stress of yield value. A prime merit of this technique is that accuracy of the measurement technique is no longer operator sensitive.

Beaney and Procter[88] concluded that comparison between two or more mechanical measurement techniques was not possible because of the calibration difficulties of techniques due to the inability to guarantee stress free materials. The comparison is also difficult because residual stress fields cannot be guaranteed uniform. Other workers[85,92,93] have presented theoretical analyses of various sources of error, such as hole eccentricity on the strain measured by the rosette.

2.6.2 XRAY METHODS

There are several reviews[10,39,94-109] of the theoretical and practical aspects of residual stress measurements by the Xray methods. The Xray methods involve use of a back reflection technique, as shown in Figure 17, to determine the lattice parameter, the change in lattice parameter being used to calculate strain. If only the sum of the principal stresses is required, a

single exposure method may be used when the Xray is beam normal to the surface. However, if the magnitude of the individual principal stresses are required, then they are determined semi-graphically from two or more Xray exposures at different angles of incidence, ψ, in a plane encompassing the stress direction required.

$$\sigma = K(2\theta_{\perp} - 2\theta_{\psi})$$

where

σ = stress

K = constant (a function of $1/\sin^2\psi$ and the elastic constant)

$2\theta_{\perp}$ = angle of refraction $\perp = 0^{\circ}$

$2\theta_{\psi}$ = angle of refraction $\psi = \psi$

ψ = angle of incidence of Xrays

This is commonly referred to as the $\sin^2\psi$ method because the stress is proportional to the slope of 2θ versus $\sin^2\psi$ graph, providing the relationship between two is linear.

The Xray method only measures surface stresses because Xray penetration is of the order 0.02mm, but it is a completely non destructive method. The technique is argued to be susceptible to errors arising from microscopic values of elastic constants, Young modulus and Poisson's ratio being different from the bulk engineering values used.[69] These variations can, however, be accounted for by employing various techniques.[71]

The Xray technique is designed for the measurement of macroresidual stresses but micro residual stresses can also be detected.

Various methods for determination of residual stresses have found limited application, a few being reported below;

a) Ultrasonic method;[10,39,71,73,110]

Stressed metals are birefringent to an ultrasonic shear wave (frequency of the order of 5MHz) similar to transparent materials being birefringent to a beam of polarised light. In a shear wave, the wave front moves at high velocities perpendicular to the surface and the particles in motion move parallel to the surface. A polarized shear wave is resolved into two wave components lying in the planes of the principal stresses. These wave components move at different velocities which are dependent upon the magnitude of the principal stresses.

Limitations of this technique arise from the fact that birefringent may also arise as a result of anisotropy.

b) Stress Corrosion method;[39,73]

Corrodants, which cause cracking of the surface of certain metals when a tensile stress field exists, may be used to detect residual stresses. The method may be quantitative if carried out under controlled conditions, since the time to cracking is roughly proportional to the level of tensile stress. It is, however, usually considered to be highly qualitative because of small changes in metal composition, corrodant, temperature and metal anisotropy have a large effect on the cracking tendency.

2.7 PREDICTION OF THE RESIDUAL STRESSES

Prediction of residual stresses is based upon the analysis of mechanical and thermal causes. The mechanical contribution is due to externally applied forces causing non-uniform plastic flow, whilst thermal stresses are caused by a non-uniform temperature distribution, which may set up stresses sufficiently high to cause local plastic flow. Stresses due to non-uniform phase transformation also fall into this thermal category.

THE PREDICTION OF RESIDUAL STRESSES ARISING BY MECHANICAL METHODS;

This initially involves calculation of stresses in the loaded body, taking into account the plastic properties of the material. This may be done analytically in a few simple cases, but more complex shapes require the use of the finite element method. The stresses are then re-calculated, but with all the external loads reversed, and assuming elastic properties. Finally the two solutions to calculations are superimposed, the external forces become zero, the summed stresses being the residual stresses required.

THE PREDICTION OF RESIDUAL STRESSES ARISING BY THERMAL MEANS;

Analysis of the thermal problem generally depends upon the times necessary for plastic flow to occur. However, for short time intervals for plastic flow, the analysis may be considered to be time independent. In the absence of phase transformation the usual solution is

iterative, proceeding by equal small intervals of time. Stressarising from the temperature distribution over each time interval (i.e. by thermal expansion or contraction) are added to the stresses present at the start of the interval. The sum of the stresses are then compared with the known yield stresses. Where these yields are exceeded, the stresses are readjusted to maintain equilibrium. If phase transformation is present, the dilations arising from it are added to thermal expansions/ contractions in calculating the increments of stress.

The thermal stress model, applicable to 'casting stresses,' involves determination of the temperature gradient followed by determination of Stresses using temperature gradient data obtained previously. Temperature data can usually be obtained by analysing the problem and for these purposes analytical, analogue and numerical methods are available

Analytical methods[111,112] involve the derivation of the mathematical solution for the temperature as a function of space or space-time co-ordinates. The solution must satisfy the basic governing partial differential equation, together with certain initial and boundary conditions appropriate to the particular problem. Usually, the actual problem must be simplified in order for this approach to succeed. Thus the solution so found is by no means exact, as far as the physical problem is concerned. Analogue or Graphical[113,114] methods are based on the properties of

the characteristic field equations and numerical principles, and have the singular advantage of giving a rapid first approximation to the required solution. Numerical methods[113-115] are usually based on finite difference approximations and hence derive an approximate computational solution, but one whose accuracy can usually be increased to any desired degree. Finite difference methods offer a powerful technique for the solution of heat transfer problems. The domain in which solution is sought is replaced by a finite set of points and then approximate values for the temperature at these points are found. Values at these points are required to satisfy finite difference equations obtained either by replacing the governing partial difference quotients, or by direct heat flow considerations. Finite difference methods have largely been applied to ingot solidification, solidification of simple bodies, and quenching,[117-122] however, with a few exceptions the treatment has been of a unidirectional nature.

Tein and Koump[123] explored the factors responsible for the development of thermal stresses. They suggested that the mathematical treatment of thermal stresses occurring during solidification is based on three features; stress-strain relationship at elevated temperature, time dependent temperature distribution in the solid layer and using appropriate pertinent boundary conditions. Because an analytical solution of the model, including these three aspects was inherently difficult with an inadequate knowledge of mechanical behaviour of metal at elevated temperatures,

two basic features were employed for calculation of stress i,e. heat transfer analysis and boundary conditions. The solid layer was assumed to behave elastically, but with a temperature dependent Young's modulus. However, in reality, the stress may be reduced by plastic flow at elevated temperature resulting in over estimation of stresses.

Weiner and Boley[124] calculated thermal stresses in a solidifying metal slab. The solid was regarded as elastic/perfectly plastic with a yield stress which was a linear function of temperature and was considered zero at the solidification temperature.

Sakwa and Parkitny[125] presented generalised equations for stress and strain conditions in castings as a function of temperature or cooling rate. Temperature distribution, and material constants expressed as functions of temperature were used for determination of the initial strain function. A critical temperature was defined so that, when the casting temperature was above this critical temperature, the casting would undergo free plastic deformation and hence be free of stresses. When casting temperature was below critical temperature, the casting would be in a condition of elastic-plastic strain. Three stages of a casting solidifying were identified;

a) The range of free thermoplastic deformation in the time interval (T1-T2)

b) The range (T2-TC) in which one part of casting is in the thermo elastic range whilst the other is still in the range of free thermoplastic deformation.

c) The range of thermoelastic deformation (TC-T4)

T1 = Mould filling time

T2 = Time at which any part of the casting first reaches critical temperature

TC = Time to reach critical temperature

T4 = Time to reach ambient temperature

To simplify modelling casting was assumed to be subjected to thermoplastic deformation during stage b. Generalised equations for casting stresses were derived by superimposing the thermal conditions prevailing at times, the later times characterising the temperature drop for the plastic/elastic transition in the behaviour of the casting.

Mathew and Brody[126] simulated thermal stresses in continuous casting of cylindrical sections, using the finite element method. The total strain was considered to consist of elastic, plastic, thermal and creep components. Elastic strain was obtained by Hooke's law, thermal strain was obtained on basis of affects of dilations, and plastic strains were related to deviatoric stresses and were not influenced by hydrostatic stresses. The creep strains were related to equivalent stress by the creep law of the material. Variations of material properties with temperature were also considered good, agreement being found between the measured and calculated temperature fields. They also found their stress analysis for simple, ideal cases (not continuous casting), whose analytical solution were available, to be in good agreement.

casting of Al-Si alloy ingots and further good agreement was established.

Grill, Brimacombe and Weinberg[127] developed a mathematical model to predict thermal stresses in continuous casting of steel. The thermal analysis section of the model used a finite difference approach and calculated the temperature history of steel for a given set of operating conditions. The stress section of the model was based on finite element theory and computed the stress field from a knowledge of computed temperature gradients and the roll pressure. The solid shell was treated as an elasto-plastic body, thermal and plastic strains being accounted for in the model. In order to calculate the stresses in the solidifying shell of continuously cast steel section, knowledge of following mechanical properties at elevated temperature was required;

i) Young's modulus
ii) Strain limit of elasticity (or yield stress)
iii) Plastic modulus
iv) Poisson's ratio

Owing to limited data available for the above properties, it was difficult to calculate values of stress that are absolutely correct. Sorimachi and Brimacombe[128] re-evaluated the stresses in continuous casting of steel using more reliable mechanical property data for steel.

Oki, Okumoto and Niyama[129] applied creep theory to the analysis of thermal stresses and deformation developed

in castings. The magnitude of the stresses were estimated by solving simultaneous equations of creep versus thermal shrinkage of the casting. The knowledge of temperature distribution, cooling rate and material constants was pre-requisite, and the analyses was applied to simple shapes.

More recently, various workers,[34,35,129,130] with Havlicek[35] being notable have reverted to basic strength of materials approach. The residual stress in castings is expressed as product of modulus of elasticity and deformation values, material properties being assumed to be constant. Predicted residual stresses were very high but they were substantially reduced and brought in agreement with the measured value by introducing correction factors influenced by casting geometry, heat passage between the parts of the castings, and coefficients characterizing temperature gradients.

3.1 INTRODUCTION

The experimental work was designed to measure residual stresses in theta rings after both casting and subsequent heat treatment (annealing, normalizing and tempering) stages and to facilitate the correlation between experimental data and theoretical explanations. The theta ring design was selected because this shape is less complex than industrial gear castings so that it is more amenable to correlate the effect of certain casting variables on residual stress patterns.

The theta ring was designed so that the thickness of central tie bar may be varied. This thickness variable provides different constraint and thermal history which will change the stress distribution in the castings.

3.2 DETAILS OF THE CASTING/MATERIALS

The theta ring, with its dimensions, is shown in Figure 18. The maximum size of the ring was chosen taking into account the constraints imposed by the available melting, casting and heat treatment facilities, and to amplify the effects of different casting variables.

The casting material used was BW2, as specified by British Standard[131], BS3100 being a low alloy steel designed for resistance to abrasion. This steel was preferred due to its basic composition without more complex alloying additions. Table 4 gives the chemical composition of the steel as given in the British Standard Specifications. All theta rings were analysed for chemical composition and were found to be within the range of

ring was produced in an aluminium casting, slots allowing tie bars of varying thickness to be fitted.

3.2.1. DESIGNING FOR A SOUND CASTING

The procedure for designing a sound casting was based upon the method outlined by Beeley[37] and Flinn[36], also known as Caine's method. The objective was to have an adequate and optimum feeding system so as to achieve a defect (mostly arising from shrinkage) free casting upon completion of the solidification.

Two critical requirements dictating the size and shape of feeder heads are:

a) Freezing time of feeding heads must exceed that of the casting, thus enabling directional solidification from Casting to feeding head. This is also known as Freezing time criteria.[37]

b) Feeding head must supply sufficient liquid metal to compensate for the liquid and solidification shrinkage. This is also known as the Volume feed capacity criteria.

Ratio of area to volume was intuitively assumed to determine the cooling rate, and hence is inversely related to freezing time[36]. For a sound casting, the ratio of freezing time of the feeding head to that of the casting being greater than 1. The liquid to solid shrinkage is approximately 3% by volume for steel[36], this requiring the riser volume to be at least 3% greater than the casting volume.

Total volume of theta ring was based on a tie bar of 30mm (maximum) thickness = 938405 mm^3

Total surface area of theta ring based on a tie bar of 30mm thickness = 123321 mm^2

Casting is symmetrical and hence may be divided into zones, each being fed by its own individual feeding head.

Therefore, volume of half the casting = V_c = 469203 mm^3

Surface area of one half the casting = A_c = 61660 mm^2

Area to volume ratio of casting = 0.131

Taking into account 3% for liquid-solid shrinkage, additional volume of feed metal necessary to supply one half casting is 14076 mm^3.

In order to employ Naval Research Laboratory method of feeding head calculation, as described by Flinn[36], it is necessary to calculate Shape factor for the casting;

Shape factor = $\frac{L+W}{T}$

Total length of half the casting = L=Circumferential length of half the ring (using mean diameter)+ length of half the tie bar = 523mm

Depth of the casting = T = 30mm

Width of the casting = W = 30mm

Shape factor for the half of the casting = 18.44

This shape factor was used to find a value of V_r/V_c (Volume of feeding head/volume of casting) from figure 19, later was used to give the value of freezing ratio (A_cV_r/V_cA_r) from the figure 20 for a sound casting.

0.5 and 1.4 for V_r/V_c and freezing ratio produce a sound casting.

$$V_r/V_c = 0.5$$

$$(A_c/V_c)/(A_r/V_r) = A_cV_r/A_rV_c = 1.4$$

$$A_r = 0.5A_c/1.4 = 0.357\ A_c$$

$$A_r = 22012mm^2$$

$$A_r = 2\pi D_r H \qquad H = D_r/2$$

D_r = Diameter of feeding head

H = Height of feeding head

$$\pi D_r^2 = 22012$$

$$D_r = 84mm$$

$$H = 42mm$$

The casting therefore required two risers, each of diameter 84mm and height 42mm. The sprue was funnel shaped with its area at the bottom greater than the cross-sectional area of the runner, $20x20mm^2$ square, thus ensuring a slightly pressurized system. The runner was S shaped, placed underneath the casting and separated by a core, entering the castings under the feeding heads (Plate 1). This S shaped design was selected with the objective of minimising the stresses imposed by the runner of the casting itself.

Chelford (60) sand was used for the mould and core, utilizing the carbon dioxide moulding process in order to strengthen the mould. The mould was thoroughly vented to avoid any gases being trapped inside the castings.

3.3 DETAILS OF HEAT TREATMENT

Theta rings after casting and post casting residual stresses analysis were heat treated, the heat treatment being divided into three natural stages;

a) Annealing at 950°C furnace cooled,

b) normalizing at 870°C

c) tempering at 640°C followed by air cooling

After each stage the casting was analysed for residual stress.

The heat treatment temperatures were those recommended by Steel Casting Research and Trade Association for the low alloy steel, BW2. The time for all treatments was 70 minutes, as dictated by the theta ring section size (30mm). Special care was taken to exclude any exterior effects during the air cooling of theta rings. Potential sites for residual stress measurement were painted with 'Berkatekt' to prevent decarburisation of the surface and hence minimise surface preparation effects.

3.4 THERMAL ANALYSIS

The objective of this analysis was to determine the thermal history of the castings during the casting and various heat treatment stages (Annealing, normalizing and tempering). Variable tie bar dimensions introduce varying thermal gradients and hence the thermal history was obtained for each casting.

Before introducing thermocouples into the mould and determining the precise solidification times in the casting, the liquidus and solidus temperature of the low alloy steel BW2 were determined. For this purpose, a cylindrical ingot 150mm long and 100mm diameter was cast with 13% Rh-Pt/Pt thermocouples placed in the centre. The metal solidified slowly, allowing solidus and liquidus temperatures to be recorded distinctly.

1468°C and 1382°C were the liquidus and solidus temperatures determined. These temperatures are in reasonable agreement with those determined by Jerkontoret[132] for low alloy steel of similar composition to BW2.

In sand moulds, six 13% Rh-Pt/Pt thermocouples were placed in the theta ring casting in the vicinity of the locations at which residual stresses were to be determined. Figure 21 shows the exact location of thermocouples denoted by the 'T_c' (subscript c referring to casting stage), 'S' denotes the position at which residual stress measurement were carried out. Thermocouples $T1_c$, $T2_c$ and $T3_c$ were located essentially to check for temperature profiles along the ring. $T2_c$ and $T6_c$ were diametrically opposite to each other to measure the thermal assymetry of the theta ring due to location of the sprue in top two quadrants. $T4_c$ and $T5_c$ were underneath the riser at hot spot and in about the mid position of the tie bar respectively These two locations were critical because this has direct effect on the temperature differentials across the two location as tie bar width is altered.

'Credshire' 200, 500 and 700 units which continuously recorded temperatures and times onto a tape cassette which, when replayed in conjunction with computer terminal, produced results on a printout.

Thermal history of the sand in the vicinity of the theta ring of 30mm tie bar was also recorded. Positions of thermocouples are shown in Figure 22, the approximate distance of thermocouples from the theta ring being 15mm.

3.4.2. HEAT TREATMENT STAGE

Thermal histories, i.e. the temperature profiles during cooling of theta rings were recorded during annealing, normalizing and tempering. Following observations that diametrically opposite locations in a theta ring had very similar thermal histories due to the absence of the sprue, the locations at which thermal histories were recorded were T4, T5 and T2 or T6 (both being interchangeable), as shown in Figure 23, and as the stress measurements to be carried out at different sites was also restricted. Subscript 'a', 'n' and 't' will refer to the annealing, normalizing and tempering stages respectively. Datalogger was used to record the temperatures using Chromel Alumel thermocouples.

3.5 RUNNER SECTIONING

An S shaped runner system was used to minimise constraints which would have been imposed by a simplified runner system. In order to check whether there was any further constraint effect on the theta ring, the runner was sectioned to isolate the effect.

the tie bar on the runner. Another line was drawn perpendicular to these lines on the centre line of the runner, as shown in Figure 24. The intersection of lines along X and Y axes were marked and distance EF measured. The runner was sectioned, using a junior hacksaw, parallel and equidistant from lines AB and CD, and the distance between the marked points measured. Any change in this distance indicated the shift of runner along the Y axis. Any shift along the X axis would lead to misalignment of two halves of scribed lines joining two marked points along Y axis.

3.6 STRESS ANALYSIS

The Centre hole drilling technique was used to measure the residual stresses at different locations in the casting. This method has the following advantages over the other methods described elsewhere in this study;

i) The method is semidestructive in the respect that only a 1.5875mm diameter hole needs to be drilled in the component. This can often be tolerated, and may be plugged if necessary.

ii) It is possible to measure stresses with reasonable accuracy.

iii) The method is very simple and quick. A complete measurement can be made in approximately one hour.

3.6.1. THE TECHNIQUE IN PRACTICE

The strain rosettes used were Micromeasurements type EA-06-062RE-120, as shown in Figure 25. These are made

foiled elements in a standard 45° format. The rosette incorporates centering marks for aligning the drill precisely at the centre of the gauge circle.

Standard procedure[133] for strain gauge installation required a small area slightly larger than the rosette to be abraded, polished and degreased. The rosette was attached with pressure sensitive adhesive M200 bond onto the surface. The 'Jig' for guiding the microscope for alignment and milling bar was mounted onto a fixture, the fixture being designed and constructed to locate, support and clamp the theta ring so as to prevent its movements in all six degrees of freedom. This method allowed the theta ring to be held independently of the jig over the rosette in order to obtain accurate alignment with the centre of rosette and vibration free drilling.

Strain measurements were made at equal intervals of depth in a 1.5875mm x 1.8mm deep hole. These strains were then used to calculate the principal stresses and their directions employing following equations[88].

$$\sigma^{max}_{min} = \frac{E}{2}\left[\frac{1}{K1}\right]\left[\frac{\epsilon_1+\epsilon_3}{1-\frac{\nu K2}{K1}} \mp \frac{1}{1+\frac{\nu K2}{K1}}\sqrt{(\epsilon_1-\epsilon_3)^2+(2\epsilon_2-(\epsilon_1+\epsilon_3))^2}\right] \qquad 3.6.1$$

$$\alpha = 0.5 \tan^{-1} \frac{2\epsilon_2-(\epsilon_1+\epsilon_3)}{\epsilon_1-\epsilon_3} \qquad 3.6.2$$

Determination of calibration constants 1/K1 and ν K2/K1;

26) of low alloy steel subjected to uniaxial tensile stress, the specimen being loaded in a Hounsfield tensile testing machine 20 KN capacity. A rig was designed and constructed to enable the 'jig' to be supported over the specimen in the testing machine. A EA-XX-062RE-120 type strain gauge rosette was attached to the specimen with a gauge in the direction of the major principal stress. A single strain gauge was attached to the underside of the specimen to indicate the presence of any bending stresses under the loading. With the specimen subjected to a load of 20 KN, the hole was drilled and the strain relieved, as indicated by the change in resistance noted at 0.1mm increments of the hole depth.

The specimen was machined to final dimensions, the machining introducing residual stress additional to those already existing in the test piece. The specimen was therefore given a stress relief anneal treatment at 650°C followed by furnace cooling, but even this treatment did not guarantee a residual stress free specimen. Therefore, to eliminate the effect of these residual stresses on the readings, the strains were noted as the specimen was loaded - After the hole had been drilled, the strains due to unloading were noted. The differences between the strains on the loading and unloading parts of the cycle is then equal to the relaxed strains in the ideal stress free case. Data obtained from experiment are shown in Table 6.

loading and unloading parts of the cycle were;

$$\epsilon'_a = -93\mu\epsilon \quad \epsilon'_b = -51\mu\epsilon \quad \epsilon'_c = -10\mu\epsilon$$

A value of $31\mu\epsilon$ was added to these values to allow for induced machining stresses, this allowance was determined as indicated in section 3.6.2. The actual relieved strains then became;

$$\epsilon'_a = -62\mu\epsilon$$
$$\epsilon'_b = -20\mu\epsilon$$
$$\epsilon'_c = +21\mu\epsilon$$

The calibration constants can be determined as described as by Beaney and Procter[88]

$$1/K1 = -\epsilon_a/\epsilon'_a \quad \text{and} \quad \nu K2/K1 = -\epsilon'_c/\epsilon'_a$$

$$1/K1 = -206/-62 = 3.322 \qquad \nu K2/K1 = -21/-62 = +0.339$$

The values of these constants were verified by substituting into equations with strains relieved, to obtain the values of σ_{max} and σ_{min}. σ_{max} is the known axial stress of 44.4 MN/m^2 and, since the stress field is uniaxial, then $\sigma_{min}=0$. Because σ_1 is in direction of the maximum principal stress, then $\alpha = 0.0^\circ$. The value for Modulus of elasticity(E) to be used for BW2 low alloy steel was 196×10^9 N/m^2 as given by Mechancal Design and Systems Handbook[134] for Cast steel. From equation 3.6.1.

$$\sigma_{max} = \frac{196\times10^9}{2}(-3.322)\left[\frac{-41}{0.661} - \frac{1}{1.339}\sqrt{(83)^2+(-40+41)^2}\right]10^{-6}$$

$$\sigma_{max} = 325.56\left[-62.027 - 62.005\right]10^3$$

$$\sigma_{max} = 40.38 \text{ MN/m}^2$$

$$\sigma_{min} = 325.56(-62.027 + 62.005)10^3$$

$$\sigma_{min} = 0.007 \text{ MN/m}^2$$

$$\alpha = 0.5 \tan^{-1}\left[\frac{-40-(-41)}{83}\right]$$

$$\alpha = 0.35^{\circ}$$

The constants are valid because of agreement between the maximum stress (σ_{max}) and uniaxial stress. The slight discrepancies, in these two stresses may be attributed to the sources of error described in the section 2.6.1. The values of constants 1/K1 and K2/K1 compared favourably with results obtained by previous investigators as shown in Table 7. Beaney and Procter[88] also indicated that as hole diameter increases, the value of 1/K1 decreases. The line was constructed by Beaney and Procter, Figure 16, to show the variation of 1/K1 with hole size and it cannot be extrapolated since a linear function is invalid for this relationship. If a linear function were valid, then the value of 1/K1 would become zero at some value of diameter, and thus σ_{max}, and σ_{min} would also become zero.

These constants and strains relieved were substituted into equations 3.6.1 and 3.6.2, 1/K1 being read from figure 16 for hole diameter 1.79mm. Hence

$$\sigma_{max} = 39.59 MN/m^2 \quad (actual = 44.4 MN/m^2)$$

$$\sigma_{min} = 1.7\ MN/m^2 \quad (actual = 00.00 MN/m^2)$$

$$\alpha = 0.35^{\circ} \quad (actual = 0.0^{\circ})$$

The σ_{max} has an error of 10.83% which is of the order Beaney and Procter[88] calculated for the centre hole drilling technique.

logical to use the values of constants as suggested by Beaney and Procter[88]. The nominal value of $\nu K2/K1$ was 0.3 and values of 1/K1 were read off from the graph as shown in figure 16, after determining the hole diameters.

Description of the Jig:

The jig for the hole drilling performs the following functions;

i) it correctly aligns the milling cutter so that it is concentric with the centre of the strain gauge rosette.

ii) the milling cutter is accurately supported during the drilling operation to ensure a perfectly formed hole without side pressure.

iii) it facilitates incrementing the depth of drilling and accurate measurement of the depth of the hole.

iv) while being held rigidly to the bed it ensures that no vibrations occur during drilling operation.

The Jig as shown in Figure 27 and 28 has a three legged arrangement for stability. Legs (item 9) were threaded to allow the height and angle of jig to be adjusted, the locking ring (item 13) finally securing the setting. The main body of the jig (item 2) allows the lateral movement of the hardened steel bush (item 3) by means of four aligning screws (items 5). Locking ring (item 4) finally secures the bush when alignment is achieved.

The focusing screw and locking ring (items 8 and 7 respectively) give focusing facility for the microscope

magnification with a cross-scaled gratitude to enable accurate alignment and measurement of hole diameter to be made.

For the drilling operation, a ground hardened steel mandrel (item 15) is designed to be accurately fitted with a precision chuck (item 21). For depth measurements, a milling arbor spacer is so designed to allow the spacer to rotate when the tool reaches the desired depth. The milling mandrel is fitted with a universal joint to remove side thrust during the drilling operation.

A complete operation involves cementing the jig onto a test bed and holding the casting to stop any movement so that the centre of the jig was approximately over the centre of the strain gauge rosette. The microscope was introduced and four alignment aligning screws adjusted until the centre of jig is concentric with the centre of rosette. The bush was then secured in the position by the locking ring.

The microscope was removed and the milling mandrel introduced with the cutter in position. Drilling was carried out using a small hand drill, higher speeds of a power drill could produce a whirling effect and induce high machining stresses.

The strains relieved were recorded through a Savage and Parsons 50 way Strain recorder in conjunction with a digital voltmeter. Each strain rosette was calibrated for a known change in resistance in terms of millivolts. A

computer program was established which converted strain relieved (in millivolts) into change in resistance, microstrains and finally calculated principal stresses.

3.6.2. INDUCED STRESSES

The major sources of error inherent in the centre hole drilling technique are concerned with;

a) stresses induced while preparing the surface for the installation of the strain gauges and

b) stresses induced due to drilling of the hole.

In the 'as cast' condition, it was not possible to install a strain gauge because of an extremely poor surface finish. For general stress analysis application, a relatively smooth surface (to the order of 2.5μm,rms) was suitable. The surface preparation of cast surface can be carried out by two alternative methods:

i) Using a grinding machine and grinding down the surface to required finish at very low speeds and feeds and flooding the workpiece with coolant to minimise the temperature gradient within workpiece, or

ii) using a portable electric drill onto which is mounted a rubber bobbin with emery sleeves of various grades, the cast surface being initially cleaned/abraded with coarse followed by fine emery sleeve.

The above two methods were compared to select the surface preparation process inducing minimum stress. Two small discs 12.5mm x 25.0mm of BW2 composition were fully annealed at 950^{o}C and furnace cooled. The surface was pre-

machine for one disc and the surface hand grinder for the second.

Induced stresses were measured in both discs, and are shown in figure 29. It was evident that stresses induced due to the grinding machine was considerably higher than those due to surface hand grinder, and surface hand grinder method was selected.

MACHINING STRESSES

All residual stress measurements were corrected by accounting for the machining stresses. It has been standard practice to drill stress free specimens, i.e. annealed discs, and record the induced strains. The machining strains are always negative and hence the error in the calculated stresses is tensile. Beaney and Procter[88] found the average value of induced strain to be $40\mu\epsilon$, this value being operator dependent.

It was experienced that the 'as cast' material required more streneous drilling compared with annealed material. This led to the conclusion that machining stresses in 'as cast' material would be higher than in the annealed condition. Two specimens, one in 'as cast' state and the other in annealed state were drilled assuming that both were stress free initially. Values of $68\mu\epsilon$ and $31\mu\epsilon$ were found as machining strains in as cast and annealed specimens respectively. It was therefore decided to use different machining strain values for determination and computation of residual stresses in Theta rings in 'as cast' and heat treated states.

3.6.3 ACCURACY OF THE CENTRE HOLE DRILLING TECHNIQUE

The accuracy of the basic technique has been quoted to be about 10% by various workers.[88,89,91] However, it was pertinent to determine the accuracy using Procter's method[91].

Maximum probable errors were determined as follows:

1.	Due to errors in $\gg K2/K1$	$\pm 5\%$*
2.	Error in hole diameter measurement	$\pm 1\%$
3.	Misalignment of hole in rosette	$\pm 5\%$
4.	Error in stress measurement	$\pm 1\%$
	Total	$\pm 12\%$

*This error, quoted by Procter[91], is due to $\gg K2/K1$ and depends on the stress field. The largest error of $\pm 5\%$ is in an equi-biaxial system but, in a uniaxial system, the error reduces to $\pm 1\%$, and in pure shear is $\pm 2.5\%$.

3.6.4 EFFECT OF THE RUNNER

The S shaped runner for theta ring casting was selected in order to minimise the constraint effect, if any. This constraint effect would be exhibited by the runner sectioning method.

In addition to the runner sectioning method, residual stress was determined in the runner on the position 'O' shown in figure 24. A theta ring with a tie bar of 30mm was selected to investigate the effect of the runner on the residual stress level in the theta ring. Feeding heads were sawn off and residual stress was measured using centre hole drilling technique on the ring and tie bar,

positions, S3 and S5 as shown in figure 21. The runner, after sectioning, was sawn off and residual stress again determined in the vicinity of the previous measurements.

3.6.5. CASTING STRESS ANALYSIS

A series of theta rings with tie bar widths varying from 5 to 30mm in steps of 5mm had their thermal history recorded. Theta rings were then subjected to Stress analysis employing centre hole drilling technique. The sites at which Stress analyses were carried out in Theta rings were as shown in figure 21 and represented by letter 'S'. In the case of theta ring with 5mm tie bar width the stress measurement was not carried out at location S5 because tie bar width was insufficient to put the strain gauge on.

It is relevant to explain the locations selected. The location S1 the hot spot underneath the feeding head was expected to be the slowest cooling section irrespective of the tie bar width. Location S5 in the middle of the tie bar, had the relative cooling rate dependent on the tie bar width. These two locations were of prime importance and interest from a thermal history point of view, and hence they were the logical sites. A temperature gradient was expected from the junction of the tie bar and the ring to the middle of the ring, forming a 90^{o} angle. This was interesting from a stress analysis point of view, however, because the theta ring was symmetrical geometrically and could be split up into four symmetrical quadrants, two locations were selected for stress analysis in the first

quadrant. Location S2 was at 45° to S1 at the hot spot, and S3 was at 45° to the S2 and 90° to S1. However, as discussed in section 3.4.1, due to location of the sprue between the tie bar and ring in one half, the thermal history of ring in upper half would differ from the lower half. The effect of this unsymmetry was investigated by carrying out stress measurement at another location S4 diametrically opposite to location S3.

3.6.6 HEAT TREATMENT STRESS ANALYSIS

This was a multi-stage analysis consisting of annealing, normalising and tempering stress analysis employing centre hole drilling technique.

Theta rings of tie bar widths 30mm and 10mm only, were heat treated and subjected to stress analyses. Stress measurements were restricted to three locations as compared with five in the casting stage.

Criteria for location of stress measurements were the same as described in the previous section. Due to absence of a sprue, the casting was geometrically and thermally symmetrical. Hence location S4 and S2 of the casting stage were considered redundant. Locations at which stress measurements were carried out are shown in figure 23 and are represented by letter 'S'.

3.7 TIE BAR SECTIONING TECHNIQUE

The technique of measuring residual stresses in tie bar was carried out on the series of theta rings with varying tie bar width after their thermal history had been recorded and stress analysis carried out after casting.

Heat treated theta rings, in which stresses had been measured employing Centre hole drilling technique, also had the stress in their tie bar determined employing this technique.

Straight lines were scribed at the intersection of the centre line of the tie bar and the ring, as shown in figure 13, the distance . between these lines being measured on the Universal measuring machine. After cutting the tie bar, the distance measured between the scribed lines indicated the contraction or expansion. Any contraction or expansion (Δl) due to stresses relieved were then substituted in the following equations to calculate the stresses.[35]

$$\sigma_T = \frac{E}{\alpha A+1} \cdot \Delta L \qquad 3.7.1$$

$$\text{where } \alpha = \frac{R}{B}\left[\frac{1}{\chi}\left\{\frac{\pi}{4} - \frac{2}{\pi}\right\} + \frac{2}{(1+\chi)}\right] \qquad 3.7.2$$

$$\text{where } \chi = \frac{1}{3}\left(\frac{e}{R}\right)^2 + \frac{1}{5}\left(\frac{e}{R}\right)^4 \qquad 3.7.3$$

The tie bar was sectioned on the hack saw machine flooded with coolant to minimise any temperature rises. All measurements were carried out at the constant temperature, 20°C. The technique has an accuracy of ±10%.

3.8 METALLOGRAPHY

A series of microscopic examinationswere made of the microstructure in relation to the varying tie bar width and hence the different cooling rates imposed. The series of theta rings subjected to stress analysis using both Centre hole drilling technique and tie bar sectioning

technique, in the "as cast" condition, had specimens taken from the central portion of the tie bar. Specimens were also taken from the region of junction of tie bar and the ring, and the ring itself at approximately 90° from the junction . Similarily, specimens were taken from the tie bar of the heat treated theta ring. The specimens were polished and examined employing photomicrography.

Specimens were hardness tested and microhardness of tie bar was also measured adjacent to the surface of tie bar employing Reichert micro hardness attachment The hardness was also measured in the centre of cross-section of the tie bars of varying widths.

3.9 EPOXY RESIN MODEL

A theta ring was cast in Araldite epoxy resin to study the stress distribution, if any, that may occur during curing.

A mould of 30mm tie bar width theta ring was prepared of Silastic 9161 RTV silicone rubber, with small addition of liquid catalyst Dow corning N9162[135,136], employing an aluminium pattern of the theta ring.

Araldite CT200 and Hardner HT901 in 100:53 proportion were heated and mixed thoroughly at 110°C and then poured into a preheated silicone rubber mould to 110°C. This was followed by curing the casting for 24 hours at 110°C followed by cooling at a rate not exceeding 10°C per hour.[135]

This Araldite model was, finally, then examined in a field of polarized light.

Finally the summaries of experimental procedures are shown in Figure 30 and 31.

4.0 COMPUTER SIMULATION OF SOLIDIFICATION PROCESS

The process of solidification, involving temperature change with heat flow as a function of time, internal generation of heat and varying conditions at the boundaries can be described in terms of partial differential equations. These equations often have complex boundary conditions imposed by the realities of foundry operations, and can be solved in their original form only by using numerical techniques.

A numerical technique often applied to the solution of partial differential equations, and particularly to those which apply to solidification problems, is that of 'finite difference approximations.' Finite difference approximation (FDA) represents the differential changes in dependent variables such as temperature by finite differences. FDA's can be used for all orders and types of derivatives. By using a set of FDA's over discrete steps in an independent variable such as time, the dynamic behaviour of a variable such as temperature can be computed. A finite difference solution using FDA is only sufficiently accurate when the time step limit approaches zero and certain criteria are met. With small time steps sequential applications of FDA's over a range of a variable will provide an accurate description of the actual physical behaviour of a system, in so far as it is characterized by the proposed partial differential equations.

4.1 FORMULATION OF HEAT FLOW DURING SOLIDIFICATION

Temperature is a function of position co-ordinate(x) and time

$$T = T(x,t)$$

in the x direction, there will be a resulting heat flow by conduction in the direction of the decreasing temperature. This is expressed by Fourier's law of heat conduction:

$$q_x = \frac{-k\partial T}{\partial x} \qquad 4.1.1$$

An energy equation which governs the temperature variations with space and time will be established for the conducting medium. Assuming a unidirectional case with dimensions along other axes to be unit and using an element as shown in figure 32.

Equating net rate of heat input to the rate of accumulation of thermal energy by element

$$q_x - (q_x + \frac{\partial q_x}{\partial x} \cdot dx) = \rho . Cp . dx . \frac{\partial T}{\partial t}$$

or

$$-\frac{\partial q_x}{\partial x} = \rho . Cp . \frac{\partial T}{\partial t} \qquad 4.1.2$$

Substituting value of q_x from equation 4.1.1 into equation 4.1.2 gives

$$-\frac{\partial}{\partial x}(-k . \frac{\partial T}{\partial x}) = \rho . Cp . \frac{\partial T}{\partial t} \qquad 4.1.3$$

$$\frac{k}{\rho . Cp} \cdot \frac{\partial^2 T}{\partial x^2} = \frac{\partial T}{\partial t}$$

replacing $\frac{k}{\rho . Cp}$ by α

$$\alpha \left(\frac{\partial^2 T}{\partial x^2} \right) = \frac{\partial T}{\partial t} \qquad 4.1.4$$

The above equation provides the basis for formulation

of the solidification problem.

EQUATIONS FOR INTERFACE

a) Metal-Sand interface:

An equation must be derived for the metal sand interface because of their vastly differing physical properties. The interface is shown in figure 33.

The first equation expresses the fact the heat flux is continuous at the interface (and elsewhere). Hence, from Fourier's law it can be deduced that:

$$k_m \left(\frac{\partial T_m}{\partial x}\right)_{x=x_o-} = k_s \left(\frac{\partial T_s}{\partial x}\right)_{x=x_o+} \qquad 4.1.5$$

x_o is the position of the interface and subscript;- and + refer to the left and right of the interface.

The second equation establishes an interfacial temperature T_i, immediately after the metal at a pouring temperature T_{po} has been brought into contact with the sand at an initial temperature T_{so}. Considering the case of a semi-infinite medium, as shown in figure 34 (with a single face at x=0, then extending indefinitely in the positive x direction). This medium has a uniform initial temperature T_{so}, and at time t=0 the interface is maintained at temperature T_i.

The subsequent temperature inside the semi infinite medium is known to obey the relation

$$T(x,t)=T_o + (T_i-T_o)\,\mathrm{erf}\,\frac{c}{2\sqrt{\alpha t}} \qquad 4.1.6$$

where $\operatorname{erfc} z = \frac{2}{\sqrt{\pi}} \int_{z}^{\infty} e^{-y^2}\, dy$ 4.1.7

From Fourier's law in conjunction with equation 4.1.6 and 4.1.7 the heat flux density into the semi infinite medium is

$$q = -k \left(\frac{\partial T}{\partial x}\right)_{x=0} = \frac{k(T_i - T_o)}{\sqrt{\pi \alpha t}} \qquad 4.1.8$$

Both metal and sand behave as semi infinite media for a short duration after they have been brought into contact. Thus, equating heat flux from metal to that into the sand, and noting that both obey a relation of the type given by equation 4.1.8, it follows that

$$\frac{k_m (T_{mo} - T_i)}{\sqrt{\pi \alpha_m t}} = \frac{k_s (T_i - T_{so})}{\sqrt{\pi \alpha_s t}} \qquad 4.1.9$$

therefore the interfacial temperature is

$$T_i = T_{so} + \frac{T_{mo} - T_{so}}{1 + \frac{ks}{km}\sqrt{\frac{\alpha m}{\alpha s}}} \qquad 4.1.10$$

The above relationship is valid for short time intervals and to simplify the latent heat effect has been ignored.

b) Sand-Air interface

This boundary is assumed to be a convective boundary condition (transient). A unidimensional approach is adopted with properties ρ, C_p and k subject to the convective boundary condition as shown in figure 35. Over a

small interval of time Δt, the energy balance method gives the following equation for the boundary node 0

$$\rho . Cp . V_o \frac{\Delta T_o}{\Delta t} = \frac{k}{\Delta x} (T_i - T_o) + h(T_A - T_o) \qquad 4.1.11$$

4.2 NUMERICAL SOLUTION FOR THERMAL ENERGY BALANCE

4.2.1 FINITE DIFFERENCE APPROXIMATIONS OF THE ENERGY EQUATIONS

In the previous section the following equations were derived for thermal energy balance

$$\rho . Cp . \frac{\partial T}{\partial t} = -\frac{\partial q_x}{\partial x} \qquad 4.2.1$$

$$\rho . Cp . \frac{\partial T}{\partial t} = k \frac{\partial^2 T}{\partial x^2} \qquad 4.2.2$$

$$\alpha \frac{\partial^2 T}{\partial x^2} = \frac{\partial T}{\partial t} \qquad 4.2.3$$

A network of grid points at different time levels, as shown in figure 36, needs to be established when using finite difference technique (FDT) to solve partial differential equations (PDE) given above in association with the initial and boundary conditions derived in the previous section.

Approximation to temperature, to be computed by Finite difference method can be denoted by $T_{i,n}$ at a typical grid point (i,n). The partial derivatives of the original PDE are then replaced at interval grid points by suitable Finite difference approximations (FDA) involving Δx, Δt and $T_{i,n}$.

4.2.2 SPACE AND DERIVATIVE APPROXIMATIONS

Approximations for a first order derivative, $\frac{\partial T}{\partial x}$, for a network of grid points are shown in figure 37, at mid-way points $(i-\frac{1}{2},n)$ and $(i+\frac{1}{2},n)$ of elements of thickness Δx.

$$\left(\frac{\partial T}{\partial x}\right)_{i-\frac{1}{2},n} = \frac{T_{i,n} - T_{i-1,n}}{\Delta x} \qquad 4.2.4$$

$$\left(\frac{\partial T}{\partial x}\right)_{i+\frac{1}{2},n} = \frac{T_{i+i,n} - T_{i\ \ ,n}}{\Delta x} \qquad 4.2.5$$

Second order derivative, $\frac{\partial^2 T}{\partial x^2}$ at grid point (i,n) can be written as follows

$$\left(\frac{\partial^2 T}{\partial x^2}\right)_{i,n} = \left[\frac{\partial}{\partial x}\left(\frac{\partial T}{\partial x}\right)\right]_{i,n}$$

$$\left(\frac{\partial^2 T}{\partial x^2}\right)_{i,n} = \frac{1}{\Delta x}\left[\left(\frac{\partial T}{\partial x}\right)_{i+\frac{1}{2},n} - \left(\frac{\partial T}{\partial x}\right)_{i-\frac{1}{2},n}\right]$$

Hence FDA for second order derivative employing equations 4.2.4 and 4.2.5 can be written as

$$\left(\frac{\partial^2 T}{\partial x^2}\right)_{i,n} = \frac{T_{i-1,n} - 2T_{i,n} + T_{i+1,n}}{(\Delta x)^2} \qquad 4.2.6$$

The FDA of second order derivative, $\frac{\partial^2 T}{\partial x^2}$ can also be derived using Taylor's series. This derivation is pertinent because of its use later when incorporating boundary conditions.

Assuming $\frac{\partial T}{\partial x} = T_x$ and $\frac{\partial^2 T}{\partial x^2} = T_{xx}$

$T_{i+1,n}$ and $T_{i-1,n}$ can then be expanded about $T_{i,n}$ as follows:

$$T_{i+1,n} = T_{i,n} + \Delta x\, T_x + \frac{(\Delta x)^2}{2!} T_{xx} + \frac{(\Delta x)^3}{3!} T_{xxx} + \frac{(\Delta x)^4}{4!} T_{xxxx} \qquad 4.2.7$$

$$T_{i-1,n} = T_{i,n} - \Delta x T_x + \frac{(\Delta x)^2}{2!} T_{xx} - \frac{(\Delta x)^3}{3!} T_{xxx} + \frac{(\Delta x)^4}{4!} T_{xxxx} \qquad 4.2.8$$

Adding equations 4.2.7 and 4.2.8 and rearranging

$$\left(\frac{\partial^2 T}{\partial x^2}\right)_{i,n} = T_{xx} = \frac{T_{i-1,n} - 2T_{i,n} + T_{i+1,n}}{(\Delta x)^2} - \frac{(\Delta x)^2}{12} T_{xxxx}$$

Δx, being made smaller than the last term of the above equation can be neglected and it then becomes equation 4.2.6.

$$\left(\frac{\partial^2 T}{\partial x^2}\right)_{i,n} = \frac{T_{i-1,n} - 2T_{i,n} + T_{i+1,n}}{(\Delta x)^2} + O\left[(\Delta x)^2\right] \qquad 4.2.9$$

where $O\left[(\Delta x)^2\right]$ is the order of the term neglected. FDA's for the first order derivative, $\frac{\partial T}{\partial x}$ can be obtained by subtracting equation 4.2.8 from equation 4.2.7 or by rearranging

$$\left(\frac{\partial T}{\partial x}\right)_{i,n} = \frac{T_{i+1,n} - T_{i,n}}{\Delta x} + O(\Delta x) \qquad 4.2.10$$

$$\left(\frac{\partial T}{\partial x}\right)_{i,n} = \frac{T_{i+1,n} - T_{i-1,n}}{\Delta x} + O\ (\Delta x)^2 \qquad 4.2.11$$

$$\left(\frac{\partial T}{\partial x}\right)_{i,n} = \frac{T_{i,n} - T_{i-1,n}}{\Delta x} + O(\Delta x) \qquad 4.2.12$$

These forms are known as Forward, Central and Backward FDA's respectively. The equation 4.2.11 with higher order form is preferred because of its greater accuracy.

$T_{i,n}$ is the temperature at grid position,i, and time level n. In order to predict $T_{i,n+1}$, the temperature at the same grid position but next time level, n+1, it is required to replace the thermal energy balance given in equation 4.2.3 by a simple FDA at grid point (i,n).

FDA of the second order derivative $\frac{\partial^2 T}{\partial x^2}$ is already known as shown in equation 4.2.6 or 4.2.9 i.e.

$$\alpha \left(\frac{\partial^2 T}{\partial x^2}\right) = \frac{\partial T}{\partial t} \qquad 4.2.3$$

$$\frac{\partial^2 T}{\partial x^2} = \frac{T_{i-1,n} - 2T_{i,n} + T_{i+1,n}}{(\Delta x)^2} \qquad 4.2.6$$

Derivative $\frac{\partial T}{\partial t}$ can be written as

$$\frac{\partial T}{\partial t} = \frac{T_{i,n+1} - T_{i,n}}{\Delta t} \qquad 4.2.13$$

By substituting equations 4.2.6 and 4.2.13 into the equation 4.2.3 it follows that

$$\alpha \frac{(T_{i-1,n} - 2T_{i,n} + T_{i+1,n})}{(\Delta x)^2} = \frac{T_{i,n+1} - T_{i,n}}{\Delta t}$$

replacing $\frac{\alpha \Delta t}{(\Delta x)^2}$ by F_o and with $T_{i,n+1}$ being the only unknown and with all temperatures at grid position at time level 'n' assumed to be known, the above equation can be written as

$$T_{i,n+1} = F_o(T_{i-1,n} - 2T_{i,n} + T_{i+1,n}) + T_{i,n}$$

Further simplification gives

$$T_{i,n+1} = F_o(T_{i-1,n}+T_{i+1,n})+T_{i,n}(1-2F_o) \qquad 4.2.14$$

Since all temperatures at time level n are known, $T_{i,n+1}$ can be calculated and this process is repeated over successive time steps given the temperature at all grid point as time progresses.

4.2.3 FDA FOR THE BOUNDARIES

a) Metal Sand Interface

Figure 38 shows the vertical interface between Metal and Sand, i being the grid position of the interface. Temperatures T_{i-1} and T_{i+1} can be expanded about the interfacial temperature, T_i employing Taylor's series.

$$T_{i-1} = T_i - \Delta x\ T_{xs} + \frac{(\Delta x)^2}{2!}\ T_{xxs} \qquad 4.2.15$$

$$T_{i+1} = T_i + \Delta x\ T_{xm} + \frac{(\Delta x)^2}{2!}\ T_{xxm} \qquad 4.2.16$$

where $T_{xs} = \frac{\partial T}{\partial x}$ in sand at point i

and $T_{xm} = \frac{\partial T}{\partial x}$ in metal at point i

Equations 4.2.15 and 4.2.16 can be rewritten as follows

$$T_{xxs} = \frac{2}{(\Delta x)^2}\ (T_{i-1} - T_i + \Delta x\ T_{xs}) \qquad 4.2.17$$

$$T_{xxm} = \frac{2}{(\Delta x)^2}\ (T_{i+1} - T_i - \Delta x\ T_{xm}) \qquad 4.2.18$$

Substituting the above two equations individually in the thermal energy balance i.e. equation 4.2.3 gives the following equations :

$$\frac{2}{(\Delta x)^2}\ (T_{i-1} - T_i + \Delta x\ T_{xs}) = \frac{1}{\alpha_s}\ \frac{\partial T}{\partial t} \qquad 4.2.19$$

In Metal (M)

$$\frac{2}{(\Delta x)^2}\ (T_{i+1} - T_i - x\ T_{xm}) = \frac{1}{\alpha_m}\ \frac{\partial T}{\partial t} \qquad 4.2.20$$

From Fourier's law, according to continuity of heat flux at interface, it has been already deduced that

$$k_s\ (\frac{\partial T}{\partial x})_s = k_m\ (\frac{\partial T}{\partial x})_m \qquad 4.1.5$$

Hence equation 4.2.19 can be rewritten as

$$T_{i-1} - T_i + \Delta_x\ T_{xs} = \frac{(\Delta x)^2}{2\alpha_s}\ \frac{\partial T}{\partial t}$$

and further simplifying gives and multiplying by Δx

$$k_s\ T_{xs} = \frac{k_s T_i}{\Delta x} - \frac{k_s T_{i-1}}{\Delta x} + \Delta x\ \frac{k_s}{2\alpha_s}\ \frac{\partial T}{\partial t} \qquad 4.2.21$$

Similarily equation 4.2.20 can be rewritten as follows

$$k_m\ T_{xm} = \frac{-k_m T_i}{\Delta x} + \frac{k_m T_{i+1}}{\Delta x} - \Delta x \cdot \frac{k_m}{2\alpha_m}\ \frac{\partial T}{\partial t} \qquad 4.2.22$$

It has already been pointed out that T_{xs} and T_{xm} are first order derivative symbols. Hence equations 4.2.21 and 4.2.22 can be equated on basis of equation 4.1.5

$$\frac{k_s T_i}{\Delta x} - \frac{k_s T_{i-1}}{\Delta x} + \frac{\Delta x k_s}{2\alpha_s}\ \frac{\partial T}{\partial t} = \frac{-k_m T_i}{\Delta x} + \frac{k_m T_{i+1}}{\Delta x} - \frac{\Delta x k_m}{2\alpha_m}\ \frac{\partial T}{\partial t}$$

Simplifying the above equation and dividing it throughout by $\frac{k_s + k_m}{(\Delta x)^2}$ and simplifying it further gives

$$\frac{\partial T}{\partial t} \cdot \frac{(\Delta x)^2}{(k_s + k_m)} \left\{ \frac{k_s}{\alpha_s} + \frac{k_m}{\alpha_m} \right\} = \frac{2 \cdot k_s\ T_{i-1}}{k_s + k_m} - 2T_i + \frac{2k_m\ T_{i+1}}{k_s + k_m} \qquad 4.2.23$$

and if $z = \frac{(\Delta x)^2}{\Delta t(k_s+k_m)} \left(\frac{k_s}{\alpha_s} + \frac{k_m}{\alpha_m}\right)$ 4.2.24

Equation 4.2.23 can be rewritten as

$$\left(\frac{\partial T}{\partial t}\right).\Delta t.z = \frac{2.k_s}{k_s+k_m} \cdot T_{i-1} - 2T_i + \frac{2k_m}{k_s+k_m} \cdot T_{i+1} \qquad 4.2.25$$

Derivative $\frac{\partial T}{\partial t}$ can be replaced in the above equation by $\frac{T_{i,n+1}-T_{i,n}}{\Delta t}$ as in equation 4.2.13, with all temperatures being at time level 'n'.

Equation 4.2.25 can be rewritten as

$$T_{i,n+1} = \frac{1}{z}\left[\left(\frac{2k_s}{k_s+k_m}\right) T_{i-1,n} - T_{i,n}(2-z) + \left(\frac{2k_m}{k_s+k_m}\right)T_{i+1,n}\right] \qquad 4.2.26$$

where $z = \frac{(\Delta x)^2}{\Delta t(k_s+k_m)} \left[\frac{k_s}{\alpha_s} + \frac{k_m}{\alpha_m}\right]$ 4.2.24

b) Sand Air Interface

Equation 4.1.11 and figure 35 represent a Sand-Air interface which is depicted as convective boundary condition (transient).

$$\rho.C_p.V_o \frac{\Delta T_o}{\Delta t} = \frac{k_s}{\Delta x}(T_i - T_o) + h(T_a - T_o) \qquad 4.1.11$$

Small time intervals can be represented as

$$\Delta T_o = T_{o,n+1} - T_{o,n}$$

$V_o = \frac{\Delta x}{2}$ assuming the heat flow to be unidemensional, equation 4.1.11 can be rewritten as follows

$$\rho.C_p.V_o\left(\frac{T_{o,n+1}-T_{o,n}}{\Delta t}\right) = \frac{k_s(T_i - T_{o,n})}{\Delta x} + h(T_a - T_{o,n})$$

The above equation can be rewritten as

$$T_{o,n+1} = 2F_o(T_i - T_{o,n}) + \frac{2h.F_o.\Delta x}{k_s}(T_a - T_{o,n}) + T_{o,n} \qquad 4.2.27$$

where $$F_o = \frac{\alpha_s \Delta t}{(\Delta x)^2} \qquad 4.2.28$$

and $$\alpha_s = \frac{k_s}{\rho . C_p}$$

Equation 4.2.28 can be further simplified into the form

$$T_{o,n+1} = 2F_o \left[T_i + B_i . T_a + T_{o,n} \left(\frac{1}{2F_o} - 1 - B_i \right) \right] \qquad 4.2.29$$

where Biots number $$B_i = \frac{h.\Delta x}{k_s} \qquad 4.2.30$$

4.2.4 CONVERGENCE, CONSISTENCY AND STABILITY

Convergence means that the computed Finite Difference Approximations approach the exact solution of the corresponding Partial differential equation (equation 4.1.4) as increments Δx and Δt, are made small. If F_o is greater than 0.5 (which can readily occur if Δt is not taken small enough), it can also be shown that the convergence does not generally occur for the method. Thus, if F_o is greater than 0.5, the temperatures can be computed which have no physical reality. Lack of convergence is always to be avoided.

The difference between the finite difference approximation and exact solution of the partial differential equation at any point in the grid is known as Local discretization error 'w'.

$$w = T_{exact} - T_{computed}$$

Thus, the convergence implies that w approaches zero as Δt and Δx approach zero. For the method described it can be shown that

$$w = 0\left[\Delta t + (\Delta x)^2\right]$$

'0' designates 'order of'.

Stability and Consistency are two other concepts closely associated with the convergence of a particular finite difference method. Stability means that the solution, at a given time t, is bounded (i.e. does not tend to infinity) as Δt (and hence Δx, for a given value for F_o) tends to zero. However, stability alone does not necessarily mean that discretization error will be small. The finite difference method described in previous pages will be stable if F_o is less than 0.5

Consistency, essentially means that the finite difference method has made a suitable approximation of the derivatives involved. For example that

$$\alpha\left(\frac{\partial^2 T}{\partial x^2}\right) = \frac{T_{i,n+1} - T_{i,n}}{\Delta t} \qquad 4.2.31$$

is a good approximation of the equation

$$\alpha\left(\frac{\partial^2 T}{\partial x^2}\right) = \frac{\partial T}{\partial t} \qquad 4.2.32$$

The truncation error of an approximation is defined as the difference between the finite differences and the derivatives they are to represent. With the aid of Taylor's expansion it can be shown that truncation error for equation 4.2.31 and 4.2.32 is $0(\Delta t+(\Delta x)^2)$. Since

this error tends to zero as Δt and Δx tend to zero the finite difference approximation is consistent with the original Partial differential equation.

4.3 MATERIAL PROPERTIES

Thermal properties of the alloy and moulding sand are the most critical inputs in any mathematical modelling of solidification process. Data, however, at elevated temperature is scarce and often conflicting. For moulding sand, the variance in reported properties is greater than for the steels[121]. The thermal properties of materials involved are taken to be functions of temperature, a necessity in any realistic simulation of heat flow in real materials over wide range of temperatures.

Pehlke et al[121] established relationships between the thermal properties of Steel and moulding sand using the reported values in the literature.[138-153] They assumed a linear relationship between the thermal properties of steel and temperature. This assumption was made in view of two considerations. First, the computation of thermal properties must be made at every spatial grid point in the casting and mould for every step of simulation. As this may involve many separate determinations of thermal properties for a long simulation with small time steps, the computing time saved by evaluating a linear equation instead of more complicated form is significant. Secondly, definite trends are apparent in the data for steel and a series of linear segments adequately represents them.

a) Thermal Conductivity of Steel[121,138-140]

The thermal conductivity of low carbon steel was represented by four linear segments. The mushy zone conductivity was assumed to drop linearly from its value at solidus to the liquidus value, an average value being used over this temperature range. Liquid steel was assumed to have a constant thermal conductivity but, however, Pehlke's relationship between thermal conductivity and temperature was modified for low alloy steel BW2 to take into different liquidus and solidus temperatures. The relationship used is shown in Figure 39.

b) Specific heat of metal[121,139,143-146]

The specific heat for liquid steel was assumed to be constant. Latent heat of fusion was accounted for over the freezing range i.e. from Solidus(T_s) to liquidus temperature (T_l), by the following relationship[121]

$$H_{fusion} = \int_{T_s}^{T_l} (C_p^* - C_p)dT$$

where C_p^* represented an approximately large value of specific heat in freezing range.

The relationship of Pehlke[121] was modified to account for different Liquidus and Solidus temperatures of low alloy steel BW2 and is shown in Figure 40. The inset shows the latent heat of fusion with area under the triangle and above the base line C_p being numerically equal to latent heat of fusion.

c) Thermal conductivity of Sand.[121,139,140,147-151]

Original data reported in the literature was scattered and did not allow linear correlation to be used. However, Pehlke et al[121] performed polynominal regression to four best quadratic curve fits based on least square criterion. No modification was made to Pehlke's relationship but it is important to note that Pehlke et al[121] were not using the CO_2 moulding process. The relationships are those as shown in figure 41.

d) Specific heat of Sand[121,152,153]

Pehlke et al[121] fitted a curve to the data existing in the literature, no mathematical relationship being given. However, a polynominal relationship was computed from the values read off the graph. The relationship is shown in figure 42 and no modification was considered necessary.

e) Density and Thermal diffusitivity

Density of moulding sand was taken as 1600 kg/m^3, this value being recommended by Steel Casting Research and Trade Association (SCRATA) Sheffield. The density of Steel was selected at 7850 kg/m^3.[154]

The thermal diffusitivity was calculated by the following relationship for both sand and metal.

$$\alpha = \frac{k}{e.c_p}$$

f) Heat transfer coefficient

The heat transfer at the sand-air interface was that

by natural convection, the fluid being air at atmospheric pressure. A simplified expression quoted in literature[155-158] for heat transfer coefficient is

$$h = A\left(\frac{\Delta T}{L}\right)^{b} \qquad 4.3.1$$

where A and b are constants, depending on geometry and flow conditions, and L is the significant length, also a function of geometry and flow. ΔT is the temperature difference between surface and air. Mcadams[155] recommended the value of A to be 0.29 and 0.27 for a plane surface depending if it is vertical or horizontal. 0.25 was the recommended value for the 'b'. Values of h in the above equation have dimensions in British thermal units and had to be converted into SI units.

4.4 MODEL

The theta ring is a complex configuration for computer simulation of solidification. Because the tie bar is one of the most critical variables in the investigation, it is useful to predict solidification times and temperature profiles in the tie bar commencing when the molten metal is poured in. Complications in predicting solidification times of tie bar along its length restricted the computer simulation to the direction of the width of the tie bar.

This approach was adopted because an attempt was made to simulate the solidification of ring and tie bar together in one dimension along axis XX as shown in figure 43. This had to be abandoned because the uni-directional nature of the model failed to extract heat from the sand in

between the ring and tie bar. To deal with this problem the model needed to be two dimensional, but this was too complex at this stage because of the need to include edges and curves of the ring.

The simulation of solidification process for a tie bar was carried out along the line TT as shown in Figure 43. A simplified version of the model is indicated by a slab of sand of definite thickness, as shown in Figure 44, with infinite length in x and y direction. In the middle of sand is the tie bar of thickness 'a'. The simulation of solidification process is based on the heat flow along the direction of the arrow i.e. through the thickness. Dimensions along other axes were assumed to be unity. Figure 45 shows the side view of the mould.

The outline of the computer model follows:

Initial values of temperature at time zero were assigned. In sand areas S1 and S2 the room temperature will be assigned to all grid points. Temperature at grid points N1 and N4 will also be sand ambient temperature. In the region M, the temperature assigned to grid points will be the pouring temperature of liquid metal. The interface grid points N2 and N3 temperature values are assigned on basis of equation.

$$T_{N2} = T_{N3} = T_{s\delta} + \frac{T_{po} - T_{so}}{1+\frac{k_s}{k_m}\sqrt{\frac{\alpha_m}{\alpha_s}}} \qquad 4.4.1$$

Assumptions in this model were:

i) At zero time, the metal-sand interface acquired the interfacial temperature as calculated using equation 4.4.1.

ii) The liquid metal is stagnant and its temperature is uniform as soon as the mould is filled.

iii) Mould is filled instantaneously with liquid metal at pouring temperature

iv) Thermal contact at the sand-metal interface was complete

v) Convective heat and mass transfer were neglected.

At time Δt, which is time level n+1 after pouring the computation begins from right hand side of the model shown in Figure 45. At the air-sand interface, the new temperature at N1 was calculated from equation 4.2.29, although this equation really becomes operative as temperature of sand increases with the passage of time. The new temperatures at all grid points within sand, S1, are calculated using equation 4.2.14 and temperature at previous time level 'n'. At the interface N2 the temperature at new time level is calculated using equation 4.2.26 and temperatures of previous time level 'n'. The new temperature within tie bar is also calculatedusing equation 4.2.14 and temperatures of previous time level 'n'. The interface N3, S2 sand area and interface N4 are treated exactly as interface N2, S1 sand area and interface N1 respectively. Once temperatures for all grid points in the mould have been calculated, these may be

printed out. These values then are saved for computation of temperatures at next time level n+2 as shown on right hand side of Figure 46. An efficient procedure is to replace temperature levels at previous time level by new temperatures at new time level and use these for calculation of temperatures at next time level and so on, as shown on left hand side of figure 46.

The thermal properties used at all grid points to calculate temperatures at new time level were calculated on the basis of temperatures at previous time levels.

VARIABLES EFFECTING THE RESULTS

Concepts of stability, consistency and discretization error have already been described in the section 4.2.4. It was established that the truncation error was of the order, $\Delta t+(\Delta x)^2$. This would require making the value of Δt and Δx smaller to make results more accurate. Another factor to be controlled is the Fourier's number, it should always be equal to or less than 0.5, otherwise model will go unstable producing nonsensical results. The Fourier number is equal to $\alpha.\Delta t/\Delta x$, and this would require Δt and Δx to alter in a definite relationship of 2:4. Figure 47 demonstrates the effect of Δx and Δt on the temperature profile. Δx was halved to 0.0005m from 0.001m to produce finer grid on the casting and mould. For stability reasons, Δt was reduced to 0.025 secs from original 0.1 secs. It may be suggested that minimum possible values of Δx and Δt should be selected. This may not be possible because as Δt time interval is reduced so the number of calculations is increased proportionally.

This means excessive computational times with diminishing returns. It was found that 0.0005m and 0.025 secs values of Δx and Δt were optimum.

SELECTION OF THERMAL CONDUCTIVITY OF SAND

Figure 41 gives four different functional relationships for thermal conductivity. Table 8 shows the temperature in the middle of a 25mm tie bar after approximately 15secs. It is evident that thermal conductivity (a) gives the highest heat extraction rates. This thermal conductivity was selected for all computations and is justified as the original model considers heat flow in one direction only.

A flow chart presenting the summary of the computer simulation of solidification process is shown in Figure 48.

5.0 EXPERIMENTAL AND COMPUTATIONAL RESULTS

This section presents the data obtained as a result of experimentation and computation as described in section 3.0 and 4.0 respectively. Initially the data obtained has been presented graphically and then treated in various ways to interpret the results.

5.1 THERMAL ANALYSIS

5.1.1 CASTING STAGE

Temperature profiles obtained from theta rings of varying tie bar width, when cast from around 1550°C are presented in Figure 49 to 54, thermocouples being located at the positions as shown in Figure 21. Liquidus and Solidus temperatures were experimentally determined, as indicated in section 3.4.1. Chemical analysis for each casting was carried out and are presented in Table 5. This analysis allowed calculation of equilibrium transformation temperatures Ac_3 and Ac_1 for each individual casting based on Andrews emprical formulae[159], the transformation temperatures being presented in Table 9. Using solidus and equilibrium transformation temperatures, the order was deduced, as shown in table 10,11,12, in which various positions of figure 21 solidify and transform within theta rings of varying tie bar widths.

The position number 4 i.e. the junction of the ring and the tie bar is the hot spot and was found to have the slowest cooling rate and hence solidify and transform last of all. Table 13,14 and 15 represent the temperature differences, between the position 4 and positions 1,2,3,5

and 6 of figure 21, when the hot spot solidifies completely followed by transformation i.e. from Ac_3 to Ac_1 respectively. These temperature differences between position 4 and position 1,2,3,5 and 6, respectively, at solidification and transformation stage were plotted versus tie bar widths. Using STATPAK, a statistical computer package, regression was carried out on all the temperature differences versus tie bar width data and best fit line computed for all the cases except for those where correlation was poor. Actual data and best fit lines for all temperature differences versus tie bar widths at solidification and transformation stages are shown in Figures 55 to 59.

Figure 60 presents the temperature profiles in the sand mould in approximate locations as shown in Figure 22. Thermocouples in the sand may have been slightly displaced from their intended location because of blind drilling.

5.1.2. HEAT TREATMENT STAGE

Cooling curves for theta rings of 10 and 30mm tie bar width which were fully annealed i.e. heated up to 950°C followed by furnace cooling are shown in figures 61 and 62. Figures 63 and 64 show the cooling curves for the theta rings of 10 and 30mm tie bar widths which were normalised i.e. heated up to 870°C followed by air cooling. Figure 65 and 66 present the cooling curves for theta rings of 10 and 30mm tie bar widths which were tempered i.e. heated up to 640°C followed by air cooling. The location of thermocouples for all treatments mentioned above are as

shown in Figure 23. Table 16 summarises the figures 61 to 66 in terms of cooling rates and temperature differences for theta rings of 10 and 30mm tie bar widths.

5.2 STRESS ANALYSIS

5.2.1 TREATMENT OF STRESS DATA

The principal stress data computed using equation 3.6.1 in section 3.6.1 for the centre hole drilling technique can be presented according to two conventions. The first convention defines σ_1 as the maximum principal stress and σ_2 as the minimum principal stress. This may be referred to as 'Maximum tensile stress' approach, because if both σ_1 and σ_2 are tensile then σ_1 will automatically be numerically greater (neglecting the sign) than σ_2 and hence become σ_{max} and σ_{min}. However, if both principal stresses are compressive and σ_2 is numerically greater than σ_1, then σ_1 according to maximum tensile criteria is greater than σ_2 because it is more tensile or less compressive. The second convention selects the numerically greatest principal stress.

It is well known that tensile residual stresses are more detrimental than the compressive residual stresses and hence it was decided to base the presentation of the detailed and summarised results using 'maximum tensile criteria.' For comparison, the summarised results are also presented according to 'numerically greatest stress' criteria.

between different parts or positions is the Von Mises Equivalent. This equivalent is based on Distortion Energy or Von Mises Theory, which gives a relationship between principal stresses σ_1, σ_2 and σ_3 (triaxial state of stress) and the yield strength in uniaxial tension, σ_{ys}. It is based on yielding occurring in an element subjected to triaxial stresses when the distortion energy is equal to that in an axially loaded element at the beginning of yielding. The mathematical statement of this theory is:

$$(\sigma_1 - \sigma_2)^2 + (\sigma_2 - \sigma_3)^2 + (\sigma_3 - \sigma_1)^2 = 2\sigma_{ys}^2$$

The above formula is modified to present Von Mises equivalent, σ_E

$$\sigma_E^2 = \sigma_1^2 + \sigma_2^2 - \sigma_1\sigma_2$$

This Von mises equivalent will also be used to compare residual stresses at different positions. Values of principal stresses σ_1 and σ_2 used were those obtained from Centre hole drilling technique as indicated in section 3.6.1.

5.2.2. MACHINING STRESSES

In section 3.6.2 machining strains induced due to Centre hole drilling technique in an annealed and as cast specimens were determined and found to be 31$\mu\epsilon$ and 68$\mu\epsilon$. These strain values were those obtained at the depth equal to hole diameter. In Figure 67 the complete data of strain values converted into stress values were plotted

Samples. Attempts were made to fit a curve to this data employing STATPAK AND CURFIT (computer programmes) but because of certain mathematical assumptions in the programmes these attempts were not successful.

Stress data was found to gradually increase over the hole depth non-linearly and then levelled out, this levelled out stress value being assumed to be the final stress value. All stress/hole data which are presented later followed a similar pattern and hence a best fitting curve was drawn ensuring that data was accurately represented, especially in the region where it levels out.

Figure 67 presents best fitted curves for the stress versus hole depth for annealed and as cast specimens.

5.2.3 RUNNER STRESS AND ITS EFFECT

The S shape design of the runner was selected in particular to minimise the effect of the runner on the stress distribution within the theta ring.

Residual stress was determined in the runner which was then sectioned according to procedure in section 3.5. Simultaneously the residual stress was determined in the theta ring before and after runner removal, as described in section 3.6.4.

The runner after sectioning was found to shift both in X and Y directions as shown in Figure 24. The experimental arrangement only allowed measurement of shift in Y direction and this is presented in Figure 68. Correlation

STATPAK programme and a best fit line was computed using least square regression analysis, this best fit line being superimposed on the data.

Residual stress in the runner is presented in the Figure 69. The residual stress in the theta ring at position 3 and 5 before and after the runner sectioning is also shown in Figure 69.

5.2.4 CASTING STRESSES

Stress analysis was carried out on Theta rings with tie bar widths 5,10,15,20,25 and 30mm at the positions as presented in Figure 21. The residual stress versus hole depth with best curve fitted, using method described in section 5.2.2 for all positions in each theta ring with each tie bar width is presented in Figures 70 to 75.

Data is also presented according to position in the theta rings. Residual stress versus hole depth for each position at which residual stress was determined, as shown in Figure 21, was compared with varying tie bar width and is shown in Figure 76 to 80.

Final residual stress values obtained at hole depth equal to hole diameter for each individual position were plotted versus tie bar widths of theta rings as presented in Figure 81 to 85. In order to study the effect of tie bar width on the residual stress level, correlation tests were run using STATPAK computer programme and best fit line using linear regression analysis was computed for

each case and was superimposed on actual data.

The best fitting lines for all positions, which represented variation of residual stress with tie bar width were superimposed on the same scale of residual stresses presented in Figure 86. This procedure facilitated further comparison of residual stress with respect to tie bar width.

The residual stresses in tie bar of the theta rings were also determined using the technique described in section 3.7. Expansion occurred in the tie bar lengths of all theta rings and the expansion variations with tie bar widths of theta rings are shown in Figure 87. The STATPAK computer programme was again used to test for correlation and compute a best fit line using least square regression analysis, this line also being presented in Figure 87. The stresses in tie bar of theta rings were calculated using equations in section 3.7, the residual stress values being presented in Table 17. No correlation was found between the residual stress in the tie bars of the theta rings and their widths using the STATPAK computer programme.

5.2.5 HEAT TREATMENT STRESSES

Stress analysis was carried out on Theta rings of tie bar width 10mm and 30mm as presented in Figure 23. Figures 88 to 93 show the residual stress versus hole depth with best curve fitted, using the method described in section 5.2.2 for all positions in theta rings after annealing, normalizing and tempering heat treatments.

The same data has been presented according to position in the theta rings. Residual stress versus hole depth for each position at which residual stress was determined, as shown in Figure 23, has been compared for different heat treatments and presented in Figure 94 to 97. Superimposed in the same figures are the residual stress versus hole depth curves for the Casting stage in order to facilitate further comparison.

Figure 98 to 100 compare Casting and Heat Treatment stresses for Theta rings of 10 and 30mm tie bar widths for position 1, 5 and others as shown in Figure 21 and 23.

Finally, as discussed in section 5.2.1, residual stresses are tabulated according to Numerically greatest principal stress (neglecting the sign) in Table 18. Residual stresses at position 1,2,3,4 and 5 in the theta ring were correlated to the tie bar width and best fit line were computed and are presented in Figure 101.

Von Mises equivalent has also been calculated and presented for all the residual stress measurements made and has been presented in Table 19.

Correlation tests were run for Von mises equivalents of different positions of all theta rings and their tie bar widths. Best fit lines were computed using Linear regression analysis in STATPAK and are presented in Figure 102.

5.3.1 METALLOGRAPHIC EXAMINATION

Hardness was measured in the tie bar as described in section 3.8. Figure 103 presents the Hardness data correlated to the tie bar width, hardness being measured at the centre of the tie bar. Figure 104 shows micro-hardness data, hardness measurements being taken in the decarburized layer and in the centre of tie bar thickness/ width. Data was subjected to correlation tests and best fit lines were computed and drawn.

Plates 2 to 5 present the microstructure of the tie bar in as cast conditions and Plates 6 and 7 present heat treated tie bar microstructure.

5.3.2 EPOXY RESIN MODEL

This model was viewed in polarized light in as cast condition to examine for any stress distribution. However, no residual stresses were found to exist in as cast epoxy resin model.

5.4 COMPUTATIONAL RESULTS

Experimentally obtained solidus and liquidus temperatures 1468°C and 1382°C were guide lines for the complete solidification of the tie bar computational model described in section 4. Also of interest were the temperature gradients within the model. Figure 105 presents the gradients when the centre of the tie bar reaches the Liquidus temperature, times required to reach this temperature also being presented. The tie bar centre is last

to solidify, i.e. cross solidus temperature and table 20 presents the temperature in the tie bar model when the centre of the tie bar approaches or crosses the solidus temperature. Table 21 presents the time required by the tie bar model to completely solidify i.e. solidification times for tie bars. Times for the various tie bar widths to cross liquidus temperature and completely solidify were also plotted and are presented versus tie bar widths in Figure 106.

Finally, Table 22 presents property data for BW2 steel as provided by Steel Casting Research and Trade Association to facilitate comparison and discussion.

6.1 RESIDUAL STRESS MEASUREMENT TECHNIQUE

Currently available residual stress measuring techniques are strictly speaking destructive because it is necessary to remove surface layers of metal where the measurement is made. The X-ray technique used for determining surface stresses may initially be considered non destructive but becomesdestructive when employed for stress against depth determination. The technique is also considered lengthy and tedious compared with the Centre hole drilling technique which overcomes these disadvantages. In the latter method the destructiveness is minimised by the availability of miniature strain gauges which further reduce the size of hole to 0.8mm compared to 1.5875mm hole produced in this work. A complete residual stress measurement can be completed in under 30 minutes using Centre hole drilling. technique.

The Centre hole drilling technique is considered a very useful and practical technique which can be easily adapted to measurement in an industrial situation. The technique measures surface stresses expressed as the average stress in the depth of the hole drilled. This work relates to these surface stresses. However, strain data may be subjected to an incremental analysis to derive a relationship of stress variation with depth over the hole depth. This latter analysis has a limited accuracy in the absence of insufficient calibrations in experimentally applied stress fields[90]. This makes analysis qualitative and not applicable to the present study.

As established in this study, control must be exercised over the surface preparation technique and induced machining strains, both of which are functions of the nature of the surface on which the strain gauge is bonded and the process history of the surface. Current practice of accounting for induced machining stresses based on annealed specimen is incorrect when determining residual stresses in cast components. Experience showed that Cast steel theta rings were more difficult to drill than the heat treated rings. It was also established that machining strains for Cast and annealed specimens are different and incorporating these values in calculations of casting and heat treatment stresses has given a more realistic comparison of these two processes. It was confirmed that the predicted data of residual stress direction, as discussed in section 2.6.1 (h), obtained from this technique was highly unreliable and had to be ignored. This however does not invalidate the technique which is being further investigated and developed to allow it to become an almost non-destructive testing tool.

6.2 GENERATION OF RESIDUAL STRESSES IN CAST THETA RINGS

Temperature differentials and phase transformations were described as major contributing factors to the occurence of residual stresses with other contributions from mould resistance. It has been possible to isolate the individual and combined effect of these factors in the casting and heat treatment processes.

has isolated the temperature differential effect whereas normalizing has combined it with phase transformation. However, for the full annealing treatment there was no evidence of a differential cooling effect, the whole theta ring appearing to transform simultaneously. In the casting stage all three factors combine to contribute to the occurence of residual stress. The only indication of mould behaviour can be obtained from the temperatures attained in the vicinity of the theta ring, in the mould.

The strength of the moulding sand trapped within the tie bar, ring and runner will increase after the ring has cooled down to room temperature. Moulding sand strength will increase as tie bar width is increased because the volume of molten metal increases and subsequent heat flow from sand is reduced. It is apparent from temperature data of sand that sand surrounding the ring does not reach very high temperatures. However, the strength of CO_2 sand is reported to drop sharply at high temperatures above 700°C.[39] The high temperatures ranging from 500 to 875°C within the sand were reached within 5 to 10 minutes of the pouring at about 15mm from the metal/sand interface as shown in figure 60. After the same period (5 minutes) temperatures within theta rings with 30, 25 and 20mm tie bar widths range from 960°C to 1200°C (hot spot was at about 1200 and the rest towards the lower end of this range) as shown in figure 49, 50 and 51. In case of theta rings with 15, 10 and 5mm tie bar widths, the temperature within

ring (except hot spot) range between 900 to 1100°C as shown in figure 52, 53 and 54. Temperature of the tie bar after 5 minutes reduces from 780°C to 500°C as the tie bar width is reduced. After 1 hour the temperature in some areas of sand within theta ring ranged from 500°C to 650°C, the temperature distribution within all theta ring sizes ranging from 450°C to 630°C.

These sand temperature distributions observed led to conclusion that the mould hindrance to the ring will be non-uniform because in some areas sand strength will be negligible and as different parts of mould will have various temperatures and strengths. In addition, any resistance offered in the initial stages of the casting will be overcome by plastic deformation. After about one hour the sand in the area enclosed between the ring and tie bar section will have regained its strength (increased in some cases) due to drop in its temperature and will offer increased hindrance. This effect will be additional to the effects of hot deformation of some sand adjacent to the metal[39].

The contributing factor of phase transformations also co-exists with increasing mould hindrance as the casting cools down. This factor is accentuated by the fact that different regions in the theta ring transform at various times, this being supported by the evidence of temperature differentials existing in the theta rings as shown in Tables 14 and 15.

Temperature differentials make a significant contribution to the generation of residual stresses. These temperature differentials relative to the junction of the tie bar and ring increased with the reduced tie bar width as shown in Table 13 and figures 55 to 59. They do not necessarily contribute to the occurence of the residual stresses in the theta ring at high temperatures although they do increase the probabilities of Hot tearing due to strain concentration as discussed in section 2.3.1. near the junction of tie bar and ring. However, no hot tearing was evident, which suggests that negligible hindrance was offered by the mould in the region of hot spot.

The temperature differentials in the ring section of cast theta ring ranged from 30°C to 190°C relative to the hot spot, junction of ring and tie bar, when eutectoid transformation occurred. In the tie bars the temperature differentials between middle of tie bar and hot spot varied from 18 to 280°C, increasing with the decreasing tie bar width. This evidence shown in figures 55 to 59 indicate the significant contribution of the temperature differentials. Since these differentials were calculated at instances when the hot spot transforms at calculated transformation temperature, this also provides evidence that phase transformation occuring at different times at different positions also contributed significantly to the occurence of residual stresses.

Casting stresses shown in figures 70 to 75 and table 18 were compressive in the theta ring section with 30mm tie bar, these stresses becoming less compressive (tensile in some cases) as the tie bar width was decreased. This decrement in compressiveness increased as the distance from hot spot along the ring increased, lowest stress being at the hot spot. These stresses were correlated and correlation coefficients ranged from 0.75 to 0.9 (1.0 indicating highest degree of correlation) except in case of hot spot and tie bar where it was 0.35 and 0.42 respectively as shown in Figure 86.

The tie bar sectioning technique showed that tensile stress was present in the tie bars of all theta rings investigated. Length of the tie bar increased upon sectioning, the changes in length (shifts) increasing with increase in tie bar width and giving a correlation coefficient of 0.7. However, when these shifts were converted into stresses, no correlation was found with varying tie bar width, as shown in figure 87 and table 17.

The results presented suggest that there is a variation of residual stress in the theta ring. Before providing an explanation it is relevant to present an idealized mechanism of residual stress formation of a theta ring similar to one presented in section 2.3.2. There are two extreme cases of theta rings

a) Theta ring with a thick bar, in this case the ring solidifies first - followed by the tie bar and finally the hot spot at the junction between the ring and

tie bar. As the casting cools into the plastic region any differential contraction is readily accommodated by plastic strain. On further cooling ring behaves elastically and on further contraction subjects the tie bar to compression which is still plastic producing permanent deformation. As the tie bar becomes elastic it encounters a restraint from the ring. This leads to residual compressive stresses in ring and tension in the tie bar.

b) Theta ring with a thin tie bar, in this case the tie bar is the first to solidify and transform cooling faster than the ring. As the casting cools into plastic region any differential contraction is readily accommodated by plastic strain. On further cooling it acquires elastic behaviour and on further contraction places the ring in diametrical compression. As the ring becomes elastic and contracts it encounters a restraint from the tie bar. This leads to compression in tie bar and diametrical tension in the ring.

The two cases considered are idealized but the increase in expansion of tie bar length upon sectioning with increase in tie bar width suggests a mechanisms similar to ones given above. Idealized contraction was not obtained for the 5mm tie bar but there was a much reduced expansion compared to 30mm theta ring, expansions of other theta rings lying in between these extremes. The most likely explanation for

this is the reheating or retarded cooling of tie bar which makes it act like a thicker tie bar. This also means that residual compressive stresses are to be expected in the ring and reduced tie bar widths may not always produce tensile stresses due to reduced shifts upon sectioning the tie bar.

The residual stress distribution in the ring should not be expected to be uniform along the ring, this is attributed to the fact that tie bar exerts force along one specific diameter and this effect should be maximum at the junction and minimum at the point furthest from the junction. The results presented confirm that stresses get less compressive as distance from junction increases.

A further observation concerns the scatter of actual residual stress values about the best fit lines. This scatter is maximum for tie bar, junction and at the position (on ring) furthest from the junction near the sprue as shown in figures 85, 81 and 83. This is attributable to the influence of runner, sprue and risers which lie adjacent to and reduce heat flow from these positions. The positions away from sprue and that lying in the other half of the ring have low scatter as shown in figure 82 and 84. This invariably suggests that in the positions with low scatter factors responsible for generation of residual stresses operate without any effect from external influences.

It is apparent from the data presented that temperature differentials are the most significant factor determining the generation of residual stresses in the theta ring with thinnest tie bar. Faster cooling of tie bar may not allow enough time for mould hindrance and phase transformations to contribute initially. However, cooling retarded by low temperature and mould heating will make residual stress distribution less predictable. As tie bar thickness is increased the effect of the three factors contributing to generation of residual stresses will overlap with a complex mechanism since phase transformations and temperature differentials act simultaneously and producing opposite forms of stresses.

It is not clear why residual stresses measured in the region of junction of tie bar and ring and the centre of tie bar do not follow a simple pattern, and the results for centre hole drilling are different from tie bar sectioning results. However, the following explanations highlight the complexity of the reasoning. The junction lies underneath the feeding head which is significant mass of metal (different for each casting) cooling very slowly in relation to the junction but no doubt may have radial and longitudinal residual stress distribution due to its differential cooling rate in both directions. The effect of these residual stresses is difficult to predict in localised terms as demonstrated by experimental determination of the residual stresses in the region. Similarly, the tie bar residual stresses measured by centre hole drilling

technique are surface stresses averaged over the depth. The cooling of tie bar will be of complex nature, a temperature difference existing through the thickness leading to differential phase transformations. It was not possible to quantify these effects but these will have had an accummulative effect so as to distort the original trend in residual stress initially anticipated with respect to tie bar width variable.

The significance of decarburization of the casting surface was also examined. Decarburized layers were measured microscopically on all the tie bars and were found not to exceed 0.4mm. However, this layer was removed while preparing the surface for installation of the strain gauge and hence its effect is not reflected in the residual stress values obtained. Residual stresses will also be generated along the thickness of the tie bar and the ring, results indicating that stresses are generally compressive in the ring and tie bar. Faster cooling of the surface of the theta ring tends to leave a state of surface compressive stress whereas its interior is in tension according to mechanism outlined in section 2.3. Stress data obtained from Centre hole drilling technique gives evidence of the former and tie bar sectioning for the latter. This mechanism is true for all the theta rings of various tie bar widths, but it is important to appreciate that this mechanism and the mechanism generating residual stresses due to interaction of ring and tie bar complement each other to produce a complex interaction.

Therefore a detailed analysis of the residual stress distribution in the theta rings is not possible.

6.3 EFFECT OF RUNNER ON RESIDUAL STRESS DISTRIBUTION IN THE THETA RING

The Runner was found to have a tensile residual stress of about 21MN/m^2, as shown in figure 69 and the residual stresses in ring were compressive. The residual stress became less compressive by about 67MN/m^2 in the tie bar and its junction with the ring, upon runner removal. It can be suggested that the runner cools rather slowly due to the heating up of the mould in the region due to cooling of the theta ring plus the fact that molten metal running through the runner may already have heated the region as discussed in section 2.3.2. This results in slow cooling of the runner behaving as a thick bar in relation to the ring. Spring back effect in the runner was found when it was sectioned in case of all the theta rings and the shift was found to increase with decrease in tie bar width as shown in figure 68. This does demonstrate effect of tie bar on the theta ring and runner. The runner will produce tensile stresses in the theta ring of thinner tie bar and these become more tensile upon its removal as determined experimentally. The significance of the runner system in terms of residual stress is therefore that it may contribute to distortion before or after runner removal, although the runner may be designed to minimise these effects.

The Epoxy resin model was uniformly cooled at a very slow rate and it exhibited no evidence of residual stresses confirming that uniform slow cooling of a casting tends to eradicate the problem of residual stresses. It may not, however, be possible to obtain uniform cooling of a casting because it may lead to problems such as porosity, shrinkage etc. which are often overcome by employing the principles of directional solidification. Hence objectives of directional solidification to minimise casting defects and uniform cooling to minimise residual stress may be contradictory and a balance needs to be created. A preheated mould may not be desirable in this respect and, although the pouring and cooling of the mould may achieve this objective, this method may have some practical and economic limitations. Variations of casting stripping temperature may also be considered, a high temperature knockout perhaps resulting in reduction of residual stress due to absence of mould hindrance; but this will also increase cooling rates leading to increase in temperature differentials and larger residual stresses. This situation can be corrected by furnace cooling but practical problems of handling casting in plastic state make this option prohibitive.

6.4 A COMMENT ON TIE BAR SECTIONING TECHNIQUE

The trend in shifts upon sectioning tie bar were in good agreement with that obtained by Chijiiwa for Theta rings in CO_2 mould. However, lack of similar correlation

of tie bar stresses and tie bar widths, stresses being computed from the equation 3.7.1 using shifts can be attributed to errors in the measurement of inputs and computation of crossection coefficient (χ) and constant (α). The input variables could not be measured accurately because of the cast surface roughness and hence dimensions aimed for were used in calculations, assuming that they would not be very different from the actual values.

Another problem of the sectioning technique which may have effected the stress results is the need to slightly grind the area where lines were to be scribed. This alters the distance from the neutral axis (used to calculate crossection coefficient) compared with that for the rest of the casting. The value used in computation was one aimed for. A way to overcome this problem can be to drill small holes at the centre of the junction of the tie bar and ring and insert small pins with lines scribed on its head. The pins must have interference fit with the hole, special care being taken in pin alignment which is critical to subsequent measurements.

6.5 HEAT TREATMENT STRESSES AND STRESS RELIEF

Tie bar sectioning of annealed, normalized and tempered theta ring produced a nearly zero contraction in case of 30mm tie bar width and slightly larger in the 10mm width tie bar. When translated into residual stresses in the tie bar, these contractions give stresses of zero and $-9.7 MN/m^2$ for 30 and 10mm width tie bar

respectively. These results for the tie bar very nearly approach the idealized cases.

Uniform thickness of the 30mm tie bar theta ring produces uniform cooling with insignificant temperature differentials leading to an almost stress free tie bar. The 10mm tie bar theta ring is a very different case because of the non uniform cooling of theta ring during Normalizing and tempering treatments leads to temperature differentials, as shown in Table 16, and hence leading to compressive stresses in the tie bar.

The overall effect of the annealing, normalizing and tempering of the 30mm tie bar theta ring is that the residual stresses measured by Centre hole drilling technique become less compressive. This trend is present at all the positions in the theta ring the interesting feature, as shown in figures 98 and 100, being that the residual stresses in annealed, normalized and tempered conditions are within a band of $20MN/m^2$, except for in the case of the tie bar. Significant reduction in compressive residual levels were obtained after the annealing. Subsequent normalizing followed by tempering resulted in further although not very significant reduction in residual stress levels. This suggests an almost negligible contribution from the insignificant temperature differentials along the tie bar. The contraction upon sectioning the tie bar in the heat treated condition was negligible as compared with significant

expansion in as cast 30mm tie bar. The lower compressive residual stresses in the ring section in heat treated condition compared with as cast stage provides evidence of the contribution of mould component in formation of stresses during casting. Residual stress in the tie bar, as shown in figure 99 vary significantly after annealing, normalizing and tempering treatment. Although the residual stress becomes less compressive after each treatment. This reduction in stress levels may be attributed to slow cooling of the tie bar due to being surrounded by the ring during heat treatment. Evidence for slower cooling is not, however, provided by cooling curves in figures 64 and 66. These reduction in stresses may also be caused by a situation analogous to the stress relaxation with the ring section acting as a constraint, strain remaining constant but stress changing with material properties and temperature. Complete relaxation will not be achieved because of insufficient times but nevertheless some relaxation will occur and no new residual stresses will be generated due to absence of temperature differentials in the theta ring. The lower residual stresses after heat treatment suggest two aspects for a uniform section theta ring. Firstly that annealing does not necessarily produce a completely stress free casting although the detailed explanations are not apparent. Secondly, normalizing or tempering treatments may or may not produce additional stress relief depending on the location of the residual stress measurement.

The residual stress in the 10mm tie bar theta ring presented a much more complex picture for a precise analysis to be made. Evidence for the temperature differentials and phase transformations occurring at different times were recorded as presented in Figures 63 and 65. It has been noted previously that the compressive stresses in the sectioned tie bar confirm the temperature differential leading to differential contraction which is more likely to occur during normalizing and tempering treatments as shown in the cooling curves. These two treatments introduce residual stresses into the tie bar as shown in Figure 97 and 99. The normalizing results in phase transformation and thermal contraction stress components whereas tempering only has a smaller thermal component during subsequent cooling. The transformation during normalizing is from austenite to a fine pearlite with some pro eutectoid ferrite at grain boundaries. The transformation results in an expansion although there is some stress relaxation because of diffusional nature of transformation. Tempering produces no long range transformations as evident from cooling curves although stress relief may occur. Both normalizing and tempering also have temperature differentials between tie bar centre and its junction with the ring as it cools down. This suggests that normalizing and tempering treatments for non-uniform section thickness components may not be beneficial with respect to relieving residual stress apart from improvements in mechanical properties.

It was assumed during Annealing and also normalizing that the cooling rates of the surface and centre of the crossectional thickness of the theta ring are almost constant, the centre being usually at a slightly higher temperature than the surface during normalizing. The surface undergoes transformation first and hardens relative to the centre. The transformation to pearlite relieves more stress than in hardening process, which form shear transformation products such as martensite and bainite. This is accompanied by the increase in yield strength, or plastic flow stress of the metal with the decreased temperature. The resultant stresses in the centre and surface depend upon the sign of net volumetric change occurring in the centre of crossection after the surface has cooled down. If the transformation expansion exceeds the thermal contraction the surface will be in the state of residual tension and centre in compression. However, if thermal contraction exceeds transformation expansion, reversed stress patterns will develop i.e. surface in residual compressive stress and centre in residual tension. These stress distributions are a function of relative cooling rates at surface and centre. It must be appreciated that transformation stress and cooling rates are very small compared with quenching processes forming martensitic structures.

The compressive residual stresses in the surface obtained after the annealing treatment imply that the contraction at the centre exceeded the expansion due to

transformation. It is possible to extend concept to normalizing, but is not appropriate to extend it to the case of tie bar for 10mm theta ring for the annealing.

An interesting feature of the annealing, normalizing and tempering treatment is observed by comparing the residual stress distribution in the 30mm tie bar theta ring in Figures 75, 88, 90 and 92. The range over which residual stresses in the theta ring are spread is reduced by 50% making distribution more uniform and additionally the complete spread of residual stress shifts significantly towards stress free situation. This suggests that the stresses are being relieved and redistributed in the theta ring. Some care is needed, because of lack of data, in a similar examination of stress distribution in the 10mm tie bar theta ring in Figures 71, 89, 91 and 93 but it is observed that the range over which residual stress is spread reduced also by about 50%. However, due to temperature differentials existing during normalizing and tempering treatments stresses behave in a rather complex manner giving a combination of tensile and compressive residual stresses. This confirms the previous suggestion that stresses were being relieved and redistributed subject to this being less predictable in a non-uniformly cooled casting.

It must be appreciated that the generation and relief of residual stresses in the theta ring is complex because two mechanisms are operating one along the

tie bar and the ring and another perpendicular to it. Reinforcement or cancellation of each of these effect is difficult to establish experimentally and this makes precise analysis of residual stress distribution difficult.

6.6 SIGNIFICANCE OF RESIDUAL STRESS LEVELS

The Residual stresses found in the theta ring with various tie bar widths were calculated according to maximum tensile stress and numerically greatest stress criteria. The results using the former criteria were presented in figure 86 for different positions as shown in Figure 21.

The residual stresses computed according to the numerically greatest stress criteria were also subjected to correlation tests with respect to tie bar widths. The correlation coefficients for the positions 1,2,3 and 4 on the ring section ranged from 0.63 to 0.93 (1.0 representing perfect correlation) and was found to be 0.56 for the tie bar position. The latter was not satisfactory but was never the less included for comparison. The best fit lines were computed and are presented in figure 101. The residual stresses according to both criteria became less compressive in the theta rings as the tie bar width decreased and consequently temperature differentials were increased, some of the maximum tensile criteria and actual residual stress values becoming tensile.

Consideration was given in section 2.5 to the detrimental effect of tensile stress on fatigue limit. A theta ring of uniform section and minimum temperature differentials may be perfectly suitable with respect to fatigue properties in the cast condition, although in metallurgical context it will need further processing to alter structure and improve other properties. This further processing in form of heat treatment will reduce compressive stresses therefore reduce the fatigue resistance of the theta ring. However a theta ring with non-uniform section and considerable temperature differentials will have reduced fatigue resistance and although certain positions on the theta ring have compressive stresses, the positions with tensile residual stresses are critical. Although the maximum tensile residual stress was less than 6% of the yield strength, any additional stress in the same direction may promote failure and further heat treatment may not significantly alter fatigue properties. This demonstrates the importance of uniform section size and minimum temperature differentials in castings.

The other criteria, Von mises equivalent which is presented in Table 19 for all the theta rings was also subjected to correlation tests. The correlation co-efficients for the positions 1,2,3 and 4 on the ring section ranged from 0.66 to 0.83, the co-efficient for the tie bar position was found to be 0.45 which although not satisfactory was included in the study to facilitate comparison. Best fit lines were also computed and are

presented in figure 102. Von Mises equivalent computed from two principal residual stresses will only cause yielding when equal to yield strength in uniaxial tension, but the maximum Von Mises equivalent computed for any position in the series of theta rings was found to be less than 25% of the yield strength of the material. It is important to emphasise that this is a residual stress situation with no other applied stresses, and also that failure is assumed at yielding, although the failure criteria may depend upon the product. However, the factor of safety according to Von Mises criteria decreases for all positions in theta rings as the tie bar width is increased, because the Von Mises equivalent stress is increased. This may suggest that the uniform section size theta ring is less suitable but heat treatment was found to significantly reduce the Von Mises equivalent stress for the same ring.

This reiterates the view, that depending on the mode of service of the finally processed casting the initial and final residual stress levels may or may not be beneficial.

6.7 SOLIDIFICATION MODEL AND PREDICTION OF RESIDUAL STRESS

The solidification model produced some data which reflect on its usefulness as an initial programme meant to be extended as a part of future work.

The model was for a unidimensional case and to speed up the solidification process from computational point

of view, highest thermal conductivity - temperature relationship was selected from those available in the literature. Another vital assumption was that the properties data for the interfacial temperature was calculated at the average temperature of sand and molten metal. This later assumption may not be correct in normal circumstances but for the purposes of this study it reduces the computational times by giving a lower interfacial temperature. This temperature was found to be just below the solidus temperature. The computational results indicate temperature gradients within the tie bars, being greatest when the centre of the tie bar approached the liquidus temperature. As the tie bar width was decreased the gradient was steeper as shown in Figure 105. The times at which the liquidus temperature was crossed were proportional to the tie bar width as would be expected, and as shown in Figure 105. The temperature gradient which existed in the tie bar when its centre was at liquidus temperature almost disappeared when the centre crossed the solidus temperature. However, the interfacial temperature drops by very small amounts and the most likely explanation for this is the release of latent heat of fusion which was accounted for in the specific heat relationship. This retarded the cooling rate of the tie bar during the solidification, the cooling rates being expected to increase after the tie bar has completely solidified. The times for complete solidification of the tie bar section were, as expected, also proportional to the tie bar width and are shown in figure 106.

However, it is not possible to compare these solidification times with those obtained for the tie bars experimentally because, the cooling process of tie bars is not a simple case of unidirectional solidification and, also, theta rings were not poured at identical temperatures. It is interesting to observe from table 20 that the temperature gradient, although very small, is greatest in case of 30mm tie bar and smallest for 10mm tie bar. This is to be expected in a normal heat flow situation, this situation may possibly persist as the tie bar further cools down. These gradients may be insignificant with respect of generation of Casting residual stresses but the programme does indicate the significance of the temperature differentials along the length of tie bar and its junction with the ring i.e. hot spot. This also reflects on the need to extend this study to take other directions into account which would then make it more meaningful to extend the programme in order to predict the residual stresses using temperature data obtained. Various models for predicting residual stresses in castings have been reviewed in section 2.7 in terms of their basic approach and inherent difficulties in areas such as mechanical properties at high temperatures. It would seem inappropriate at this stage to show preference for any one model in this study without progressing further with temperature distribution prediction, which will form a useful initiation for further work.

7.0 CONCLUSION

1. Centre hole drilling technique was found to be highly sensitive to the surface preparation methods. Induced machining stresses in cast samples exceeded those in annealed samples, and these stresses were accounted for in the final measured residual stresses.

2. Generation of casting residual stresses may be explained in terms of mould hindrance, temperature differentials and phase transformation using cooling curves of theta rings and sand mould.

3. Casting stresses in Theta rings were compressive but as the tie bar width was decreased they became less compressive and even tensile in certain locations. The decrement in compressiveness increased as the distance from the hot spot along the ring increased, lowest stress being at the hot spot.

4. Tie bar sectioning technique showed that tensile stress was present in the tie bars of all theta rings. Length of the tie bar increased upon sectioning, the changes in length increasing with increase in tie bar width.

5. The above results can be accounted for by considering two idealized cases of theta rings with thick and thin tie bars.

6. A runner designed to exert minimum stresses on the theta ring, was shown to contain a tensile residual stress of $21 MN/m^2$. Sectioning the runner demonstrated a spring

back effect, and upon removal made the residual stress in the theta ring less compressive.

7. An epoxy resin model cast and cooled uniformly at a very slow rate contained no residual stresses.

8. Theta rings of 30 and 10mm section in the annealed, normalized and tempered condition, were found to contain approximately zero and $-10MN/m^2$ stress levels respectively when the tie bar was sectioned.

9. A uniform section size theta ring, cooling uniformly, produced a lower residual stress in the tie bar after each treatment but tempering and normalizing treatments did not lower residual stress levels in the ring section of the theta ring.

10. Residual stresses in non-uniform section size theta ring were not lowered or relieved by heat treatments because of temperature differentials and phase transformation which also generated some additional stresses.

11. Annealing did not fully stress relieve the theta ring irrespective of section sizes.

12. Heat treatments reduced the range over which residual stresses were present in the theta ring by 50%. The spread shifted towards stress free situation for a uniform section size theta ring.

13. Uniform section size theta ring with more compressive residual stress compared with non-uniform size theta ring may have improved fatigue resistance. Heat treatment did not alter this situation significantly although the maximum von Mises equivalent for any position in series of theta ring was less than 25% of the yield strength of material.

14. A computational model indicated that temperature gradients existed across the tie bar widths during solidification, but this gradient disappeared as tie bar solidified completely. At this stage no residual stresses are expected to be generated along this axis. This model forms a basis for future investigation along the axis in the tie bar.

8.0 RECOMMENDATIONS FOR FURTHER WORK

1. This study has been primarily concerned with the generation of residual stresses in castings largely due to mould hindrance and temperature differentials. The effect of increasing the phase transformation variable may be studied more in depth by retaining the theta ring configuration and selecting a material with more complex transformation products such as bainite and martensite.

2. Annealing treatment is intended to fully stress relieve a component but this was not confirmed by this investigation. For a clearer understanding this aspect needs investigation using a basic configuration such as bar or rod.

3. The runner system adopted was shown to significantly alter residual stress levels in theta rings. Investigations into variations in the runner system such as two pouring heads placed diametrically opposite with individual runners or other alternatives will therefore be useful from the point of view of controlling residual stress levels.

4. Further investigation of the stress versus depth relationship in the theta ring may account for certain discrepancies in the Centre hole drilling and tie bar sectioning technique, the application of incremental analysis of the centre hole drilling data being desirable.

5. The computational model has been established but it requires to be extended into second direction encompassing the whole of theta ring. A first step would be to solidify and cool the theta ring down to room temperature in a programme and then incorporate the stress-strain relationship which depends upon the temperature differentials.

REFERENCES

1. Polushkin, E.P., Defects and failures of metals, Elsevier, London (1956).
2. Fugso, H., Aida, R. and Masumoto, Y., Bull.Jpn.Soc. Mech.Eng., v20, p150(1977)
3. Sach, G. and Van Horn, K.R., Practical Metallurgy, Cleveland, Am.Soc.Metals (1940)
4. Heyenti, M., Handbook of Experimental Stress Analysis, Wiley, London (1963)
5. Thomson, R.F., Proc.Symposium on Internal Stresses and Fatigue in metals, Michigan (1958)
6. Benham, P.P. and Hoyle, R., Thermal stresses, Pitman, London (1964)
7. Gatewood, B.E., Thermal Stresses, McGraw Hill, New York (1957)
8. Orowan, E.,Proc.Symposium on Internal Stresses and Fatigue in metals, Michigan (1958)
9. Orowan, E., Symposium on Internal stresses, London, Inst. Metals (1948)
10. Andrews, K.W., Physical Metallurgy Techniques and Applications, Vol.11, Allen & Unwin (1973)
11. Gensamer, M., Strength of materials under combined stresses, Am. Soc.Metals (1940)
12. Evans, W.P., Soc. Automotive Engrs. O.,n3(1963)
13. Osgood, W.R., Residual stresses in metals and construction, Reinhold, New York (1954)
14. Parlane, A.J.A., Seminar on Residual stresses and their effect on service performance, Cambridge, Welding Inst. (1979)

15. Nabarro, F.R.N., Symposium on Internal stresses, London, Inst. Metals (1948)

16. Thomson, F.C., Symposium on Internal stresses, London, Inst. Metals (1948)

17. McClintock, F.A. and Argon, A.S., An introduction to the behaviour of materials, Sec. 1, School of Eng., M.I.T., Massachusetts(1974)

18. Heindlhofer, K., Evaluation of Residual stresses, McGraw Hill, London (1948)

19. Buhler, H. and Scheil, E., Archiv fur das Eisenhullenwesen, v7, n6 (1933-34)

20. Angus, H.T. and Tonks, W.G., Br. Foundryman,v50(1957)

21. Heggie, C., Proc.Inst.Brit.Foundryman, v21(1927-28)

22. Servais, M., Proc.Inst.Brit.Foundryman,v21(1927-28)

23. Longden, E., Proc.Inst.Brit.Foundryman,v25(1931-32)

24. Longden, E., Proc.Inst.Brit.Foundryman,v41(1947-48)

25. Angus, H.T. and Tonks,W.G.,Brit.C.I.Res.Assoc.J.Res. Dev.,v3 (1949)

26. Dodd,R.A.,3.Inst.Metals,v81 (1952-53)

27. Parkins, R.N. and Cowans,A., J.Inst.Metals,v82(1933-34)

28. First Report of Subcommittee T.S.32, Foundry Trade J., v93 (1952)

29. Konstantinov, K.,Russ.Cast.Prod., n11(1963)

30. Chijiiwa,K., Eng.Kori,I. and Fujiwara,N.,IMONO,J.Jpn. Foundryman.Soc. v38(1966)

31. Chijiiwa,K.,J.Jpn.Foundryman.Soc.,v38(1966)

32. Chijiiwa,K., J.Jpn.Foundryman.Soc.,v38(1966)

33. Othahal,V., Slevarenstvi,v25,n10,BISI 16934(1977)

34. Medek,V.,Slavarenstvi,v25,n8,BISI 16535(1977)

35. Havelicek,F.,Slevarenstvi,v ,n8 BISI 17951(1978)

36. Flinn,R.A.,Fundamentals of Metal castings, Addison-Wesley,London(1963)

37. Beeley,P.R.,Foundry Technology,Butterworths,London(1974)

38. Bishop,H.E., Ackerlind,C.G. and Pellini,W.S.,Trans. Am.Foundry Assoc., v60(1952)

39. Balasingh,C., Seshadri,M.R., Ramasushan,S. and Srinuva,M.N.,J.Ind.Inst.Sci., V59,n9(1977)

40. Second Report of subcommittee T.S.32,Foundry Trade J. v101 (1956)

41. Oki,S., Okumoto, T. and Niijama,E., AFS Cast Metals. Res. J.(1970)

42. Parkins, R.N. and Cowans, A.,Proc.Inst.Brit.Foundrym., v46(1953)

43. Grishovich,N.G. and Simanovskii,M.P., Russ.Cast. Prod.(1963)

44. Kasch,F.E. and Mikelonis,P.J.,Mod.Castings,v55(1969)

45. Report of subcommittee T.S.18,Proc.Inst.Brit. Foundrym.,v42(1949)

46. Crowe,J.E., BCIRA J., Report 1009(1970)

47. Middleton, J.M. and Protheroe,H.T.,J.I & S.Inst. Aug.(1951)

48. Elliss,H.,Symposium on Internal Stresses,London, Inst.Metals(1966)

49. BISRA, Distortion of Steel during heat treatment, BSC Sheffield

50. Patterson,W. and Dietzel,G., Giesserei (Tech-wiss-Beihefts), v18,n3(1966)

51. Crane,L.W.,Proc.Conf.Heat treatment: methods and media, IMI/2, 1207-79-MT,London,Inst.Metall.Tech.(1979)

52. Bainbridge,A.T.,Paper presented at Winter Annual meeting ASME, Georgia(1977)

53. Stewart,C.W.,J.Am.Soc.Naval Engrs.v49(1937)

54. Rominskii,E.A. and Taylor,H.F.,Trans.Am.Foundrym., v51 (1943)

55. Jelm,C.R. and Herris,S.A., Trans.Am.Foundrym., v54(1946)

56. Report of subcommittee T.S.17., Symposium on Internal stresses, London, Inst.Metals(1948)

57. Saunders,G.G., Seminar on Residual stresses and their effect on service performance, Cambridge,Welding Inst. (1979)

58. Kotsyubinkii,O.Yu.,Russ.Cast.Prod.(1962)

59. Baldwin,W.M.Jr.,Residual stresses in Metals, 23rd Edgar Marburg lecture,Proc.Am.Soc.Testing Mater.(1949)

60. Claxton,R.A. and Saunders,G.G.,Metall.Mater. Tech., Dec.(1976)

61. Claxton,R.A., Heat treatment of Metals, v1,n4(1974)

62. Third Report of Subcommittee T.S.32.,Proc.Inst. Brit.Foundrym., v53(1960)

63. Novichkov,P.V.,Russ.Cast.Prod.(1970)

64. Giverney,T.R.,Paper 23, Proc.Conf. on Residual stresses in welded construction and their effects, Welding Inst.(1977)

65. Frost,N.E.,Marsh,K.J. and Pook,L.P., Metal Fatigue, Claredon Oxford (1974)

66. Found,M.S., J.Res.,SCRATA, n44/45(1979)

67. Timofeev,A.A. and Shumov,I.D.,Izv.Vuz Chern Met.,n5,BISI 10619 (1972)

68. Trueting,R.J., Lynch, J.J., Wisharl,H.B. and Richards, D.G., Residual stress measurements, Amer.Soc.Metal,Pittsburgh(1951)

69. Denton,A.A., Review 101,v11,Metallurgical Reviews(1966)

70. Barret,C.S., Metals and Alloys, v5(1934)

71. Parlane,A.J.A., Paper 8, Proc.Conf.on Residual stresses in welded construction and their effects, Welding Inst.(1977)

72. Sachs,G. and Epsey,G., Iron Age, Sept. 18, 25 (1941)

73. Report of Iron and Steel Technical committee, Soc.Auto.Engrs.Hdbk.Suppl.J936,New York (1965)

74. Barret,C.S., Exptal Stress Anal.,v2,n1(1944)

75. Tebedge,N., Allisten,S. and Tall,L., Exptal Mech., Feb. (1973)

76. Leaf,W.,Proc.Exptal.Stress Anal.,v9,n2(1952)

77. Underwood,J.H., Exptal.Mech.,Sept.(1973)

78. Stengel,B and Gaymann,Th., Paper 16, AGARD Conf. Proc.No.53, NATO(1970)

79. Oppel,G.U., Proc.Soc.Exptal Stress Anal.,v21,n1(1964)

80. Gadd,W.C.,Proc.Soc.Exptal.Stress Anal.,v4,n1(1946)

81. Mathar,J.,Trans.ASME.,v56 (1934)

82. Kelsey,R.A.,Proc.Soc.Exptal.Stress Anal.,vXIV,n1(1946)

83. Rendler,N.J. and Vigness,I.,Exptal.Mech.,Dec.(1966)

84. Bathgate,R.G.,Strain,v4,n2,April (1968)

85. Gupta,B.P., Exptal.Mech.,Jan.(1973)

86. Redner,S., Bulletin TDG-5, Welwyn Strain Measurement Ltd. (1974)

87. Tech.Data Bull.T-403, Measurement of Residual Stresses by the Blind Hole drilling method, Photolastic Inc., Pennsylvania(1977)

88. Beaney,E.M. and Procter,E., Strain,v10,n1(1974)

89. Beaney,E.M., Strain,v12,n3,July (1976)

90. Birley,S.S. and Owens,A., NDT.Int.,Feb.(1980)

91. Procter,E.,Seminar on Residual Stresses and their effect on service performance, Cambridge, Welding Inst.(1979)

92. Bijak-Zochowski,M.,VDI-Berichte,n313(1978)

93. Ajovalasit,A.,J.Strain Anal.,v14,n4(1979)

94. Thomas,D.E., J. Scientific Instruments,v18,n7(1941)

95. Clark,G.L., Ind.Radiography(1964)

96. Christenson,A.L. and Rowland,E.S., 34th Annual Convention of Am.Soc. Metals(1952)

97. Hawkes,G.A., Brit.Jnl.App.Phy.,v8 (1957)

98. Marburger,R.E. and Koistinen,D.P., Proc.Symposium on Internal Stresses and Fatigue in Metals,Michigan(1958)

99. Shimada,H. and Arakida,Y., Proc.of 4th Int.Conf.NDT. testing., London (1963)

100. Hughes,H., Strain,v3,n3(1967)

101. Doig,P. and Fewitt,P.E.J.,NDT.Int., June(1978)

102. Kirk,D., Strain, April(1970)

103. Kirk,D., Strain, Jan.(1971)

104. Larsson,L.E., Scand.J.Met.,v3(1974)

105. Kraus,I. and Kralova,R., Kovove Mat.,v2(1976)

106. Kurita,M., Bull.JSME.,V20,n149(1977)

107. Stevens,P.J., BHP.Tech.Bull.,v21,n2(1977)

108. Cullity,B.D., Proc.Conf.Adv.Xray Anal.(1977)

109. Jaensson,B.,Mat.Sci.Engg.,v43(1980)

110. Stahlkopf,K.,Egan,G.R. and Dau,G.,Paper 43, Proc. Conf. on Residual Stresses in Welded construction and their effects. Welding Inst.(1977)

111. Carslaw,H.S. and Jaeger,J.C., Conductive of Heat in Solids, Oxford (1959)

112. Hill,A.W.D., Trans.Met.Soc.AIME.,v245,July(1969)

113. Mcadams,W.H., Heat transmission, Mcgraw Hill, New York(1954)

114. Dusinberre,G.H., Heat transfer calculations using finite difference equations, Applied Science Publ., London (1977)

115. Croft,D.R. and Lilley,D.G., Heat transfer calculations using finite difference equations, Applied Sci., Publ., London (1977).

116. Adams, J.A. and Rogers, D.F., Computer-aided Heat transfer analysis, Mcgraw-Hill, New York (1973)

117. Ohnaka, I., and Fukusako,T., Trans.ISIJ.v17(1977)

118. Schniewind,J., Iron and Steel Inst., July (1963)

119. Adenis, D.J.P., Coats,K.H. and Ragone,D.V., J.Inst. Metals,v91(1962-63)

120. den Hartog, H.W., Rabenborg,J.M. and Willemse,J., Iron and Steelmaking (Quart.),n2(1975)

121. Pehlke,R.D., Marrone,R.E. and Wilkes,J.D., Computer Simulation of Solidification, Am.Foundryman's Soc. Illinois (1976)

122. Fletcher, A.J., Metals Tech., June(1977)

124. Weiner,J.H. and Boley,B.A.,J.Mech.Phy.Solids,v11(1963)

125. Sakwe,W. and Parkitny,R., Giessereiforschung in English,v23,n2(1971)

126. Mathew,J. and Brody,H.D.,Comp.Simulation for Mater. App.Nuclear Metall., v20,n2(1976)

127. Grill,A.,Brimacombe,J.K. and Weinberg,F., Iron and Steelmaking,n1(1976)

128. Sorimachi,K. and Brimacombe,J.K., Iron and Steelmaking, n4(1977)

129. Havelicek,F., Slevarenstvi, v24,n11(1976)

130. Othahal,V., Slevarenstvi, v25,n10(1977)

131. British Standard 3100,BSI., London (1976)

132. A guide to Solidification Steels, Jerokontoret, Stockholm(1977)

133. Bulletin B-127-5, Welwyn Strain Measurements Ltd., Hants (1976)

134. Rothbart, H.A., Mach.design and Systems Hdbk., McGraw-Hill(1964)

135. Bulletin 90-242A-01,Info. about Si.mater.,Dow Corning(1975)

136. Instruction Sheet No.5a, Araldite Resin for photo-elastic stress analysis, CIBA-GIEGY, Cambridge(1975)

137. Geiger,G.H. and Poirier,D.R., Transportphenomena in Metallurgy, Addison-Welsey,London(1973)

138. Ruddle,R.W., The Solidification of Castings, Inst. of Metals Monograph No.7, Inst. of Metals(1957)

139. McGannon,H.E., The Making, Shaping and Treating of Steel, United States Steel Corp. (1964)

Conductivity of Selected Materials,Nat.Std. Reference Data Series, National Bureau of Standards NSRDS-NBS 8 (1967)

141. American Society for Metals, Metals Hdbk.,vol.1, Am.Soc.for Metals (1961)

142. Powell,R.W., Proc.Phys.Soc.,v46(1934)

143. Gray,D.E., Am.Inst.of Phys.Hdbk.,Amer.Inst.Phys.(1963)

144. Darken,L.S. and Smith,R.P., 'Thermodynamics Functions of Iron', Ind.Eng.Chem.,v43(1951)

145. Am.Soc.for Metals, Metals Hdbk.,Am.Soc.for Metals(1948)

146. Schroader,D.L. and Lippit,D.L.,'Two dimensional Continuous casting Heat transfer simulation', paper presented at Fall,AIME,New York(1967)

147. Pirani,M. and Wagenheim,F.V.Z., tech.Physik,v10(1929)

148. Atterton,D.V.,J.Iron Steel Inst.,v174(1953)

149. Lucks,C.F., Linebrink,D.L. and Johnson,K.L., Trans. Amer.Found.Assoc.,v55(1947)

150. Dietart,H.W., Hasty,E.J. and Doelman,R.L., Foundry, v75,n9(1947)

151. Hodgman,C.D., Hdbk. of Chemistry and Physics, Chemical Rubber Publ. Co.(1958)

152. Kelly,K.K.,U.S.Bureau of Mines Bull.476(1949)

153. Perry,J.H., Chemical Engr's.Hdbk.,McGraw-Hill(1963)

154. North American Combustion Hdbk.,North American Manufacturing Co., Cleveland, Ohio(1952)

155. Mcadams,W.H.,Heat transmission,McGraw-Hill,NewYork (1954)

156. Welty,J.R., Engg.Heat Transfer, John Wiley,
London (1974)

157. Jakob,M., Heat Transfer,vl,John Wiley,London(1949)

158. Hsu,S.T., Engg.Heat Transfer,D.Van Nostrand,
London (1962)

159. Andrews,K.W., J. Iron and Steel Inst., July (1965)

TABLE 1 SUMMARY OF EFFECTS OF VARIOUS STRESS RELIEF TREATMENTS (After Novichkov[63])

Process	Residual stress	Stress relaxation resistance	Potential energy	Remarks
Natural ageing	Lowers RS by 7-20%	Appreciably(?) raised	Lowered slightly	
Annealing in the range 550-600°C	Lowered by 85-90%	Decreased appreciably	Lowered	
Thermal shock	Lowered	Increased	Raised	
Static over load and vibration	Lowered but amount depends on different parameters	Increased		Difficulty in case of complex castings

TABLE 2. SIGNIFICANCE OF RESIDUAL STRESSES ON CRITICAL DEFECT SIZES (After Found[66])

Steel	1½%Mn	1%Cr-0.5%C
Fracture toughness K_{1c} N/mm$^{3/2}$	3800	1900
0.2% proof stress σ_y N/mm^2	364	376
Tensile strength σ_u N/mm^2	560	794
Working stress σ_w N/mm^2 (σ_w/σ_y=0.5)	182	188
Critical defect size, mm		
(a) σ_{res}=0	138	32.5
(b) σ_{res}=80 N/mm^2	67	16
(c) $\sigma_{res}=\sigma_y$	15.5	3.5

TABLE 3 CLASSIFICATION OF RESIDUAL MEASURING METHODS

Non destructive Methods	Semi destructive Method	Destructive Methods
a. Indentation methods	a. Brittle Lacquer Method	a. Boring & Turning Met
	b. Centre hole drilling method	b. Parting set Method
		c. Layer Removal Method
		d. Cutting Deflection M
		e. Sectioning Method
b. X-Ray methods		

TABLE 4 COMPOSITION OF BW2

	min	max
C	0.45	0.55
Mn	0.5	1.0
Si		0.75
S		0.06
P		0.06
Cr	0.8	1.2

TABLE 5 CHEMICAL ANALYSIS OF THE THETA RINGS

Casting tie bar width(mm)	C	Mn	Si	Cr	Al	S	P
30C	0.45	0.75	0.3	0.99	0.001	0.011	0.015
25C	0.50	0.97	0.74	1.07	0.029	0.013	0.016
20C	0.53	1.0	0.7	1.07	0.040	0.016	0.017
15C	0.52	0.94	0.7	1.11	0.037	0.013	0.015
10C	0.505	0.93	0.68	1.08	0.037	0.012	0.016
5C	0.53	0.93	0.63	1.08	0.037	0.013	0.017
30H	0.50	0.96	0.66	1.14	0.029	0.012	0.019
10H	0.56	0.95	0.68	1.07	0.027	0.012	0.019

C refers to Theta ring used for Casting Stress Analysis

H refers to Theta ring used for Heat Treatment Stress analysis

TABLE 6 DATA OBTAINED FOR CALIBRATION TESTS

	ϵ_a	ϵ_b	ϵ_c
Strain recorded on loading	206 $\mu\epsilon$	60 $\mu\epsilon$	+57 $\mu\epsilon$
Strain recorded on unloading	-113 $\mu\epsilon$	-9 $\mu\epsilon$	-47 $\mu\epsilon$
Strain recorded in ideal case	- 93 $\mu\epsilon$	-51 $\mu\epsilon$	-10 $\mu\epsilon$

Load on Specimen: 20 kN

Specimen c.s.a: 50 x 9.01 = 450.5mm^2

Uniaxial stress on Specimen = 44.4 MN/m^2

Measured hole
diameter : 1.79 mm

VALUES OF FUNCTIONS $\overline{K_1}$ AND $\overline{K}_1$ (AFTER BEANEY & PROCTER[88])

Origin	$\frac{\nu K_2}{K_1}$	$-\frac{1}{K_1}^{\dagger}$	$-\frac{1}{K_1}^{*}$	Hole Diameter in mm	Material
Rendler & Vigness	0.333	4.94	4.99	1.498	Steel
Tebedge et al	0.324			2.997 (nom)	Steel
Kelsey	0.320			6.35 (nom)	Aluminium
Bathgate	0.307			6.35 (nom)	Aluminium
C.E.G.B., S.W.Region (Bending)	0.289	3.70	3.69	1.689	M.S.
	0.313			2.379 (nom)	M.S.
	0.285			2.379 (nom)	M.S.
	0.252			2.379 (nom)	M.S.
B.N.L. Uniaxial Tests	0.336	2.89	2.94	1.905	M.S.
	0.278	3.95	3.92	1.661	M.S.
	0.264	3.78	3.73	1.679	M.S.
	0.305	4.17	4.17	1.638	M.S.
			3.81	1.646	EN8
			3.86	1.694	EN8
			3.72	1.663	EN8
B.N.L. 2:1 Biaxial Tests			3.37	1.773	M.S.
			3.72	1.717	M.S.
			3.13	1.841	$2\frac{1}{4}$Cr.1Mo.
			3.23	1.7902	$2\frac{1}{4}$Cr.1Mo

† $\frac{1}{K_1}$ calculated from $\frac{\epsilon_A}{\epsilon_{A\,1}}$

* $\frac{1}{K_1}$ calculated from maximum stress equation substituting

$$\frac{\nu K_2}{K_1} = 0.3.$$

TABLE 8 EFFECTS ON COOLING RATES OF THERMAL CONDUCTIVITY

Thermal Conductivity of sand	After 15sec temperature in the middle of tie bar is:
a) K = 0.38171.....	1460.4 °C
b) K = 0.5244.....	1463.0 °C
c) K = 0.30215.....	1464.9 °C
d) K = 0.1634.....	1466.9 °C

TABLE 9 POURING AND TRANSFORMATION TEMPERATURE OF THETA RINGS

	Pour temp.	Ac_1	Ac_3
30C	1500	740.4	771
25C	1600	752.2	781.4
20C	-	750.7	779.6
15C	-	752	779.8
10C	1535	751	782.3
5C	1600	749.6	777.3
30H	1595	751.2	779.5
10H	1580	750.6	772

* Number refers to tie bar width in mm.

C stands for Cast theta ring

H stands for Heat treated theta ring

TABLE 10 SOLIDIFICATION ORDER IN THETA RINGS

Tie bar width - mm	30	25	20	15	10	5
1st	2	5	5	5	5	5
2nd	3(0.02)	2*	2(0.05)	2(0.72)	1(0.73)	2(1.11)
3rd	6(1.04)	6(0.09)	6(0.10)	6(0.12)	3(0.075)	1(0.18)
4th	1(0.07)	1(0.10)	1*	1(0.05)	2*	3*
5th	5(0.09)	3(0.00)	3(0.03)	3(0.15)	6(0.10)	6(0.13)
6th	4(1.16)	4(1.11)	4(1.42)	4(2.18)	4(-)	4(-)

* denotes the assumed order of position because of thermo-couple failure. Figures in brackets=time interval since previous position solidified in minutes.

TABLE 11 ORDER OF CROSSING Ac_3 LINE

Tie bar width	30	25	20	15	10	5
1st	6	6	2	5	5	5
2nd	2(0.03)	2*	6(0.8)	2(6.2)	6(2.8)	2(10.06)
3rd	1(5.2)	1(2.95)	1*	6(0.1)	2*	3(1.15)
4th	3(1.0)	3(0.5)	5(2.9)	1(4.69)	1(1.2)	6(0.0)
5th	5(3.6)	5(4.4)	3(4.6)	3*	3(3.00)	1(5.1)
6th	4(3.4)	4(5.8)	4(8.9)	4(13.8)	4(-)	4(2.6)

*denotes the assumed order of position because of thermo-couple failure. Figures in brackets=time interval since previous position transformed, in minutes.

TABLE 12 ORDER OF CROSSING Ac_1 LINE

Tie bar width	30	25	20	15	10	5
1st	2	6	2	5	5	5
2nd	6(1.0)	2*	6(0.85)	6(6.8)	6(9.05)	2(11.33)
3rd	1(4.7)	1(3.78)	1*	2(0.1)	2*	6(1.25)
4th	3(1.6)	3(1.0)	5(4.8)	1(5.43)	1(4.4)	3(0.95)
5th	5(7.8)	5(3.6)	3(3.5)	3*	3(0.6)	1(5.5)
6th	4(2.51)	4(7.0)	4(9.0)	4(14.6)	4(-)	4(2.4)

* denotes the assumed order of position because of thermo-couple failure. Figures in brackets=time interval since previous position transformed in minutes.

TABLE 13 TEMPERATURE DIFFERENTIALS AT SOLIDIFICATION STAGE

Tie bar width mm	4-1 °C	4-2 °C	4-3 °C	4-4 °C	4-5 °C	4-6 °C
30	162.2	215.4	208.2	0	155	190.1
25	189.5	127.5	176.5	0	195.2	176.5
20	-	234.4	209.7	0	297.2	219.8
15	244.5	294.2	317.9	0	524.9	273.7
10	-	-	-	0	-	-
5	253	-	-	0	-	-

TABLE 14 TEMPERATURE DIFFERENTIALS WHEN HOT SPOT CROSSES Ac_3

Tie bar width mm	4-1 °C	4-2 °C	4-3 °C	4-4 °C	4-5 °C	4-6 °C
30	79.6	127.5	75	0		190.1
25	93		81.1	0	34.2	100
20	-	139.6	64.5	0	54.6	132.7
15	86.7	136.3	-	0	134.8	164.2
10	-	-	-	0	-	-
5	25.3	101	75.4	0	283.5	75.4

TABLE 15 TEMPERATURE DIFFERENTIALS WHEN HOT SPOT CROSSES Ac_1

Tie bar width mm	4-1 °C	4-2 °C	4-3 °C	4-4 °C	4-5 °C	4-6 °C
30	60.5	120.9	48.6	0	18.2	94.8
25	77.6	-	60.6	0	25.2	115.4
20	-	135	44.3	0	29	128.4
15	52.1	127.6	-	0	112	159.3
10	-	-	-	0	-	-
5	24.5	70.1	61.6	0	246.9	32.9

TABLE 16 HEAT TREATMENT DATA

Heat treatment	Tie bar width	Position	Cooling Rate (max)	Temperature difference °C (max)	
	mm		(°C/min)	3-4	4-5
Annealing	10	3	9	4	
		4	9		4
		5	9		
	30	3	4.5		
		4	4.5		
		5	4.5		
Normalising	10	3	128		
		4	90	88	12
		5	148	62	156
	30	3	112		
		5	112		
		6	118		
Tempering	10	3	40	18	
		4	40	18	67
		5	72		72
	30	3	45		
		4	36		32
		5	45		22

TABLE 17 TIE BAR STRESSES OBTAINED FROM TIE BAR SECTIONING TECHNIQUE

Tie bar width mm	Residual Stress (MN/m^2)
Casting 30	9.11
Casting 25	12.59
Casting 20	15.67
Casting 15	24.77
Casting 10	11.71
Casting 5	7.23
Heat treated 10	-9.7
Heat treated 30	-0.625

TABLE 18 RESIDUAL STRESSES (MN/m^2)

Position → / Tie bar width ↓	1	2	3	4	5
Casting 30	-115	-127	-155	-84	-124
Casting 25	-110	- 76	- 34	-58	-43
Casting 20	- 62	- 46	- 24	-25	-125
Casting 15	-104	- 44	- 55	-43	-104
Casting 10	-100	- 25	35	20	- 34
Casting 5	- 45	- 42	- 22	16	-
Annealing 30	- 40	-	- 94	-96	- 94
10	-140	-104	-	-115	- 68
Normalising 30	- 42	-	- 56	-77.4	- 61
10	- 80	-	-	-	- 42
Tempering 30	- 45	-	- 51	-	- 50
10	-104	-	- 14	-	25
Casting 30 with Runner			-78.6		-78.5
Runner					-97.00
Machining Stress					
a) Annealed					20.71
b) Cast					30.11

TABLE 19 VON MISES EQUIVALENT STRESSES (MN/m^2)

Position → / Tie bar width ↓	1	2	3	4	5	
Casting 30	107.5	114.4	147.23	80.72	143	
Casting 25	97.54	68.02	31.43	50.22	38.97	
Casting 20	56.32	40.44	23.06	21.65	110.77	
Casting 15	90.15	38.31	51.39	37.63	97.75	
Casting 10	91.65	25	37.61	23.57	31.43	
Casting 5	40.11	38	19.28	21.16	-	
Annealing 30	37.74	-	81.70	84.86	87.84	
10	121	95.92	-	102	61.57	
Normalising 30	38	-	51.39	70.96	57.23	
10	96.37	-	-	-	37.54	
Tempering 30	39.88	-	45.90	-	44.93	
10	93.74	-	12.49	-	24.06	
Casting 30 with Runner			74.74		67.81	
Runner						110.00
Machining Stress						
a) Annealed						20.80
b) Cast						34.31

TABLE 20: COMPUTED TEMPERATURE WITHIN THE TIE BAR WHEN ITS CENTRE CROSSES SOLIDUS LINE

x/L Tie bar width mm	0.0	0.1	0.2	0.3	0.4	0.5
30	1374.7	1377.0	1379.0	1380.7	1381.8	1382.2
25	1376.2	1378.2	1380.0	1381.4	1382.4	1382.8
20	1377.5	1378.9	1380.2	1381.2	1381.8	1382.1
15	1378.6	1379.6	1380.5	1381.2	1381.6	1381.8
10	1379.5	1380.1	1380.7	1381.2	1381.5	1381.6
5	1380.0	1380.5	1380.9	1381.3	1381.5	1381.6

x is the distance from surface of tie bar in millimetres

L is the width of the tie bar

TABLE 21 COMPUTED TIMES REQUIRED FOR CENTRE OF TIE BAR TO REACH SOLIDUS TEMPERATURE

Tie bar width	Temperature at x/L=0.5 (°C)	Time after pouring (sec)
30	1382.2	200.95
25	1382.8	144.97
20	1382.1	97.98
15	1381.8	57.99
10	1381.6	26.99
5	1381.6	6.99

TABLE 22 PROPERTY DATA FOR BW2

COMPOSITION:

0.47 C, 0.85 Cr, 0.45 Si, 0.83 Mn.
P and S minimum

Yield Stress	= 661 MN/m^2
Tensile Strength	= 823 MN/m^2
Elongation	= 16%
Reduction of Area	= 40%
Charpy V	= 45 Joules
Vickers Hardness	= 260
Brinnel Hardness	= 254

Source: SCRATA, Sheffield

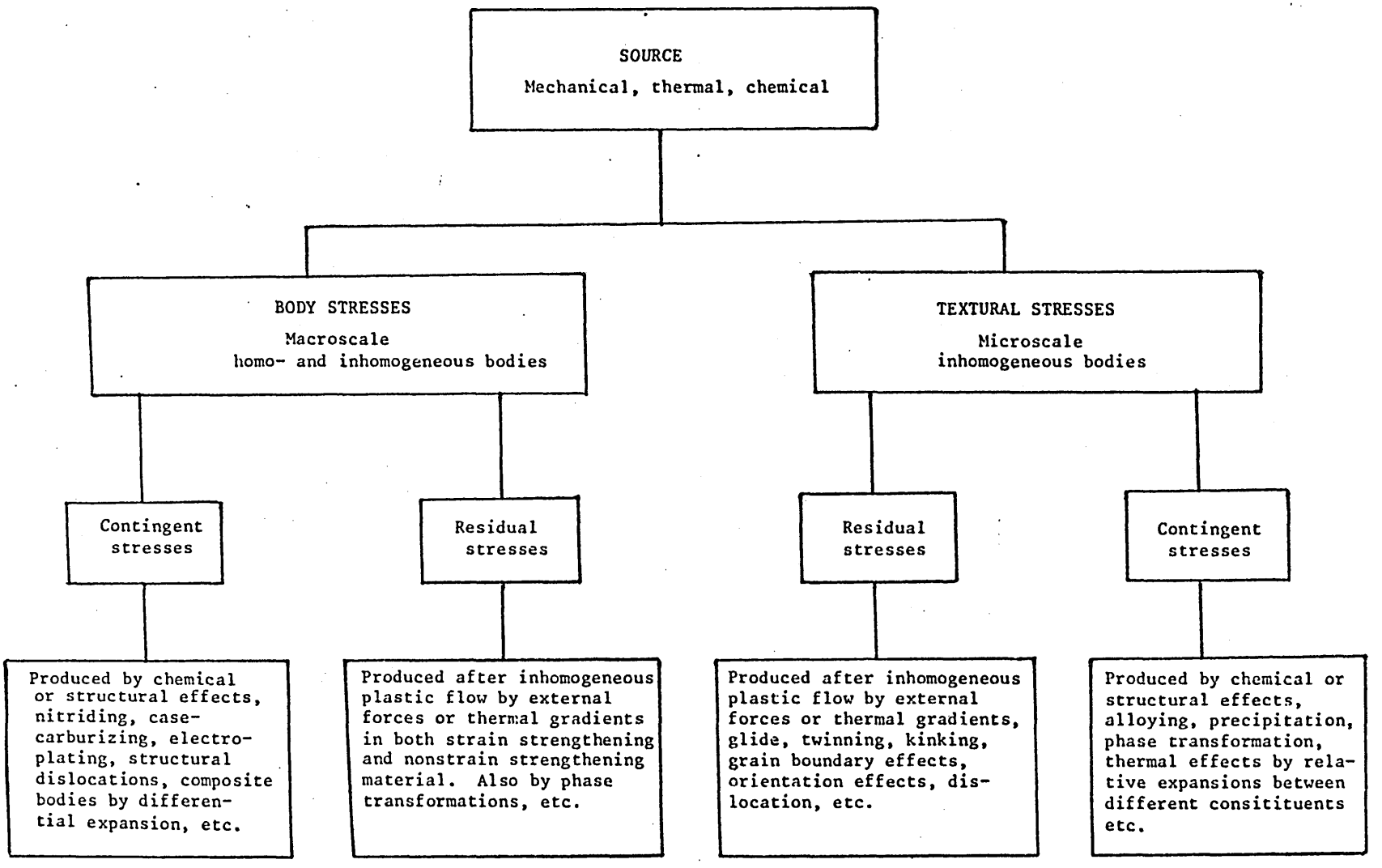
SOURCE
Mechanical, thermal, chemical
BODY STRESSES
Macroscale
homo- and inhomogeneous bodies
TEXTURAL STRESSES
Microscale
inhomogeneous bodies
Contingent stresses
Residual stresses
Residual stresses
Contingent stresses
Produced by chemical or structural effects, nitriding, case-carburizing, electro-plating, structural dislocations, composite bodies by differen-tial expansion, etc.
Produced after inhomogeneous plastic flow by external forces or thermal gradients in both strain strengthening and nonstrain strengthening material. Also by phase transformations, etc.
Produced after inhomogeneous plastic flow by external forces or thermal gradients, glide, twinning, kinking, grain boundary effects, orientation effects, dis-location, etc.
Produced by chemical or structural effects, alloying, precipitation, phase transformation, thermal effects by rela-tive expansions between different consitituents etc.

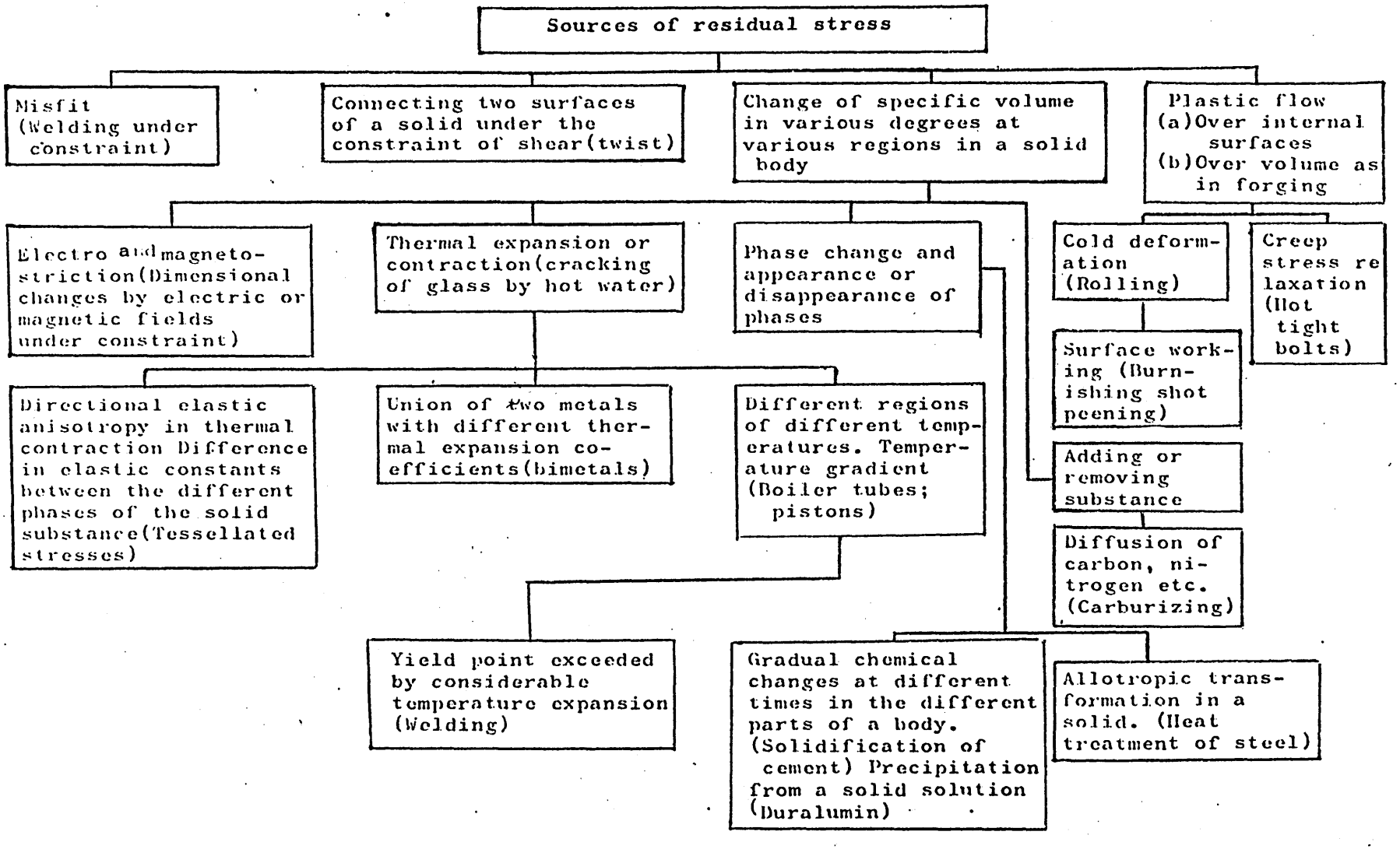
Sources of residual stress
Misfit (Welding under constraint)
Connecting two surfaces of a solid under the constraint of shear(twist)
Change of specific volume in various degrees at various regions in a solid body
Plastic flow (a)Over internal surfaces (b)Over volume as in forging
Electro and magneto-striction(Dimensional changes by electric or magnetic fields under constraint)
Thermal expansion or contraction(cracking of glass by hot water)
Phase change and appearance or disappearance of phases
Cold deformation (Rolling)
Creep stress relaxation (Hot tight bolts)
Surface working (Burnishing shot peening)
Directional elastic anisotropy in thermal contraction Difference in elastic constants between the different phases of the solid substance(Tessellated stresses)
Union of two metals with different thermal expansion coefficients(bimetals)
Different regions of different temperatures. Temperature gradient (Boiler tubes; pistons)
Adding or removing substance
Diffusion of carbon, nitrogen etc. (Carburizing)
Yield point exceeded by considerable temperature expansion (Welding)
Gradual chemical changes at different times in the different parts of a body. (Solidification of cement) Precipitation from a solid solution (Duralumin)
Allotropic transformation in a solid. (Heat treatment of steel)

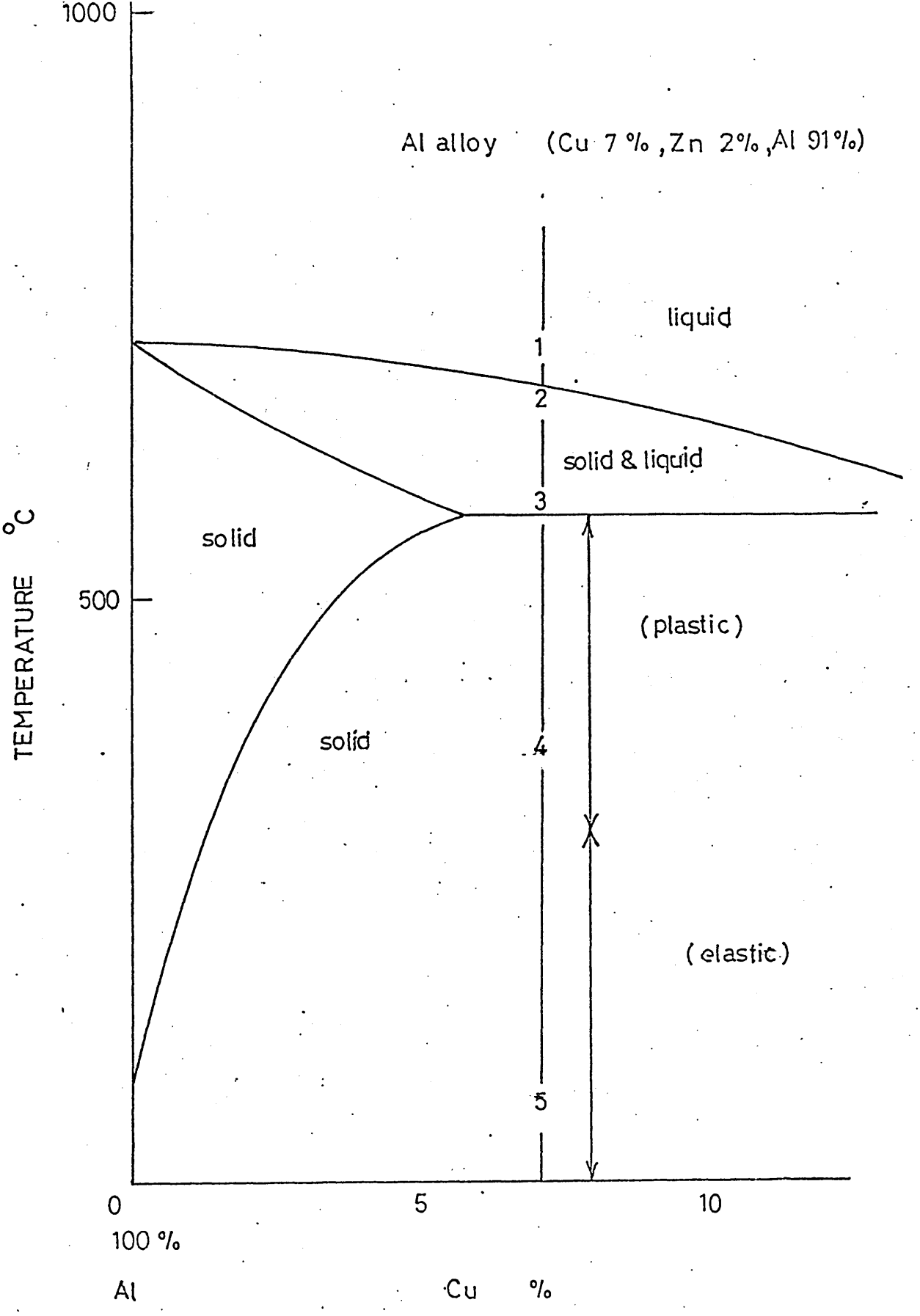
Al alloy (Cu 7 %, Zn 2%, Al 91%)
liquid
1
2
solid & liquid
3
solid
500
(plastic)
solid
4
(elastic)
5
1000
TEMPERATURE °C
0
5
10
100 %
Al
Cu %

FIGURE 4: Changes in Stress-strain curves with temperature (Flinn[36])

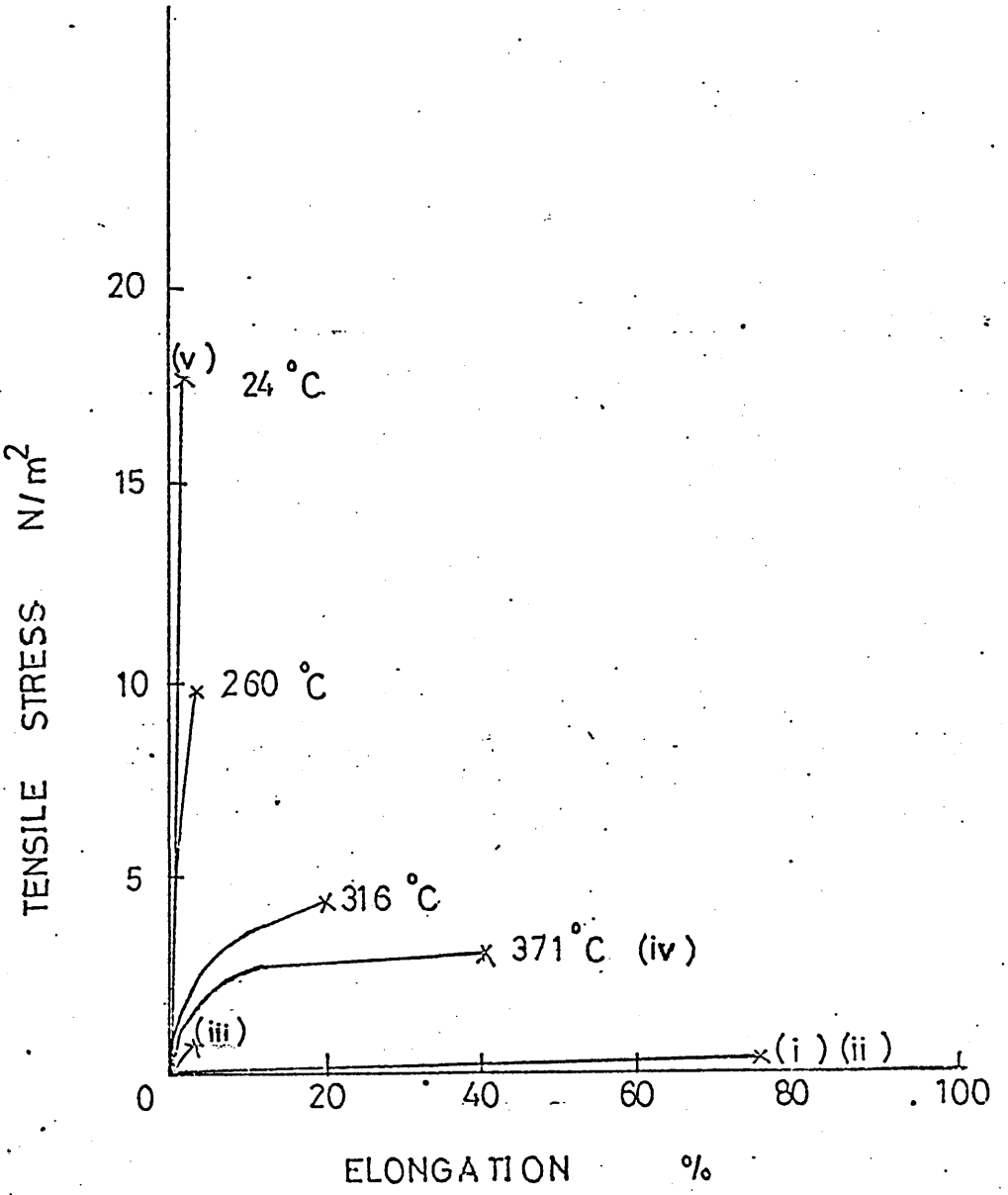
TENSILE STRESS N/m²
20
15
10
5
0
(v)
24 °C
260 °C
316 °C
371 °C (iv)
(iii)
(i) (ii)
20
40
60
80
100
ELONGATION %

FIGURE 5: Development of stresses through differential contraction

(a) Stress grid casting
(b) Schematic plot of stresses in thick and thin members illustrating change in sign during cooling (Parkins and Cowans[27])

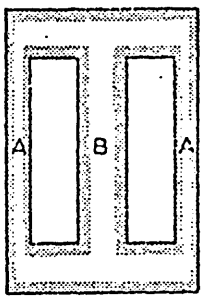
A
B
A

(a)

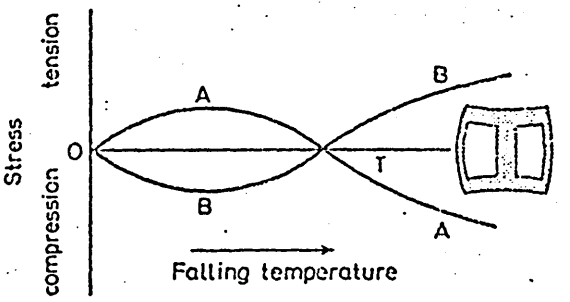
Stress
tension
compression
O
A
B
B
A
T
Falling temperature

(b)

FIGURE 6: Residual stress/maximum temperature relationship

(a) Aluminium alloy frame works
(b) Cast iron frame works

(Parkins and Cowans[27])

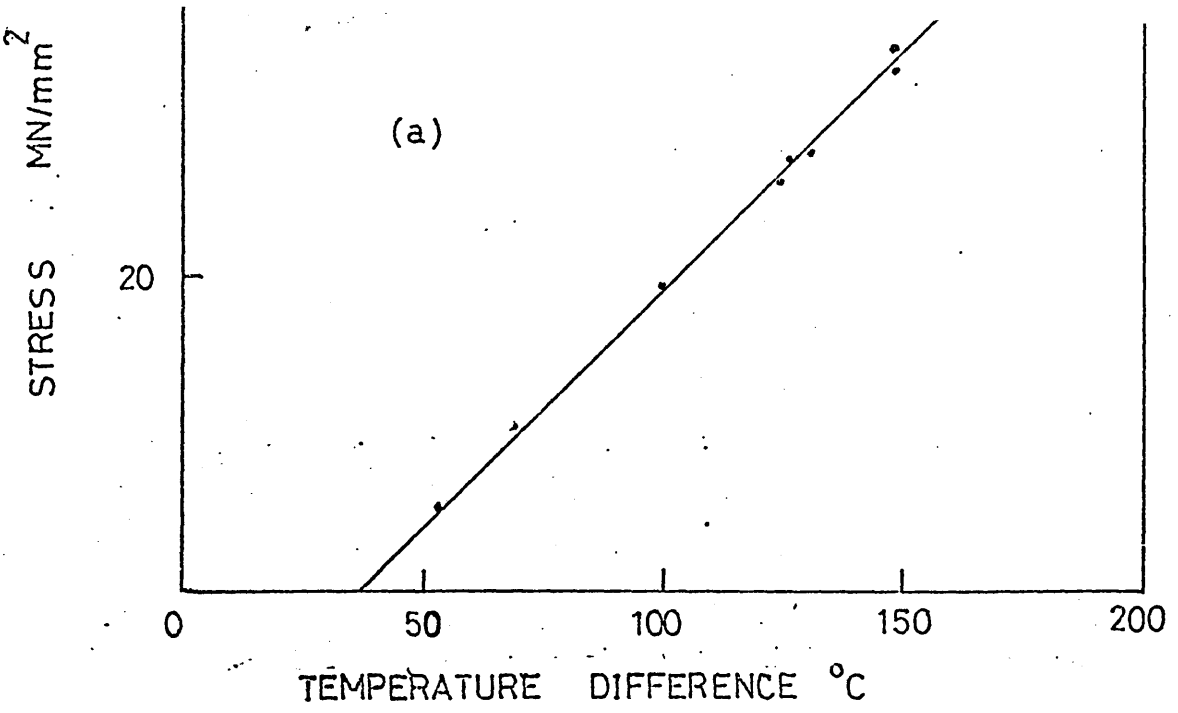
(a)
STRESS MN/mm^2
20
0
50
100
150
200
TEMPERATURE DIFFERENCE °C

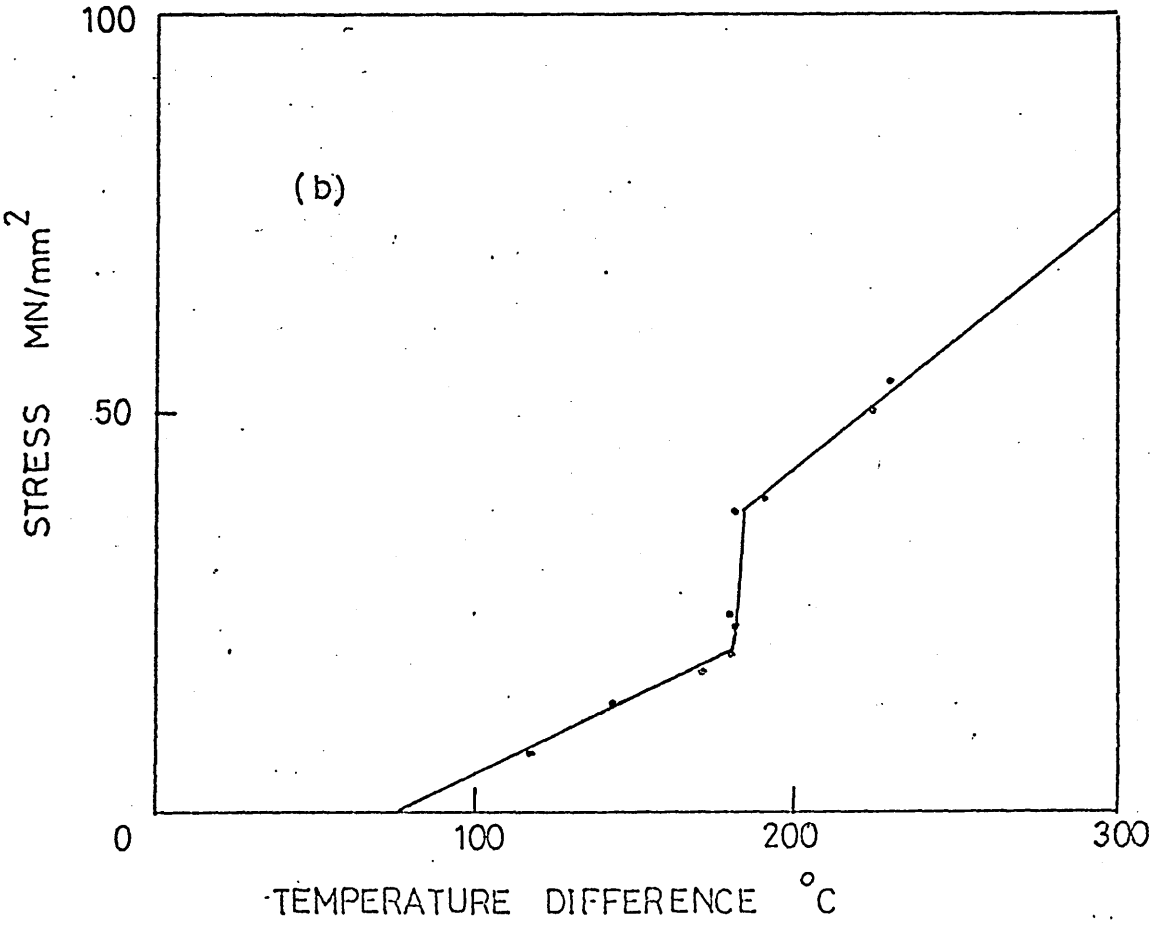
(b)
STRESS MN/mm^2
100
50
0
100
200
300
TEMPERATURE DIFFERENCE °C

FIGURE 7: Relationship between stress in centre member and ratio of cross-section of centre and outer members

A/A_o = Ratio of crossectional areas

(Dodd[26])

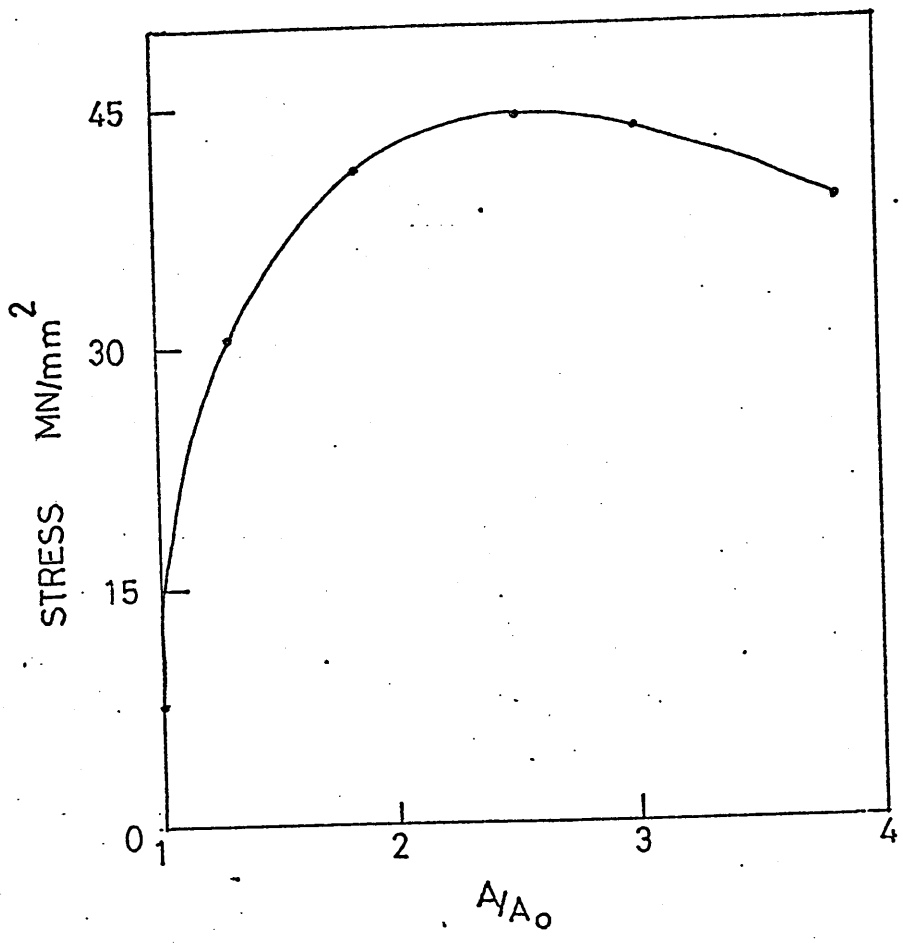
45
30
15
0
STRESS MN/mm 2
1
2
3
4
A/Ao

FIGURE 8: Effects of temperature and time on relief of residual stresses in steel castings (Jelm and Herris[55])

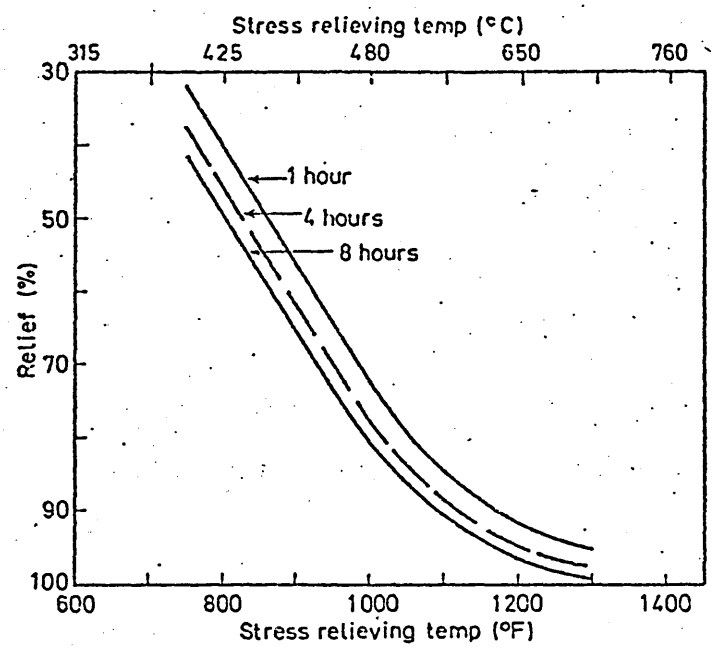
Stress relieving temp (°C)
315
425
480
650
760
30
50
70
90
100
Relief (%)
1 hour
4 hours
8 hours
600
800
1000
1200
1400
Stress relieving temp (°F)

FIGURE 9: Stress relief heat treatments of two national codes (Saunders[57])

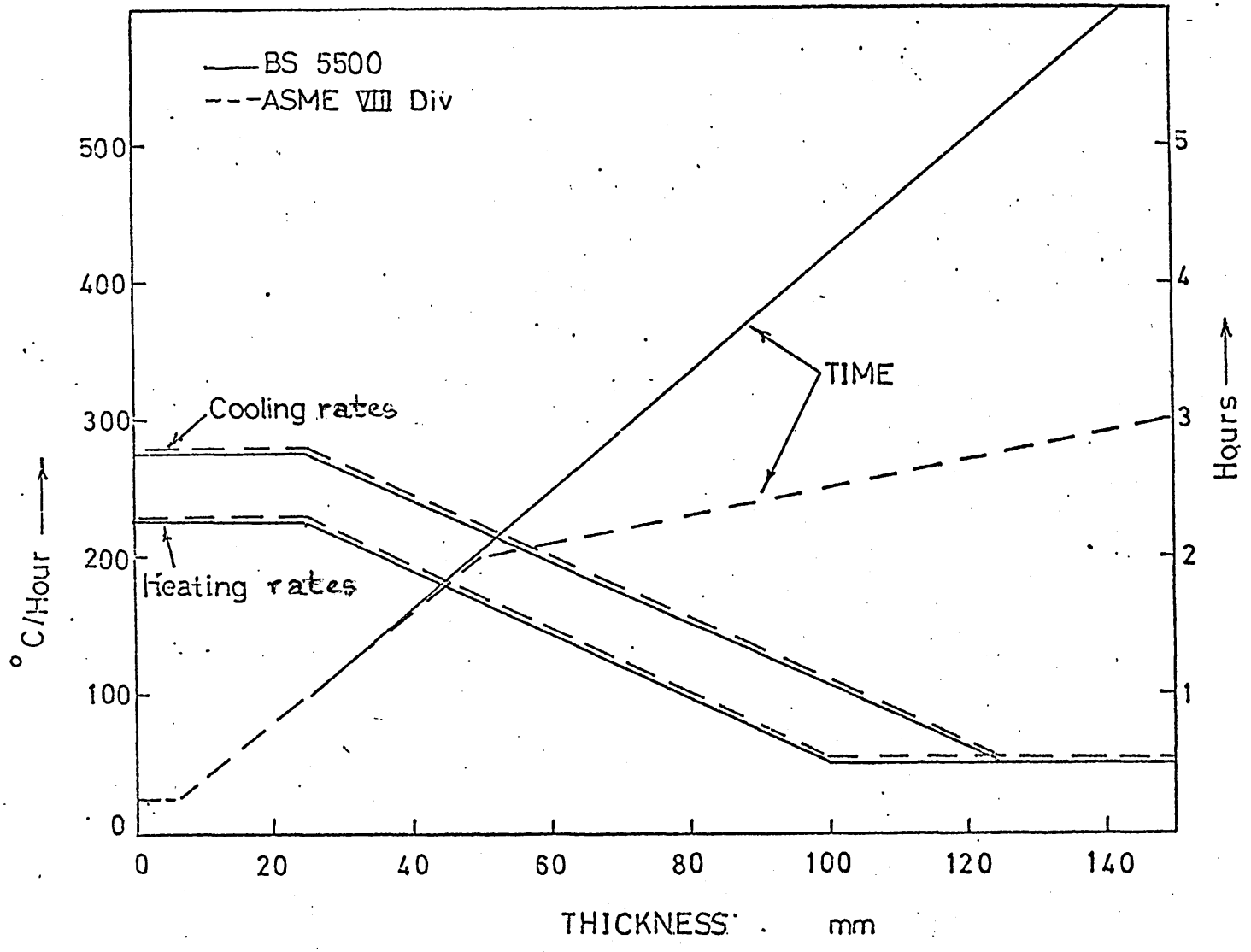
BS 5500
ASME VIII Div
Cooling rates
Heating rates
TIME
°C/Hour
Hours
THICKNESS mm
0
100
200
300
400
500
1
2
3
4
5
0
20
40
60
80
100
120
140

FIGURE 10: Strain measuring device.

1. Paxolin handle, 2. Steel body,
3. Fixed Pin, 4. Movable pin
(Parlane[71])

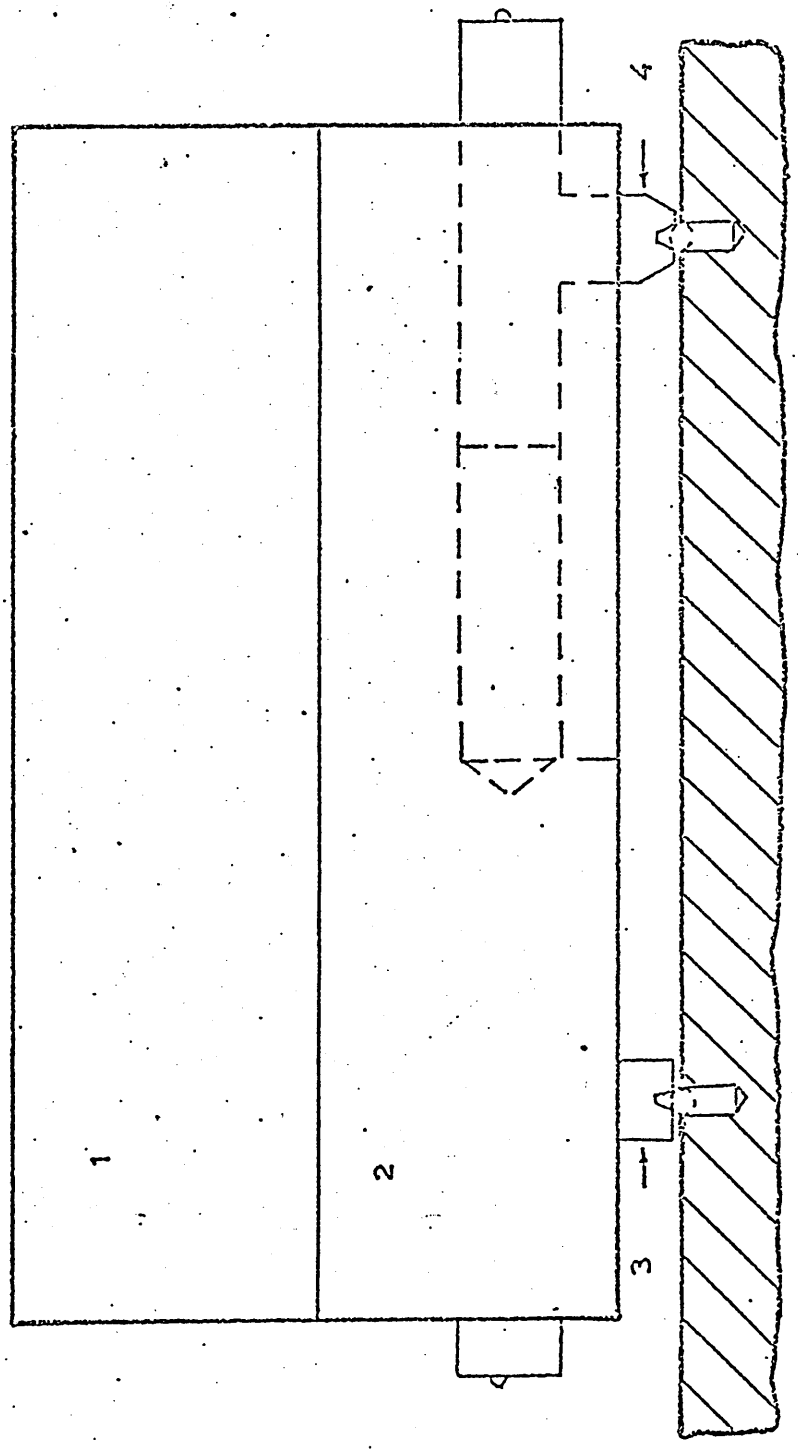
1
2
3
4

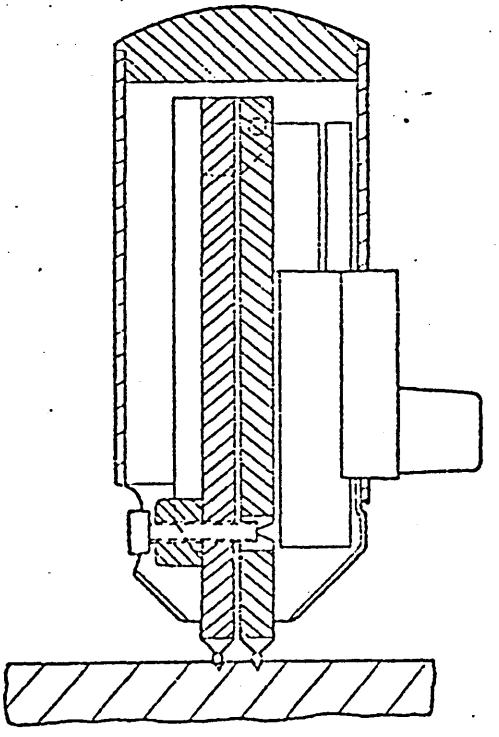

FIGURE 12: Cutting deflection methods

(a) for circumferential stress
(b) for longitudinal stress
(c) for irregular section (neglects transverse stresses)
(d) rod or bar
(e) rolled sheet or plate

(Andrews[10])

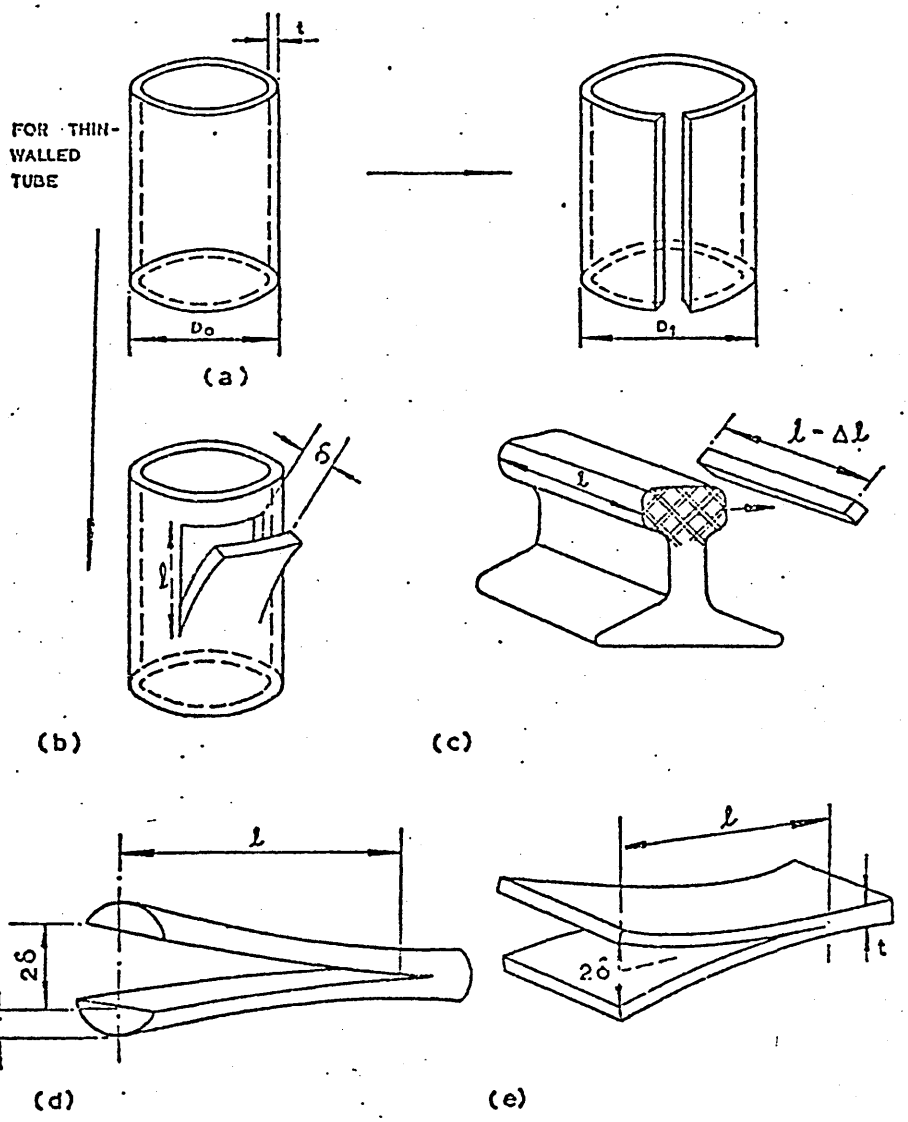
FOR THIN-WALLED TUBE
t
D_0
D_1
(a)
δ
l
(b)
l
l - Δl
(c)
l
2δ
r
(d)
l
2δ
t
(e)

FIGURE 13: Tie bar sectioning method

l = tie bar length before sectioning

l'= tie bar length after sectioning

(Chijiiwa[30])

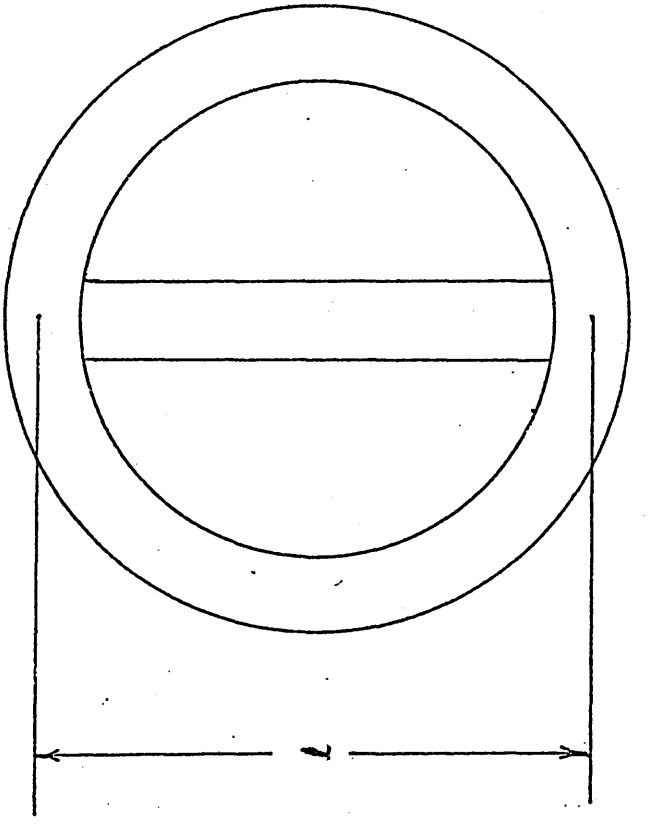

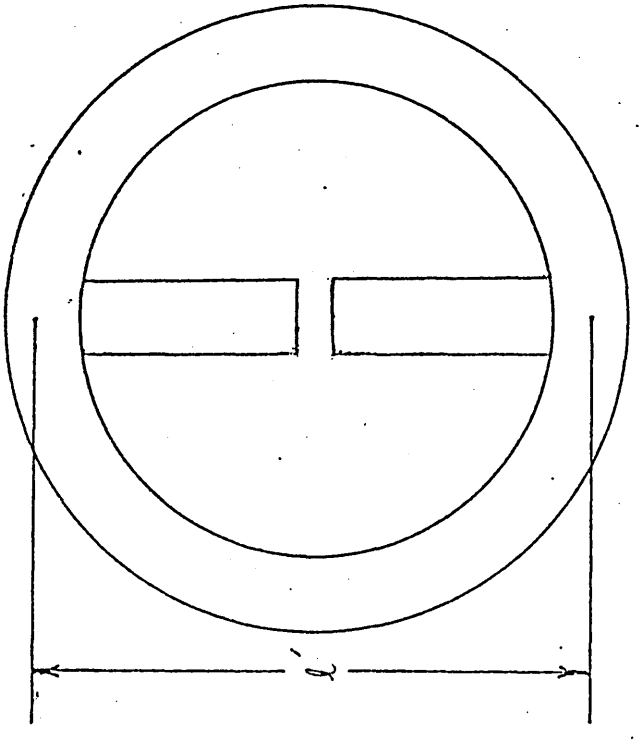

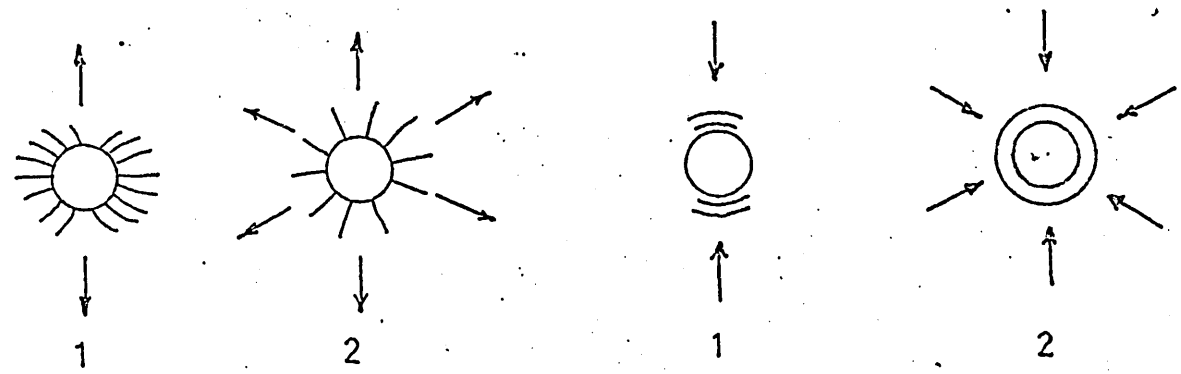
1
2
TENSION
1
2
COMPRESSION

FIGURE 15: Effect of plasticity at edge of hole (Beaney and Procter[88])

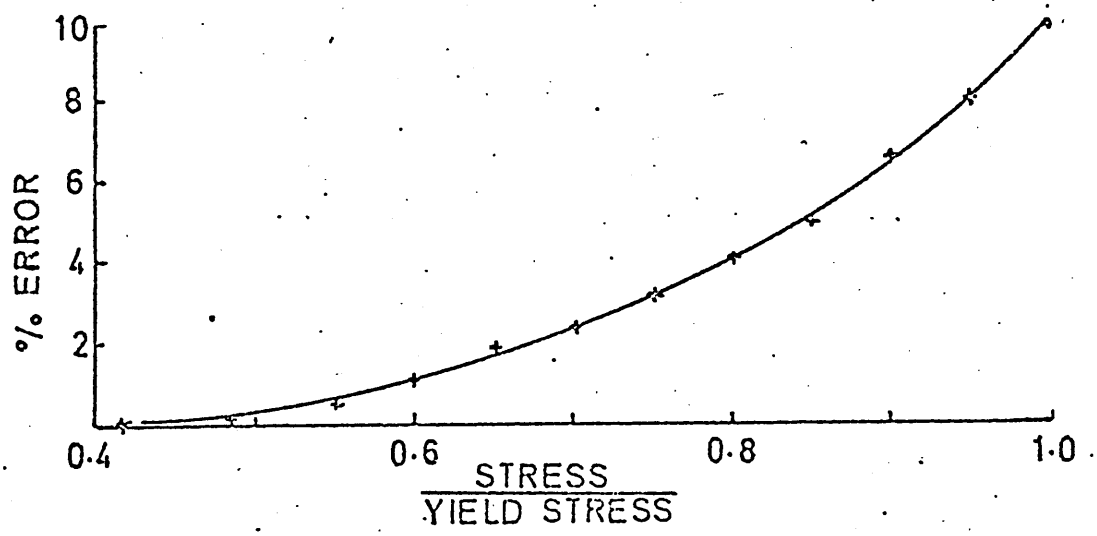
10
8
6
4
2
% ERROR
0·4
0·6
0·8
1·0
STRESS
YIELD STRESS

FIGURE 16: Variation of 1/K1 with Hole size (Beaney and Procter[88])

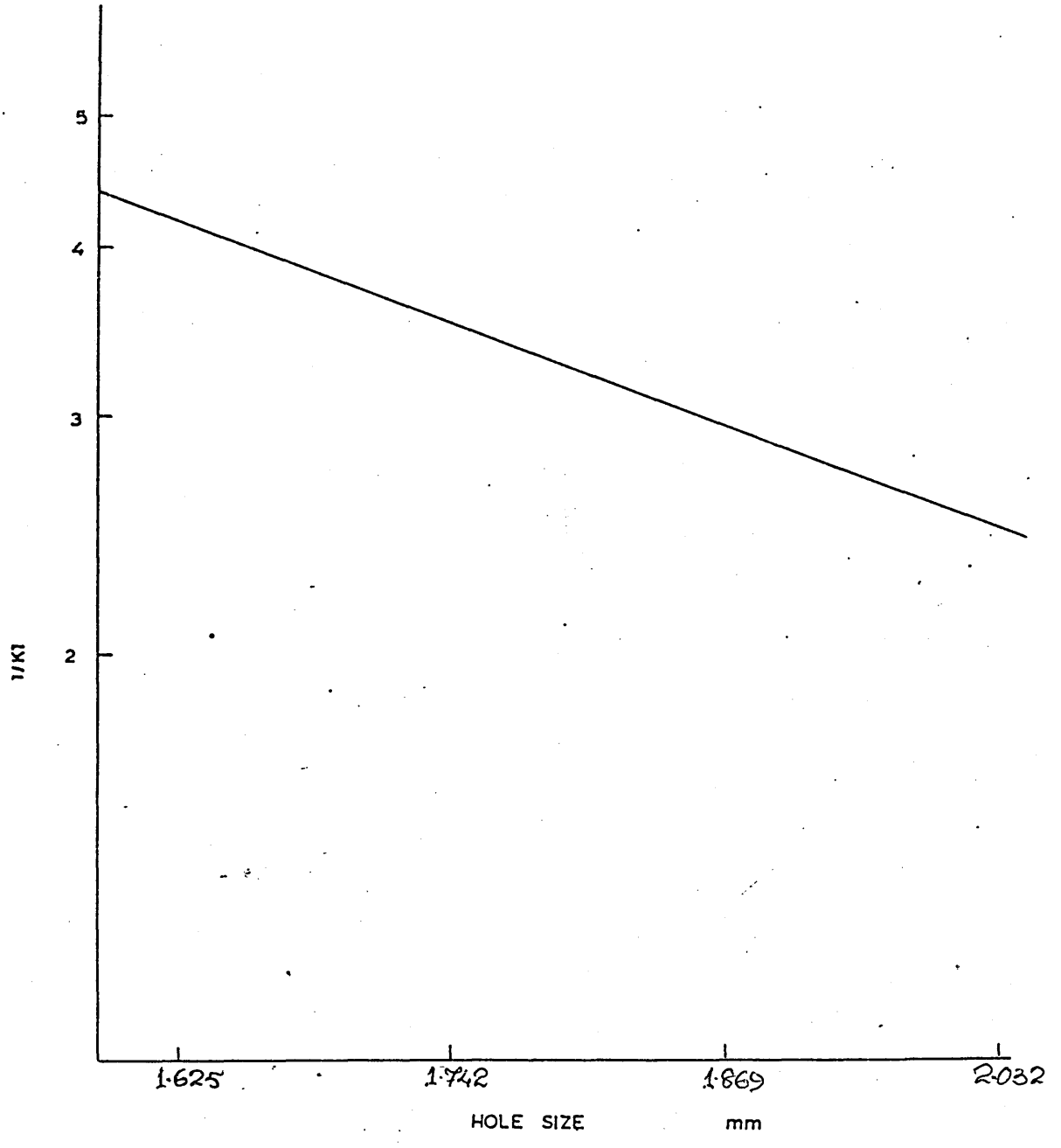
5
4
3
2
1/K1
1·625
1·742
1·869
2·032
HOLE SIZE
mm

FIGURE 17: Principle of back reflection technique for stress-strain measurement using Xray diffraction. Angle 2θ is function of lattice strain. 1. film (or diffractometer); 2. diffracted ray; 3. reflecting planes of atoms

(Parlane[71])

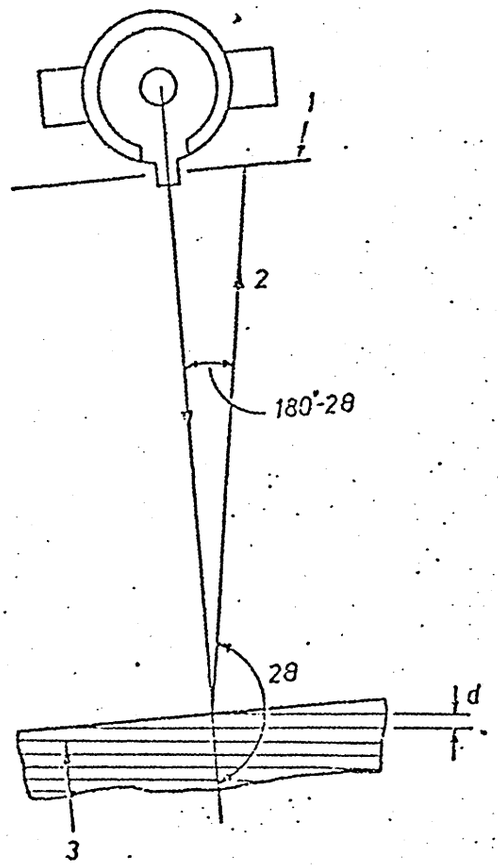
1
2
180°-2θ
2θ
d
3

FIGURE 18: Theta ring
a = 5,10,15,20,25 and 30
All dimensions are in millimeters

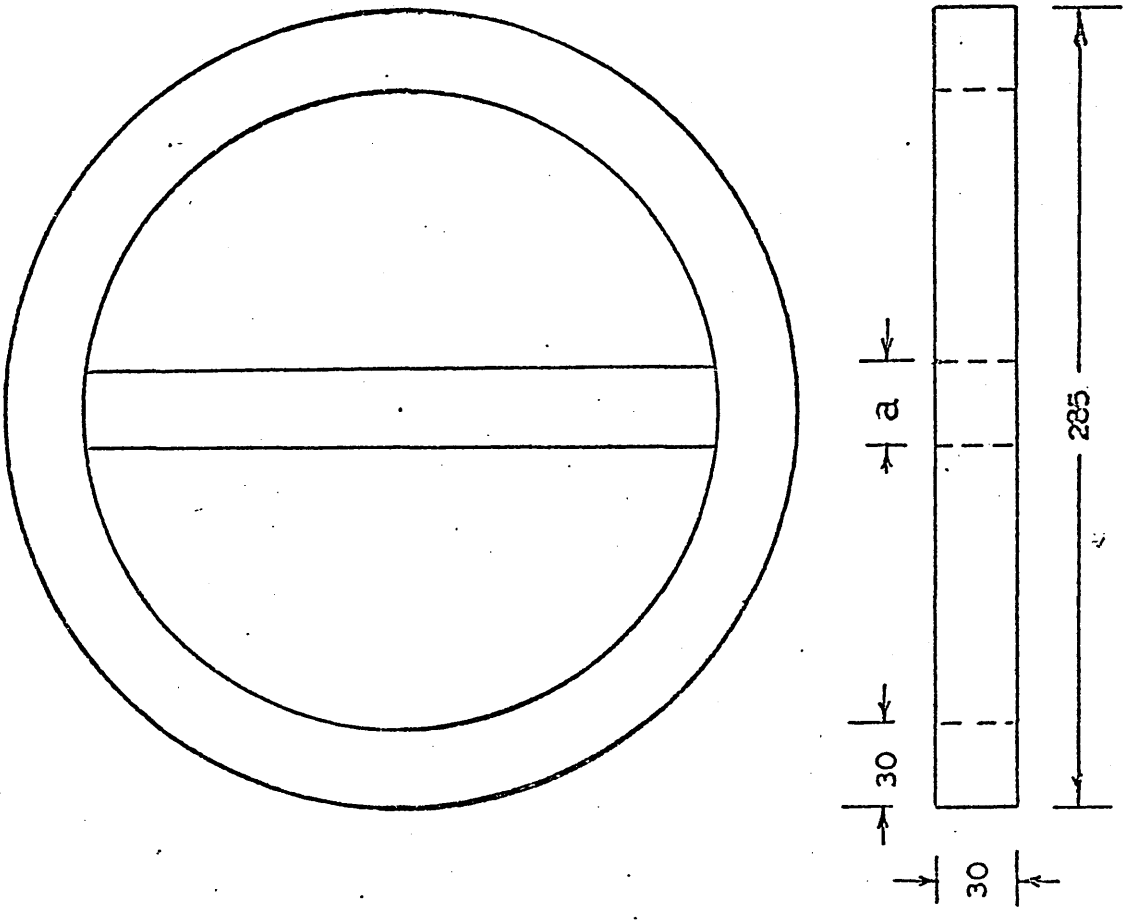
a
285
30
30

FIGURE 19: Relation of casting shape factor to minimum effective riser volume expressed as a fraction of casting volume

(Beeley[37])

FIGURE 20: Caine's curve for minimum feeder head volume based on freezing ratio

(Beeley[37])

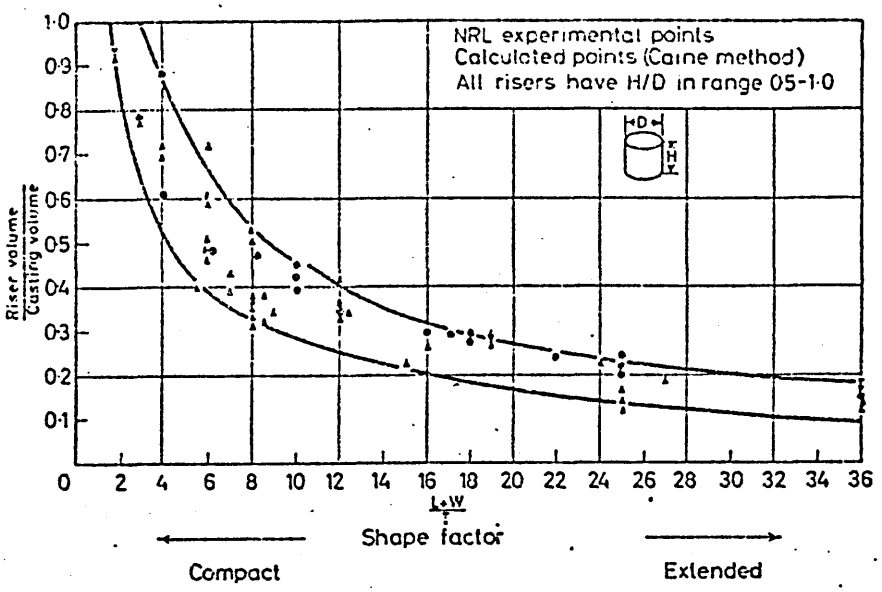
NRL experimental points
Calculated points (Caine method)
All risers have H/D in range 05-1·0
H
D
Riser volume / Casting volume
1·0
0·9
0·8
0·7
0·6
0·5
0·4
0·3
0·2
0·1
0 2 4 6 8 10 12 14 16 18 20 22 24 26 28 30 32 34 36
L+W / T
Shape factor
Compact
Extended

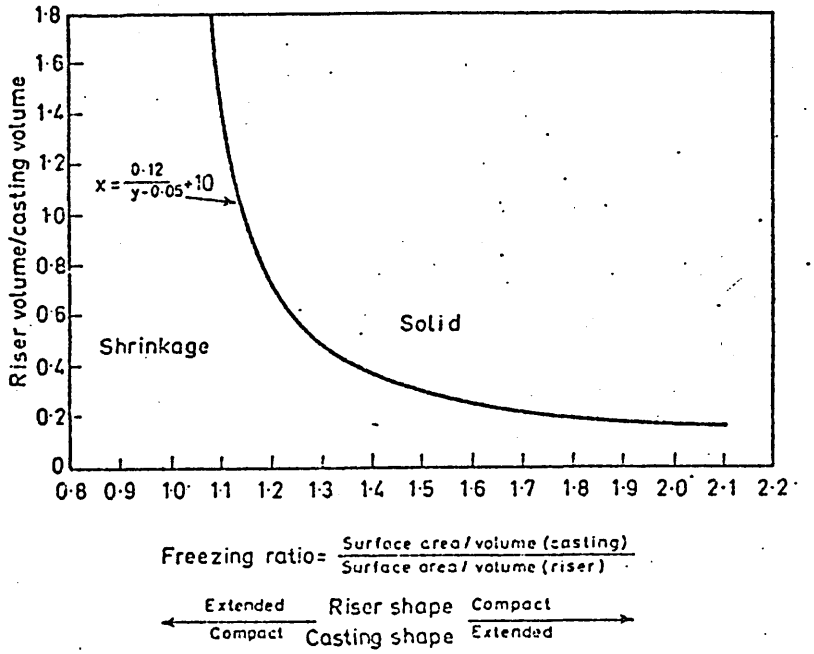
Riser volume/casting volume
1·8
1·6
1·4
1·2
1·0
0·8
0·6
0·4
0·2
0
x = 0·12 / (y − 0·05) + 1·0
Shrinkage
Solid
0·8 0·9 1·0 1·1 1·2 1·3 1·4 1·5 1·6 1·7 1·8 1·9 2·0 2·1 2·2
Freezing ratio = Surface area / volume (casting) / Surface area / volume (riser)
Extended
Compact
Riser shape
Casting shape
Compact
Extended

FIGURE 21; Location of Thermocouples and Strain gauges for Casting stage

T: Thermocouple position
S: Strain gauge position

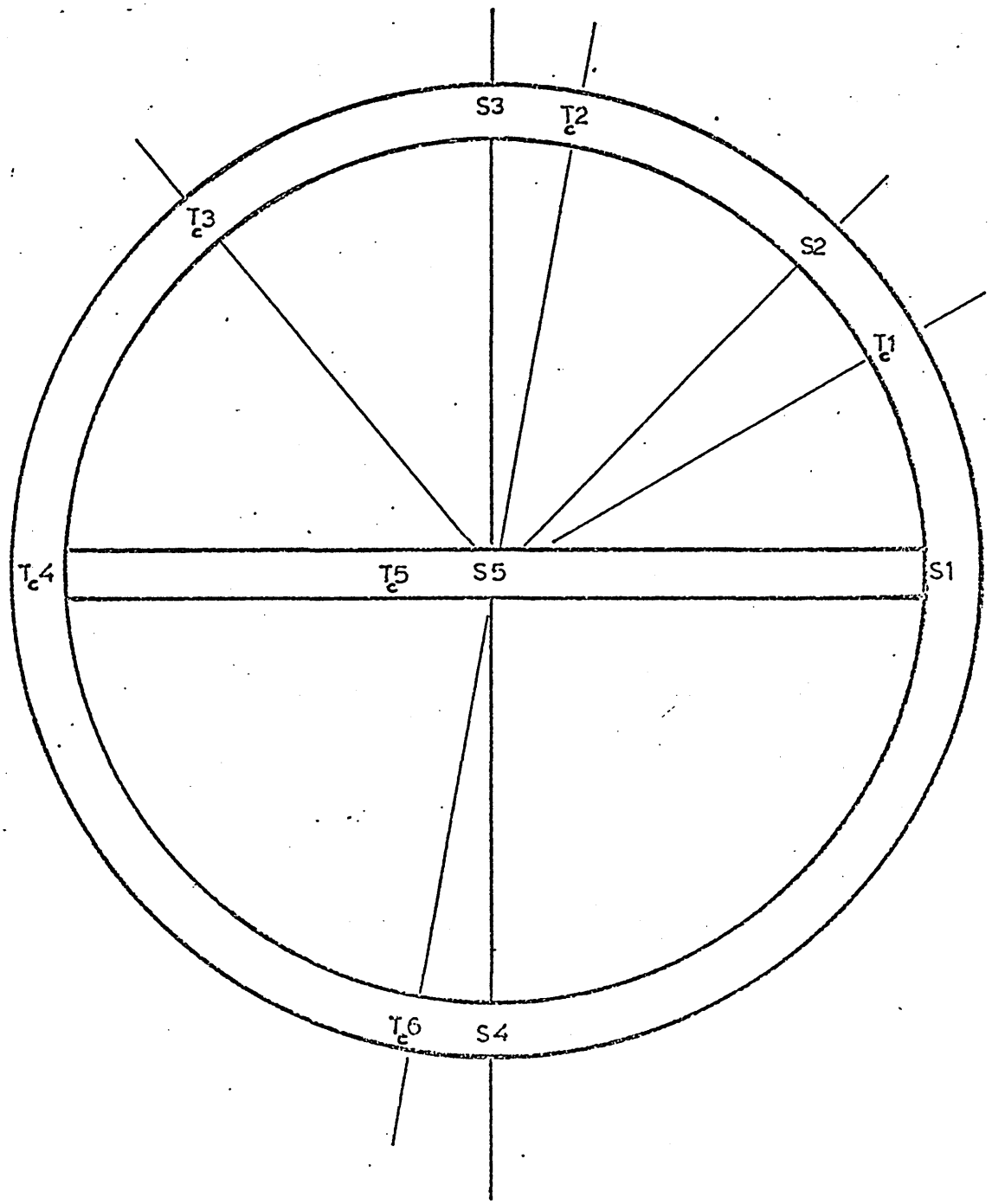
S3
T_c2
T_c3
S2
T_c1
T_c4
T_c5
S5
S1
T_c6
S4

FIGURE 22: Location of Thermocouples in the Sand mould

T_s: Thermocouple position

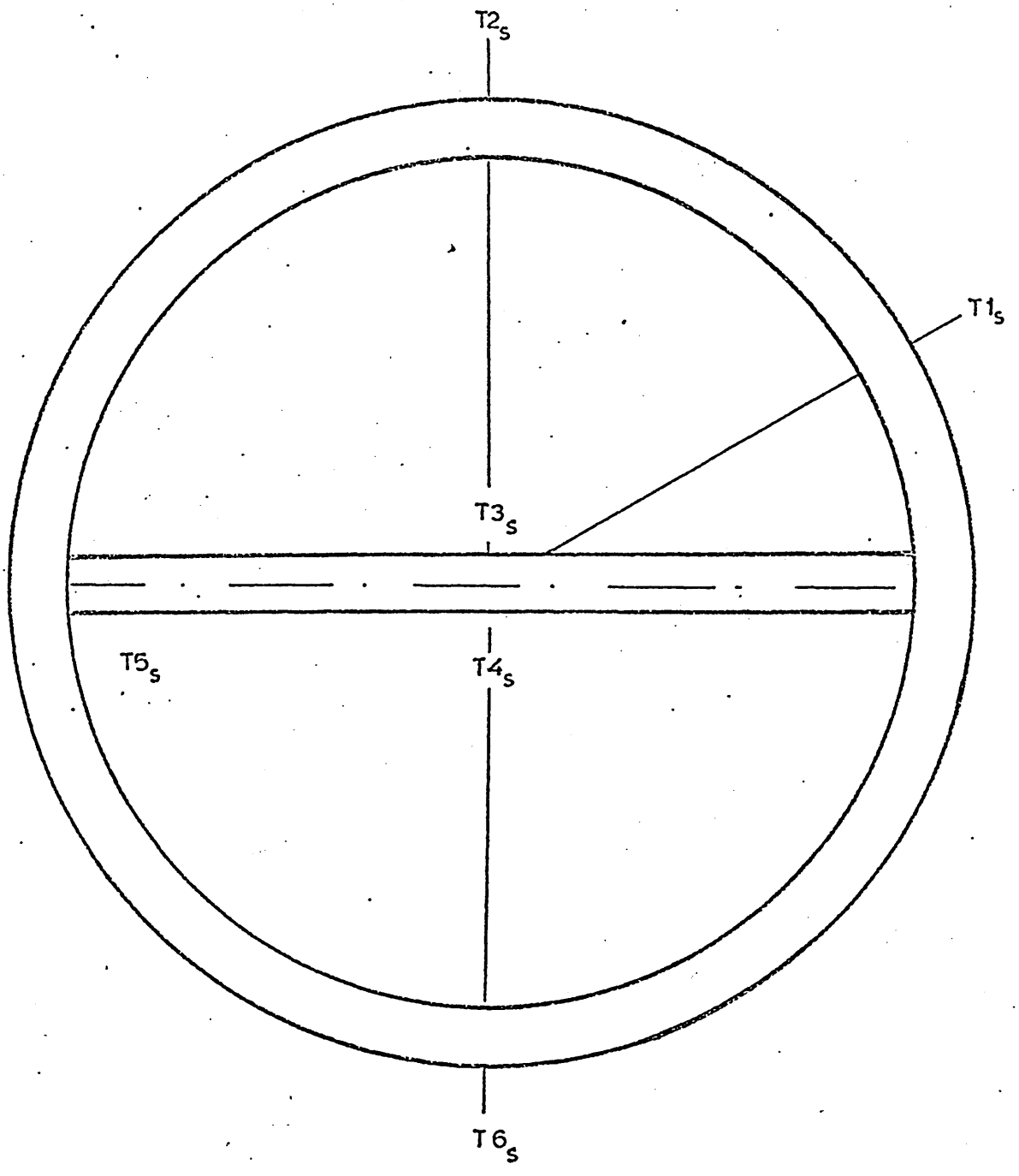
T2s
T1s
T3s
T5s
T4s
T6s

FIGURE 23: Location of Thermocouples and Strain gauges for Heat Treatment stage

T: Thermocouple position
S: Strain gauge position

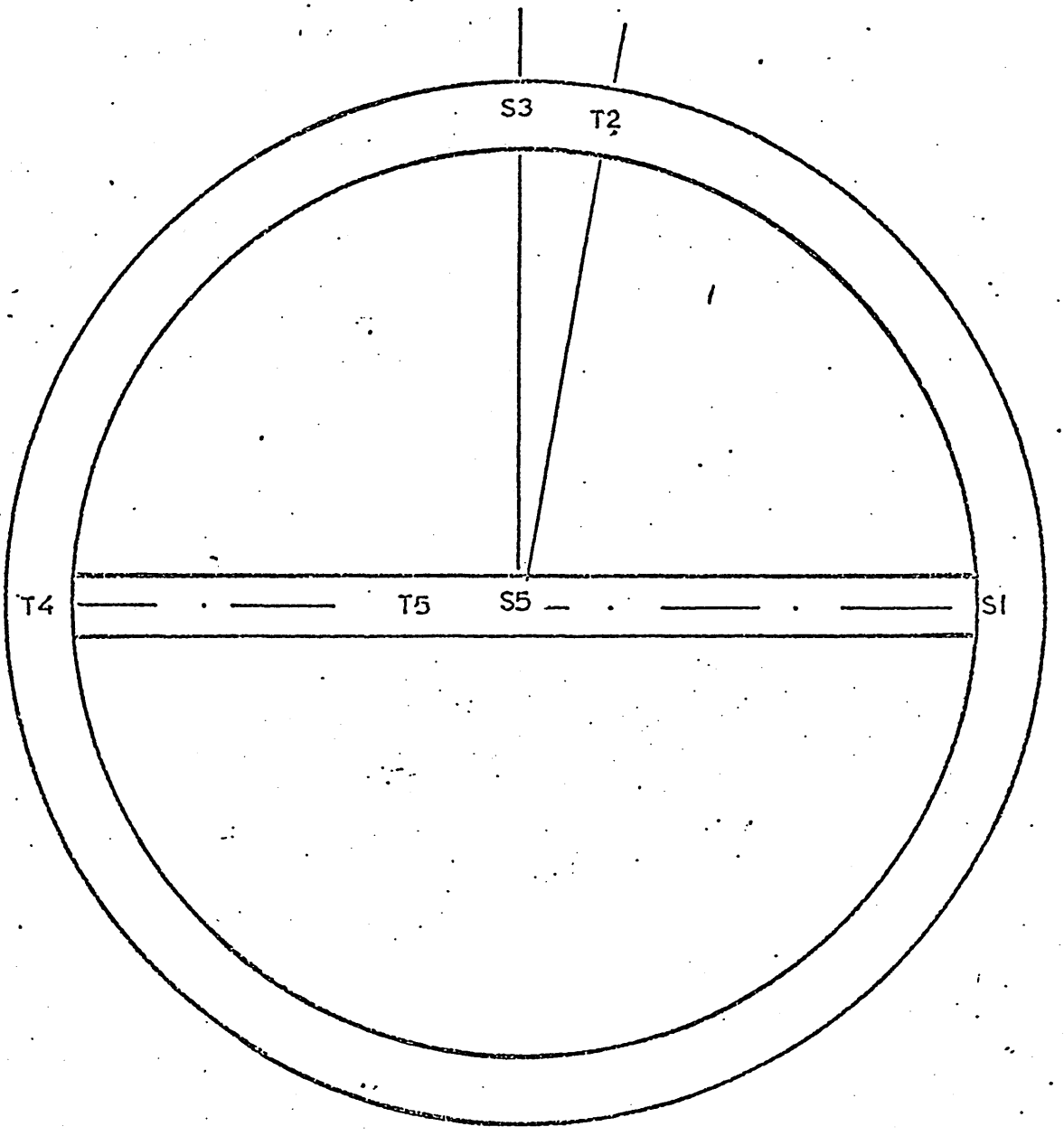
S3
T2
T4
T5
S5
S1

FIGURE 24: Layout of scribed lines for Runner sectioning method.

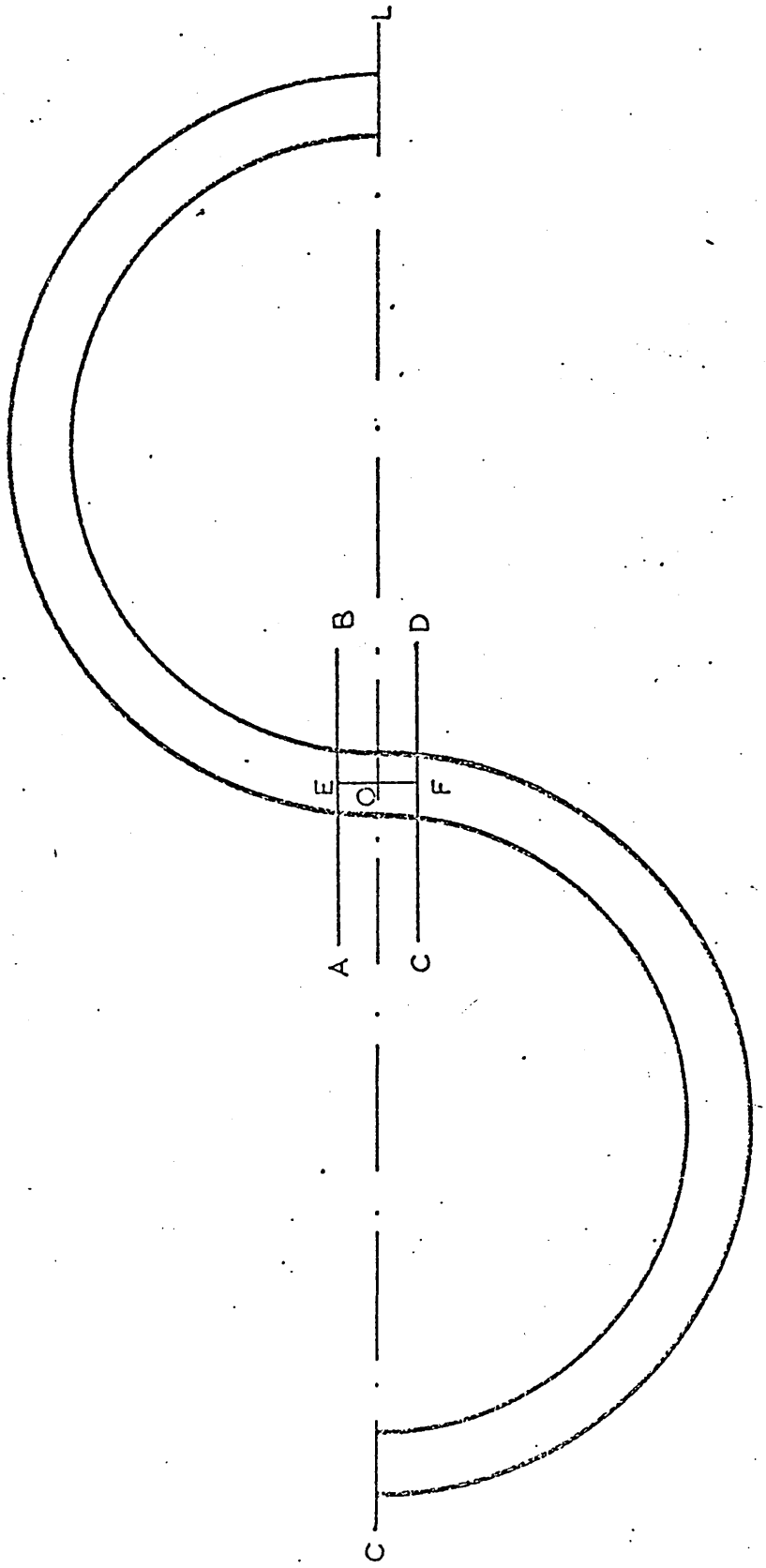
L
B
D
E
O
F
A
C
C

FIGURE 25: Rectangular rosette for residual stress measurement.

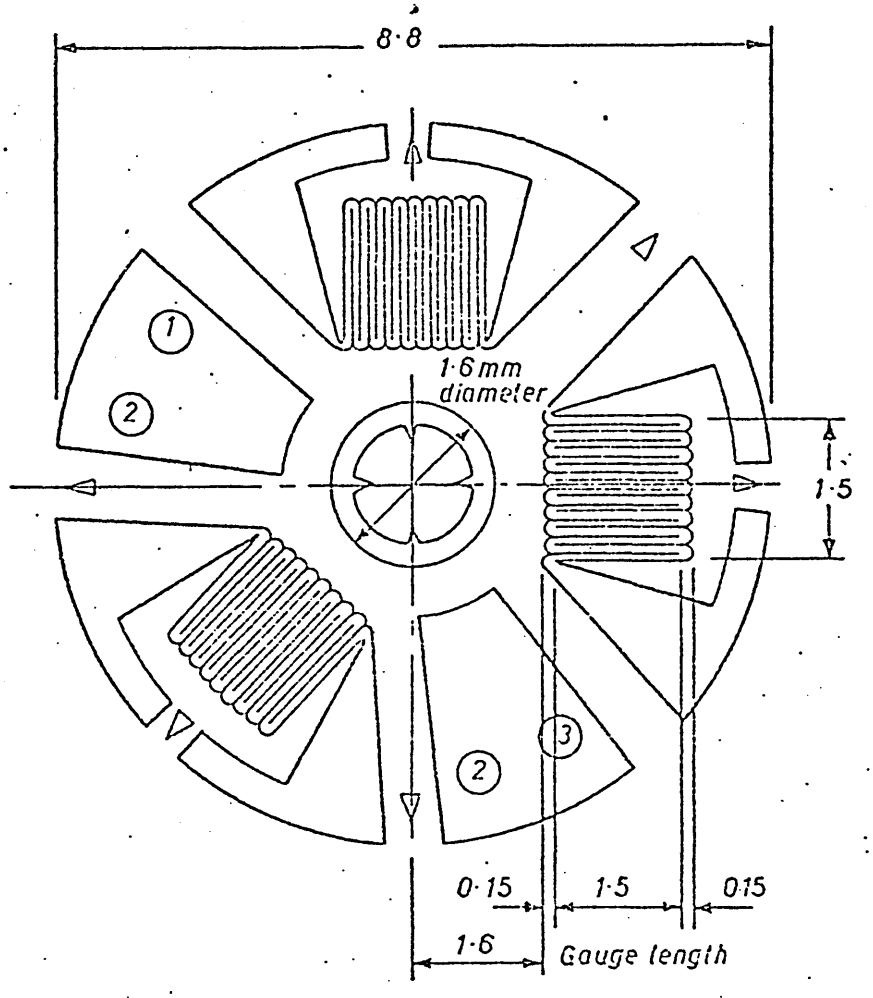
8·8
1·6 mm
diameter
1·5
1
2
2
3
0·15
1·5
0·15
1·6
Gauge length

FIGURE 26: Specimen used in Calibration tests
All dimensions in millimeters

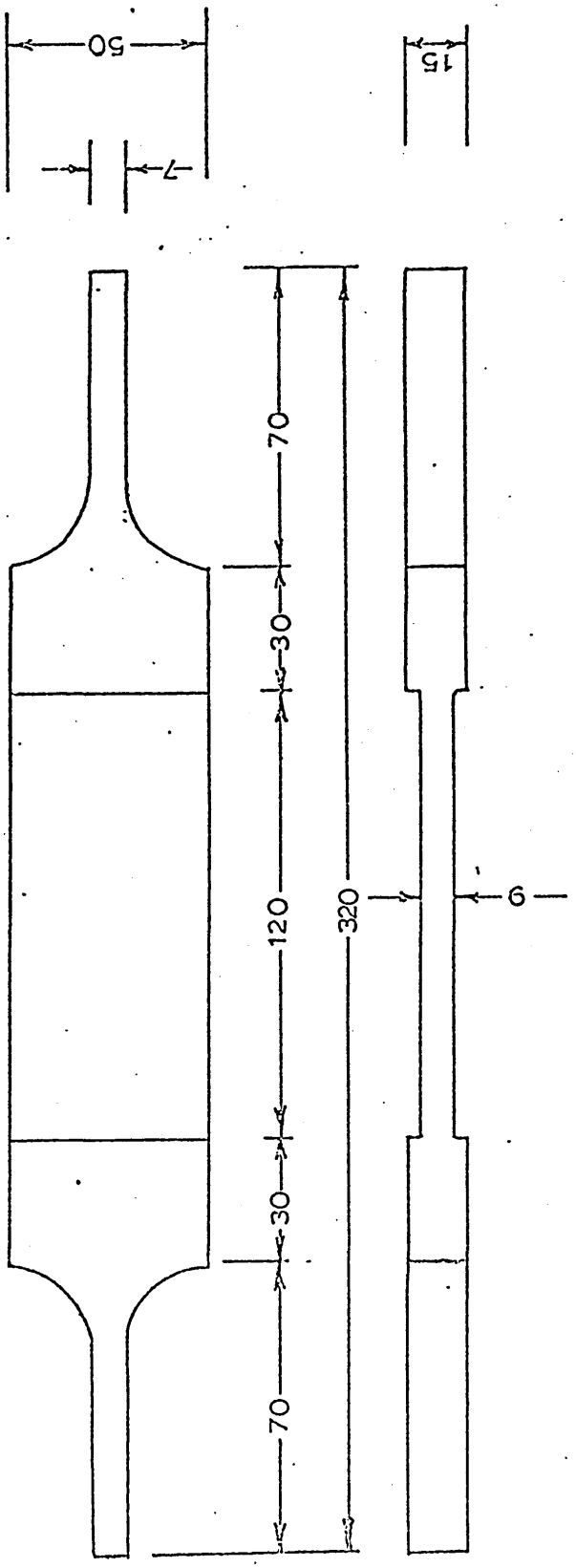
50
7
15
70
30
120
30
70
320
6

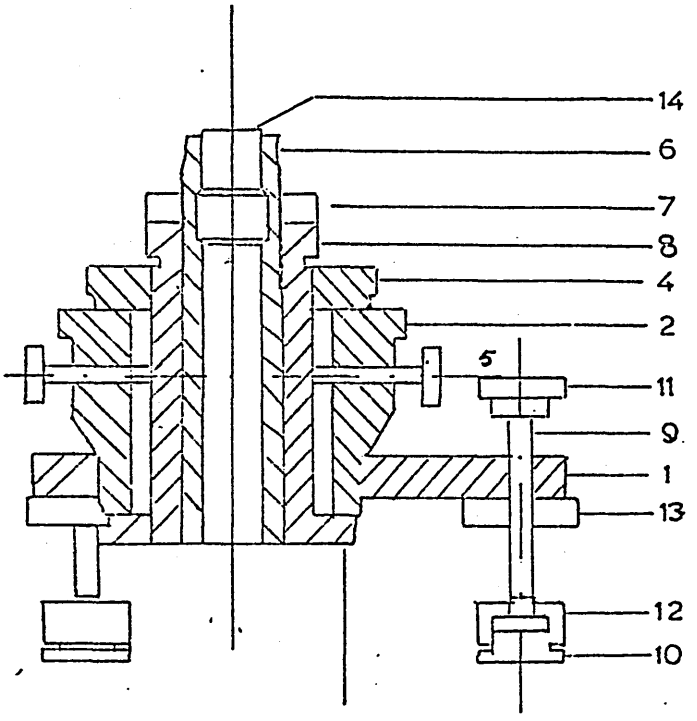
14
6
7
8
4
2
5
11
9
1
13
12
10
3

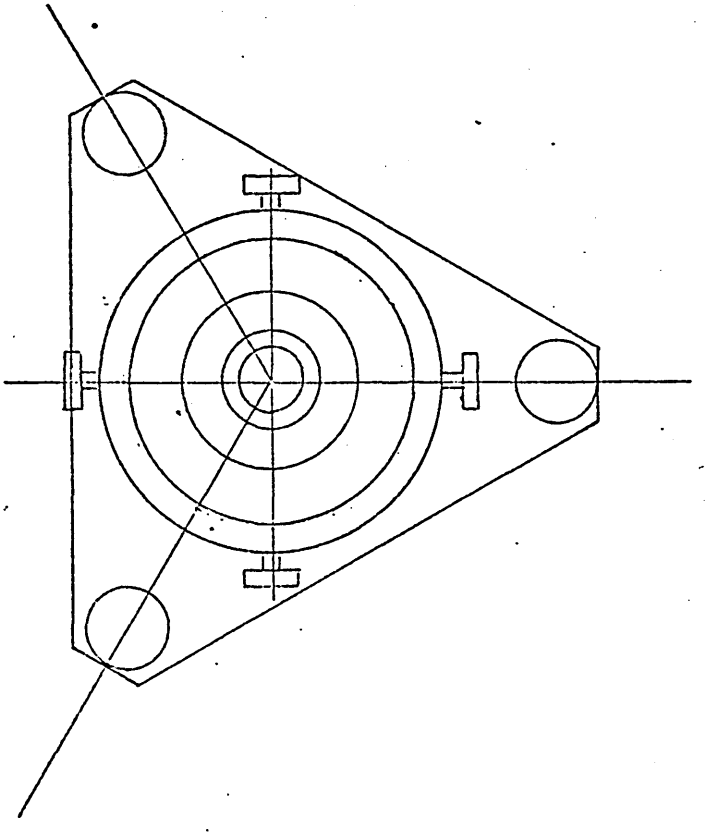

FIGURE 28: Arrangement of jig with drilling mandrell in position

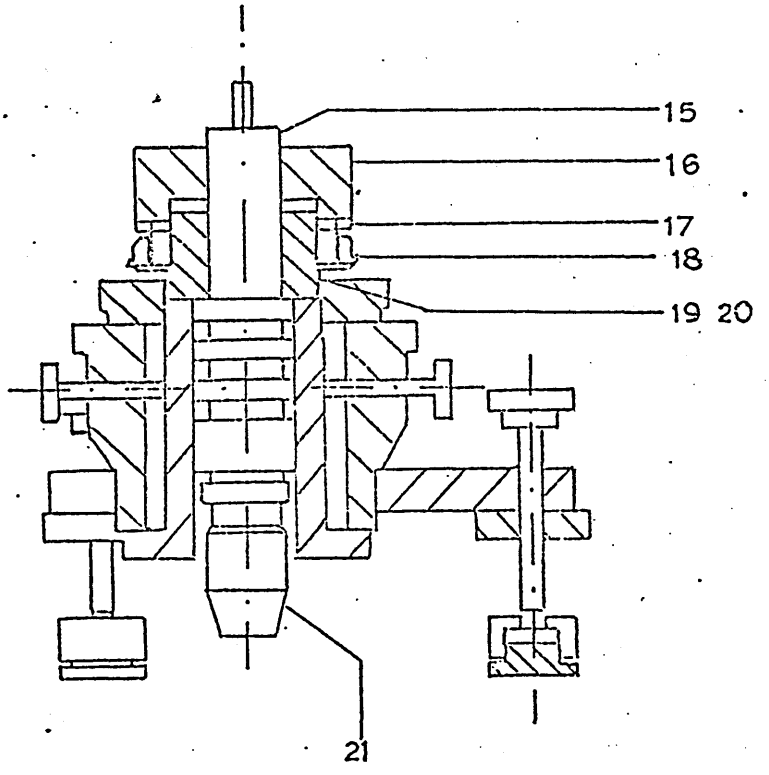
15
16
17
18
19 20
21

FIGURE 29: Residual stresses induced in hand and machine prepared surface for installation of strain gauge.

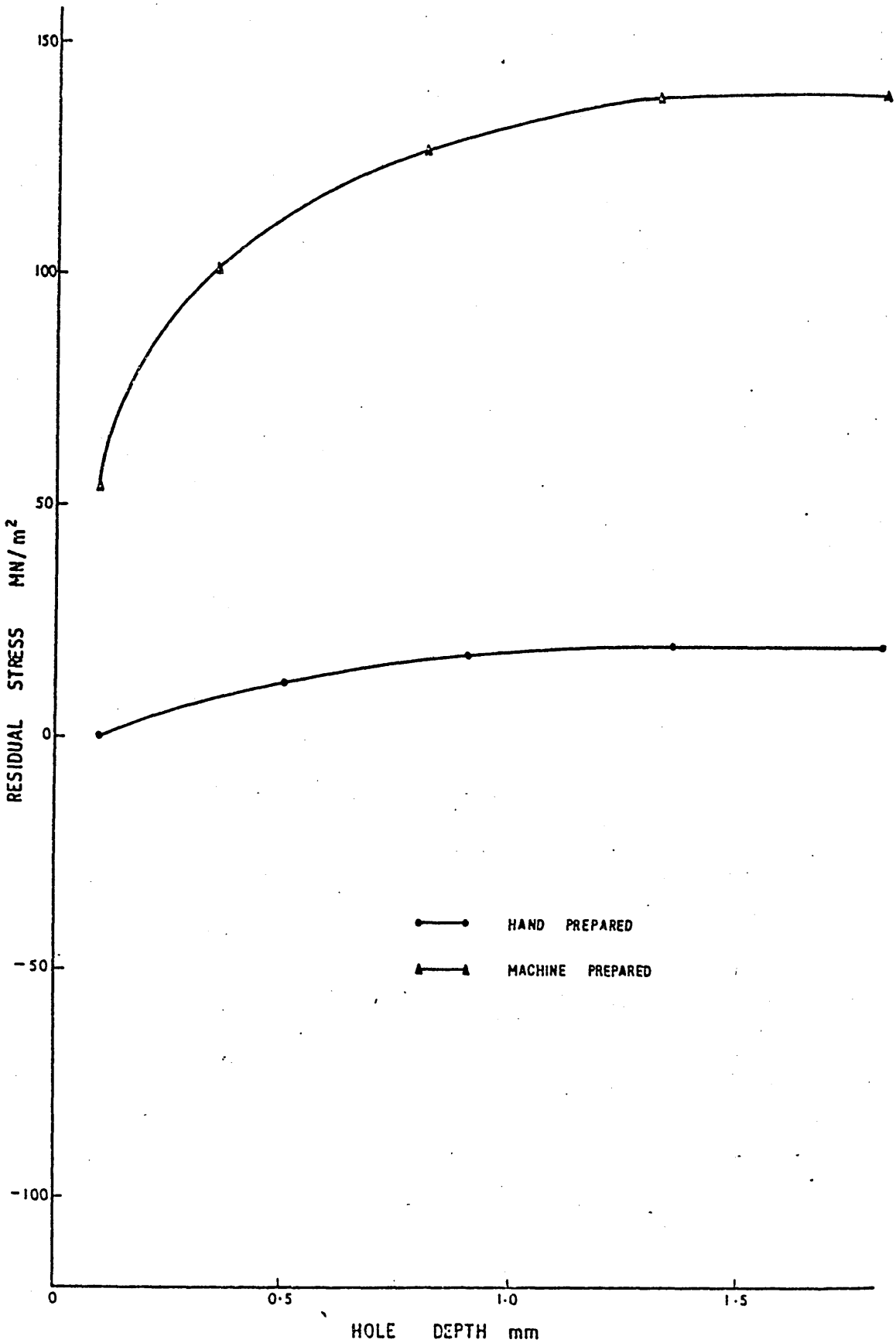
150
100
50
0
-50
-100
RESIDUAL STRESS MN/m²
HAND PREPARED
MACHINE PREPARED
0
0·5
1·0
1·5
HOLE DEPTH mm

FIGURE 30: An outline of Experimental procedure for determining Residual Stresses for Casting stage.

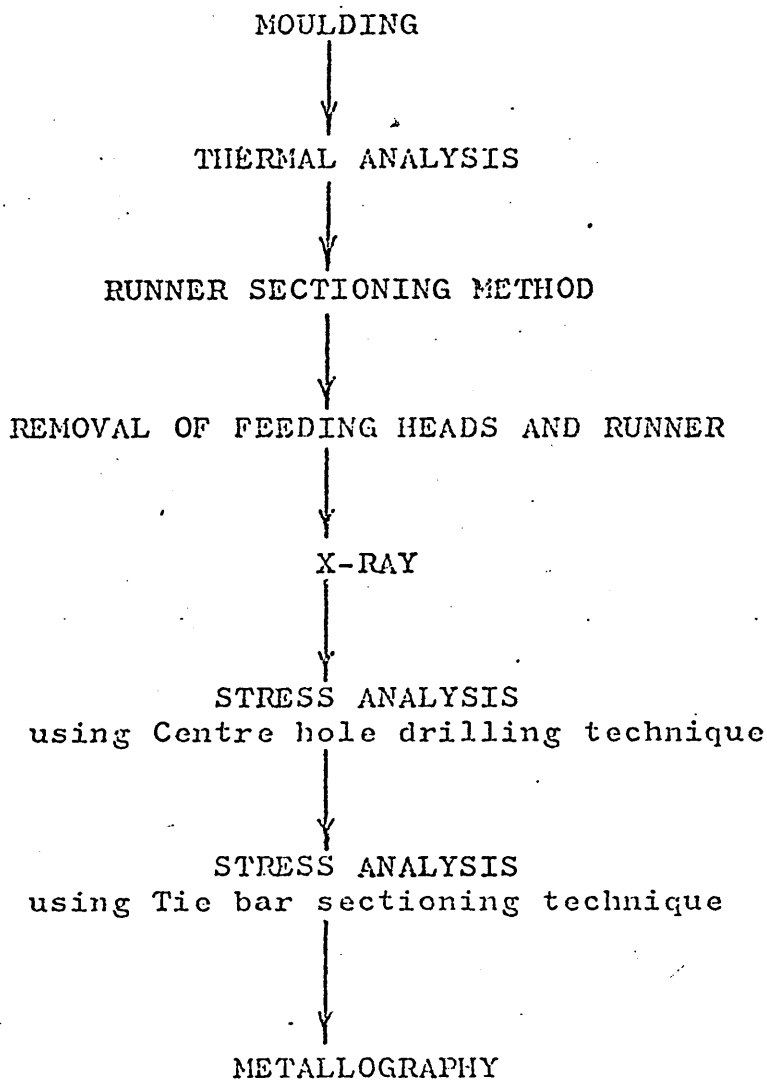
MOULDING
THERMAL ANALYSIS
RUNNER SECTIONING METHOD
REMOVAL OF FEEDING HEADS AND RUNNER
X-RAY
STRESS ANALYSIS
using Centre hole drilling technique
STRESS ANALYSIS
using Tie bar sectioning technique
METALLOGRAPHY

FIGURE 31: An outline of Experimental procedure for determining Residual Stresses for Heat Treatment Stage.

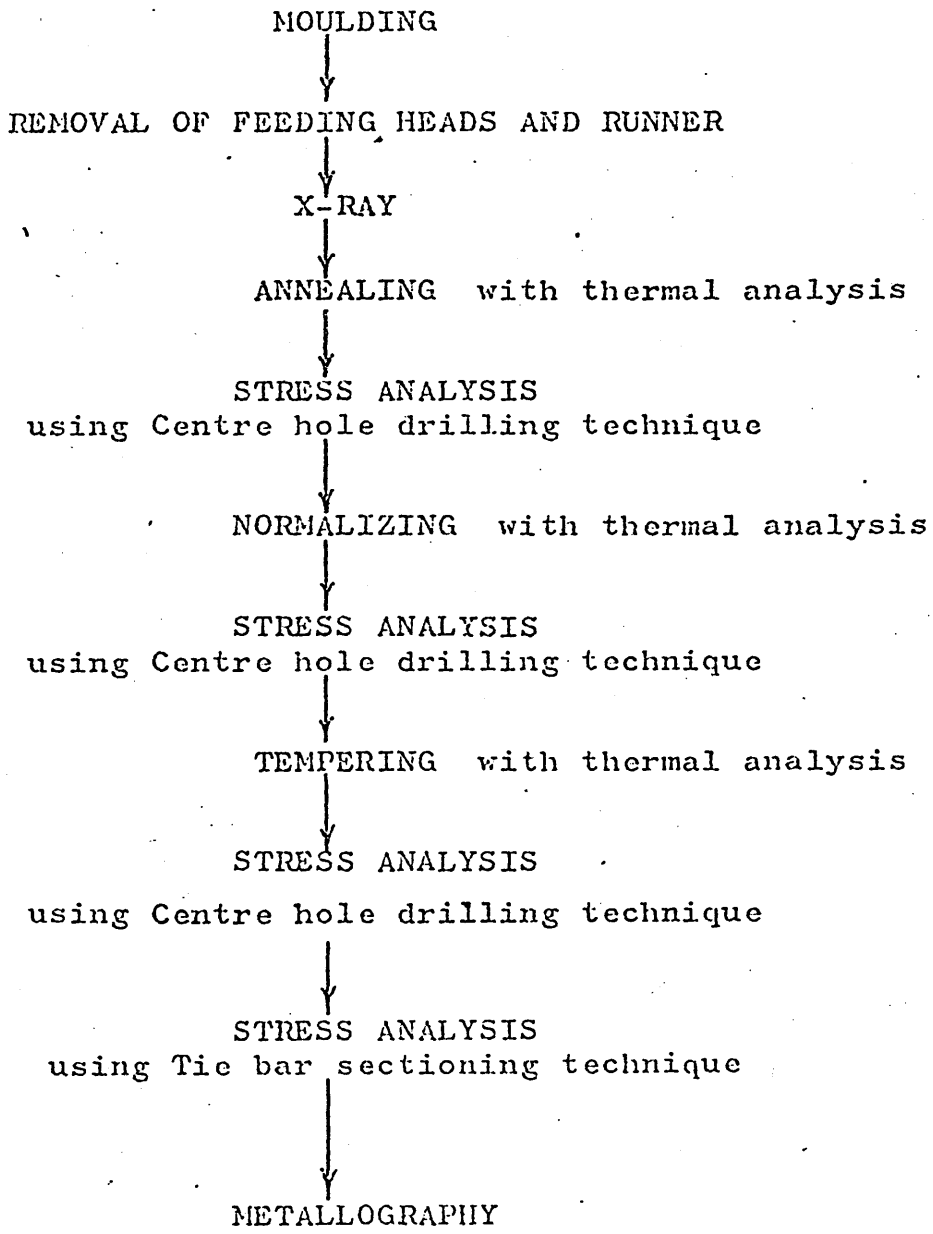
MOULDING
REMOVAL OF FEEDING HEADS AND RUNNER
X-RAY
ANNEALING with thermal analysis
STRESS ANALYSIS
using Centre hole drilling technique
NORMALIZING with thermal analysis
STRESS ANALYSIS
using Centre hole drilling technique
TEMPERING with thermal analysis
STRESS ANALYSIS
using Centre hole drilling technique
STRESS ANALYSIS
using Tie bar sectioning technique
METALLOGRAPHY

FIGURE 32: Heat fluxes to and from a differential element.

FIGURE 33: Interface between metal and sand.

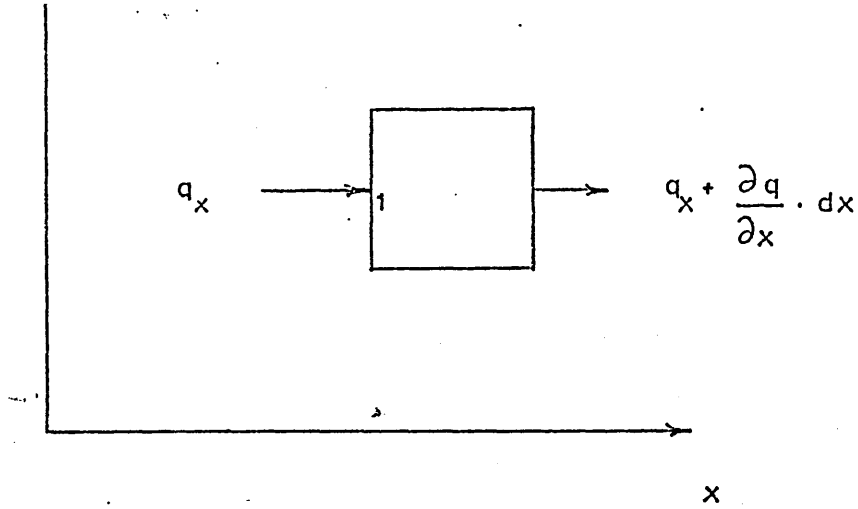
q_x
1
$q_x + \frac{\partial q}{\partial x} \cdot dx$
x

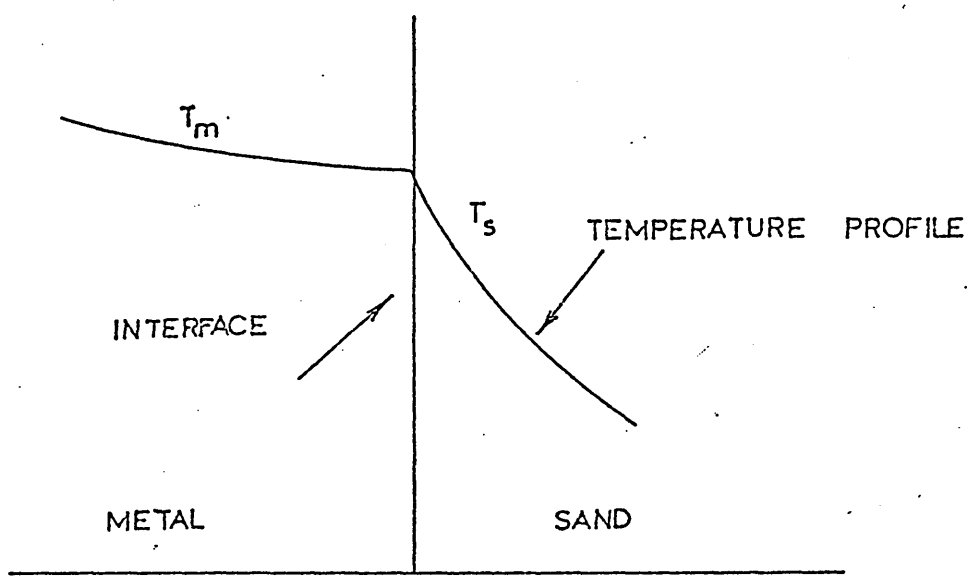
T_m
T_s
TEMPERATURE PROFILE
INTERFACE
METAL
SAND

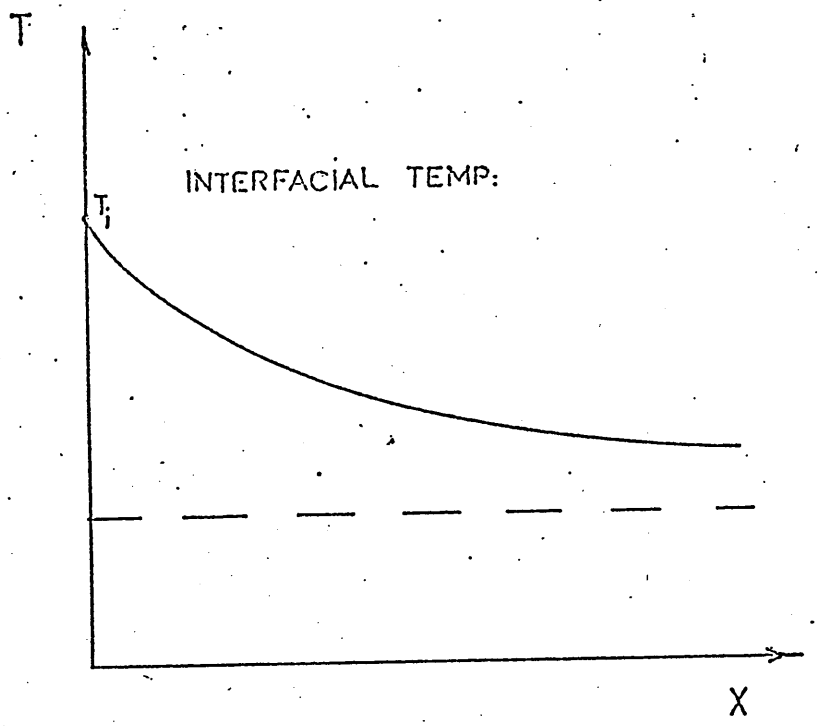
T
INTERFACIAL TEMP:
T_i
X

FIGURE 35: One dimensional convective boundary surface
(Croft and Lilley[115])

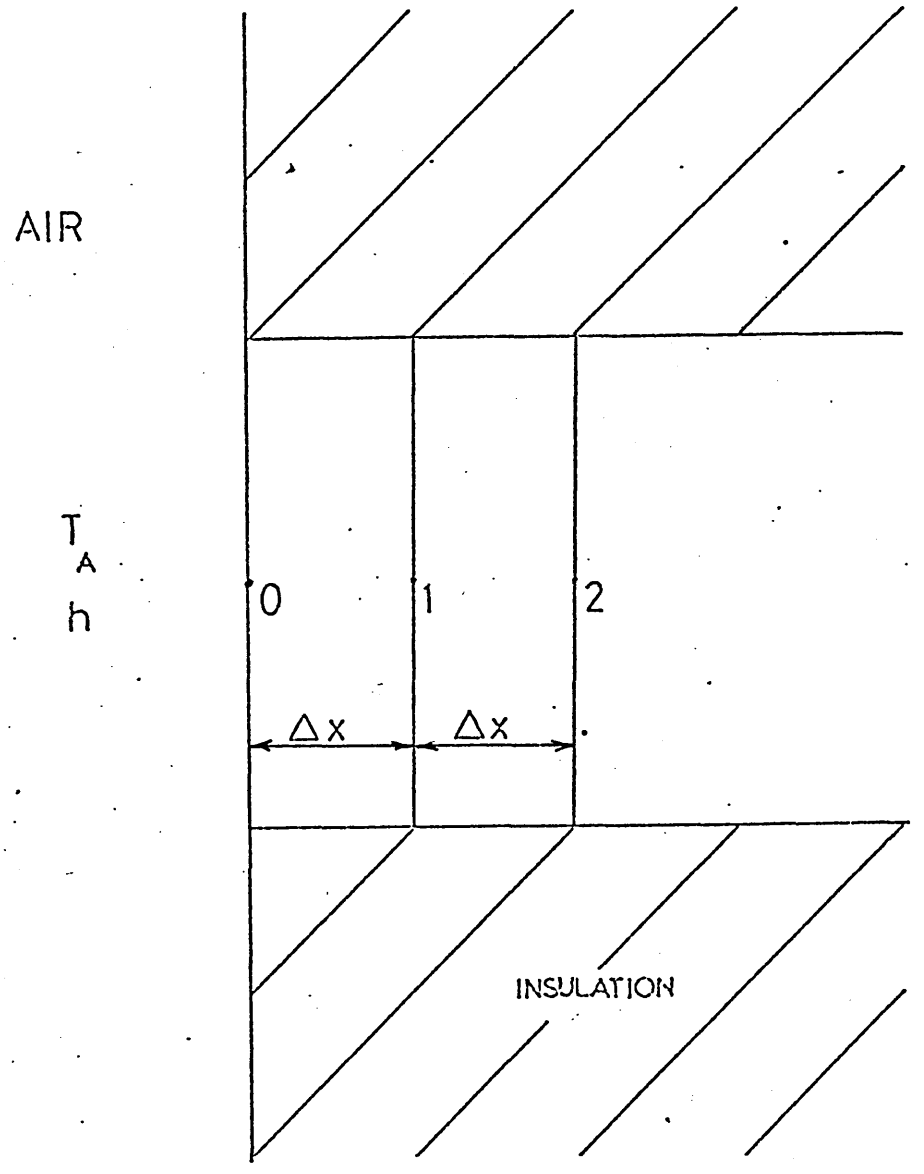
AIR
T_A
h
0
1
2
Δx
Δx
INSULATION

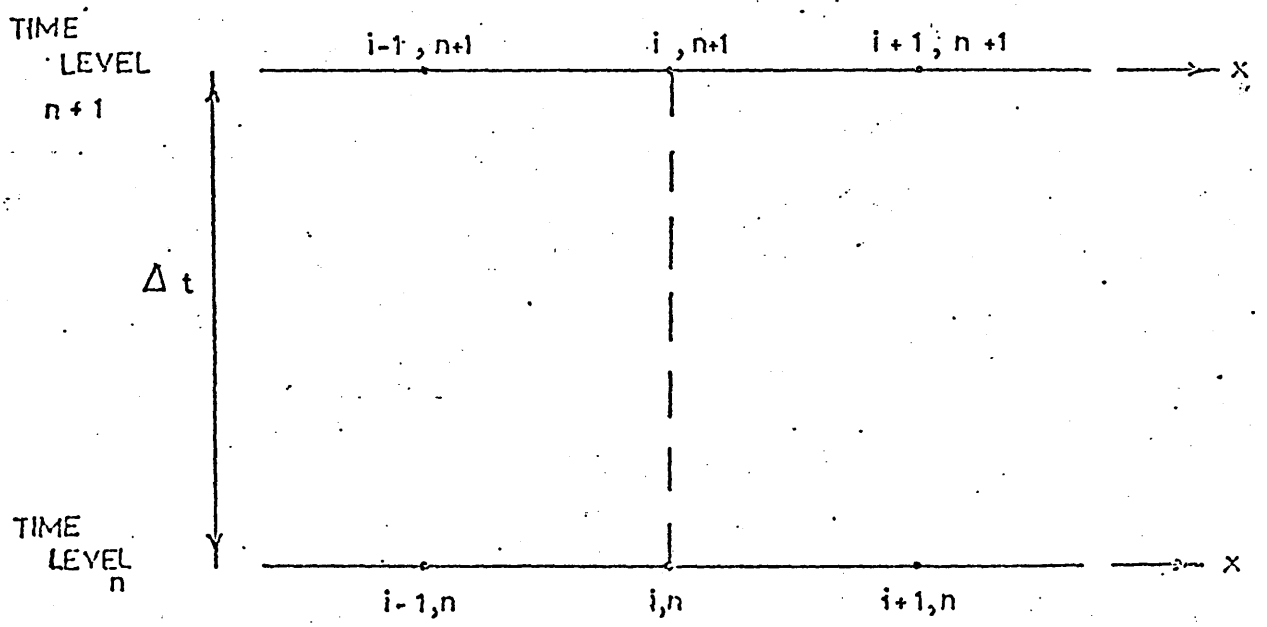
TIME
LEVEL
n + 1
i-1 , n+1
i , n+1
i + 1 , n +1
x
Δ t
TIME
LEVEL
n
x
i - 1,n
i,n
i+1,n

FIGURE 37: Approximation of first order derivative.

FIGURE 38: Vertical interface.

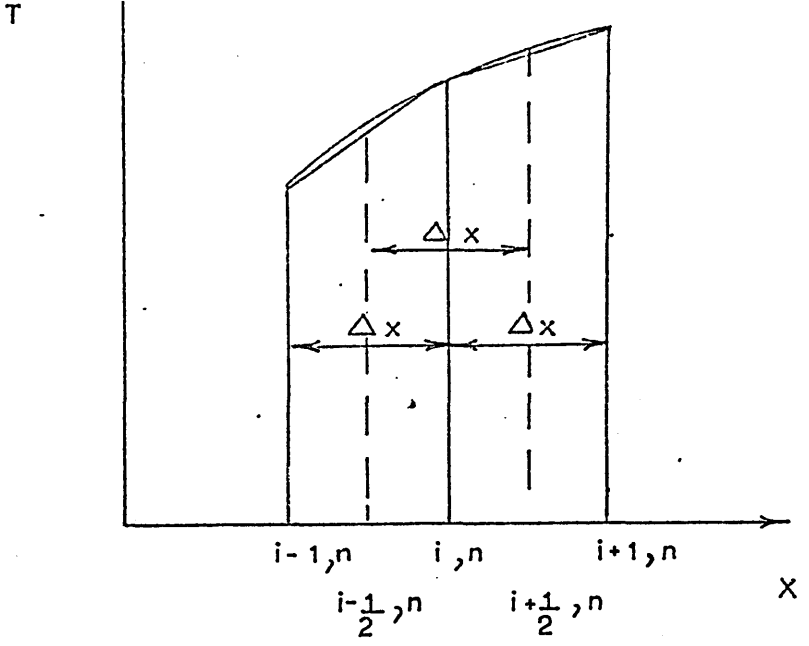
T
Δ x
Δ x
Δ x
i - 1, n
i , n
i+1, n
i-1/2 , n
i+1/2 , n
X

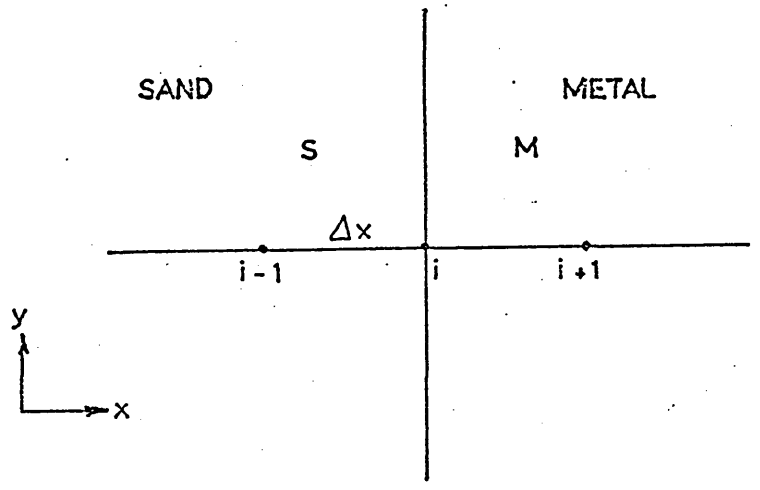
SAND
METAL
S
M
Δx
i - 1
i
i +1
y
x

FIGURE 39: Functional relationship for Thermal conductivity of steel

(a) $K = 49.1002 - 0.0225\ (T-50)$
(b) $K = 29.9752 + 0.00425\ (T-900)$
(c) $K = 32.0237 - 0.07045\ (T-1382)$
(d) $K = 25.965$

(Pehlke et al[121])

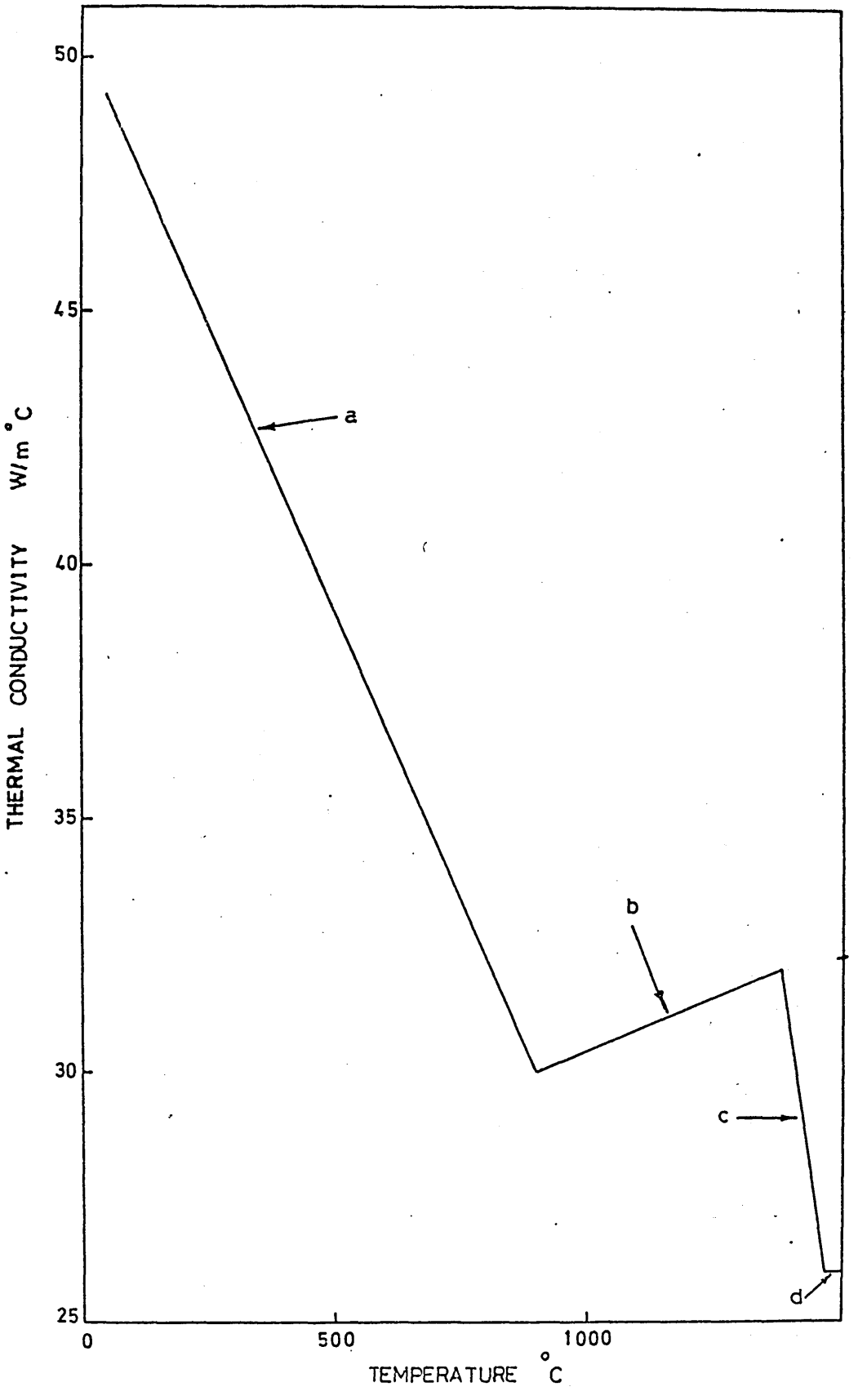
50
45
40
35
30
25
0
500
1000
THERMAL CONDUCTIVITY W/m °C
TEMPERATURE °C
a
b
c
d

FIGURE 40: Functional relationship for specific heat of steel

(a) Cp = 494.42539+0.37645 (T-100)
(b) Cp = 617.14809+1.1143 (T-426)
(c) Cp = 926.92349-0.81314 (T-704)
(d) Cp = 700.87057+0.3395506 (T-982)
(e) Cp = 7180.2288+147.52414 (T-1425)
(f) Cp = 7180.2288-146.55309 (T-1425)
(g) Cp = 878.4459

(Pehlke et al[121])

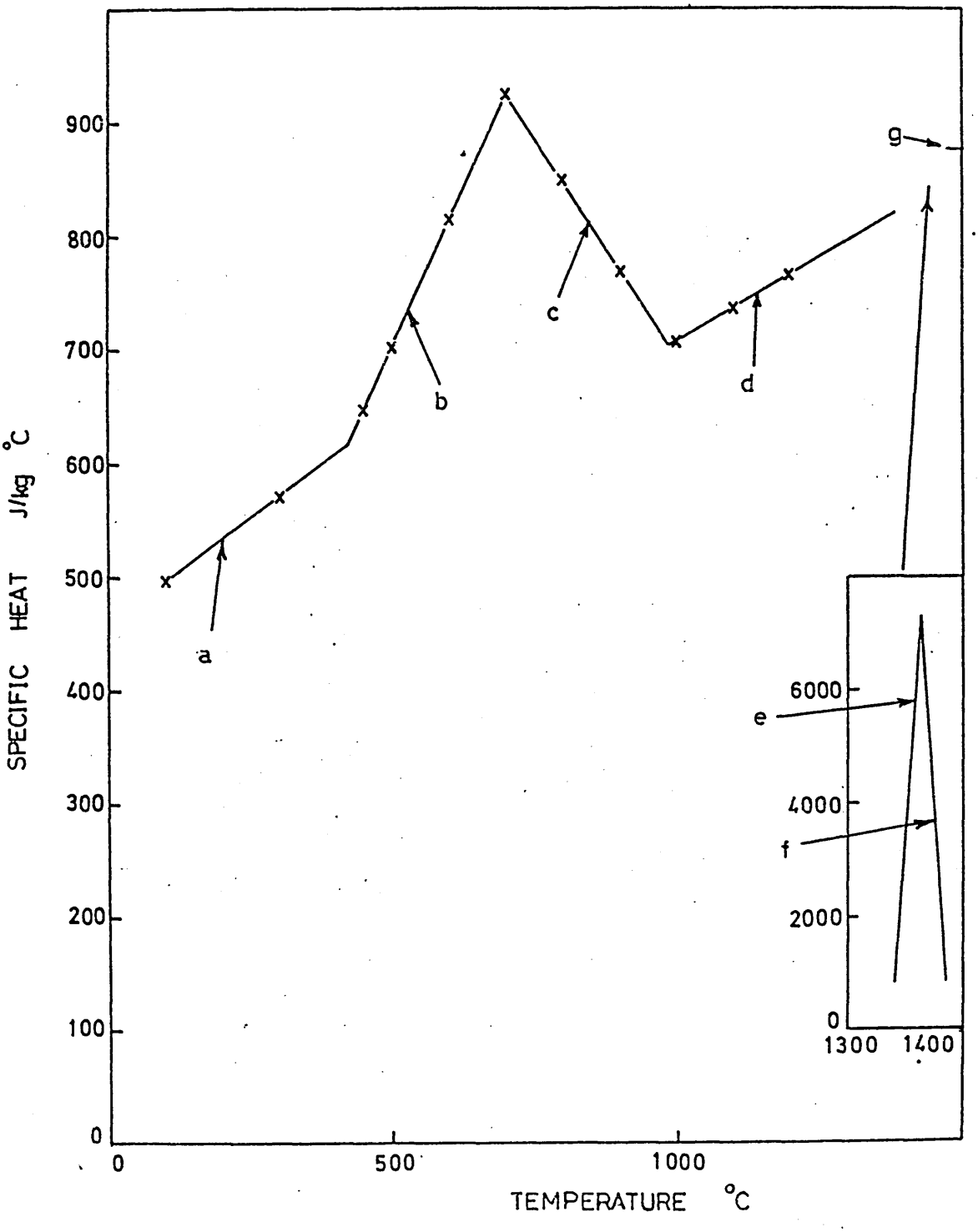
SPECIFIC HEAT J/kg °C
900
800
700
600
500
400
300
200
100
0
0
500
1000
TEMPERATURE °C
a
b
c
d
e
f
g
6000
4000
2000
0
1300
1400

FIGURE 41: Functional relationship for thermal conductivity of sand

(a) $K = (0.38171 - 6.6889 \times 10^{-5}((T+17.78)1.8) + 1.3805 \times 10^{-7}((T+17.78)1.8)^2\ 1.731$

(b) $K = (0.5244 - 3.6289 \times 10^{-4}\ ((T+17.78)1.8) + 1.66667 \times 10^{-7}((T+17.78)1.8)^2)\ 1.731$

(c) $K = (0.30216 - 1.786 \times 10^{-4}\ ((T+17.78)1.8) + 1.0522 \times 10^{-7}((T+17.78)1.8)^2)\ 1.731$

(d) $K = (0.1634 - 5.3969 \times 10^{-4}\ ((T+17.78)1.8) + 2.4113 \times 10^{-8}\ ((T+17.78)1.8)^2)\ 1.731$

(Pehlke et al[121])

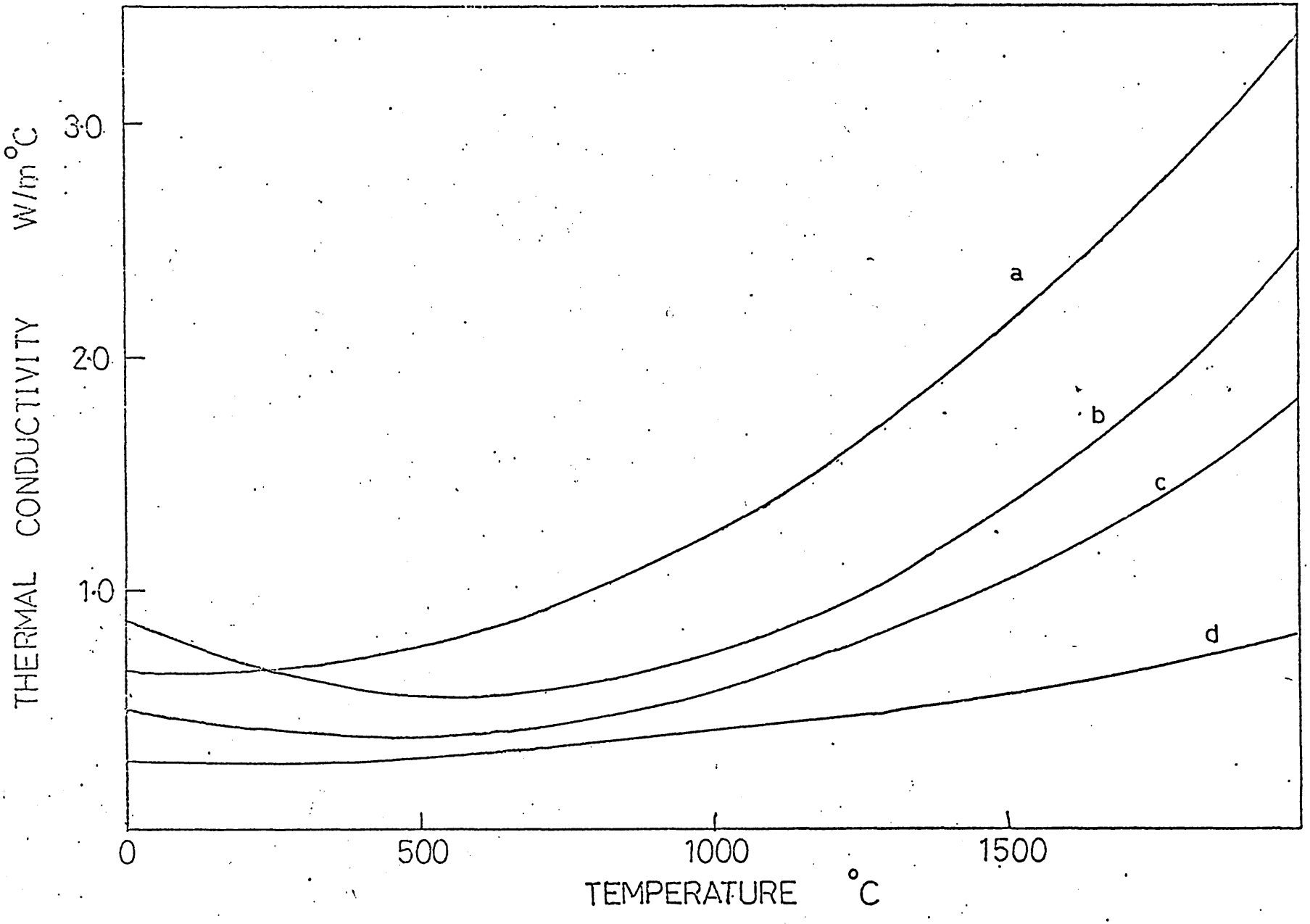
THERMAL CONDUCTIVITY W/m °C
3·0
2·0
1·0
a
b
c
d
0
500
1000
1500
TEMPERATURE °C

FIGURE 42: Functional relationship for specific heat of moulding sand

$$Cp = (0.1683035+0.2368111\times10^{-3}\ T-0.200749\times10^{-6}\ T^2+0.764947\times10^{-10}\ T^3-0.1041948\times10^{-13}\ T^4)\ 4182.82$$

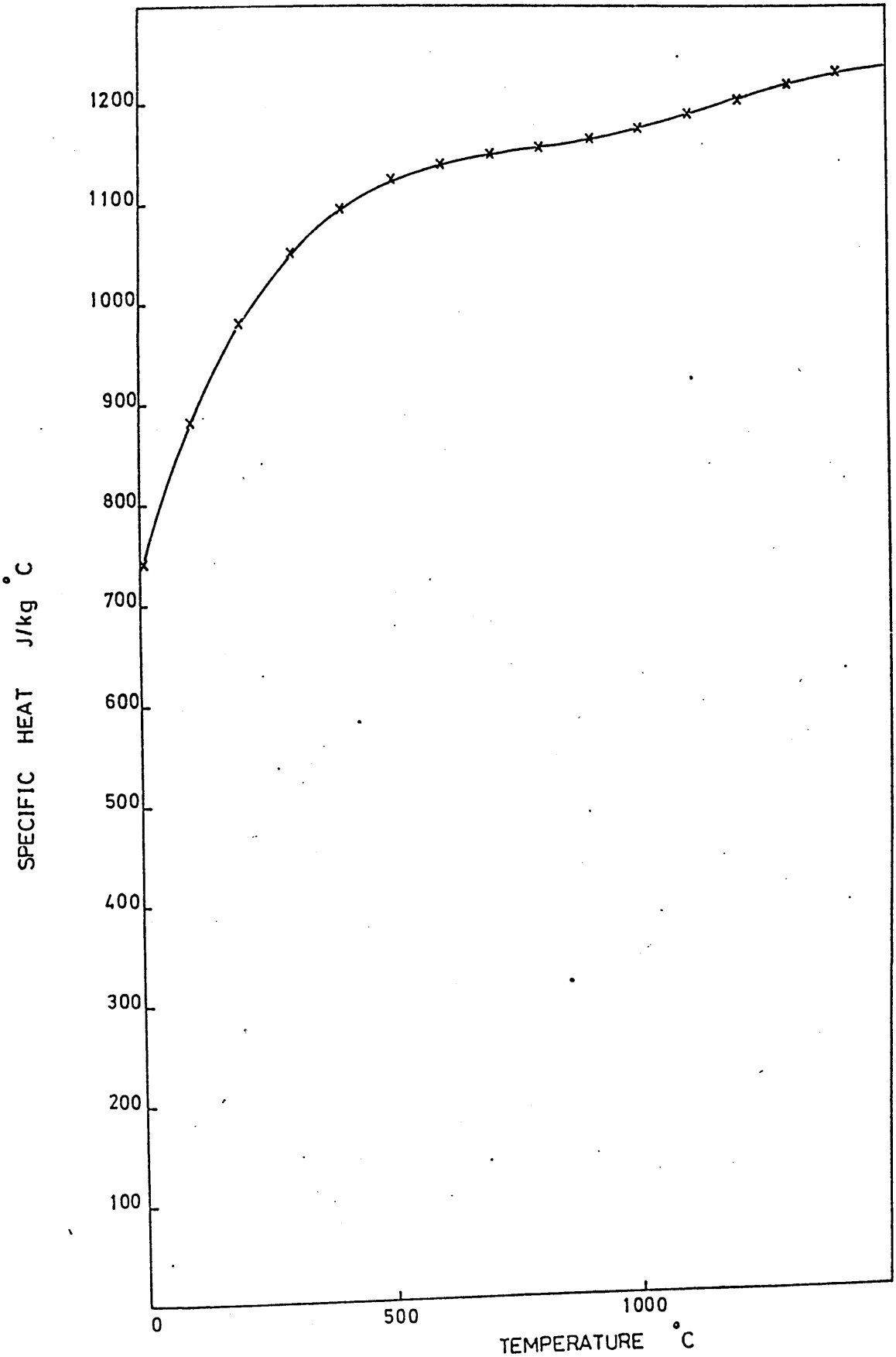
1200
1100
1000
900
800
700
600
500
400
300
200
100
SPECIFIC HEAT J/kg °C
0
500
1000
TEMPERATURE °C

FIGURE 43: Location of mould model in theta ring TT represents the model.

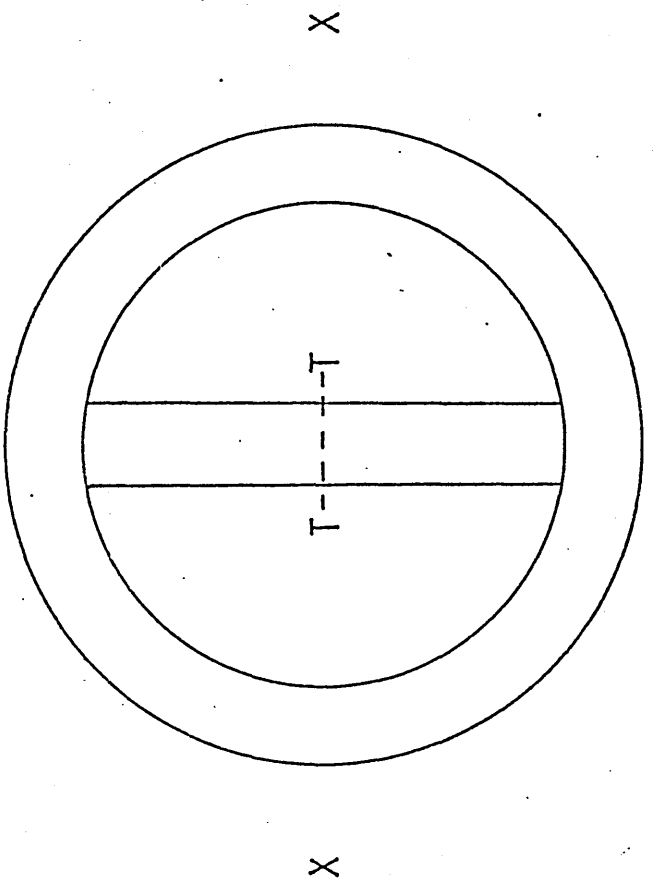
X
T
T
X

FIGURE 44: Isometric view of mould model used for simulation of solidification

a = 5,10,15,20,25 and 30

All dimensions are in millimeters

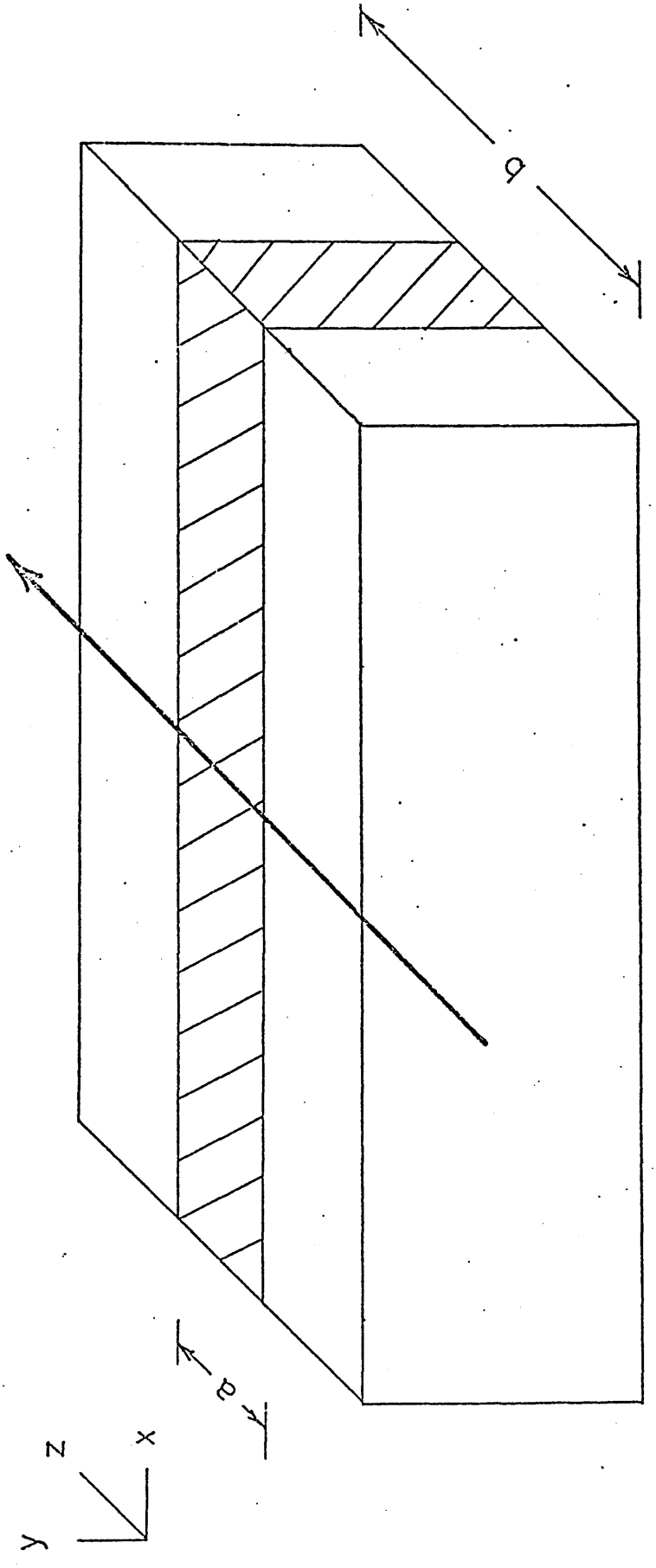
a
a
z
x
y

FIGURE 45: Mould model with interfaces.

FIGURE 46: Alternative methods for computing temperatures at new time levels.

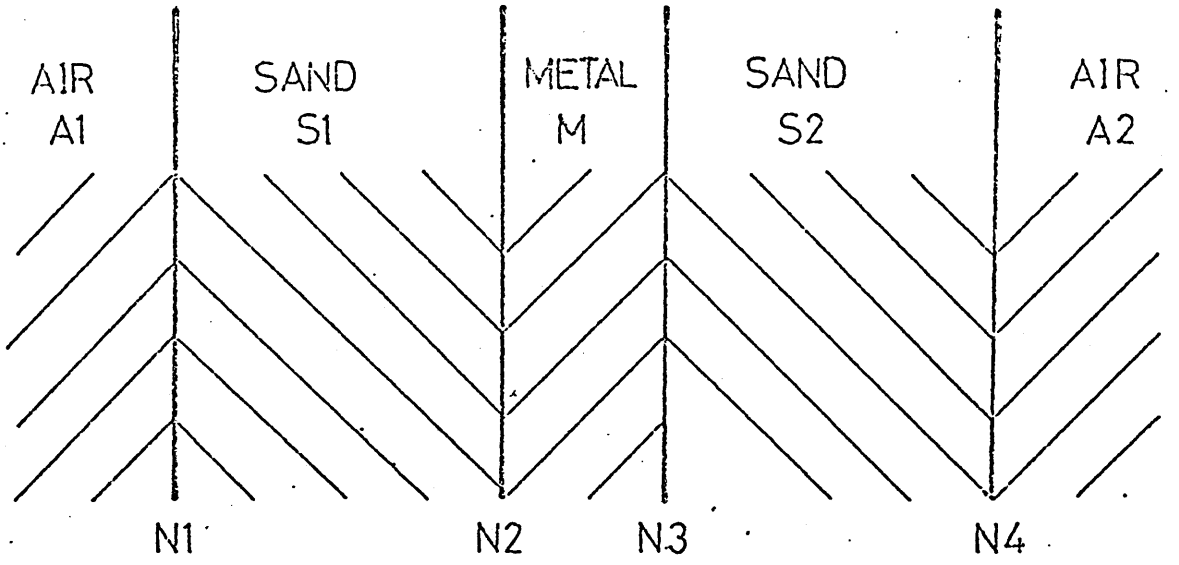
AIR
A1
SAND
S1
METAL
M
SAND
S2
AIR
A2
N1
N2
N3
N4

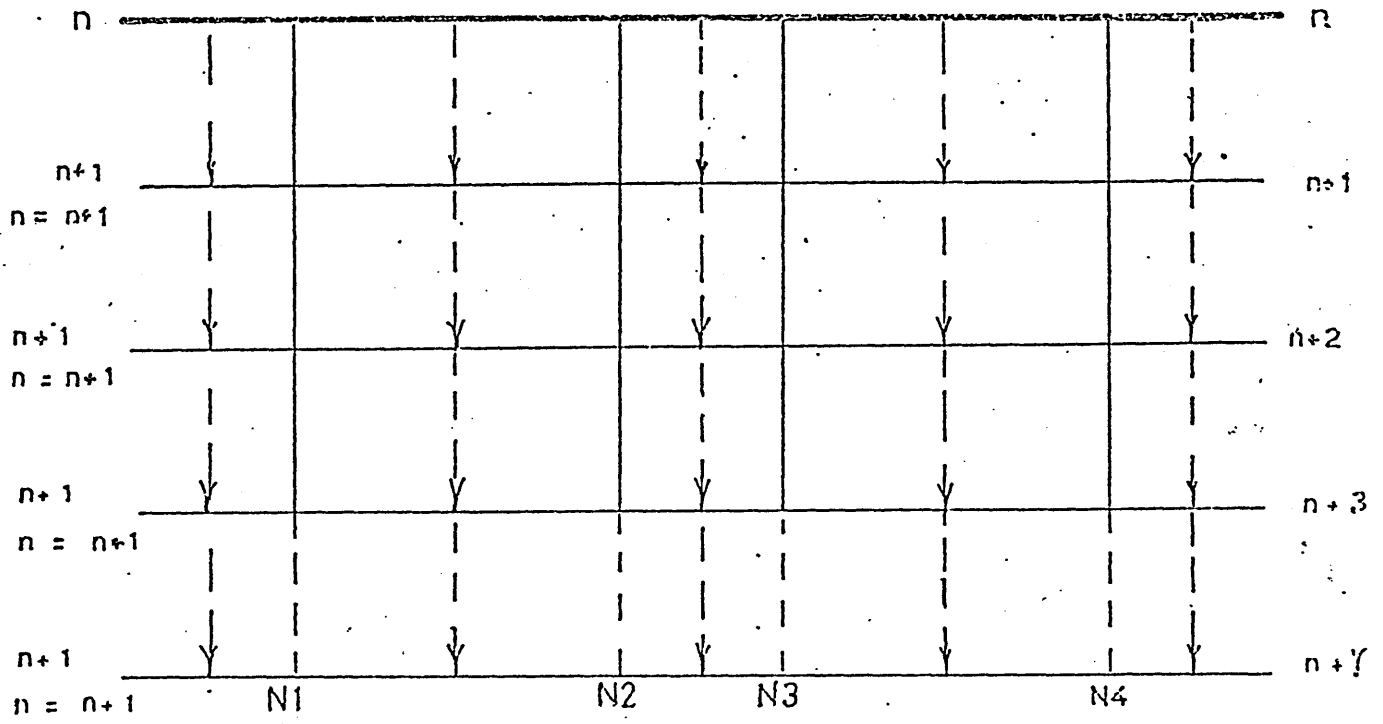
n
n+1
n = n+1
n+1
n = n+1
n+1
n = n+1
n+1
n = n+1
n
n+1
n+2
n+3
n+Y
N1
N2
N3
N4

FIGURE 47: Effect of grid spacing and time interval on the accuracy of computed results.

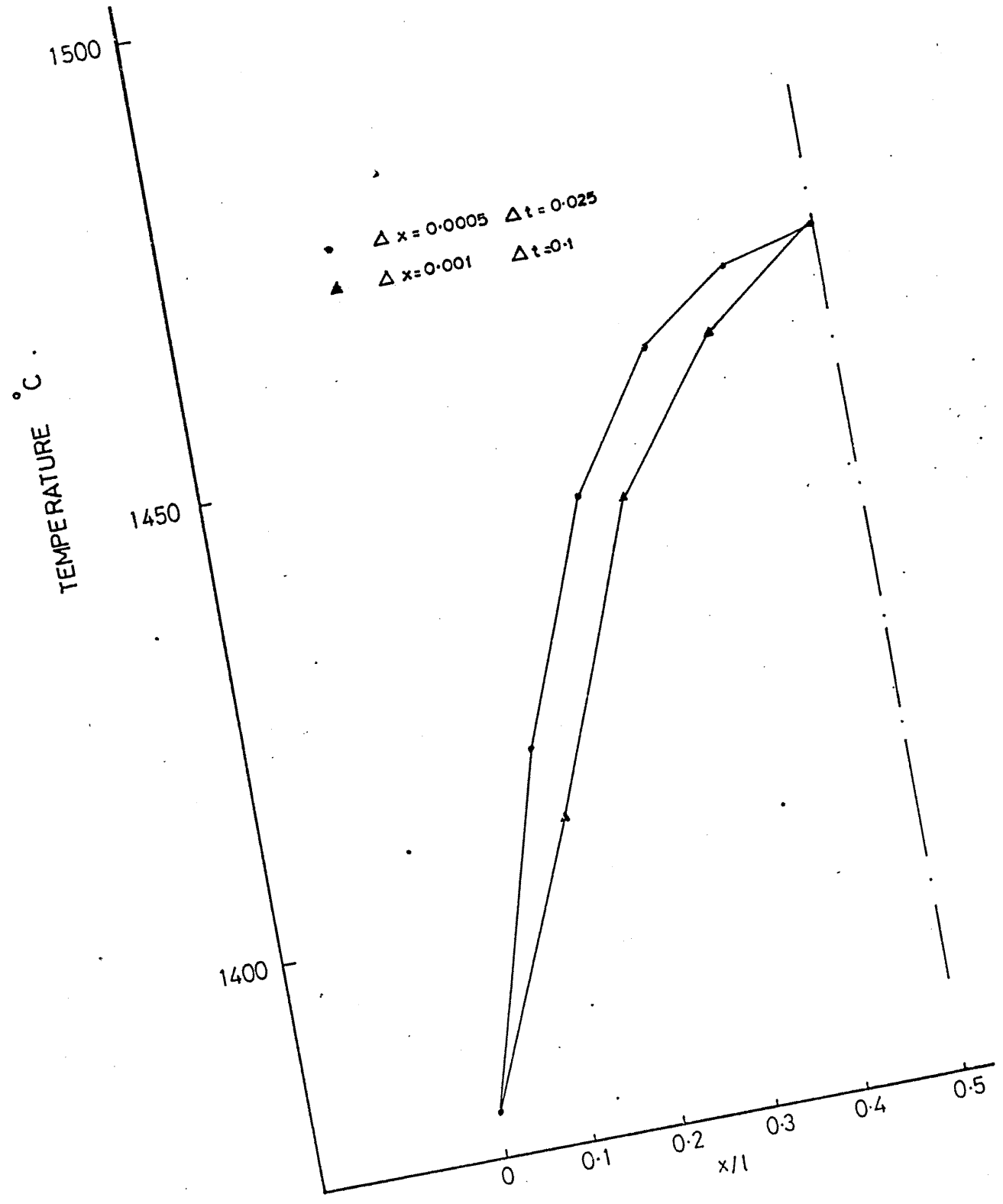
1500
1450
1400
TEMPERATURE °C
Δ x = 0·0005 Δ t = 0·025
Δ x=0·001 Δ t=0·1
0
0·1
0·2
0·3
0·4
0·5
x/l

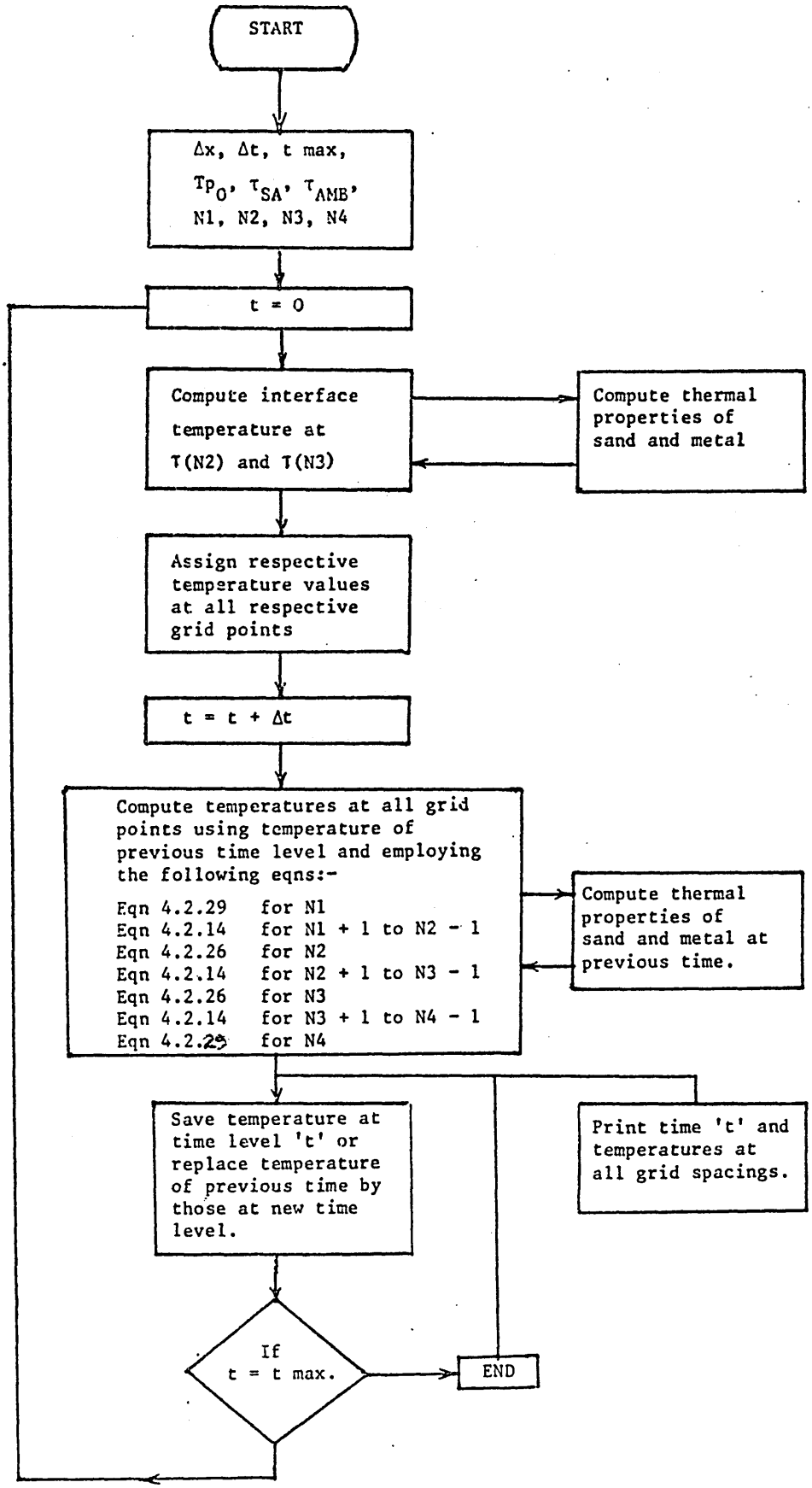
START
Δx, Δt, t max,
T_{P_0}, τ_{SA}, τ_{AMB},
N1, N2, N3, N4
t = 0
Compute interface temperature at T(N2) and T(N3)
Compute thermal properties of sand and metal
Assign respective temperature values at all respective grid points
t = t + Δt
Compute temperatures at all grid points using temperature of previous time level and employing the following eqns:-
Eqn 4.2.29 for N1
Eqn 4.2.14 for N1 + 1 to N2 - 1
Eqn 4.2.26 for N2
Eqn 4.2.14 for N2 + 1 to N3 - 1
Eqn 4.2.26 for N3
Eqn 4.2.14 for N3 + 1 to N4 - 1
Eqn 4.2.29 for N4
Compute thermal properties of sand and metal at previous time.
Save temperature at time level 't' or replace temperature of previous time by those at new time level.
Print time 't' and temperatures at all grid spacings.
If t = t max.
END

FIGURE 49: Cooling curves for the Theta ring with 30mm tie bar width. Thermocouple locations are as shown in figure 21.

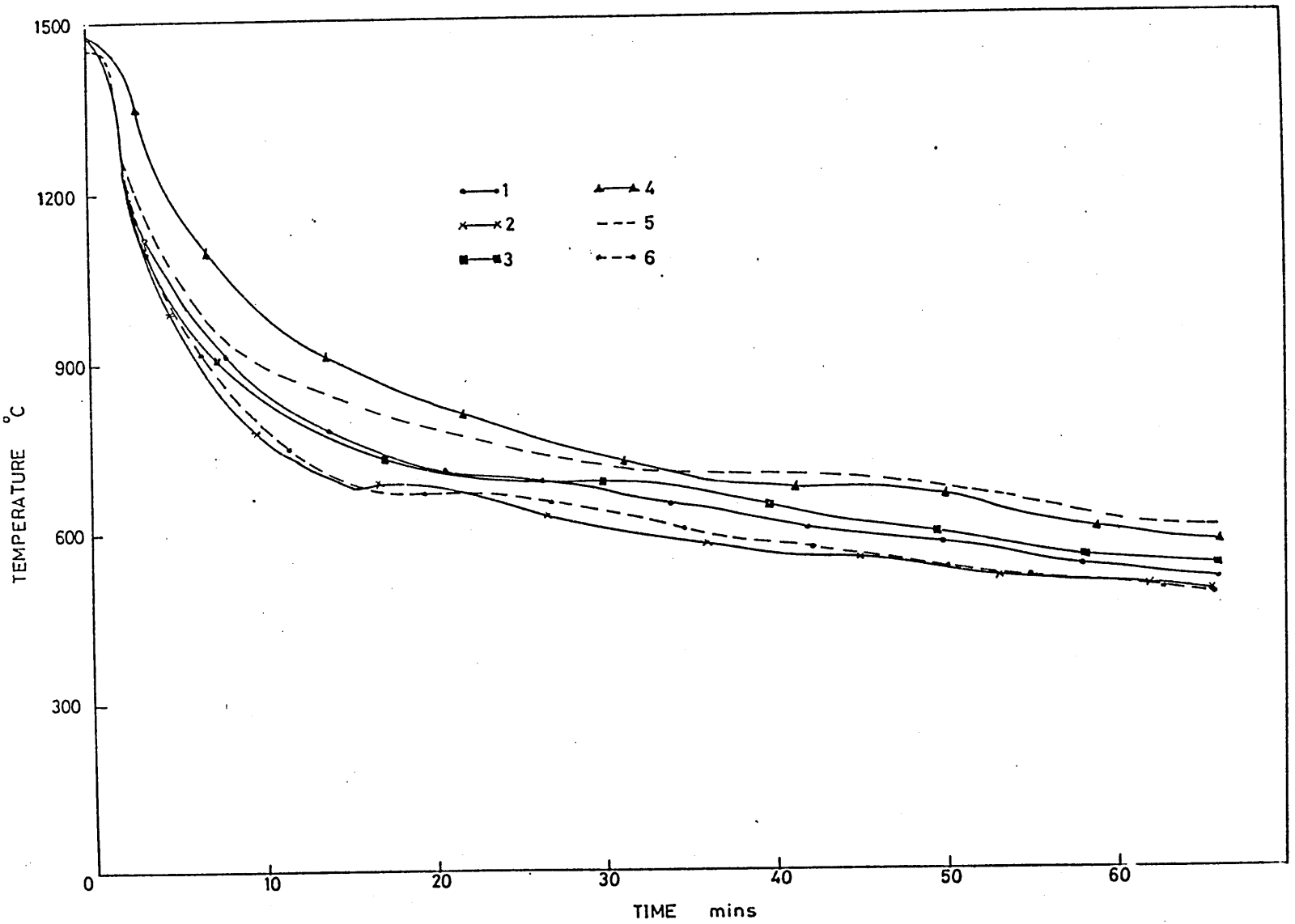
1500
1200
900
600
300
0
10
20
30
40
50
60
TEMPERATURE °C
TIME mins
1
2
3
4
5
6

FIGURE 50: Cooling curves for the Theta ring with 25mm tie bar width. Thermocouple locations are as shown in Figure 21.

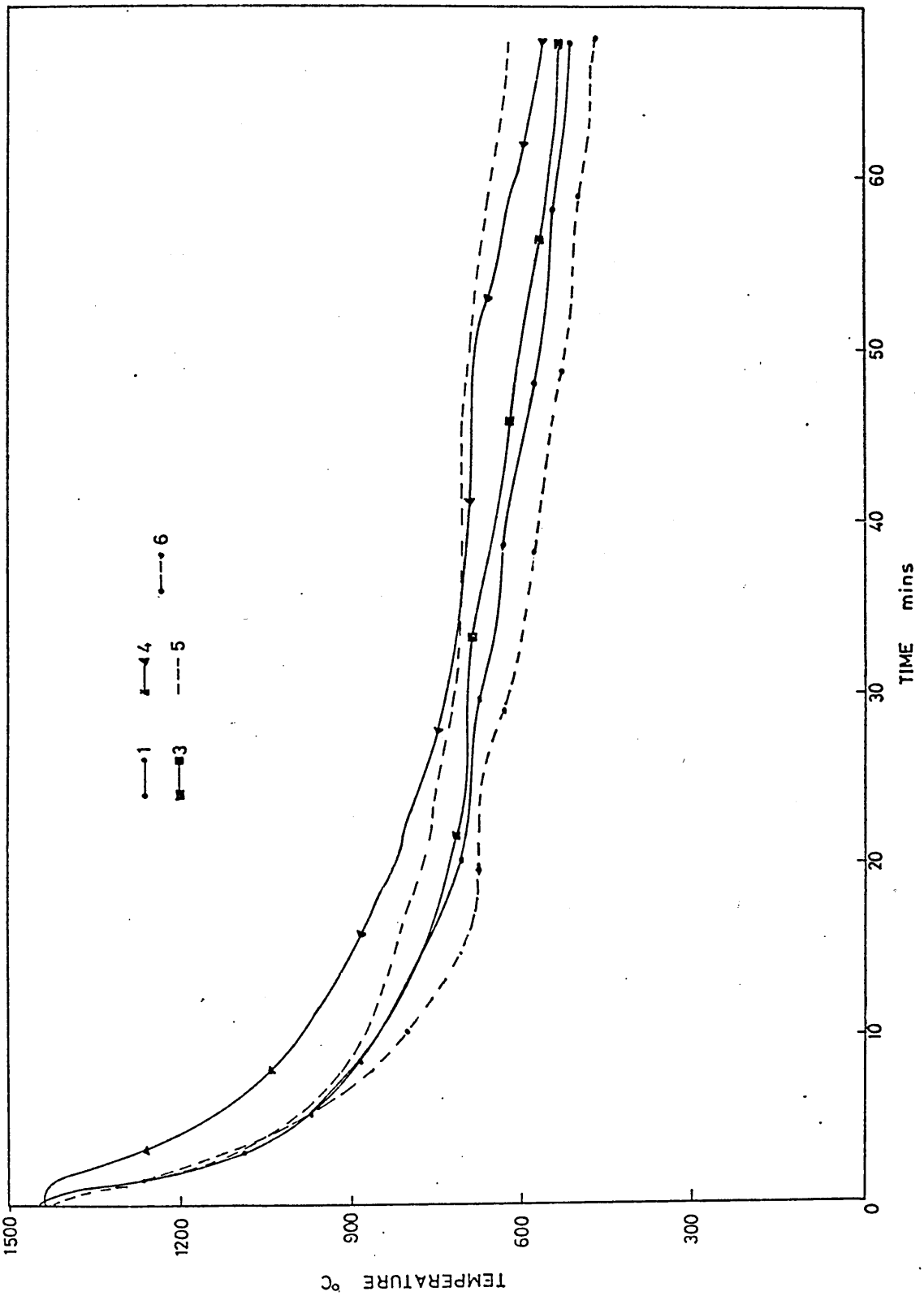
TEMPERATURE °C
1500
1200
900
600
300
0
10
20
30
40
50
60
TIME mins
1
3
4
5
6

FIGURE 51: Cooling curve for the Theta ring with 20mm tie bar width. Thermocouple locations are as shown in figure 21.

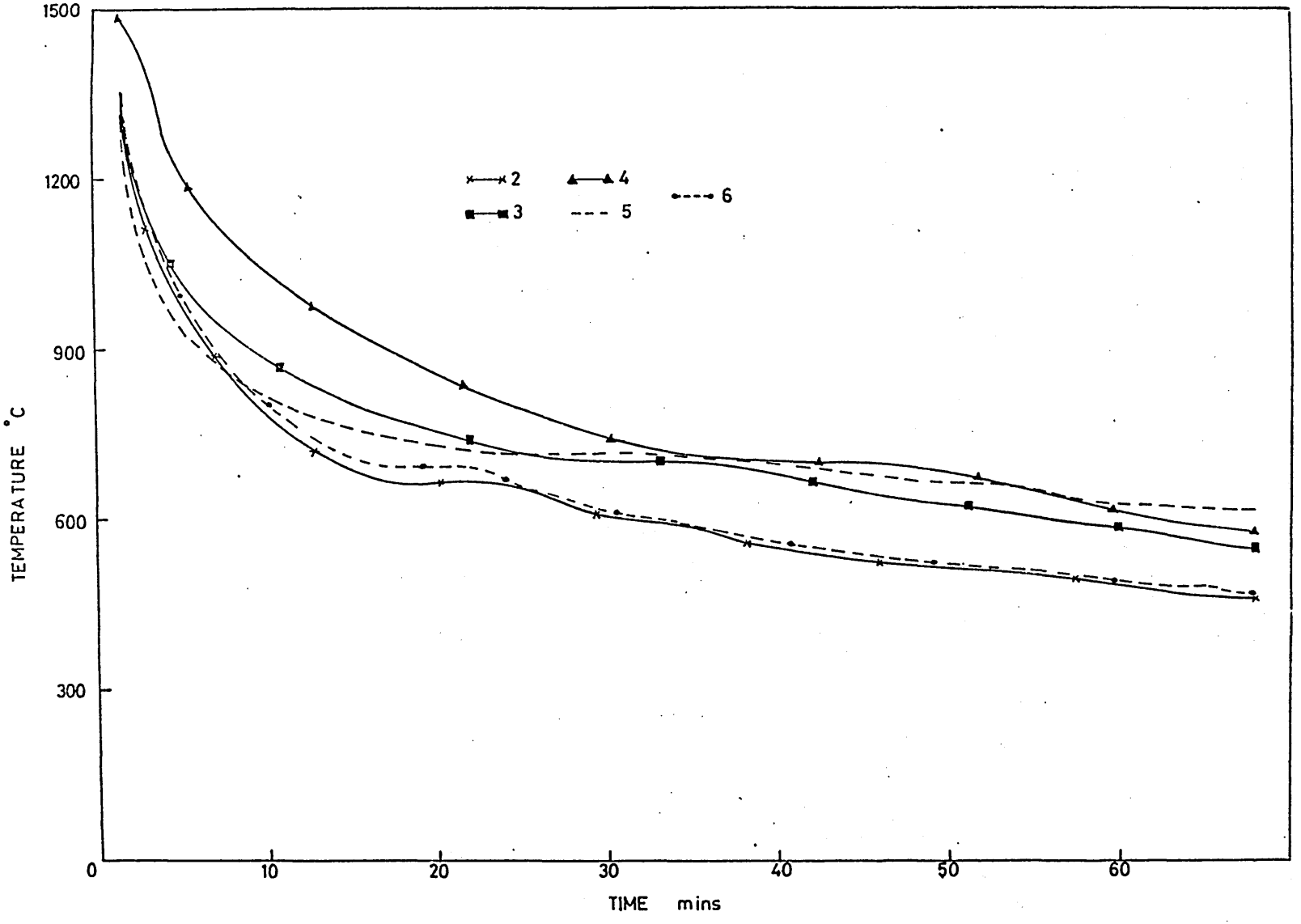
1500
1200
900
600
300
0
10
20
30
40
50
60
TEMPERATURE °C
TIME mins
2
3
4
5
6

FIGURE 52: Cooling curves for the Theta ring with 15mm tie bar width. Thermocouple locations are as shown in figure 21.

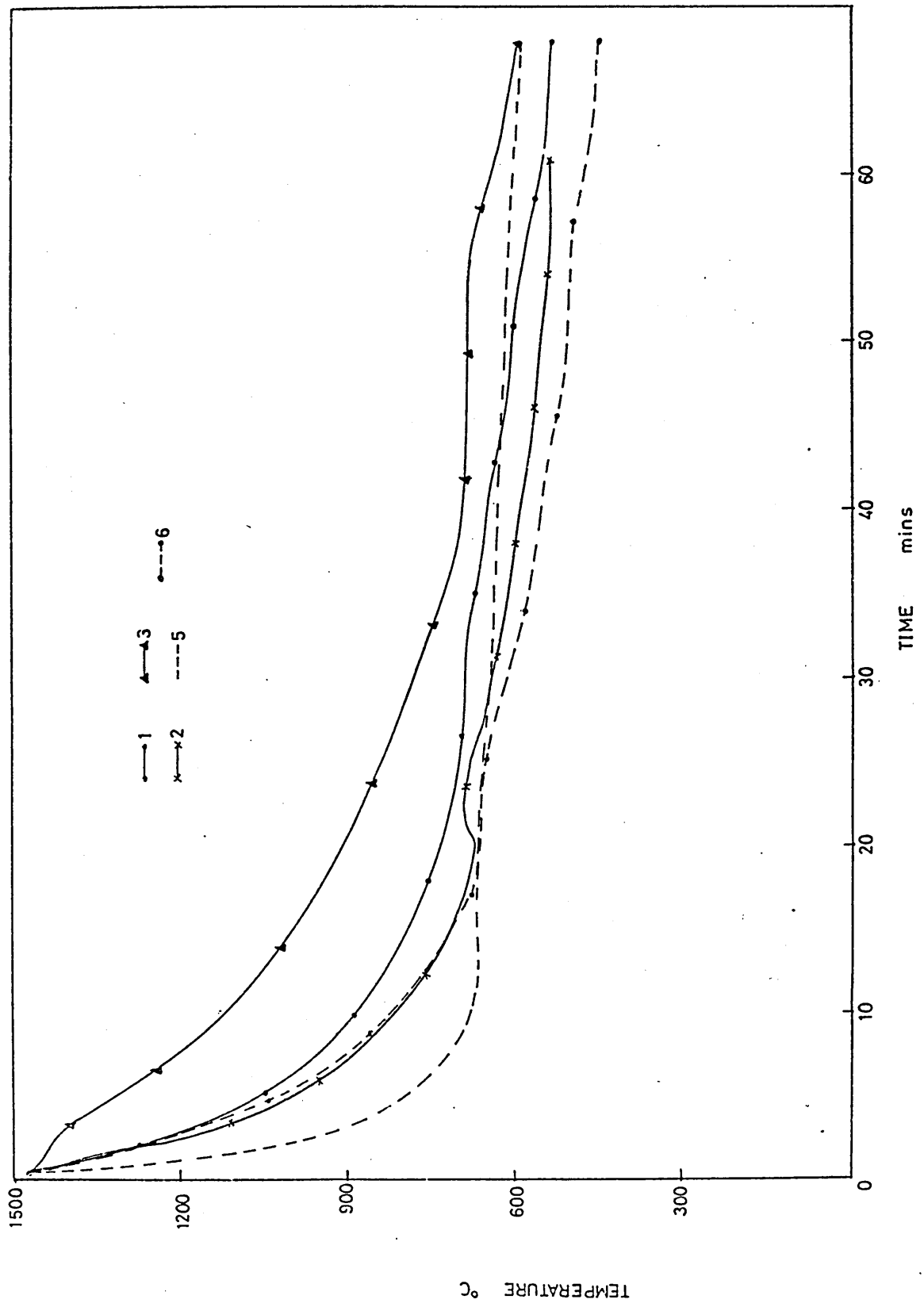
1500
1200
900
600
300
TEMPERATURE °C
0
10
20
30
40
50
60
TIME mins
1
2
3
5
6

FIGURE 53: Cooling curves for the Theta ring with 10mm tie bar width. Thermocouple locations are as shown in figure 21.

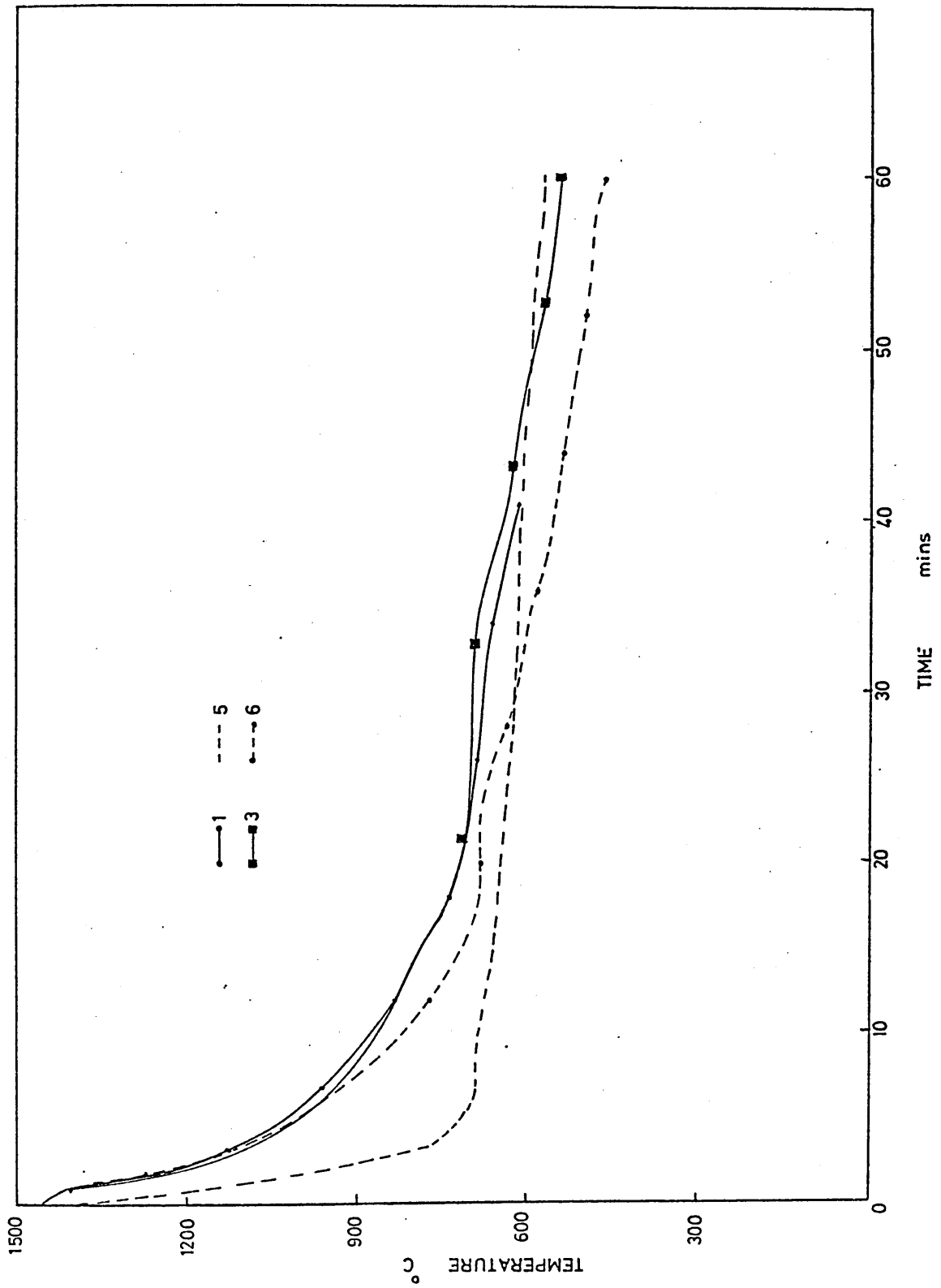
1500
1200
900
600
300
TEMPERATURE °C
0
10
20
30
40
50
60
TIME mins
1
3
5
6

FIGURE 54: Cooling curves for the Theta ring with 5mm tie bar width. Thermocouple locations are as shown in figure 21.

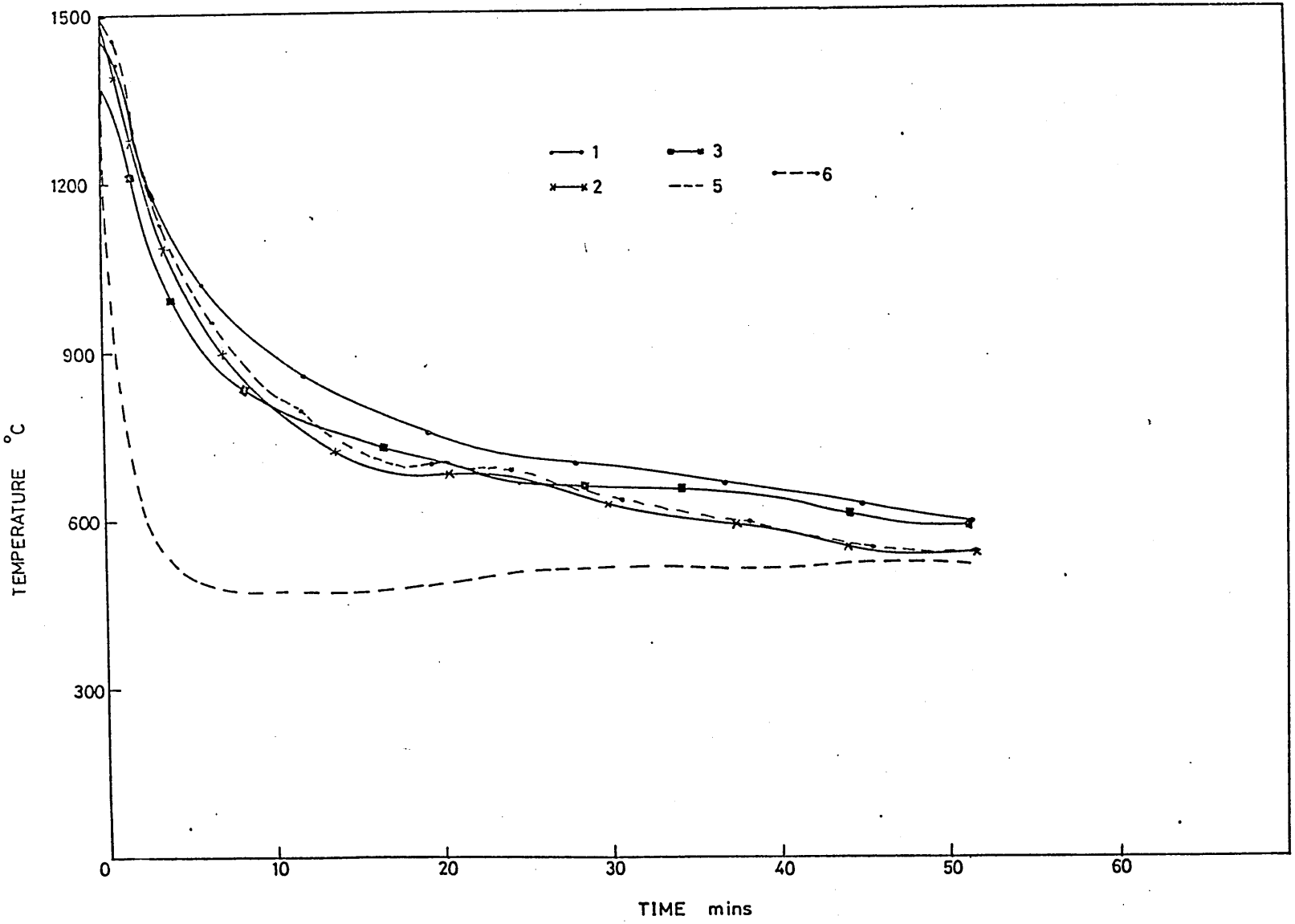
1500
1200
900
600
300
0
10
20
30
40
50
60
TEMPERATURE °C
TIME mins
1
2
3
5
6

FIGURE 55: Temperature differences between position 4(hot spot) and position 1 when the hot spot attains solidus and eutectoid transformation temperatures.

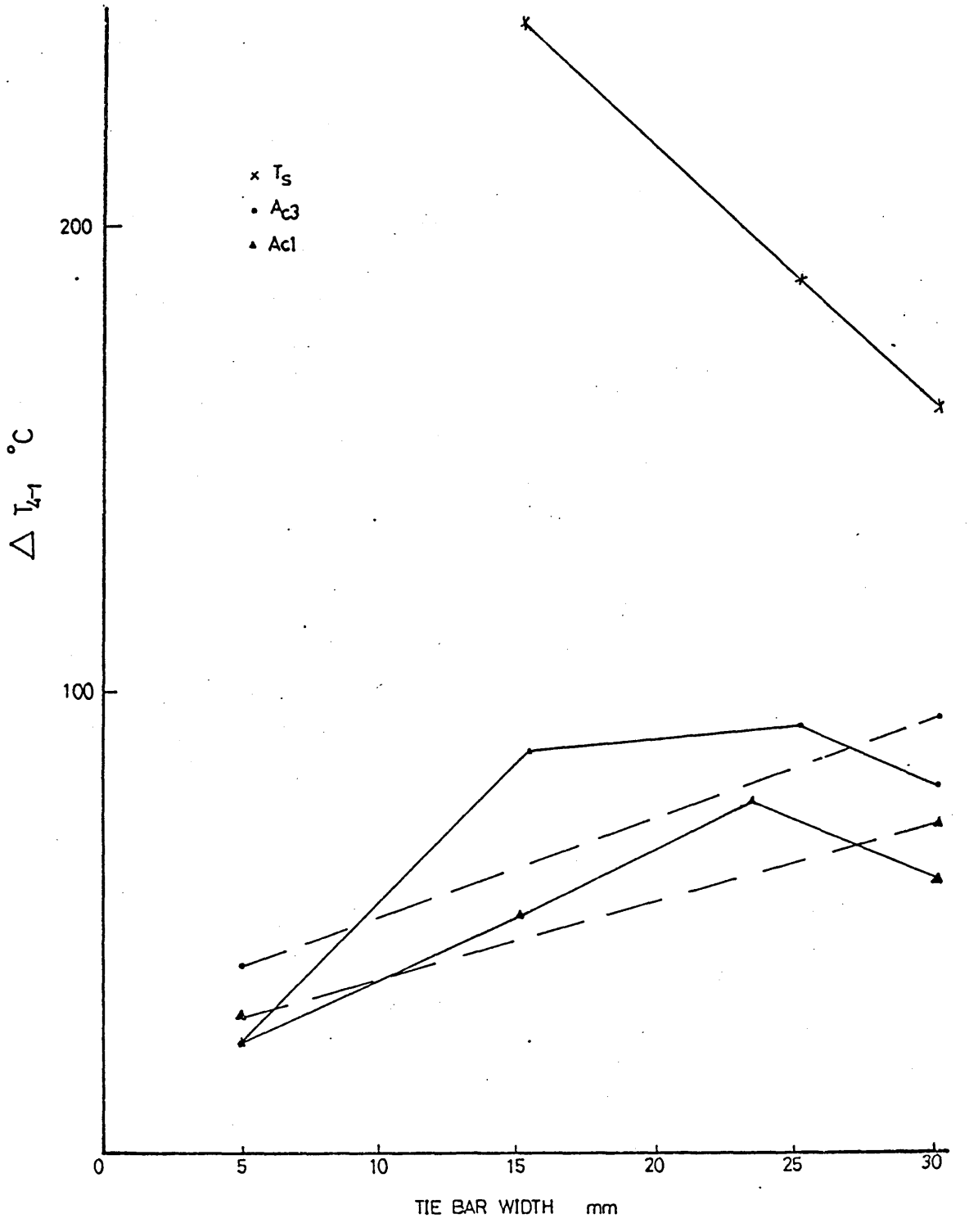
× T_s
• A_{c3}
▲ Ac1
200
100
ΔT_{4-1} °C
0
5
10
15
20
25
30
TIE BAR WIDTH mm

FIGURE 56: Temperature differences between position 4 (hot spot) and position 2 when the hot spot attains solidus and eutectoid transformation temperatures.

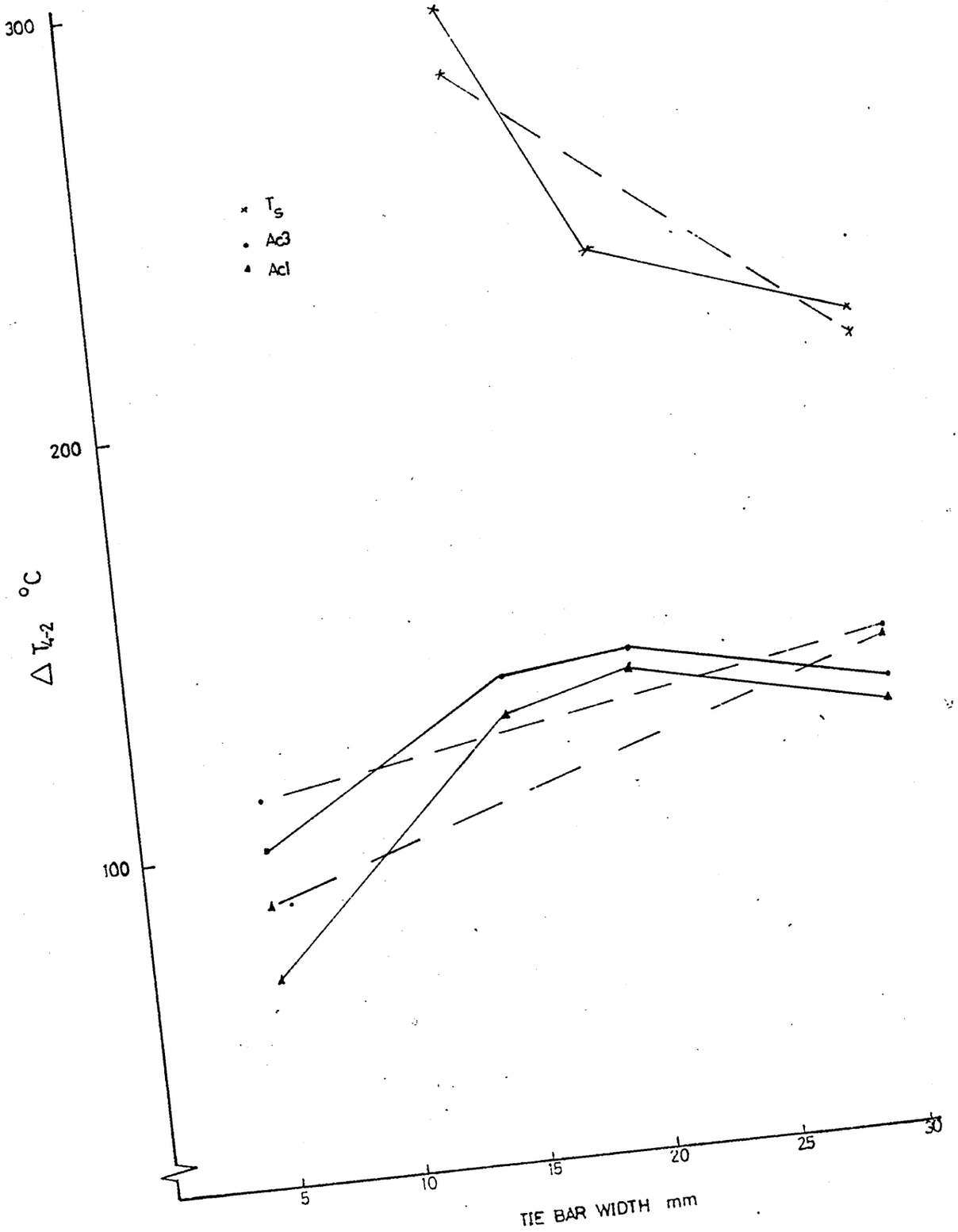
300
200
100
ΔT_{4-2} °C
T_s
Ac3
Ac1
5
10
15
20
25
30
TIE BAR WIDTH mm

FIGURE 57: Temperature differences between position 4 (hot spot) and position 3 when the hot spot attains solidus and eutectoid transformation temperatures.

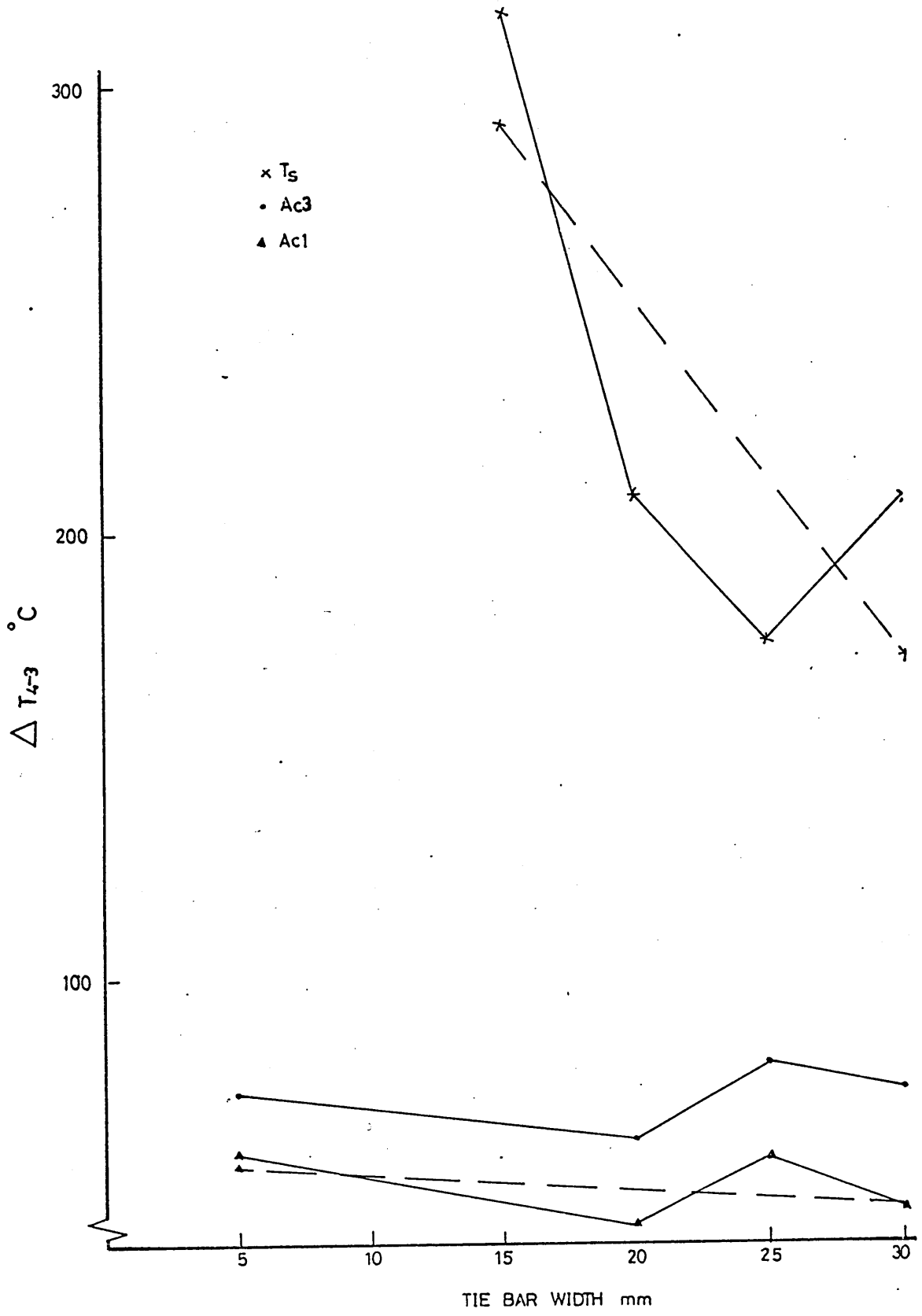
300
200
100
× Ts
• Ac3
▲ Ac1
Δ T4-3 °C
5
10
15
20
25
30
TIE BAR WIDTH mm

FIGURE 58: Temperature differences between position 4 (hot spot) and position 5 when the hot spot attains solidus and eutectoid transformation temperatures.

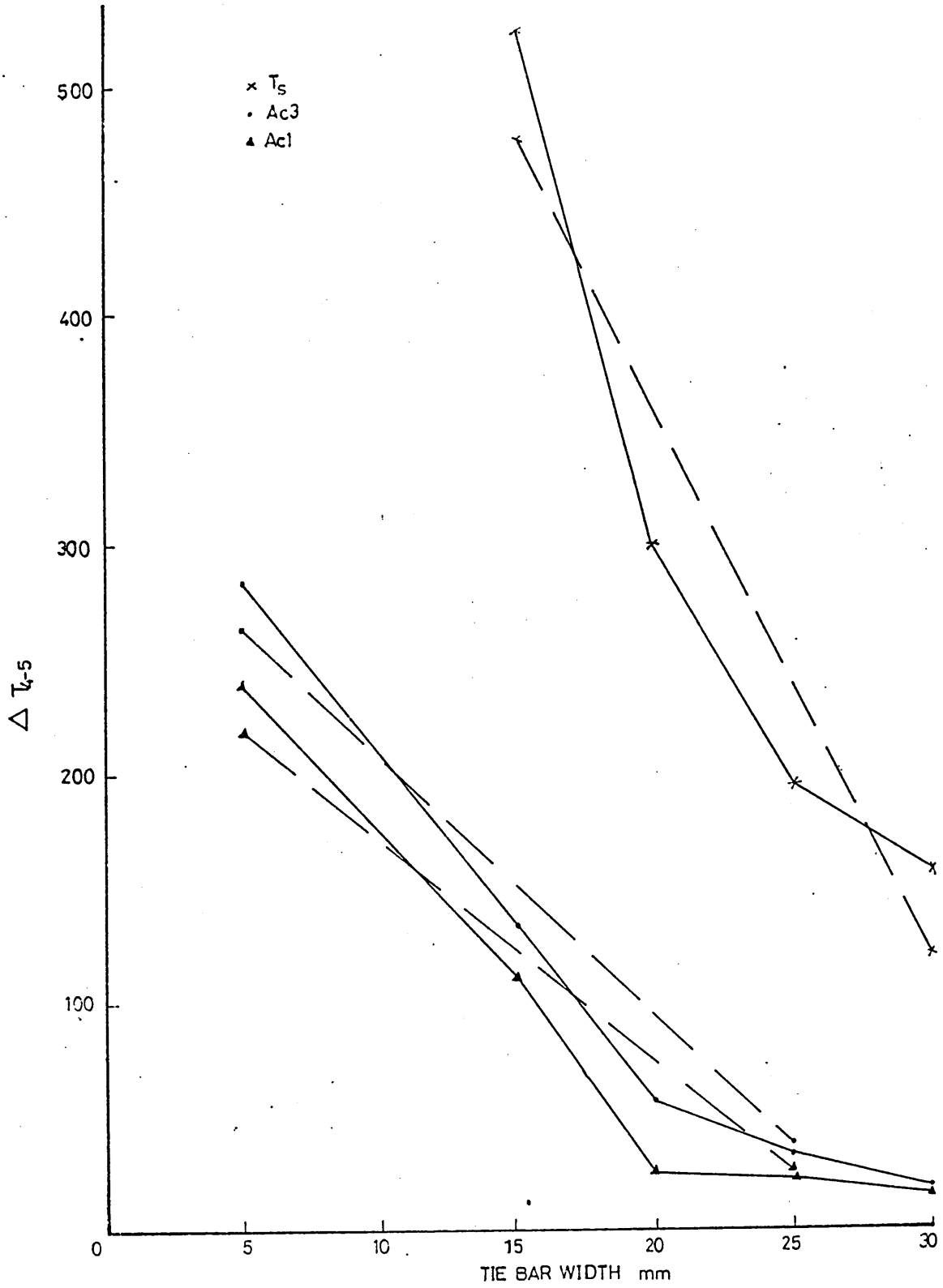
× T_s
• Ac3
▲ Ac1
500
400
300
200
100
0
5
10
15
20
25
30
ΔT_{4-5}
TIE BAR WIDTH mm

FIGURE 59: Temperature differences between position 4 (hot spot) and position 6 when the hot spot attains solidus and eutectoid transformation temperatures.

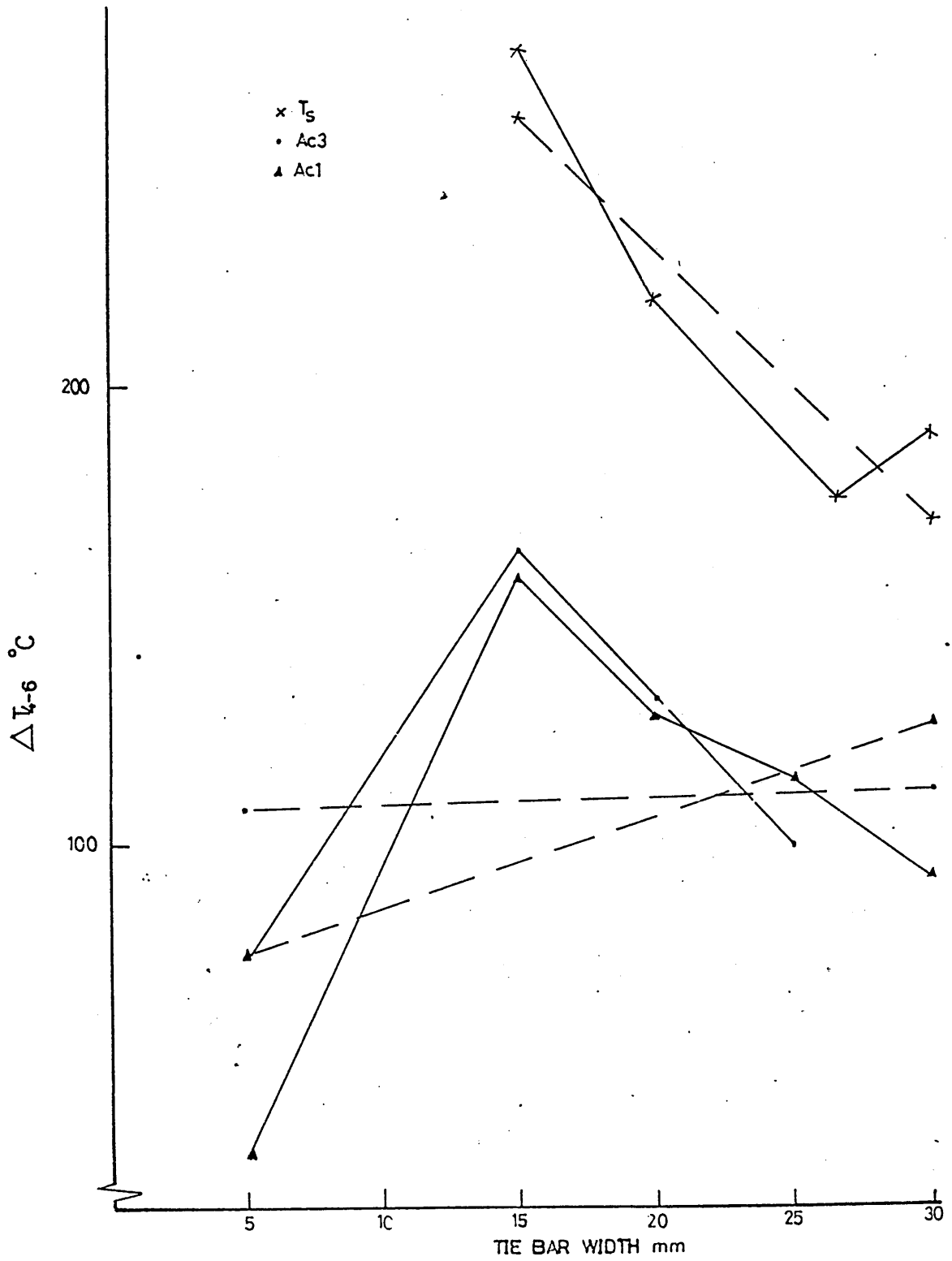
× T_S
• Ac3
▲ Ac1
200
100
ΔT_{4-6} °C
5
10
15
20
25
30
TIE BAR WIDTH mm

FIGURE 60: Temperature profiles of various locations in the sand. Locations are as shown in figure 22.

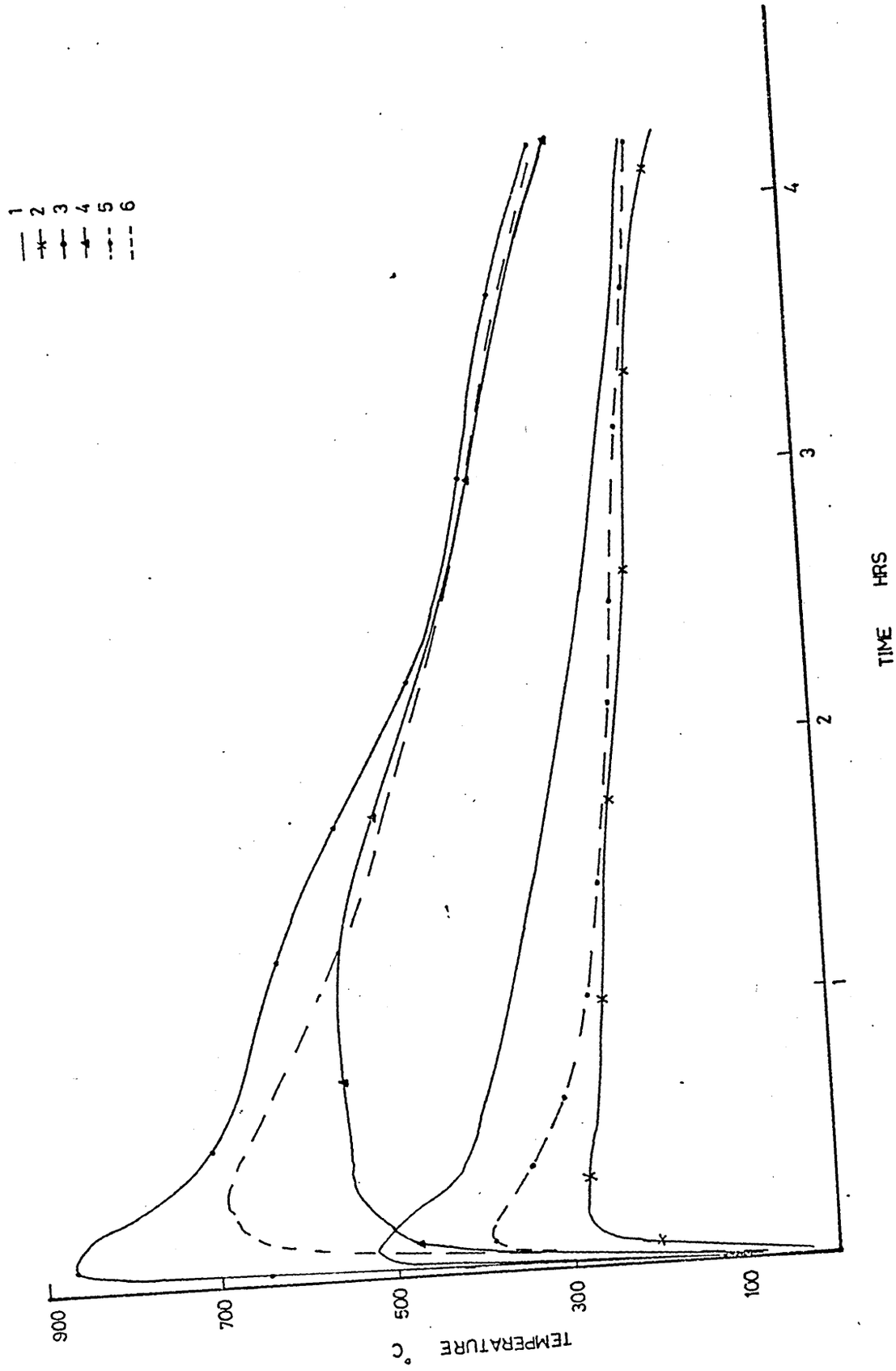
1
2
3
4
5
6
900
700
500
300
100
TEMPERATURE °C
1
2
3
4
TIME HRS

FIGURE 61: Cooling curve for the Theta ring with 10mm tie bar width during Annealing. Thermocouple locations are as shown in Figure 23.

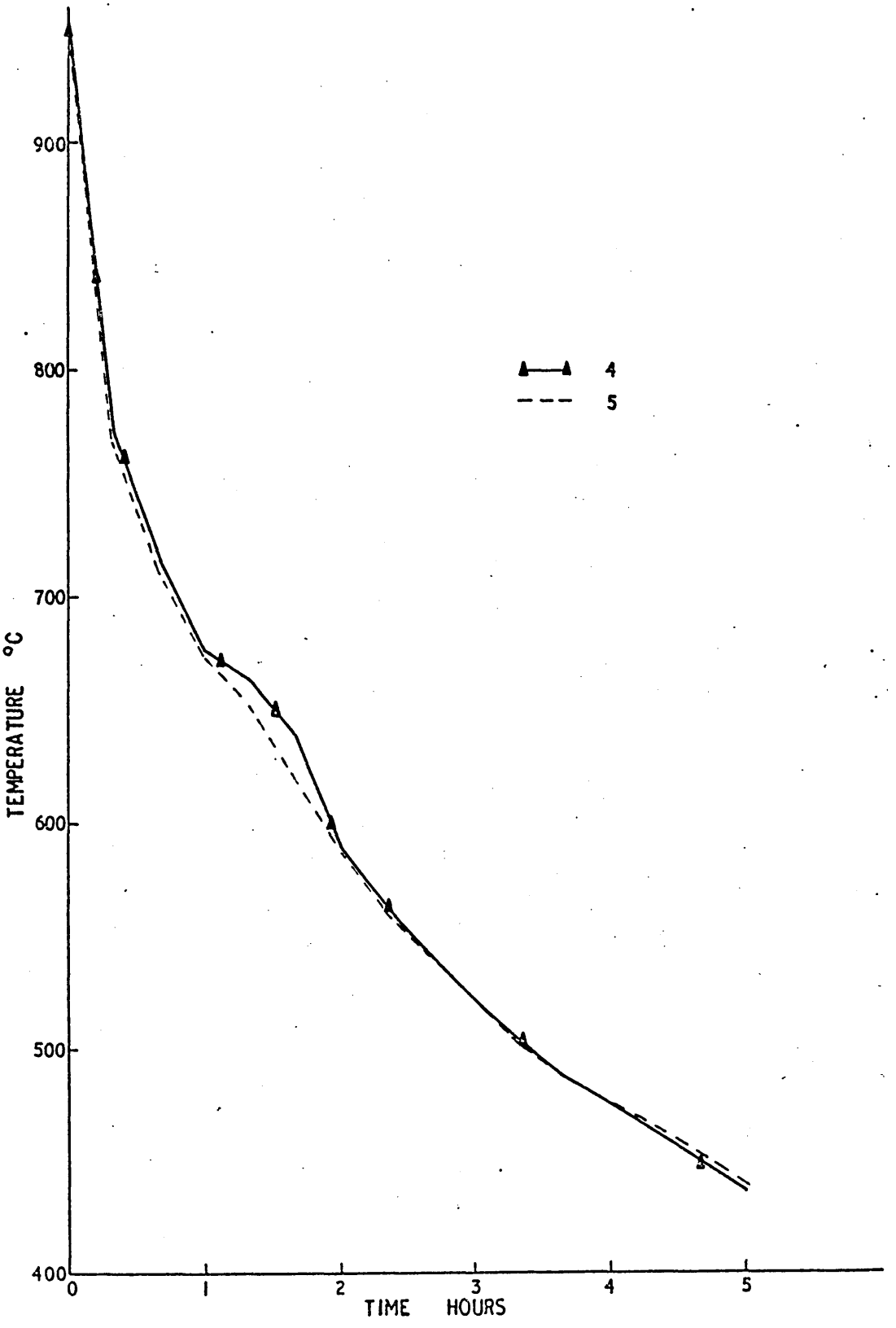
900
800
700
600
500
400
TEMPERATURE °C
0
1
2
3
4
5
TIME HOURS
4
5

FIGURE 62: Cooling curves for the Theta ring with 30mm tie bar width during Annealing. Thermocouple locations are as shown in Figure 21.

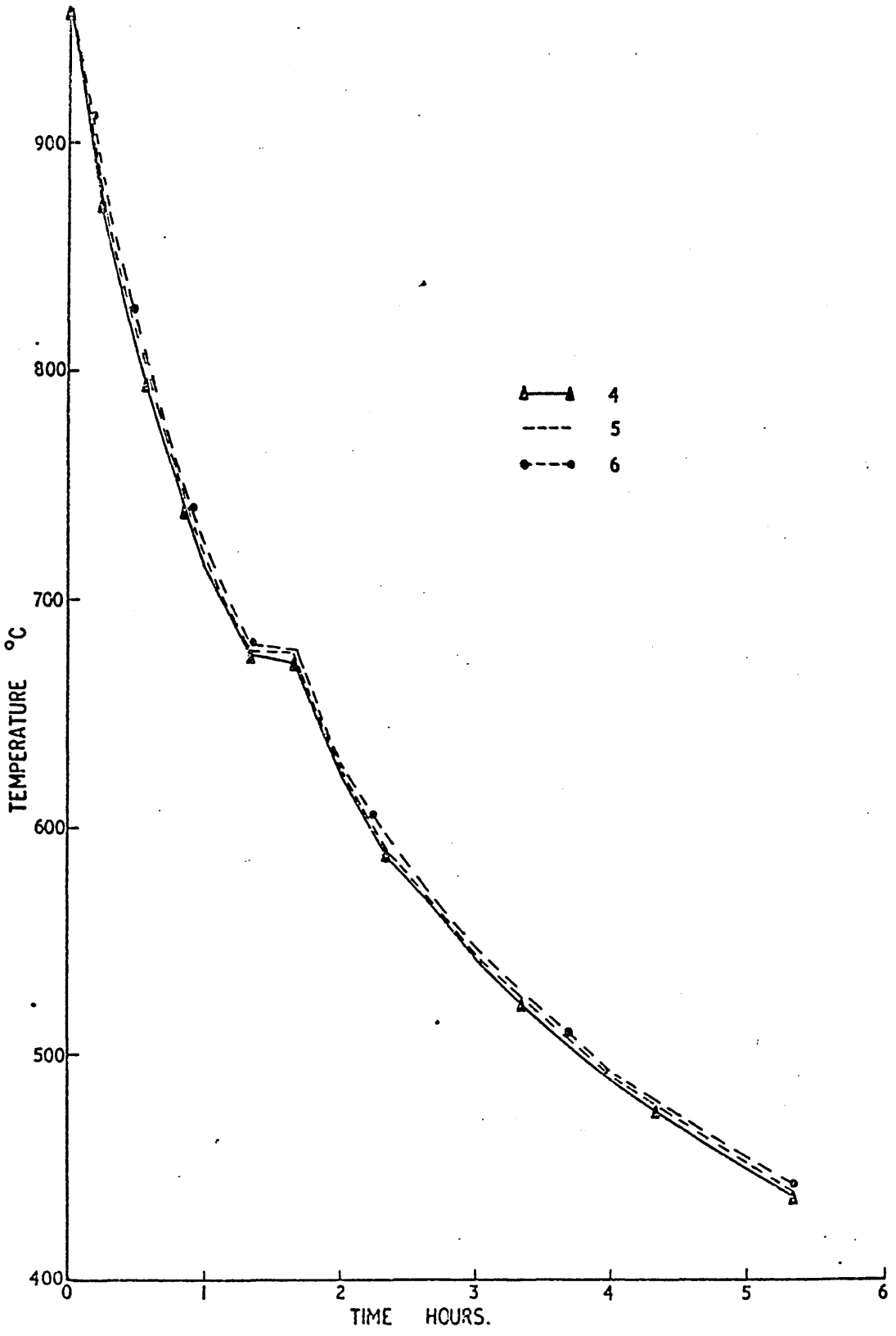
900
800
700
600
500
400
TEMPERATURE °C
0
1
2
3
4
5
6
TIME HOURS.
4
5
6

FIGURE 63: Cooling curves for the Theta ring with 10mm tie bar width during Normalising. Thermocouple locations are as shown in Figure 23.

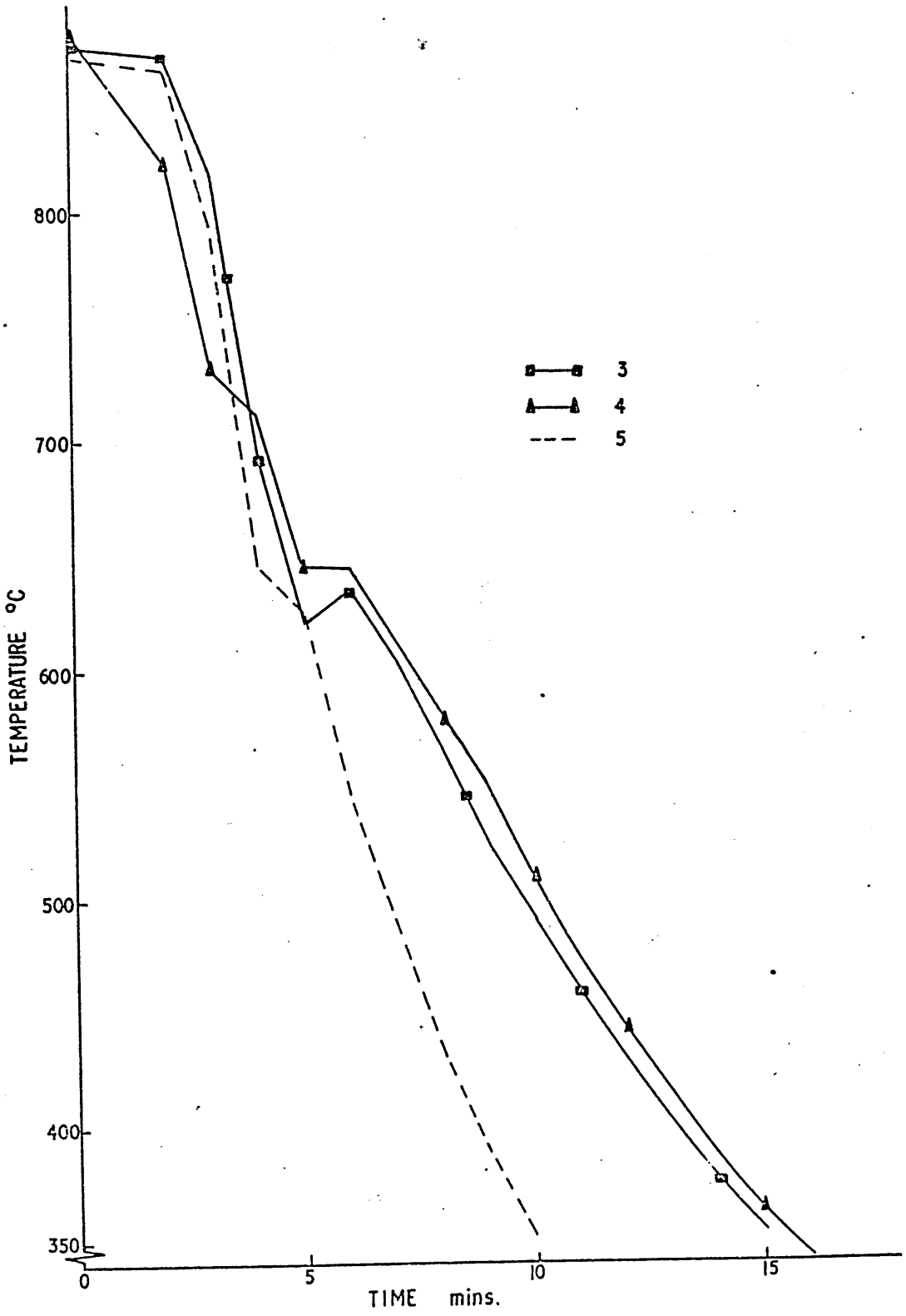
800
700
600
500
400
350
TEMPERATURE °C
0
5
10
15
TIME mins.
3
4
5

FIGURE 64: Cooling curves for the Theta ring with 30mm tie bar width during Normalising. Thermocouple locations are as shown in Figure 21.

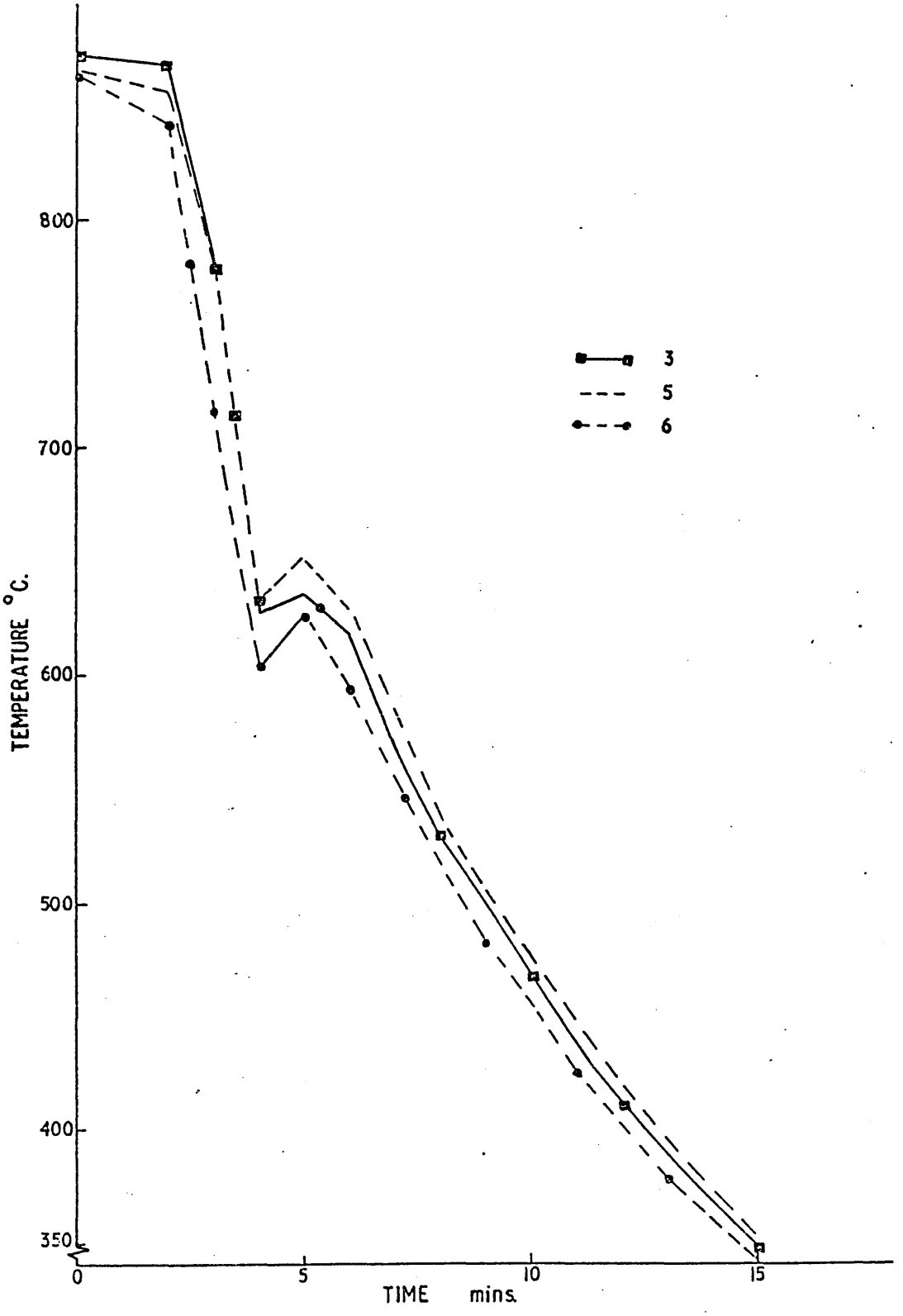
800
700
600
500
400
350
TEMPERATURE °C.
0
5
10
15
TIME mins.
3
5
6

FIGURE 65: Cooling curves for the Theta ring with 10mm tie bar width during Tempering. Thermocouple locations are as shown in Figure 23.

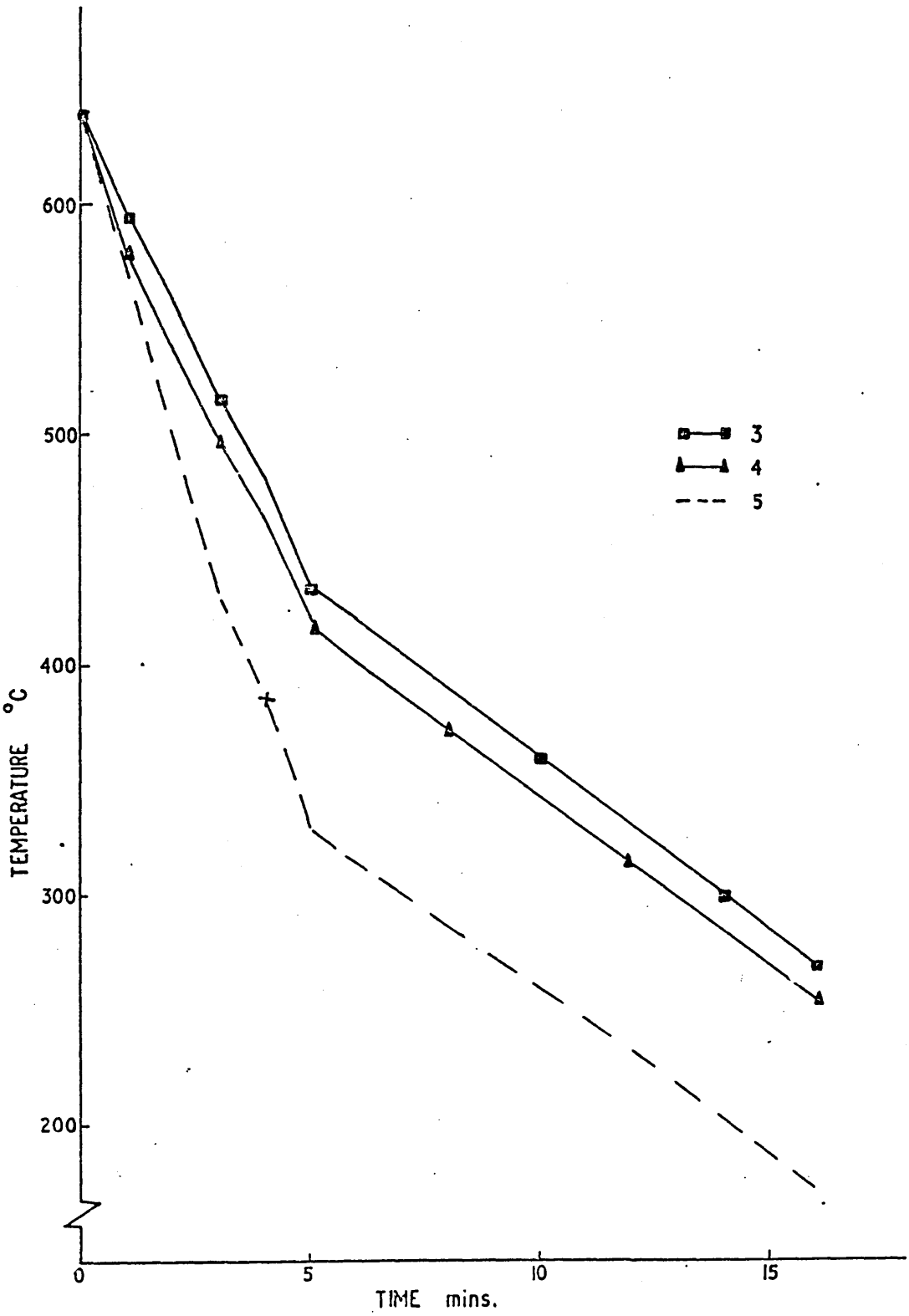
600
500
400
300
200
TEMPERATURE °C
0
5
10
15
TIME mins.
3
4
5

FIGURE 66: Cooling curves for the Theta ring with 30mm tie bar width during Tempering. Thermocouple locations are as shown in Figure 23.

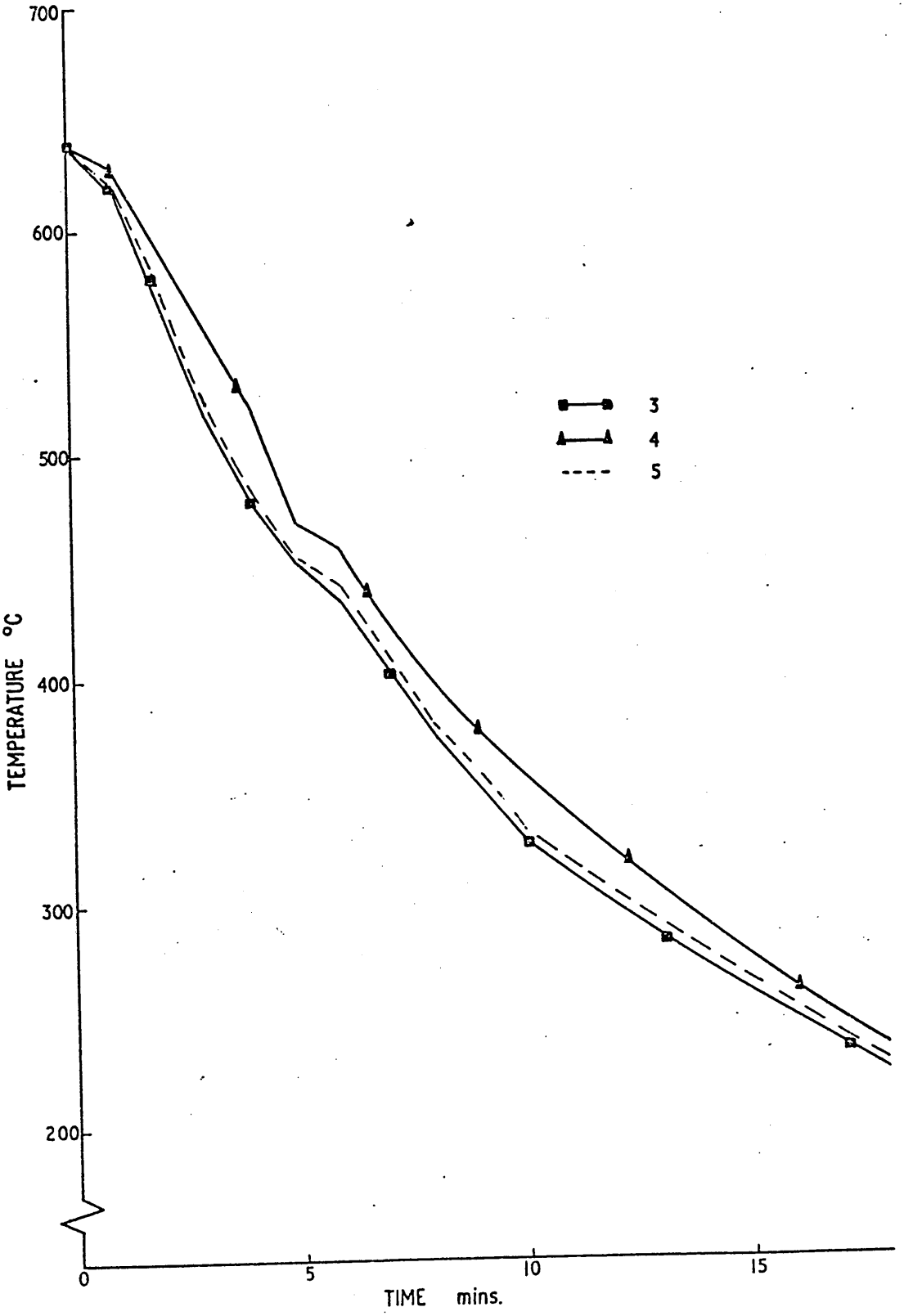
700
600
500
400
300
200
TEMPERATURE °C
0
5
10
15
TIME mins.
3
4
5

FIGURE 67: Surface preparation stresses induced in specimens in cast condition and the annealed conditions.

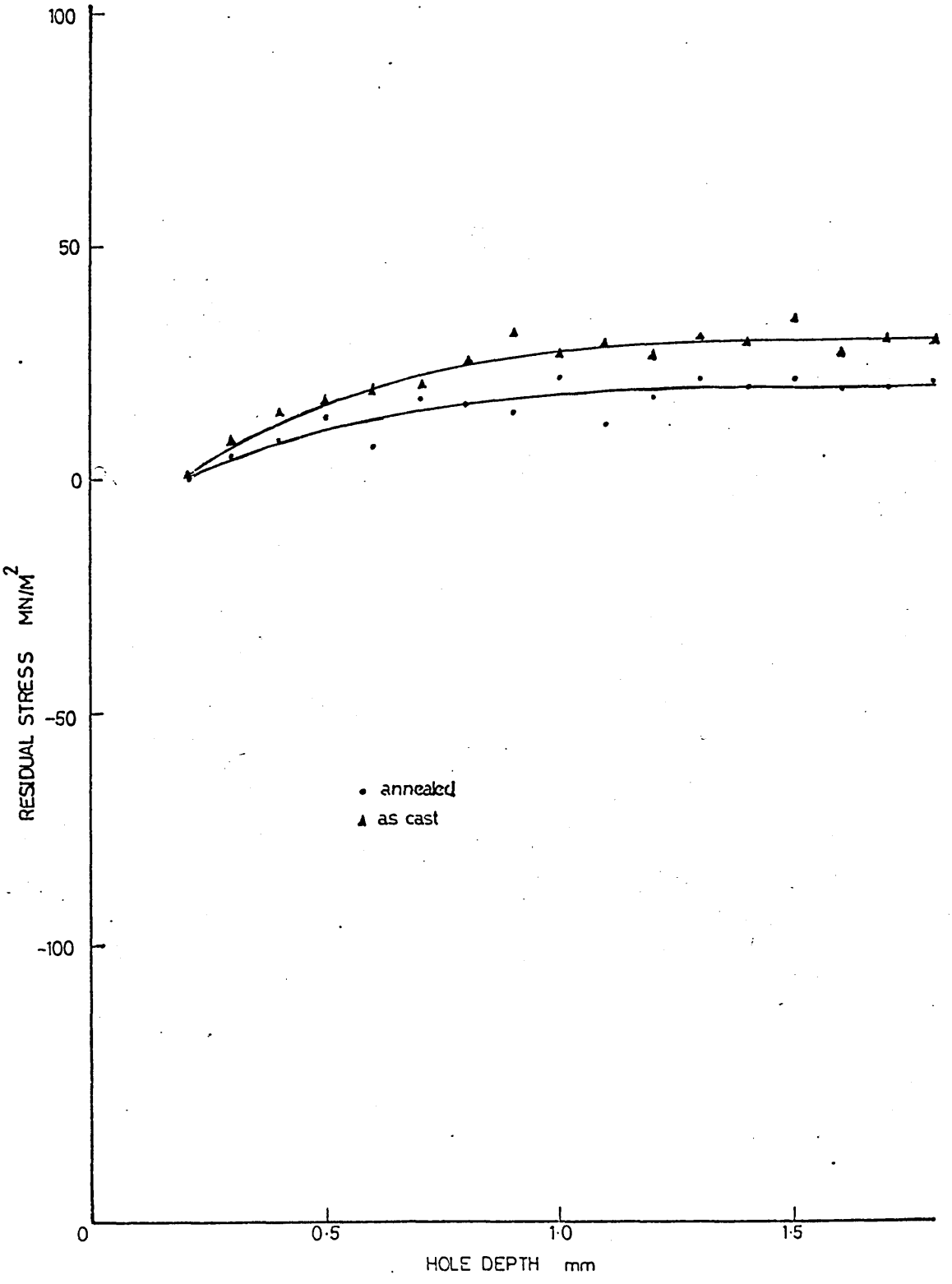
100
50
0
-50
-100
0
0·5
1·0
1·5
RESIDUAL STRESS MN/M2
HOLE DEPTH mm
annealed
as cast

FIGURE 68: Variation of the shift in runner upon sectioning with tie bar widths, best fit line is also superimposed.

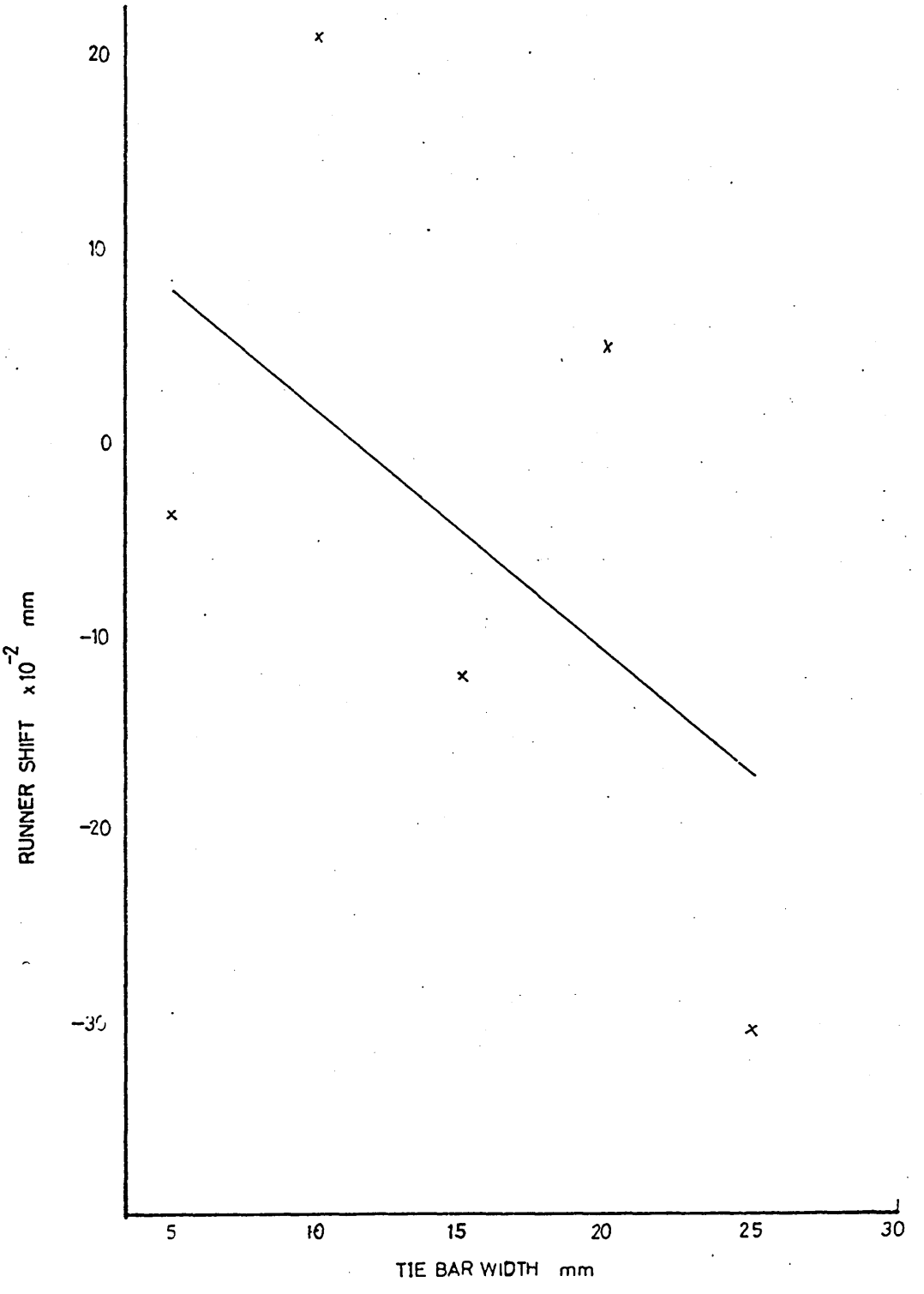
20
10
0
-10
-20
-30
RUNNER SHIFT x10^{-2} mm
5
10
15
20
25
30
TIE BAR WIDTH mm

FIGURE 69: The residual stress in the runner and its effect on as cast residual stress levels in 30mm tie bar width theta ring before and after runner removal (Locations are those shown in Figure 21).

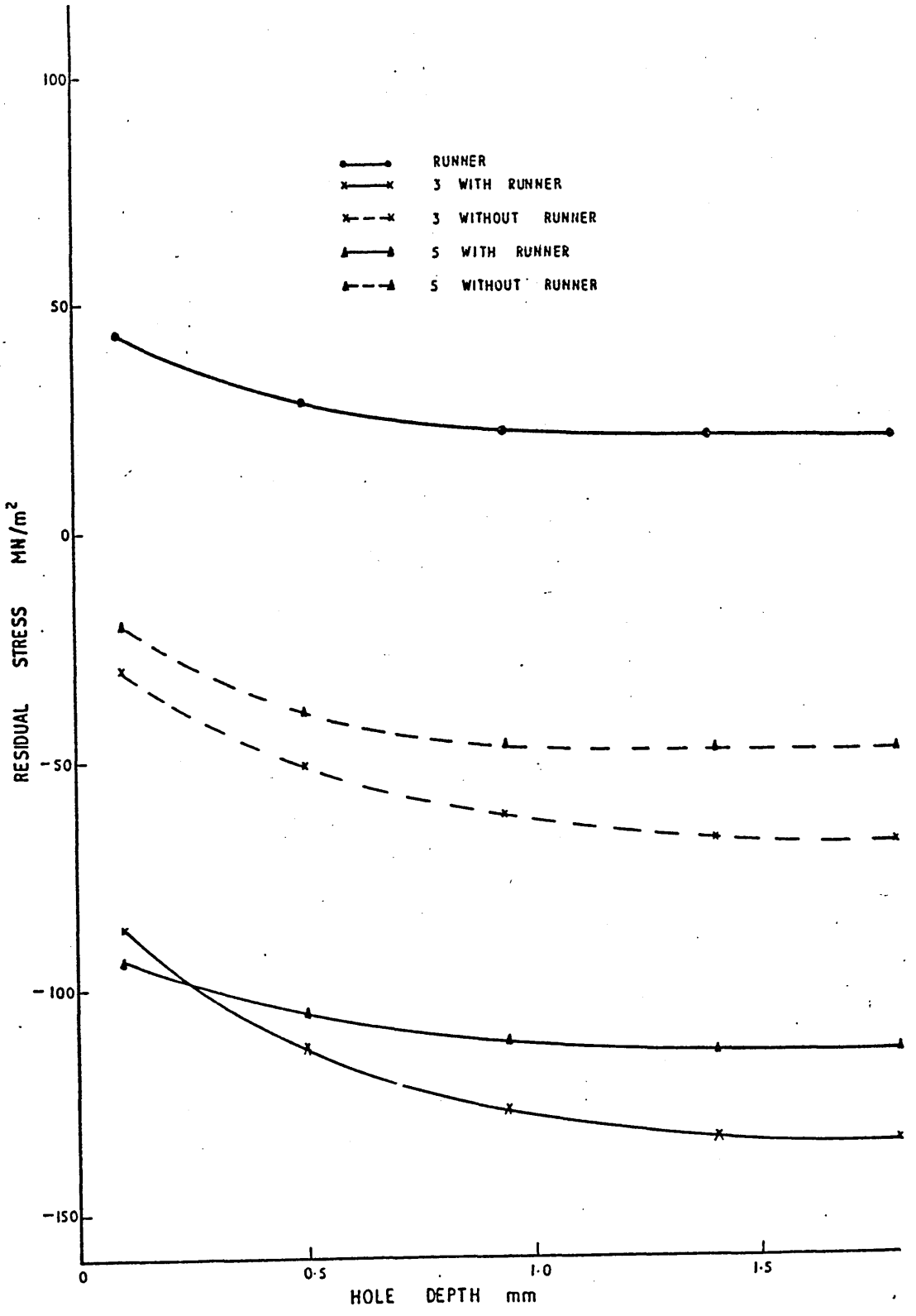
RUNNER
3 WITH RUNNER
3 WITHOUT RUNNER
5 WITH RUNNER
5 WITHOUT RUNNER
100
50
0
-50
-100
-150
RESIDUAL STRESS MN/m²
0
0·5
1·0
1·5
HOLE DEPTH mm

FIGURE 70: Variation of residual stress distribution in as cast Theta ring with 5mm tie bar width with hole depth (Locations are those shown in Figure 21).

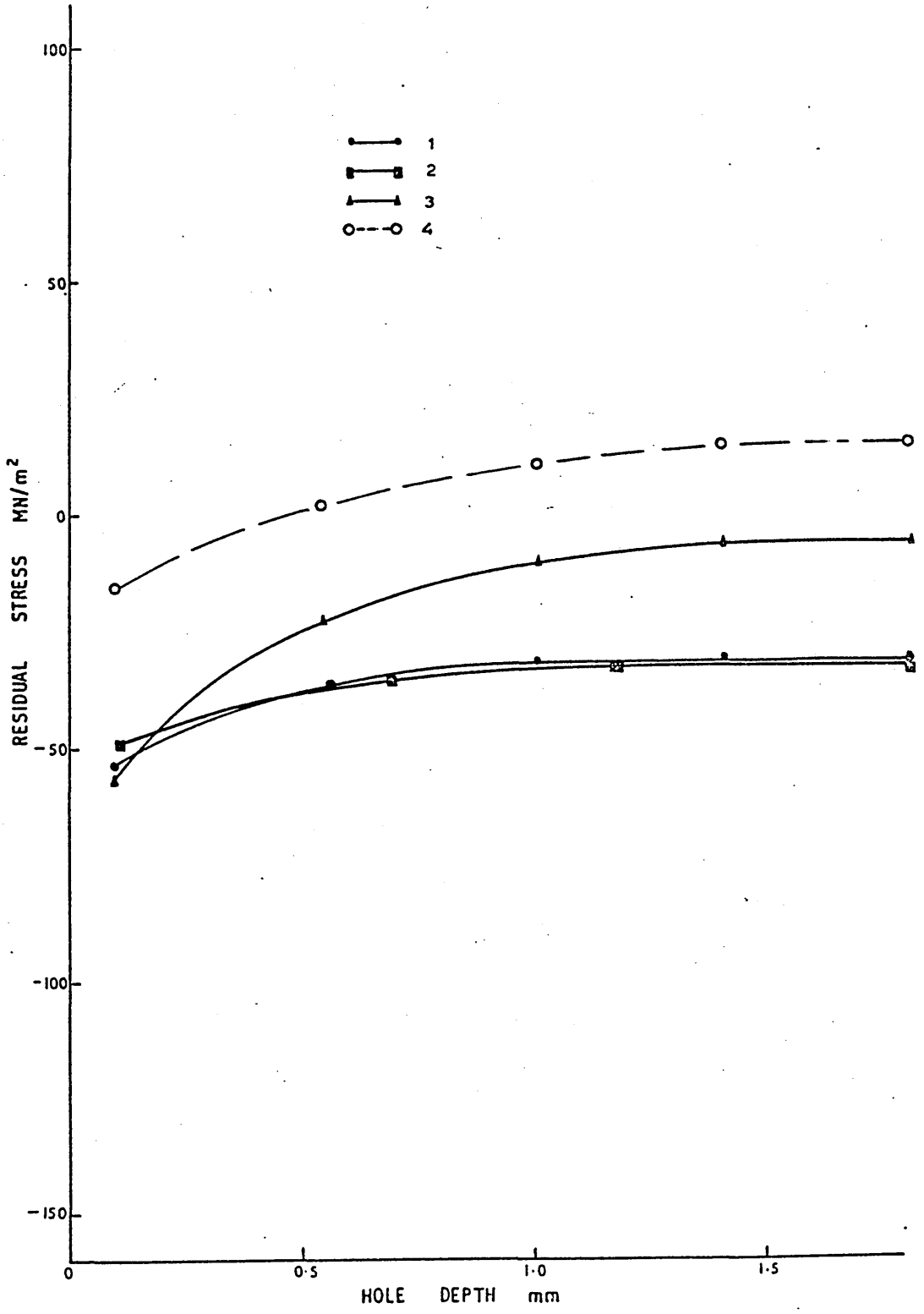
100
50
0
-50
-100
-150
RESIDUAL STRESS MN/m²
1
2
3
4
0
0·5
1·0
1·5
HOLE DEPTH mm

FIGURE 71: Variation of residual stress distribution in as cast Theta ring with 10mm tie bar width with hole depth (Locations are those shown in Figure 21).

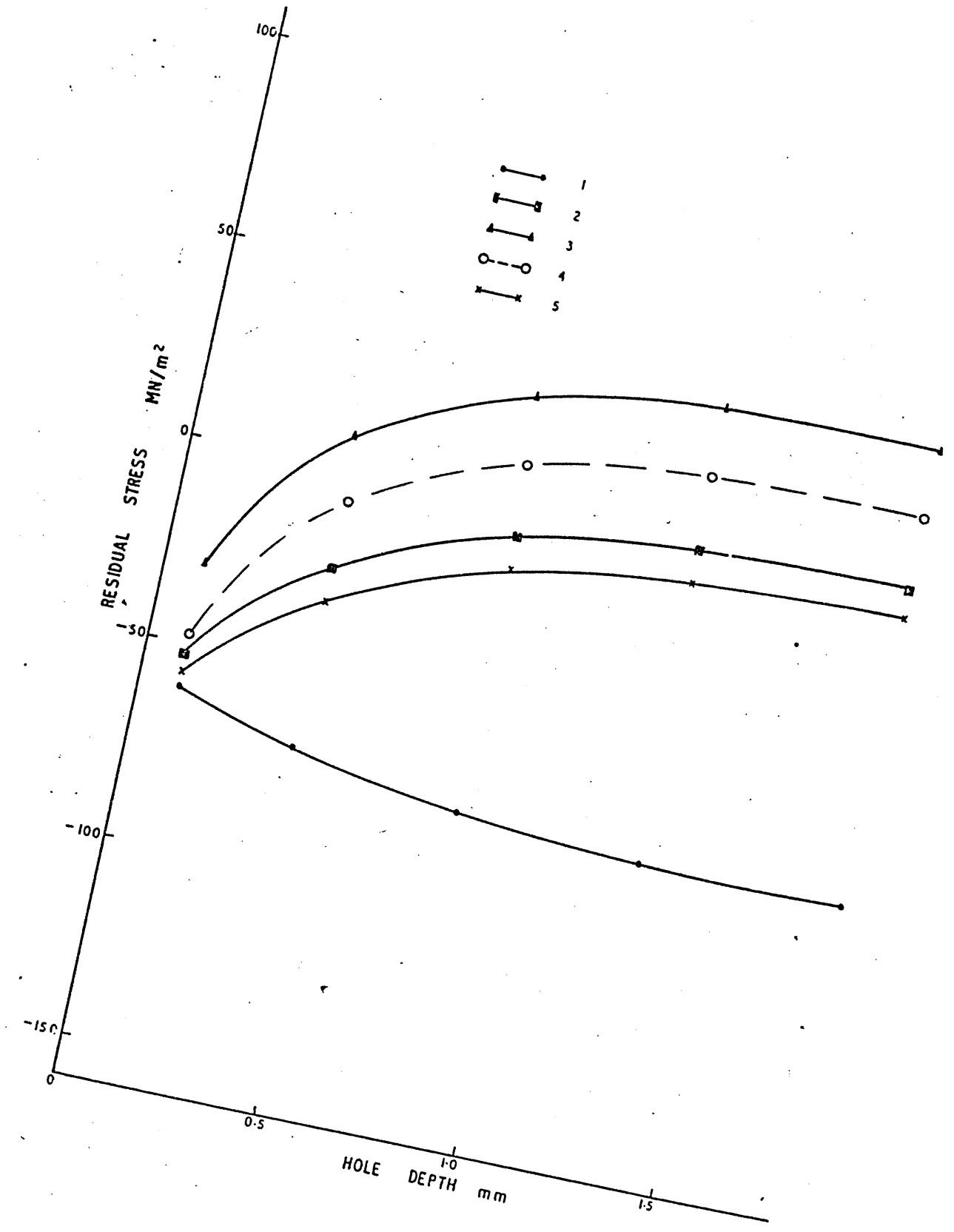
100
50
0
-50
-100
-150
RESIDUAL STRESS MN/m²
1
2
3
4
5
0
0.5
1.0
1.5
HOLE DEPTH mm

FIGURE 72: Variation of residual stress distribution in as cast Theta ring with 15mm tie bar width with hole depth (Locations are those shown in Figure 21).

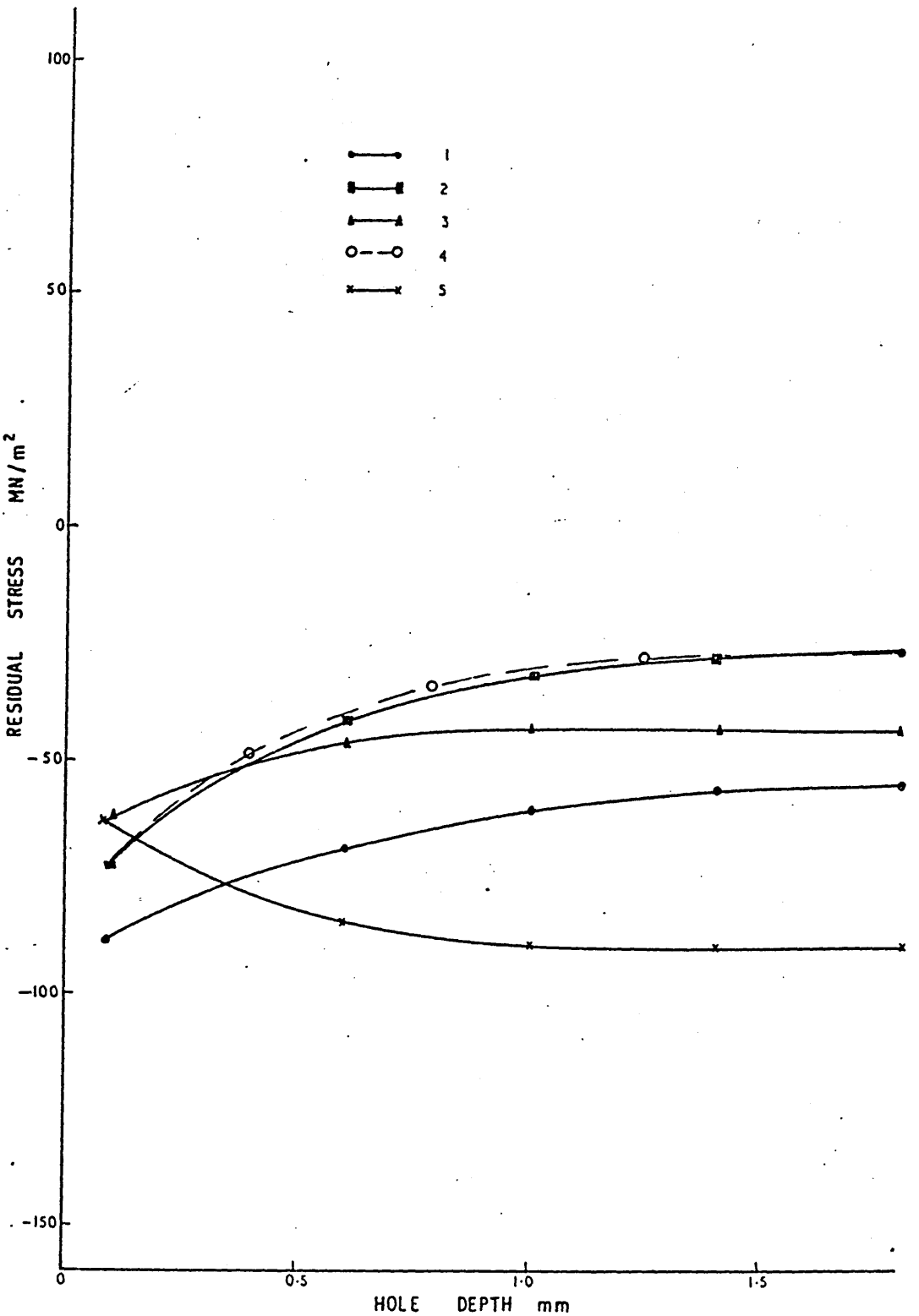
100
50
0
-50
-100
-150
RESIDUAL STRESS MN/m²
1
2
3
4
5
0
0·5
1·0
1·5
HOLE DEPTH mm

FIGURE 73: Variation of residual stress distribution in as cast Theta ring with 20mm tie bar width with hole depth (Locations are those shown in Figure 21).

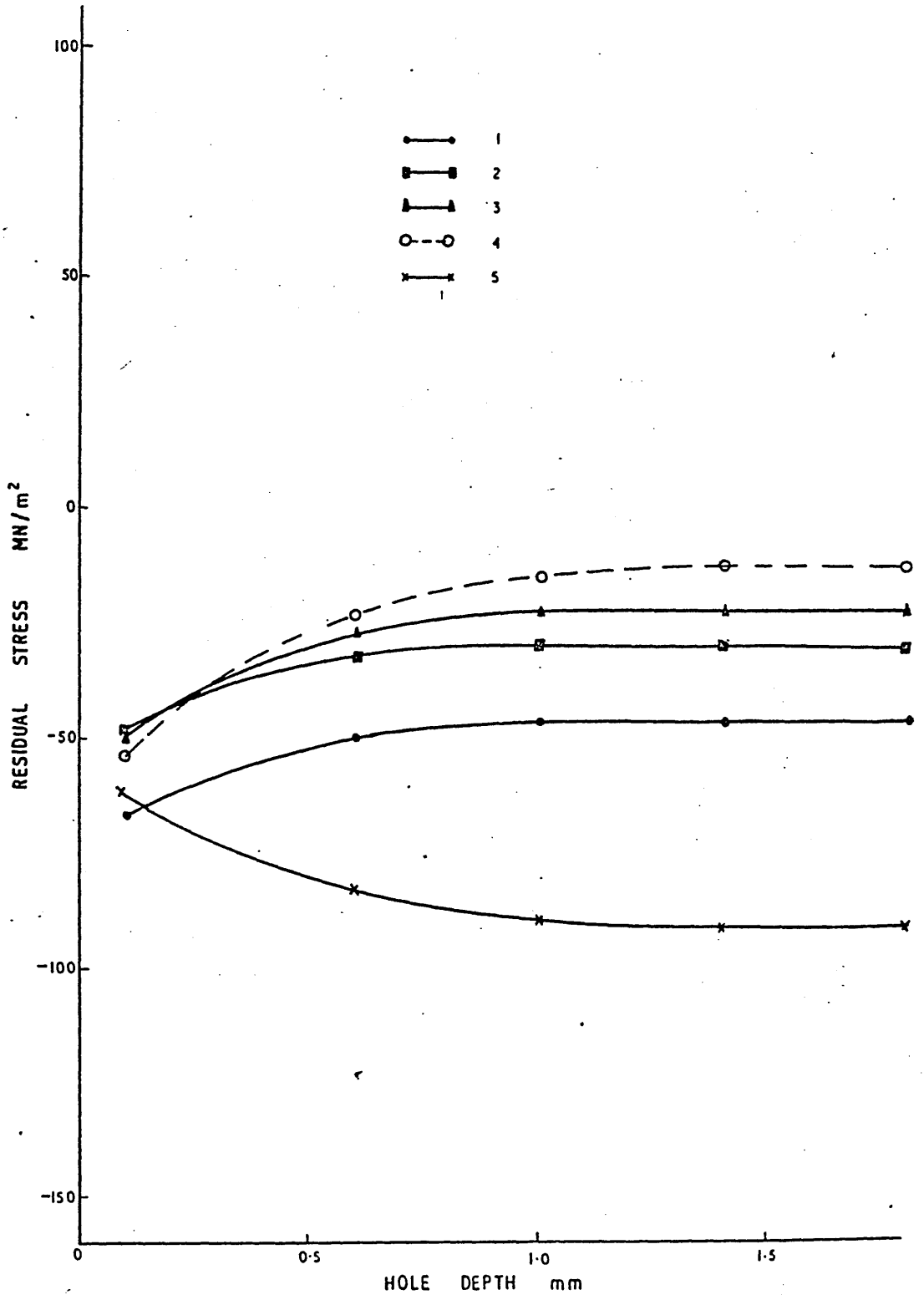
100
50
0
-50
-100
-150
RESIDUAL STRESS MN/m²
1
2
3
4
5
0
0·5
1·0
1·5
HOLE DEPTH mm

FIGURE 74: Variation of residual stress distribution in as cast Theta ring with 25mm tie bar width with hole depth (Locations are those shown in Figure 21).

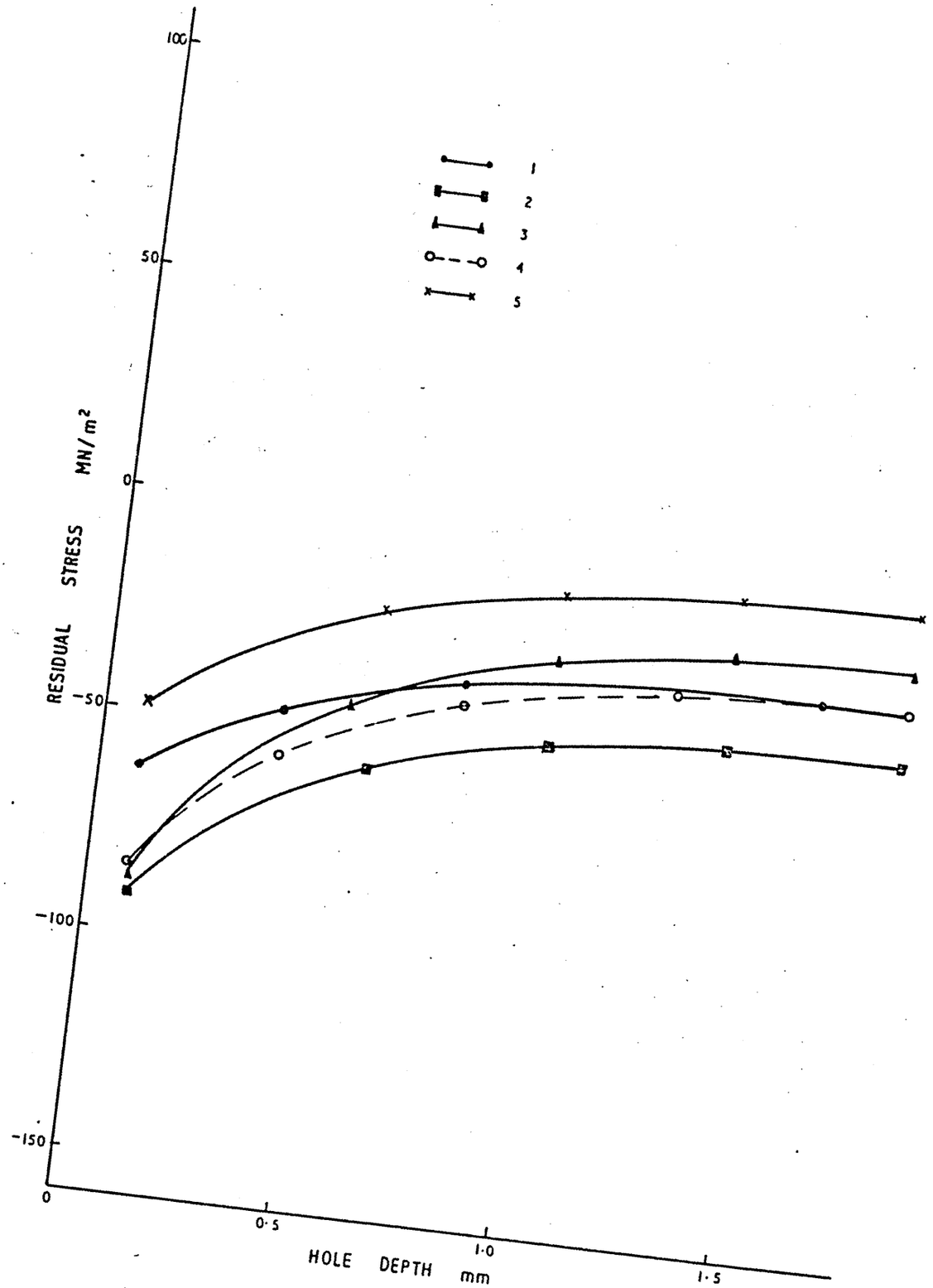
100
50
0
-50
-100
-150
RESIDUAL STRESS MN/m²
1
2
3
4
5
0
0·5
1·0
1·5
HOLE DEPTH mm

FIGURE 75: Variation of residual stress distribution in as cast Theta ring with 30mm tie bar width with hole depth (Locations are those shown in Figure 21).

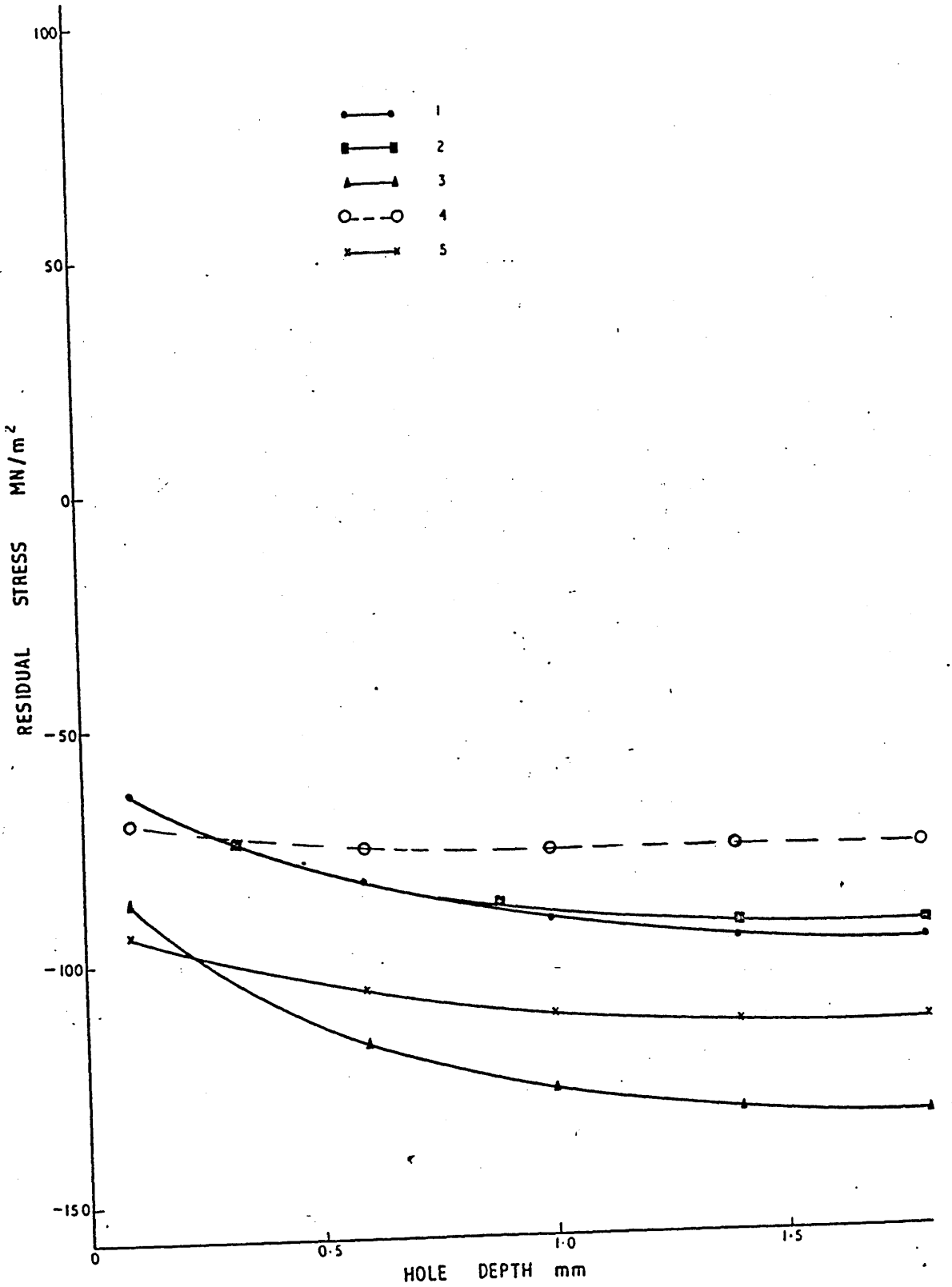
100
50
0
-50
-100
-150
RESIDUAL STRESS MN/m²
1
2
3
4
5
0
0·5
1·0
1·5
HOLE DEPTH mm

FIGURE 76: Variation of Residual stress at position 1 in theta rings with different tie bar widths and hole depth (Location of position is shown in Figure 21).

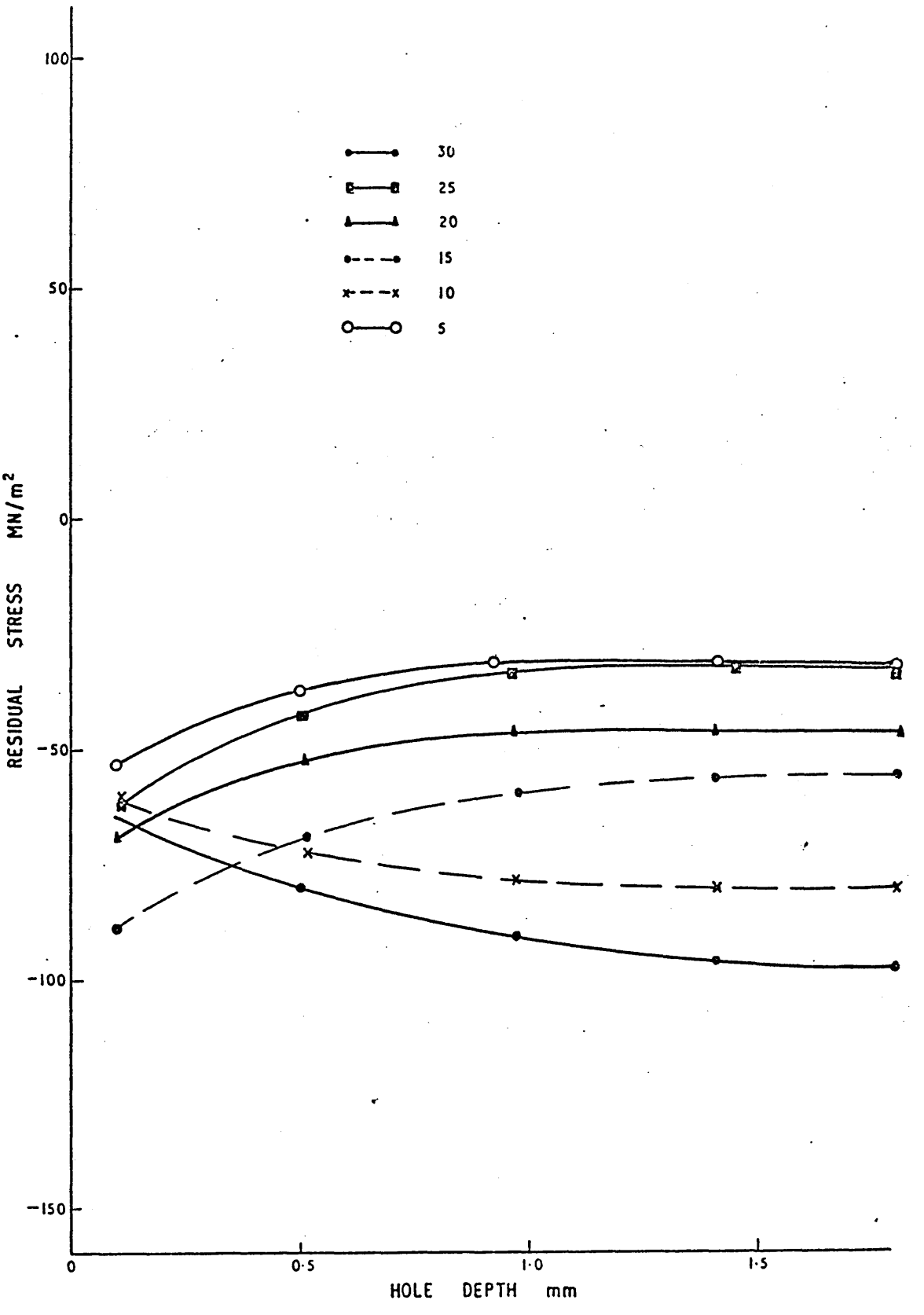
100
50
0
-50
-100
-150
RESIDUAL STRESS MN/m²
30
25
20
15
10
5
0
0·5
1·0
1·5
HOLE DEPTH mm

FIGURE 77: Variation of Residual stress at position 2 in theta rings with different tie bar widths and hole depth (Location of position is shown in Figure 21).

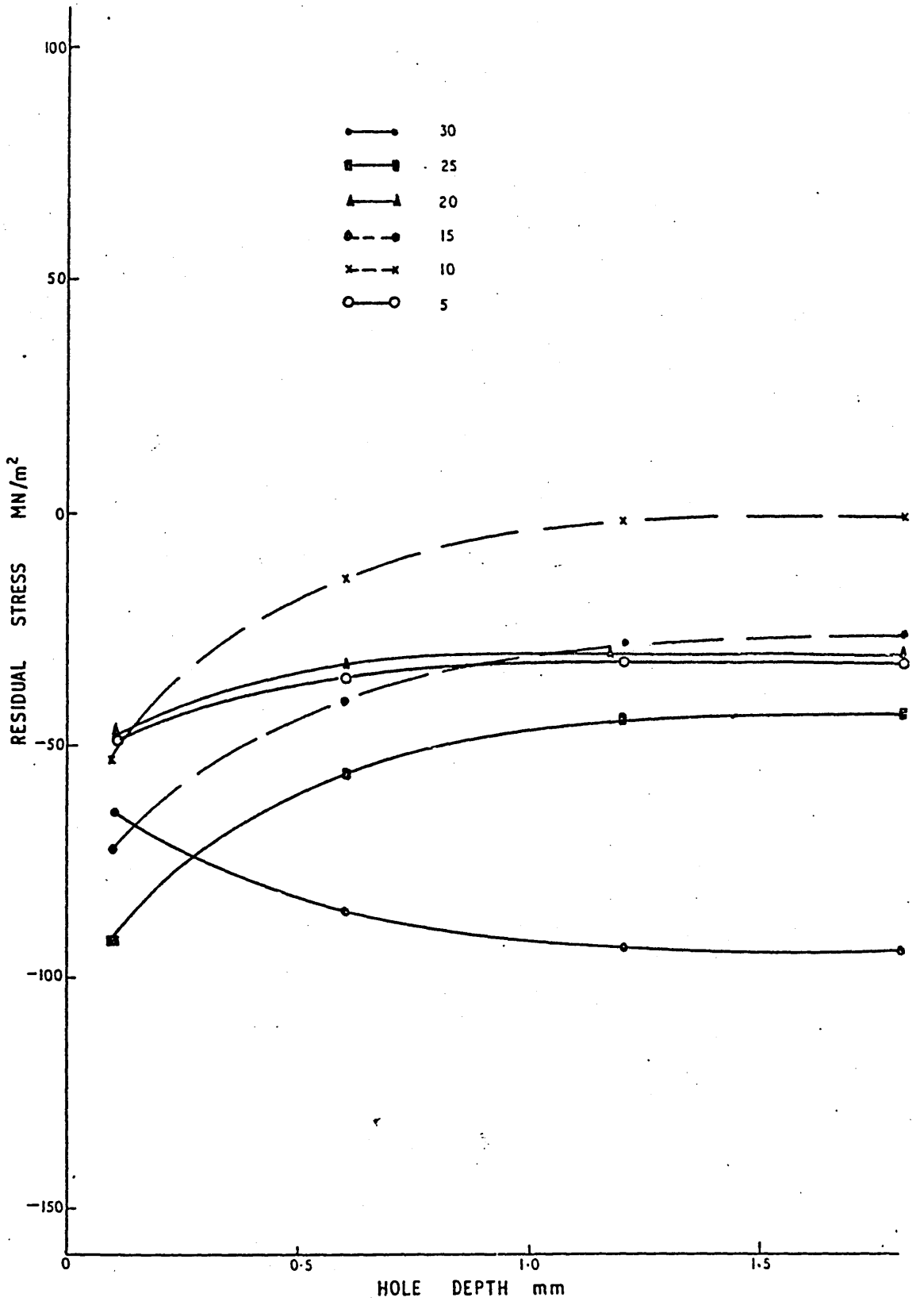
100
50
0
-50
-100
-150
RESIDUAL STRESS MN/m²
30
25
20
15
10
5
0
0·5
1·0
1·5
HOLE DEPTH mm

FIGURE 78: Variation of Residual stress at position 3 in theta rings with different tie bar widths and hole depth (Location of position is shown in Figure 21).

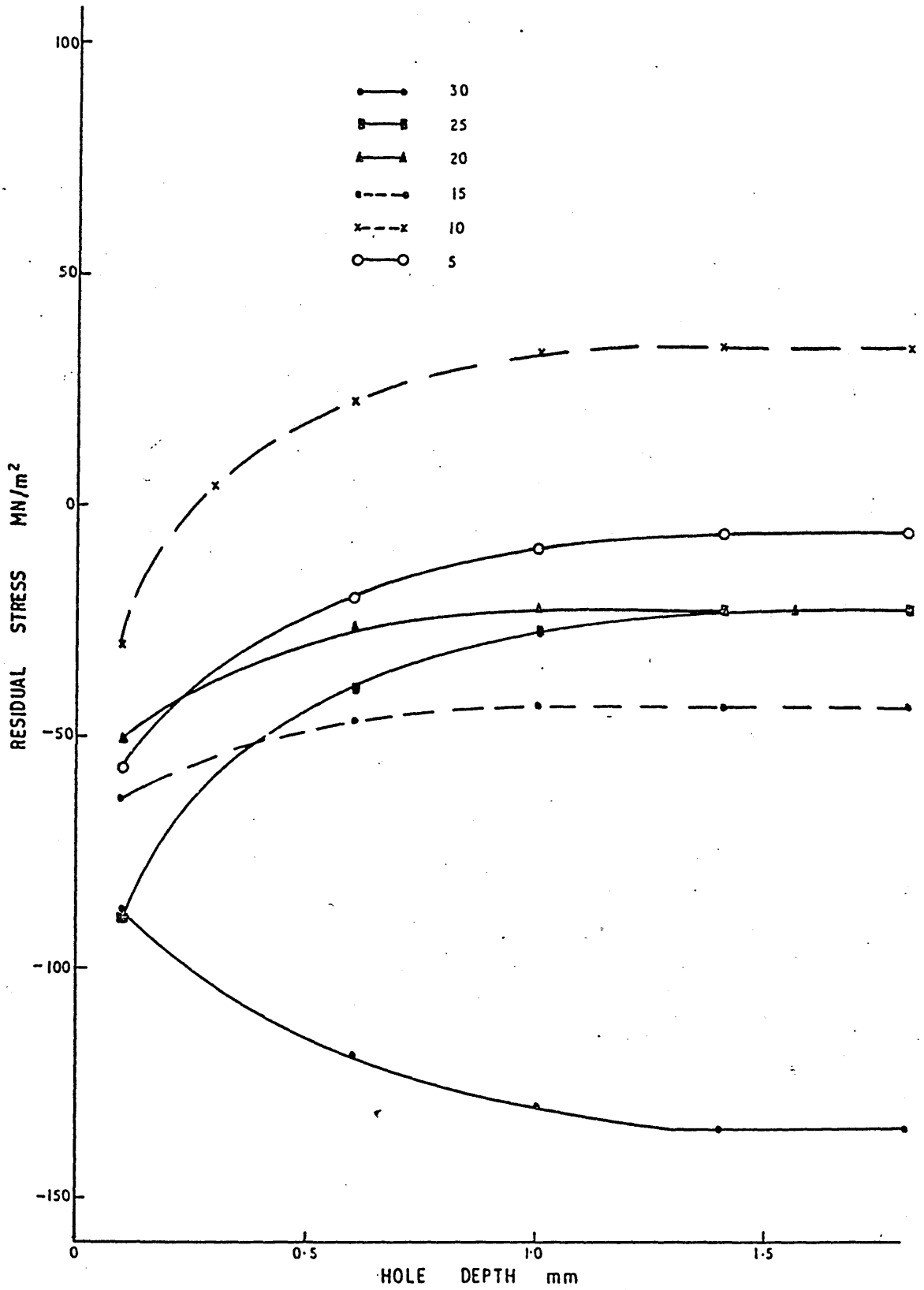
30
25
20
15
10
5
100
50
0
-50
-100
-150
RESIDUAL STRESS MN/m²
0
0·5
1·0
1·5
HOLE DEPTH mm

FIGURE 79: Variation of Residual stress at position 4 in theta rings with different tie bar widths and hole depth (Location of position is shown in Figure 21).

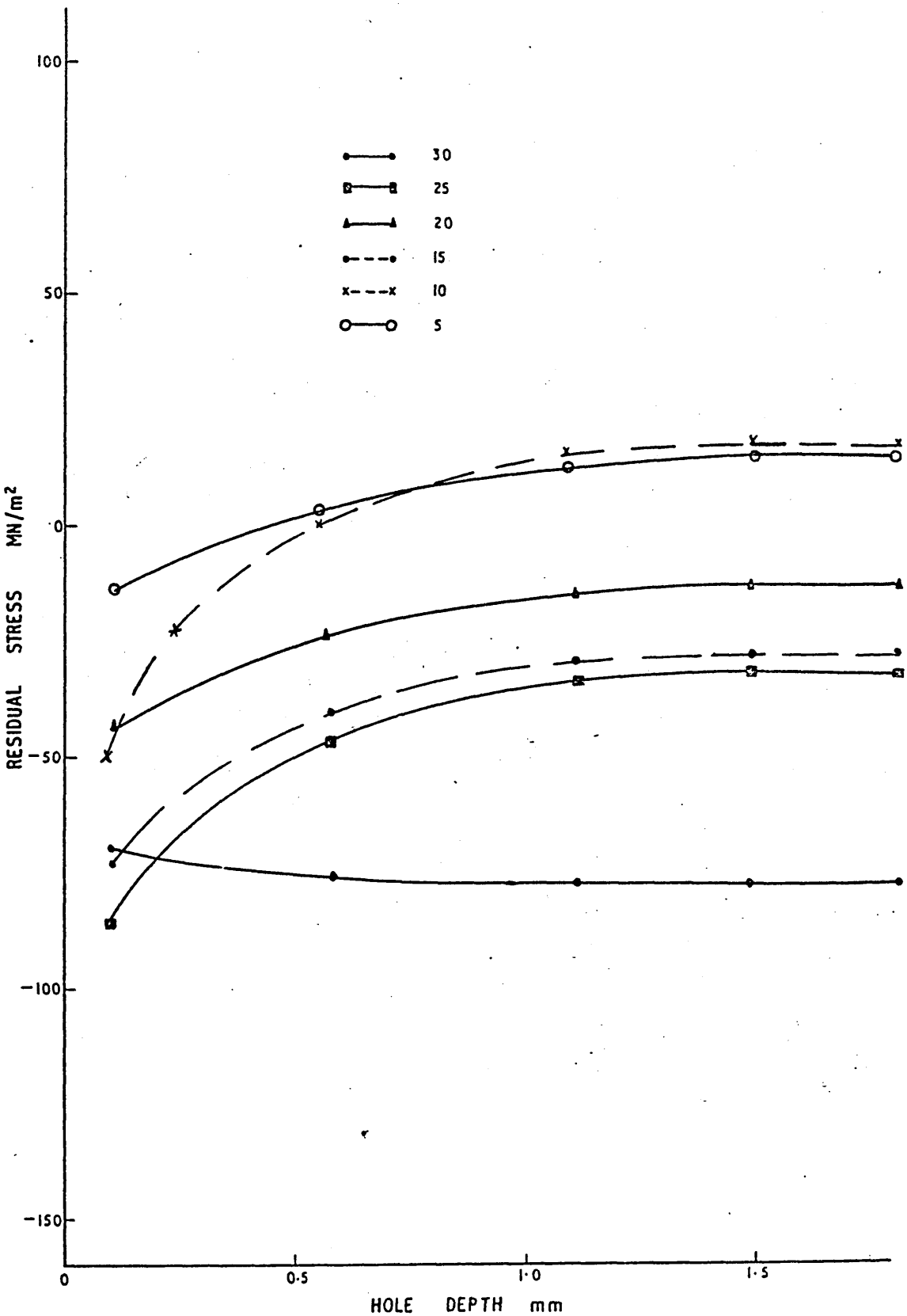
30
25
20
15
10
5
100
50
0
−50
−100
−150
RESIDUAL STRESS MN/m²
0
0·5
1·0
1·5
HOLE DEPTH mm

FIGURE 80: Variation of Residual stress at position 5 in theta rings with different tie bar widths and hole depth (Location of position is shown in Figure 21).

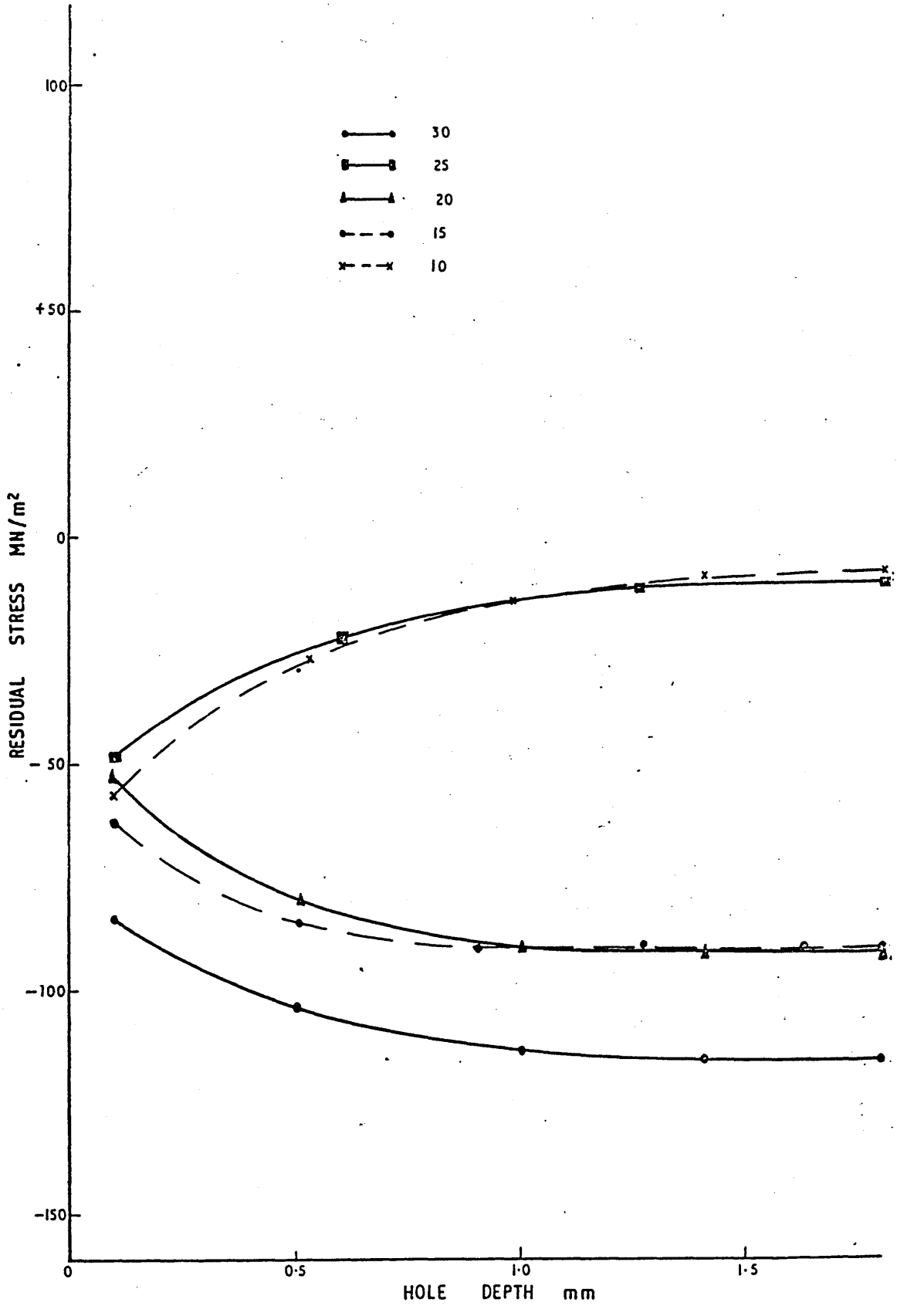
30
25
20
15
10
100
+50
0
-50
-100
-150
RESIDUAL STRESS MN/m²
0
0·5
1·0
1·5
HOLE DEPTH mm

FIGURE 81: Computed best fit line for the as cast residual stress at hole depth equal to diameter at position 1 in theta rings with different tie bar widths (Location of position is shown in Figure 21).

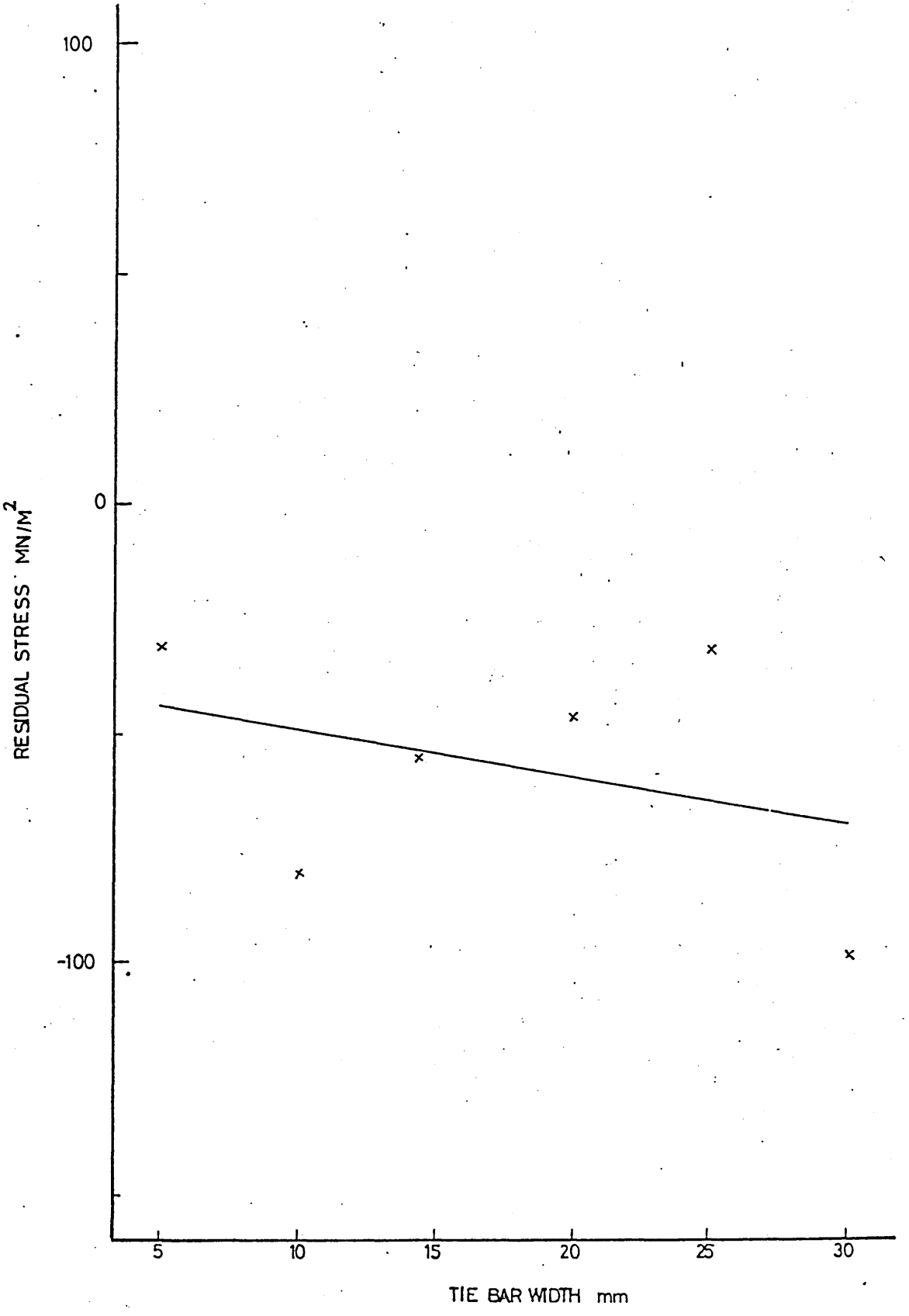
100
0
-100
RESIDUAL STRESS · MN/M2
5
10
15
20
25
30
TIE BAR WIDTH mm

FIGURE 82: Computed best fit line for the as cast residual stress at hole depth equal to diameter at position 2 in theta rings with different tie bar widths (Location of position is shown in Figure 21).

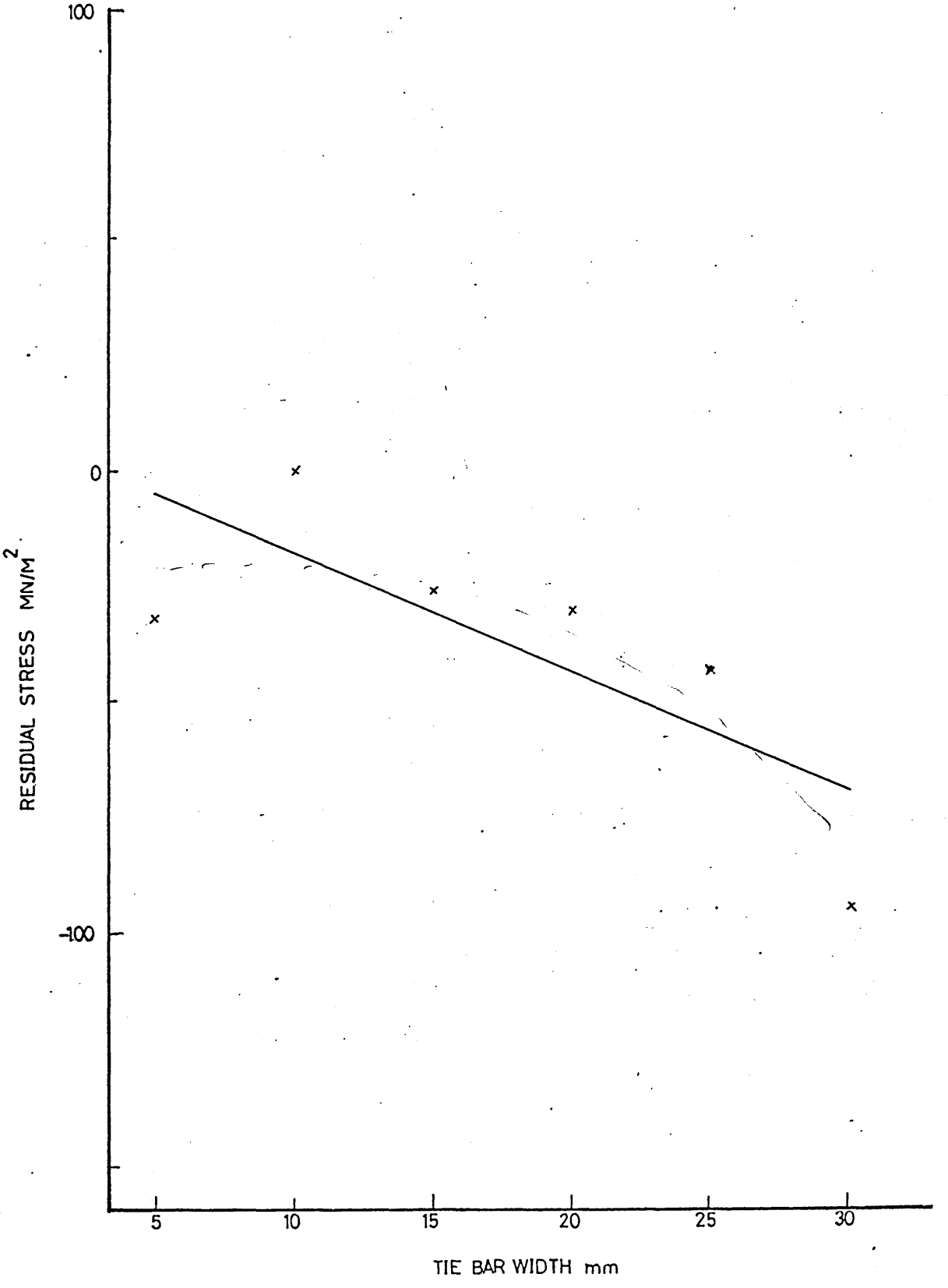
100
0
-100
RESIDUAL STRESS MN/M^2
5
10
15
20
25
30
TIE BAR WIDTH mm

FIGURE 83: Computed best fit line for the as cast residual stress at hole depth equal to diameter at position 3 in theta rings with different tie bar widths (Location of position is shown in Figure 21).

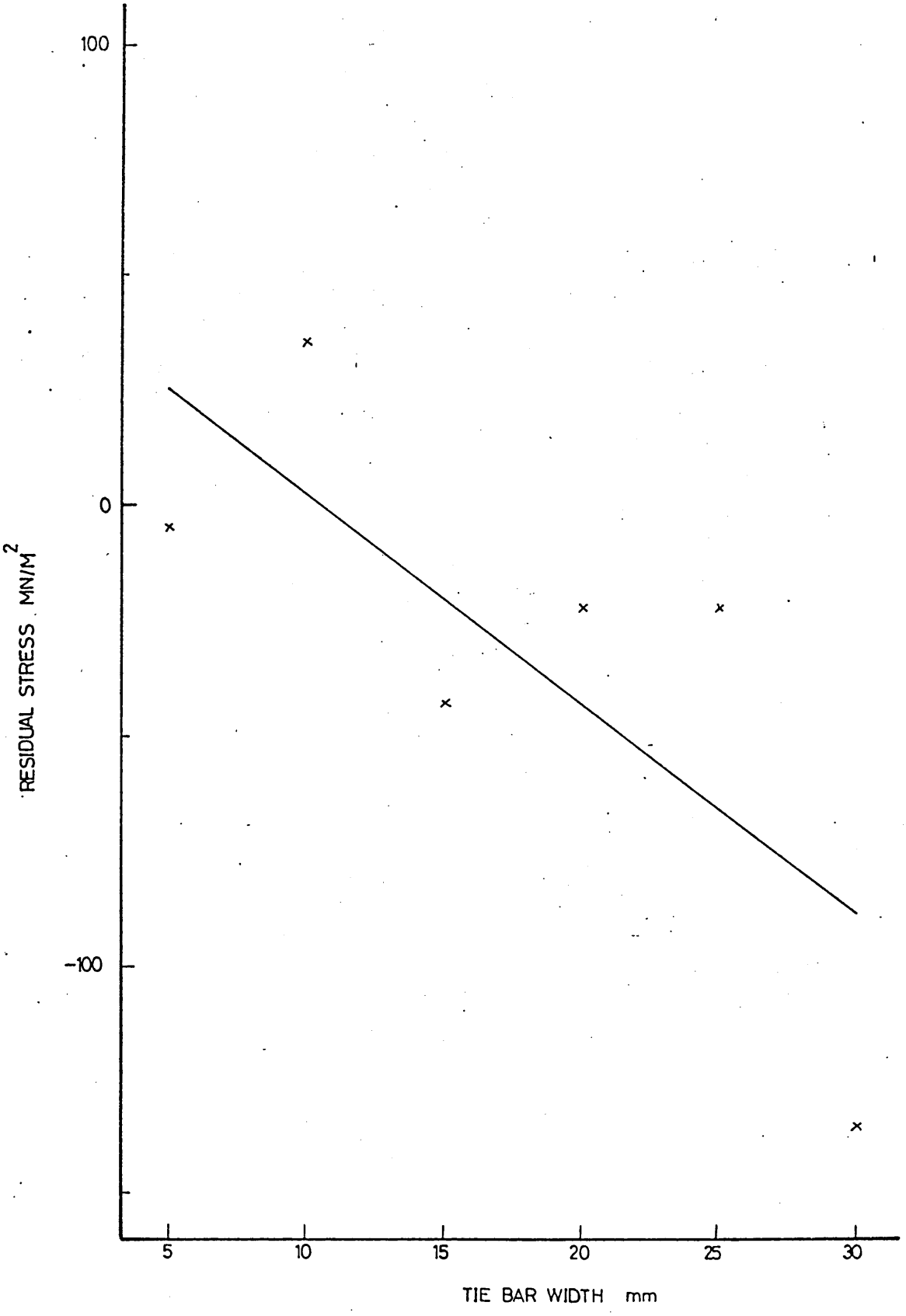
100
0
-100
RESIDUAL STRESS MN/M2
5
10
15
20
25
30
TIE BAR WIDTH mm

FIGURE 84: Computed best fit line for the as cast residual stress at hole depth equal to diameter at position 4 in theta rings with different tie bar widths (Location of position is shown in Figure 21).

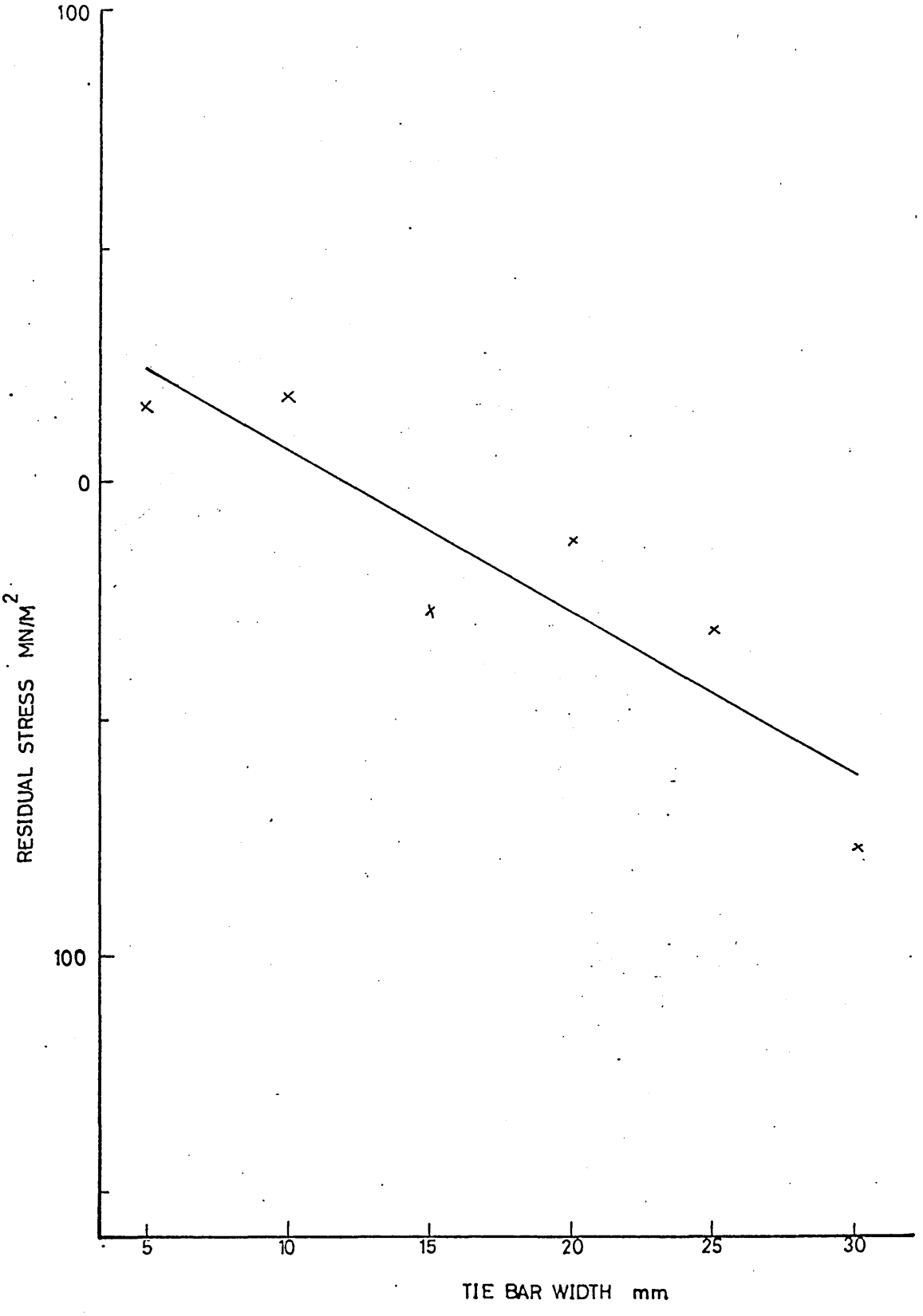
100
0
100
RESIDUAL STRESS MN/M2
5
10
15
20
25
30
TIE BAR WIDTH mm

FIGURE 85: Computed best fit line for the as cast residual stress at hole depth equal to diameter at position 5 in theta rings with different tie bar widths (Location of position is shown in Figure 21).

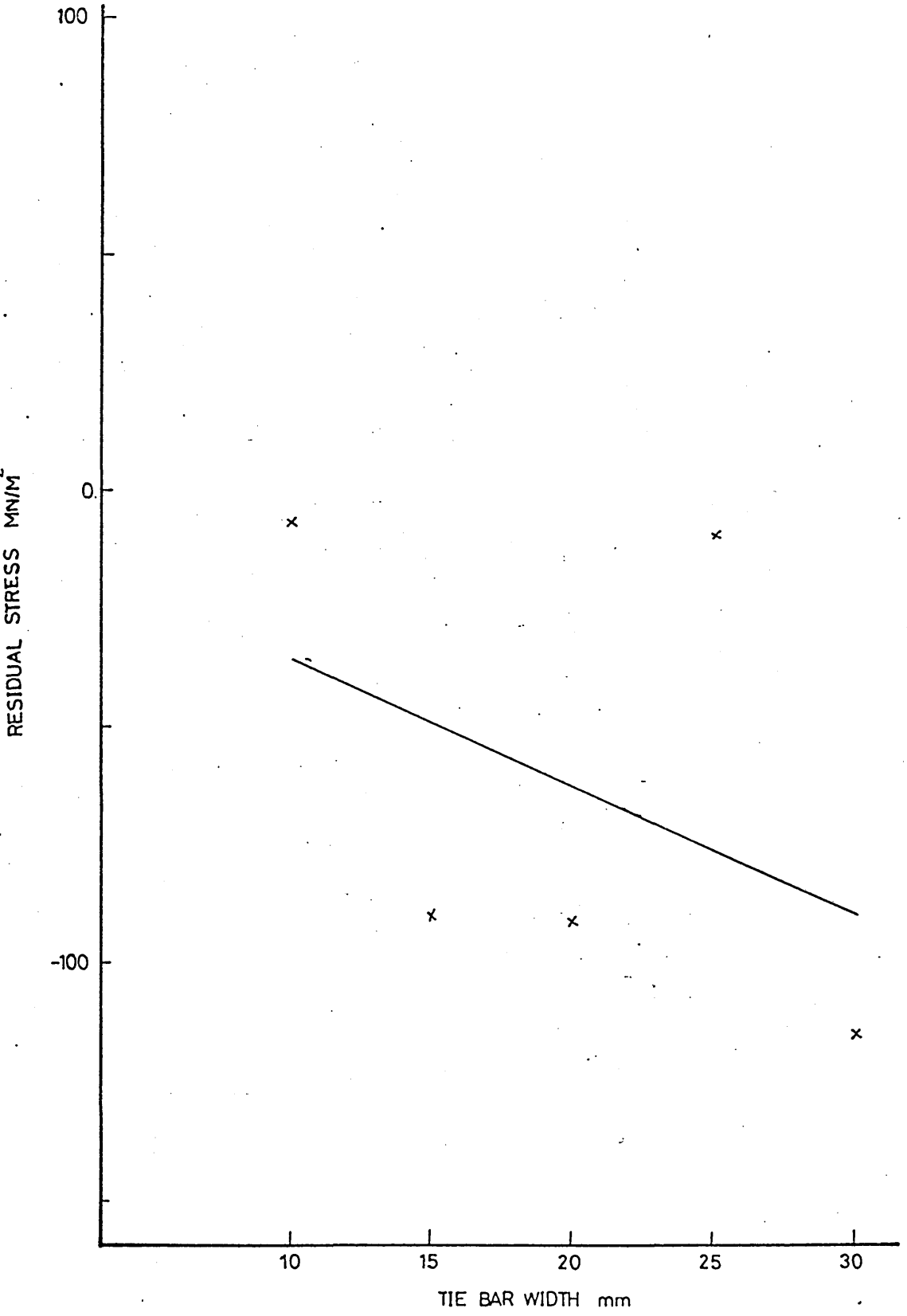
100
0
-100
RESIDUAL STRESS MN/M2
10
15
20
25
30
TIE BAR WIDTH mm

FIGURE 86: Computed Best fit lines for the as cast residual stress at hole depth equal to diameter at all positions in theta rings with different tie bar widths (Locations of the positions are shown in figure 21).

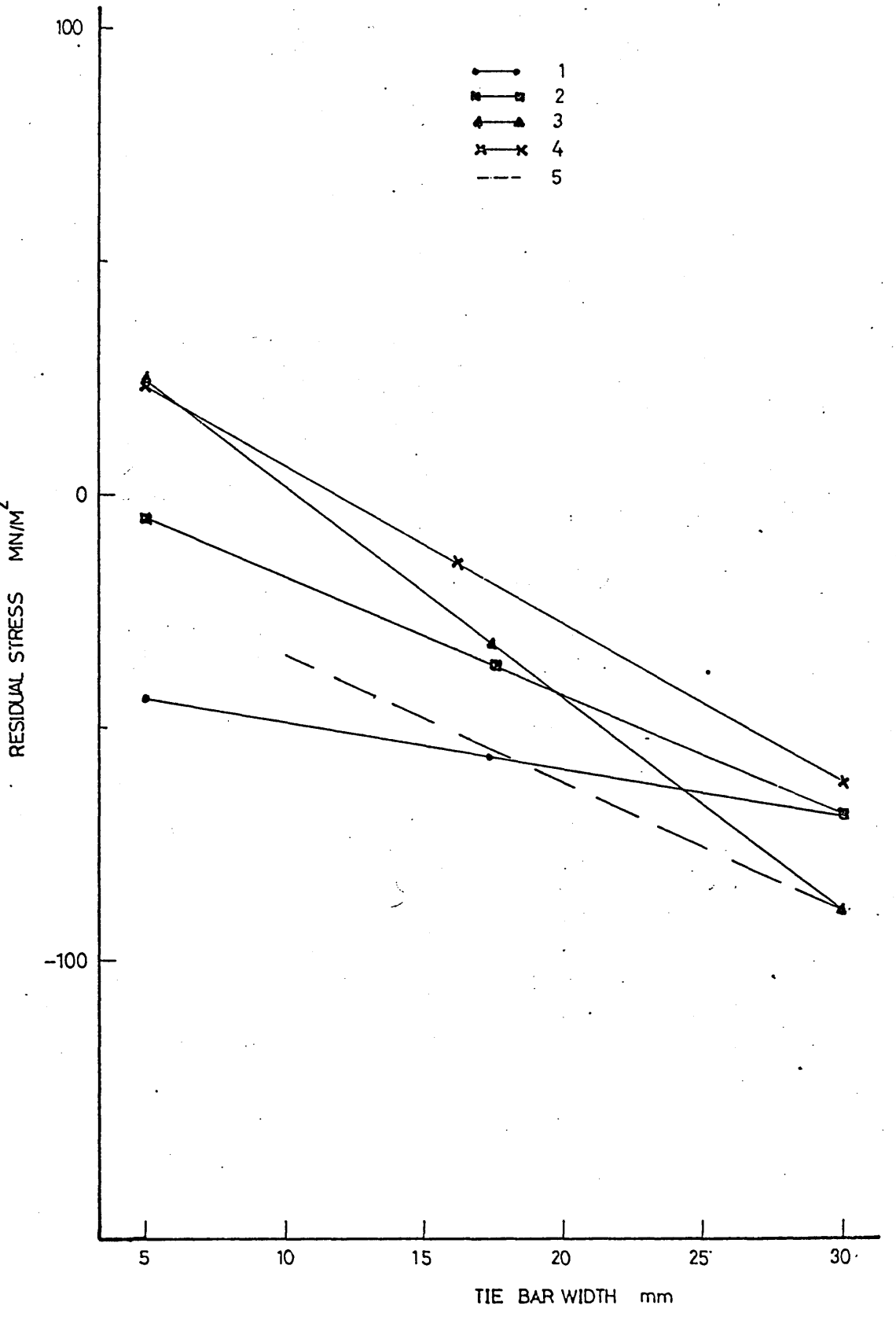
100
0
-100
RESIDUAL STRESS MN/M2
1
2
3
4
5
5
10
15
20
25
30
TIE BAR WIDTH mm

FIGURE 87: Variations of tie bar shift after sectioning for different tie bar widths, best fit line is also superimposed.

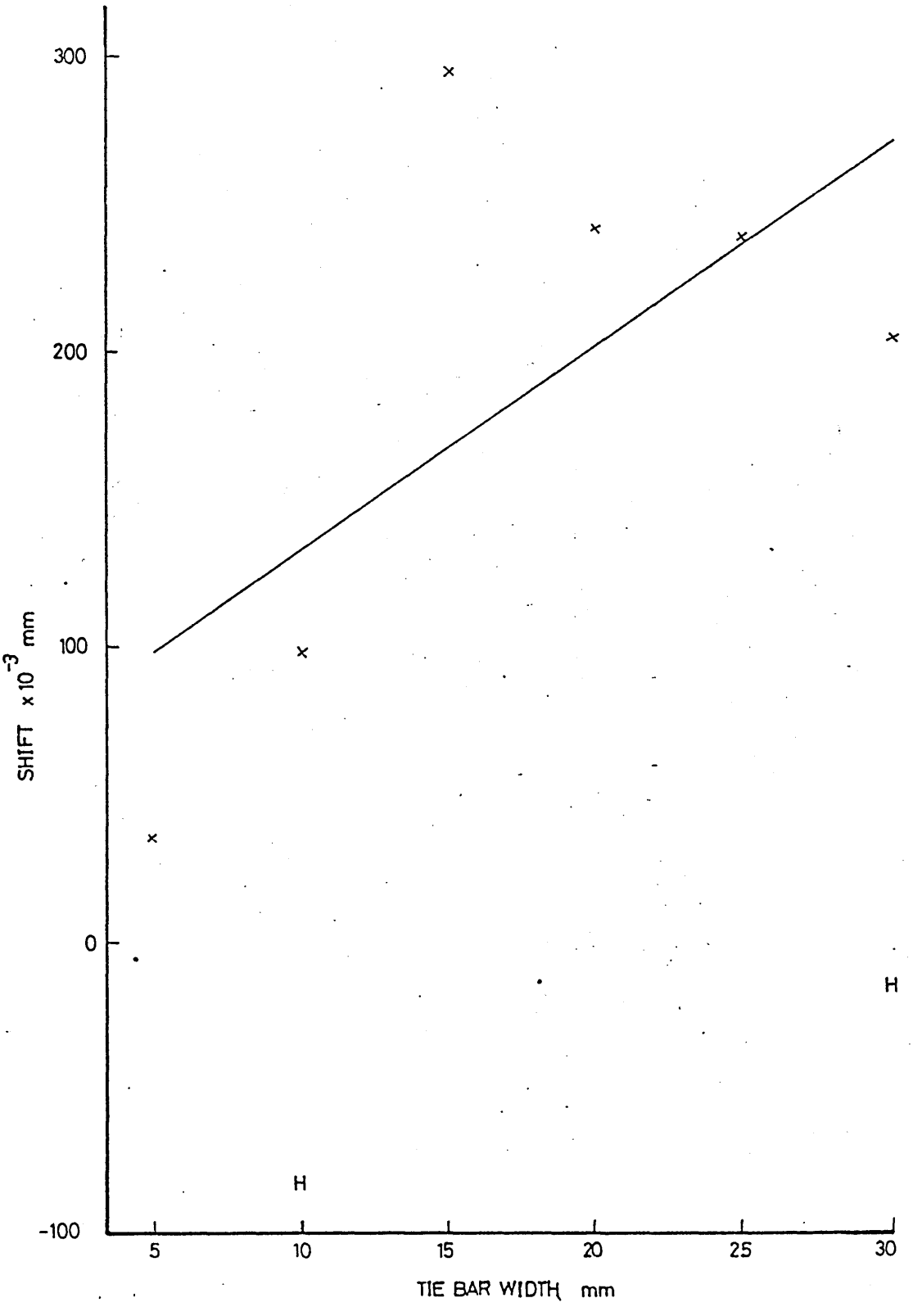
300
200
100
0
-100
SHIFT x10^-3 mm
5
10
15
20
25
30
TIE BAR WIDTH mm
H
H

FIGURE 88: Variation of Residual stress distribution in annealed Theta ring with 30mm tie bar width with hole depth (Locations are those shown in Figure 23).

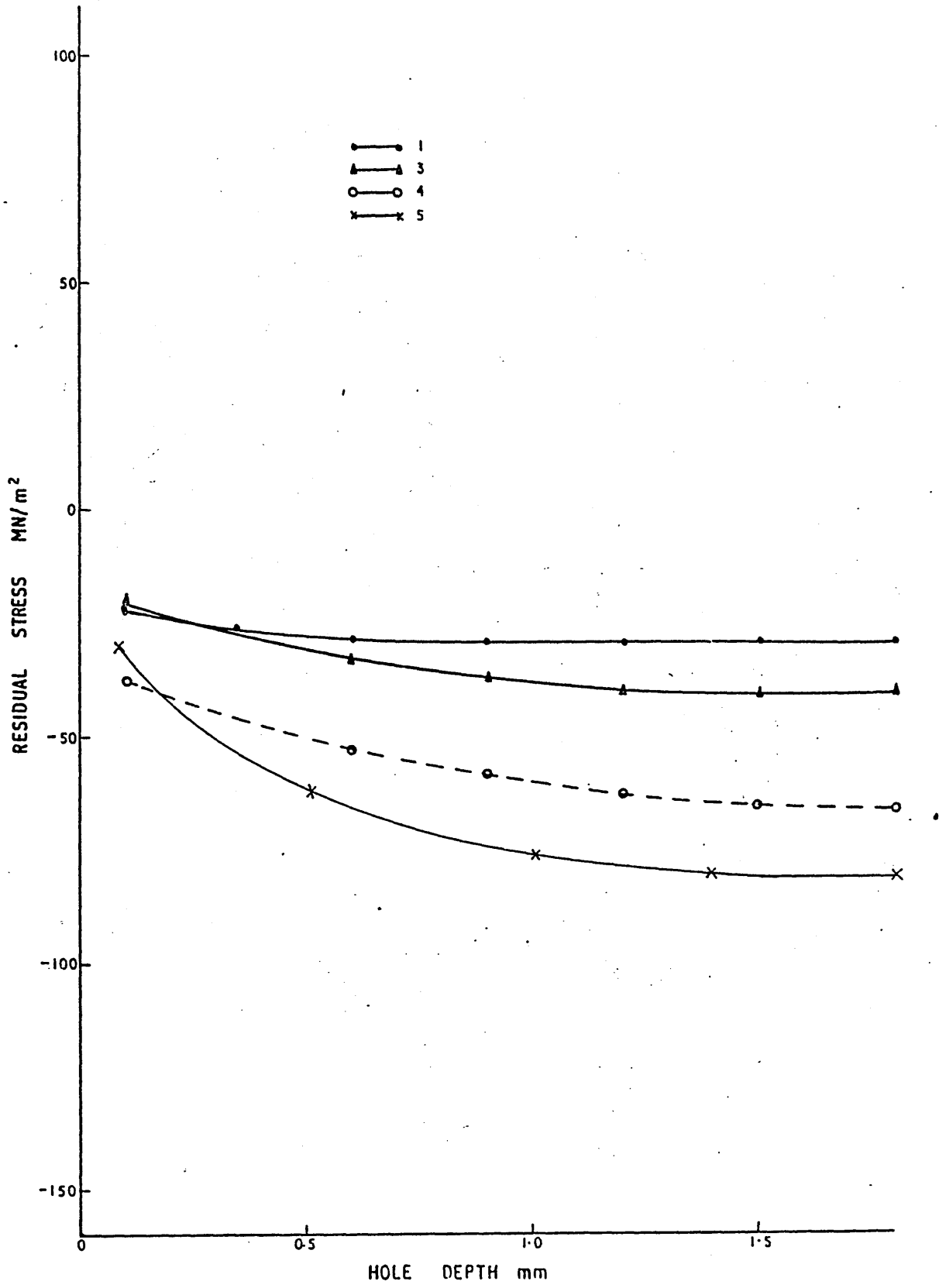
100
50
0
-50
-100
-150
RESIDUAL STRESS MN/m²
1
3
4
5
0
0·5
1·0
1·5
HOLE DEPTH mm

FIGURE 89: Variation of Residual stress distribution in annealed Theta ring with 10mm tie bar width with hole depth (Locations are those shown in Figure 23).

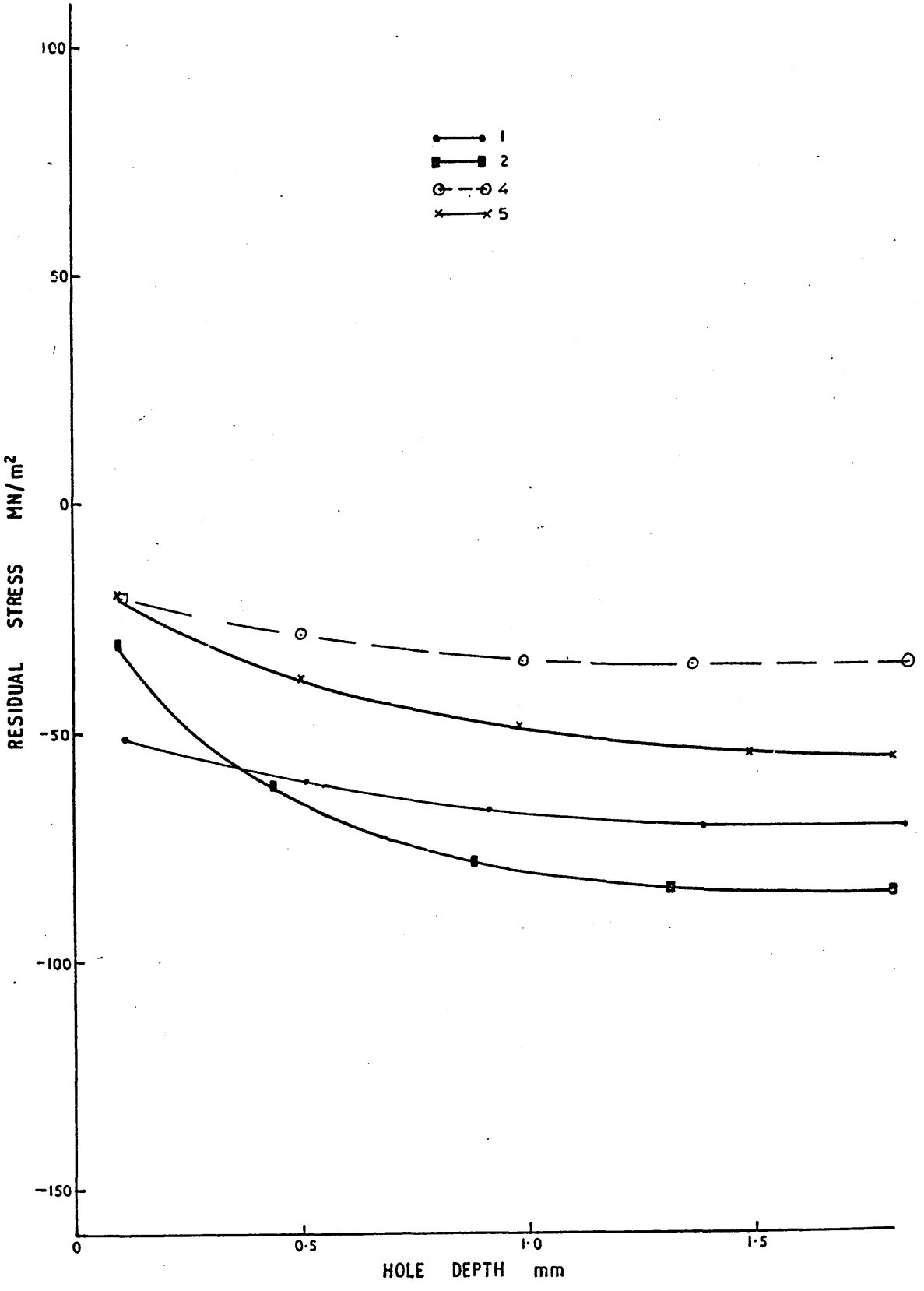
100
50
0
-50
-100
-150
RESIDUAL STRESS MN/m²
1
2
4
5
0
0·5
1·0
1·5
HOLE DEPTH mm

FIGURE 90: Variation of Residual stress distribution in normalized Theta ring with 30mm tie bar width with hole depth (Locations are those shown in Figure 23).

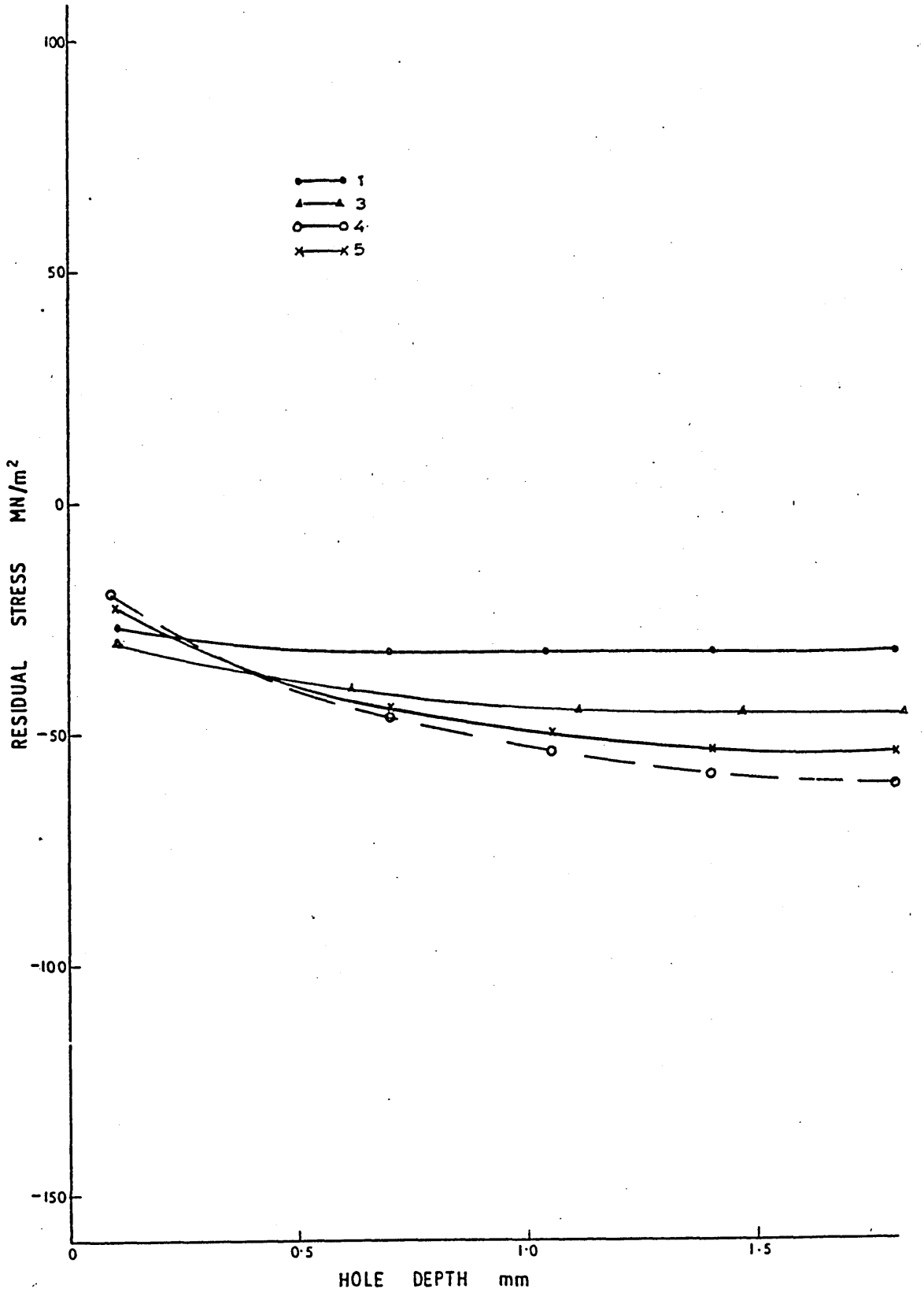
100
50
0
-50
-100
-150
RESIDUAL STRESS MN/m²
1
3
4
5
0
0·5
1·0
1·5
HOLE DEPTH mm

FIGURE 91: Variation of Residual stress distribution in normalized Theta ring with 10mm tie bar width with hole depth (Locations are those shown in Figure 23).

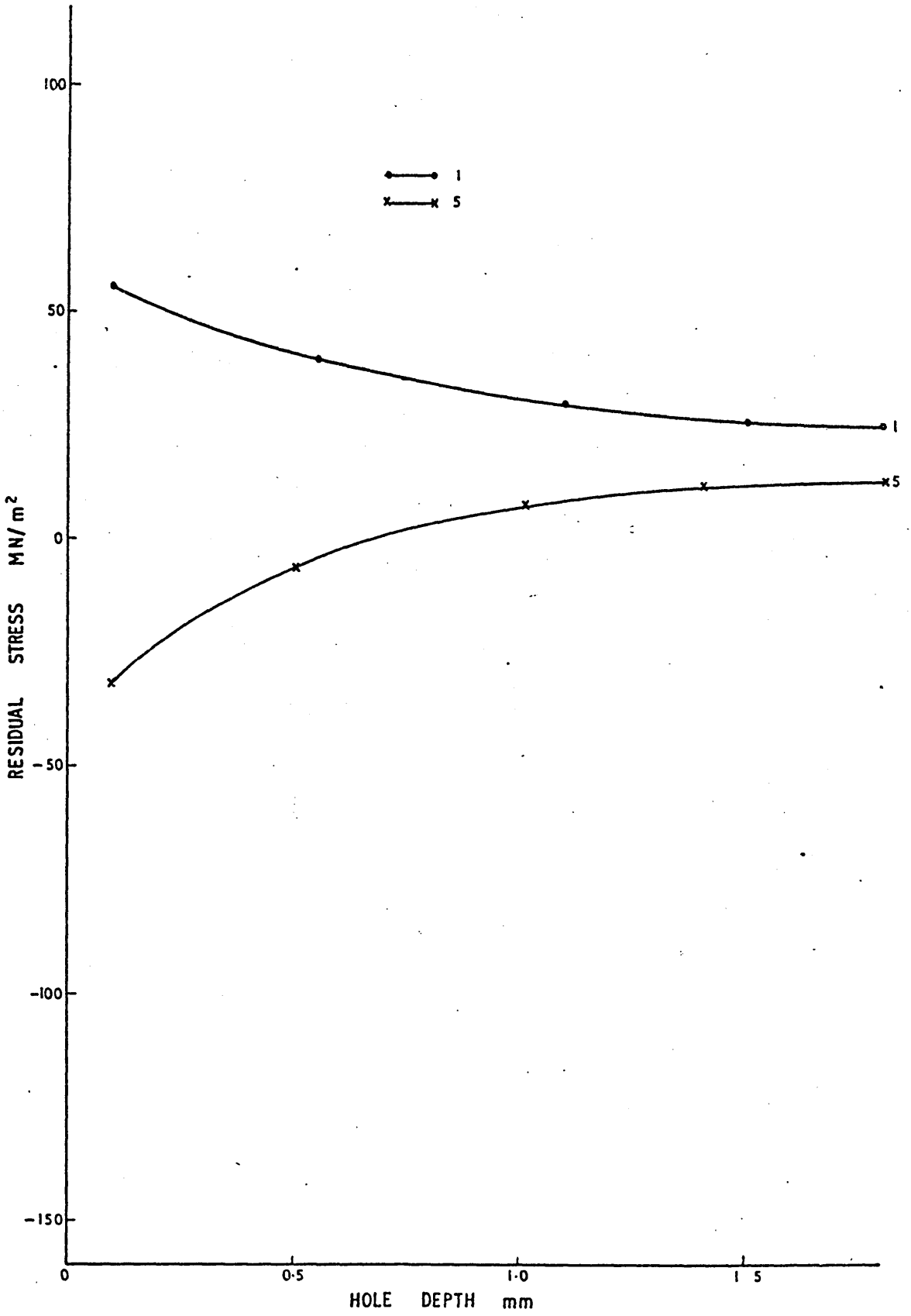
100
50
0
-50
-100
-150
RESIDUAL STRESS MN/m²
1
5
0
0·5
1·0
1·5
HOLE DEPTH mm

FIGURE 92: Variation of Residual stress distribution in tempered Theta ring with 30mm tie bar width with hole depth (Locations are those shown in Figure 23).

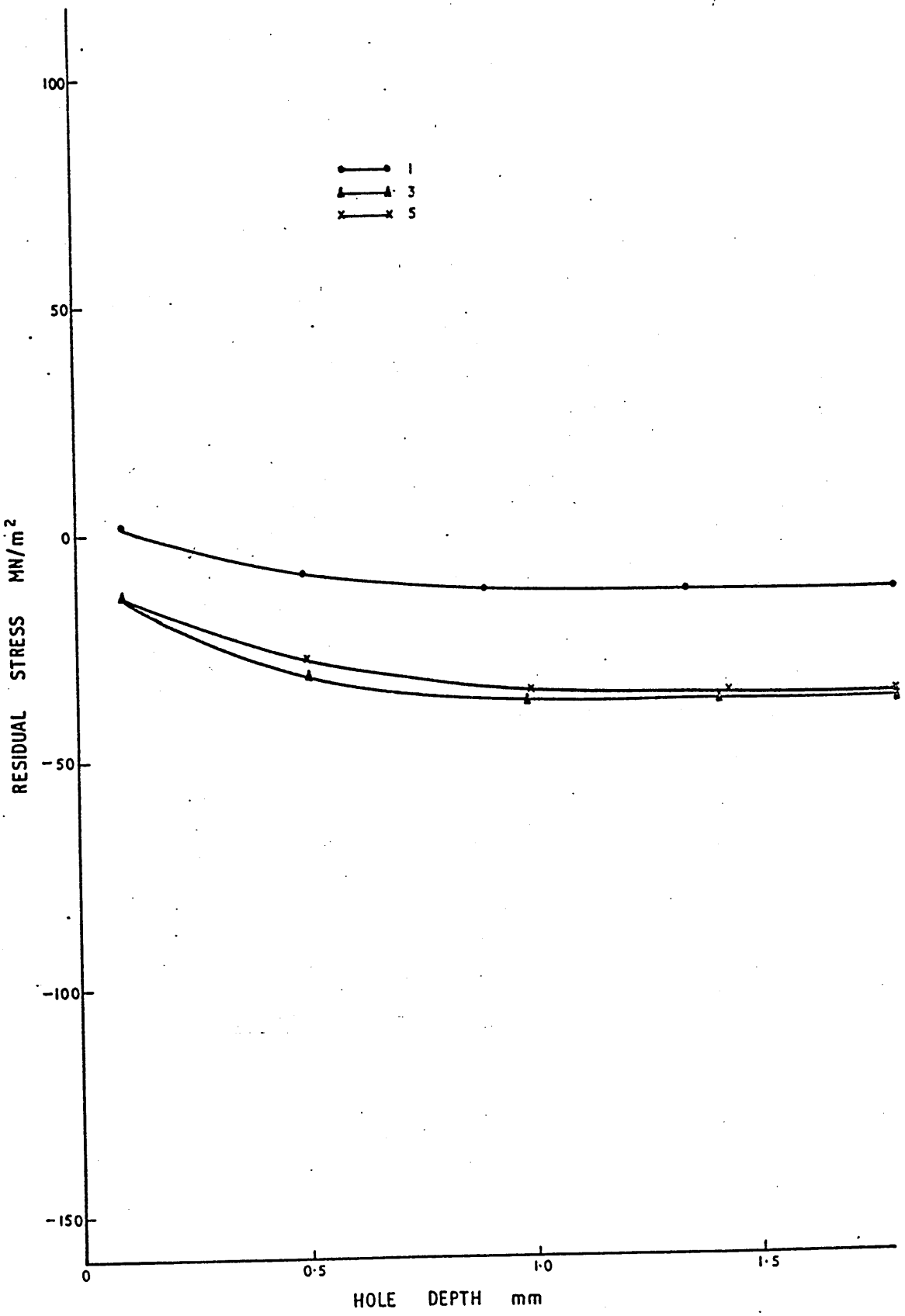
100
50
0
-50
-100
-150
RESIDUAL STRESS MN/m²
1
3
5
0
0·5
1·0
1·5
HOLE DEPTH mm

FIGURE 93: Variation of Residual stress distribution in tempered Theta ring with 10mm tie bar width with hole depth (Locations are those shown in Figure 23).

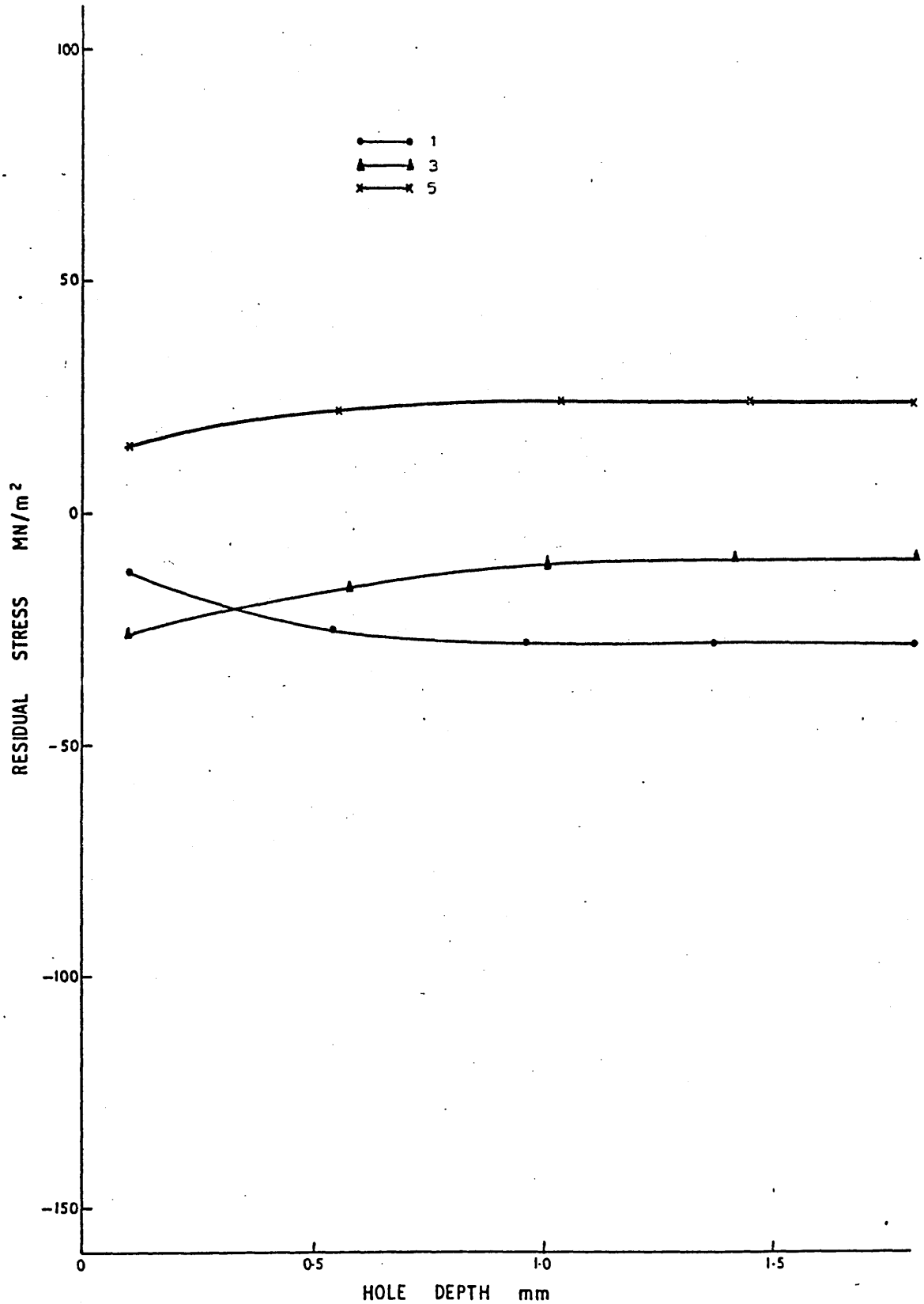
100
50
0
-50
-100
-150
RESIDUAL STRESS MN/m²
1
3
5
0
0·5
1·0
1·5
HOLE DEPTH mm

FIGURE 94: Residual stresses at position 1 of 30mm tie bar theta ring in as cast, annealed, normalized and tempered conditions (Location of position is shown in Figure 21 and 23).

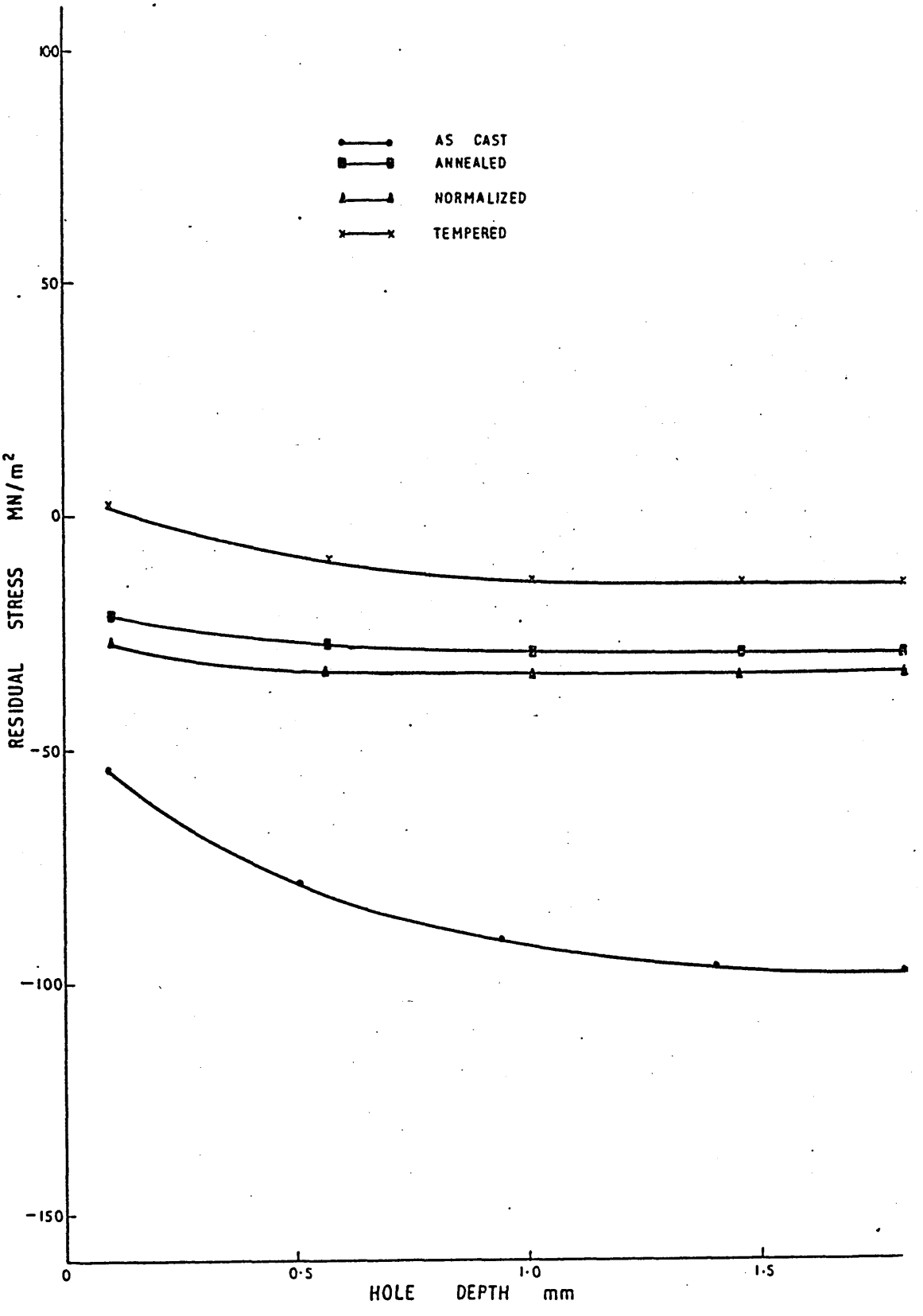
AS CAST
ANNEALED
NORMALIZED
TEMPERED
100
50
0
-50
-100
-150
RESIDUAL STRESS MN/m²
0
0·5
1·0
1·5
HOLE DEPTH mm

FIGURE 95: Residual stresses at position 5 of 30mm tie bar theta ring in as cast, annealed, normalized and tempered conditions (Location of position is shown in Figure 21 and 23).

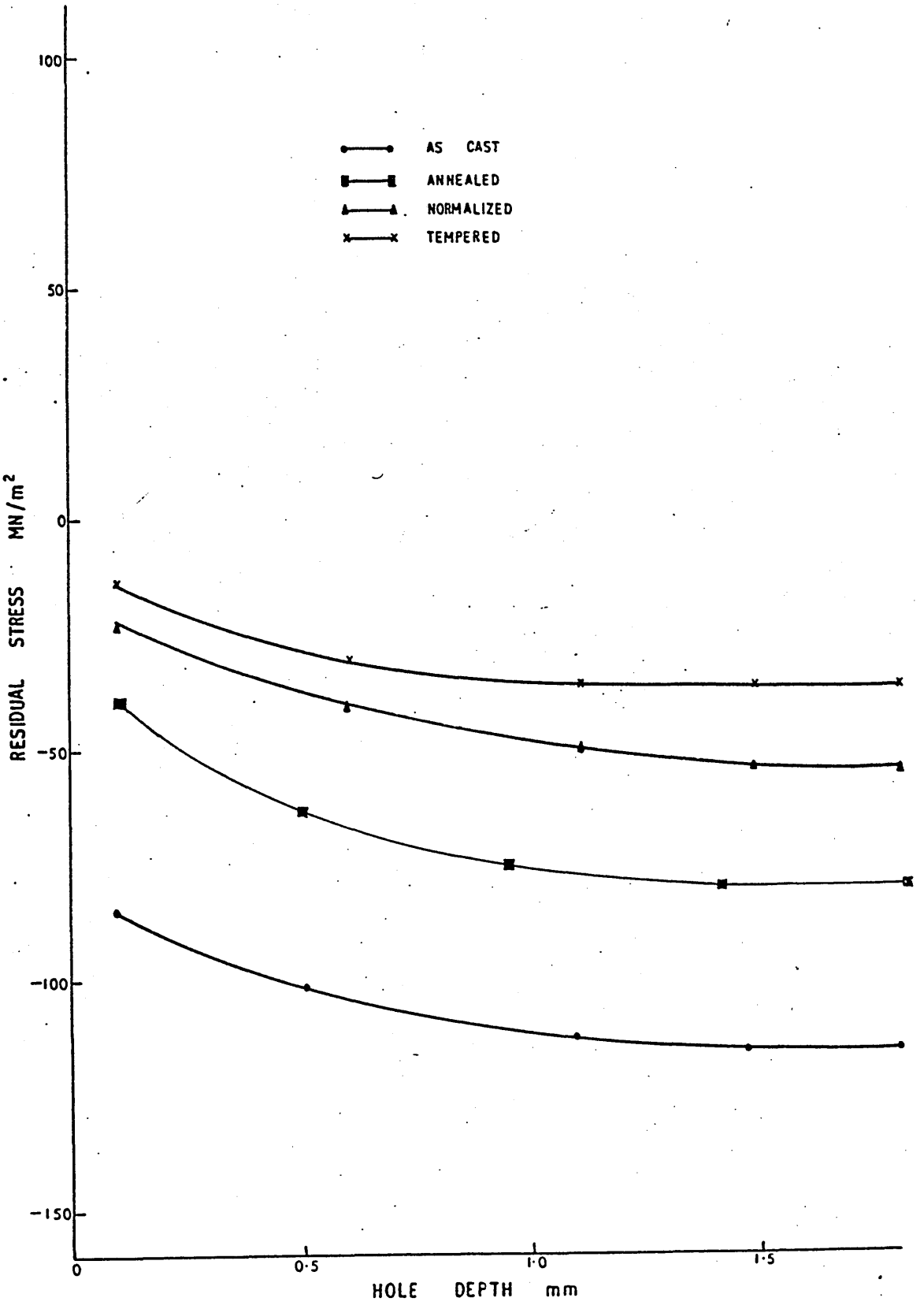
AS CAST
ANNEALED
NORMALIZED
TEMPERED
100
50
0
-50
-100
-150
RESIDUAL STRESS MN/m²
0
0·5
1·0
1·5
HOLE DEPTH mm

FIGURE 96: Residual stresses at position 1 of 10mm tie bar theta ring in as cast, annealed, normalized and tempered conditions (Location of position is shown in Figure 21 and 23).

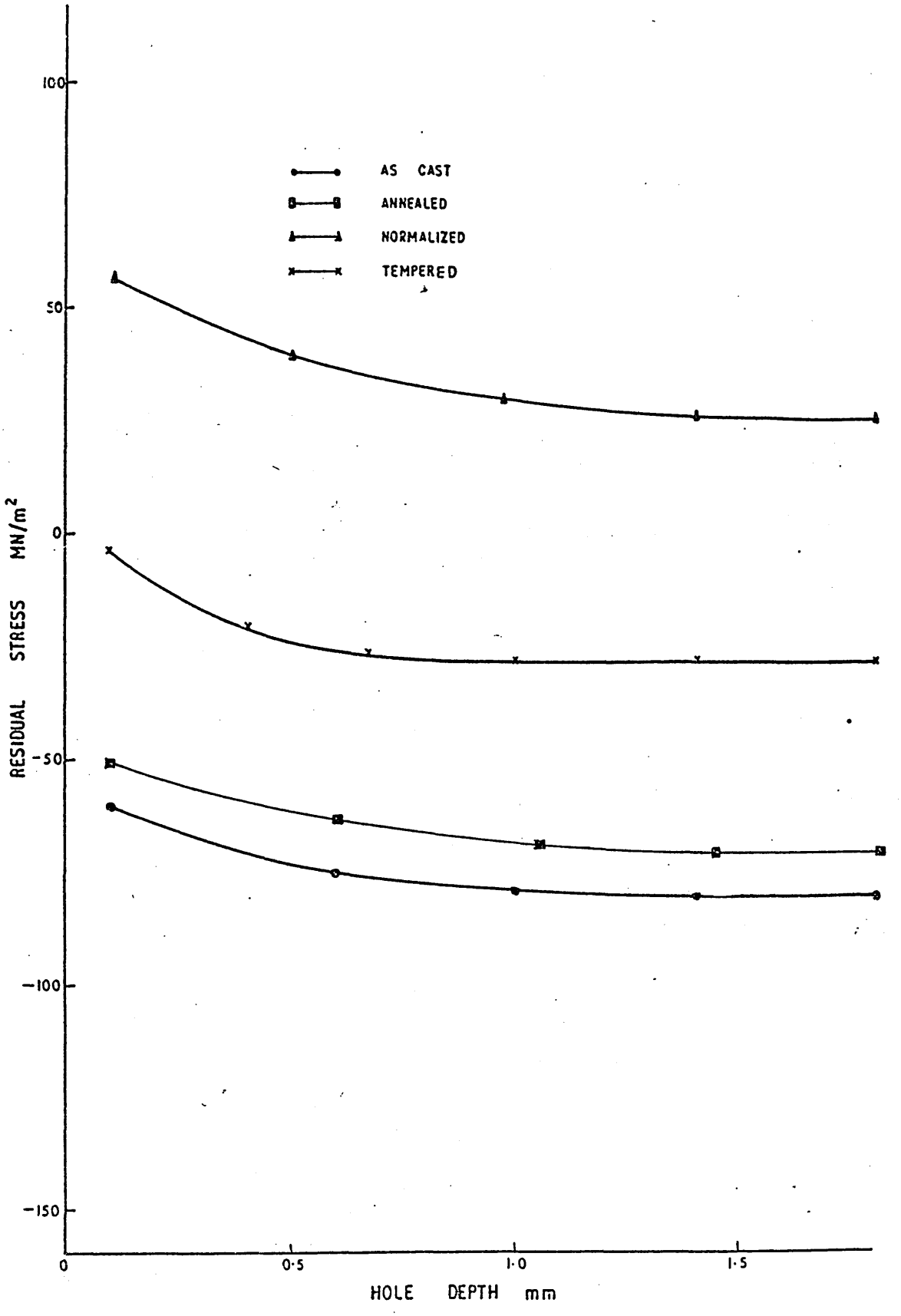
AS CAST
ANNEALED
NORMALIZED
TEMPERED
100
50
0
-50
-100
-150
RESIDUAL STRESS MN/m²
0
0·5
1·0
1·5
HOLE DEPTH mm

FIGURE 97: Residual stresses at position 5 of 10mm tie bar theta ring in as cast, annealed, normalized and tempered conditions (Location of position is shown in Figure 21 and 23).

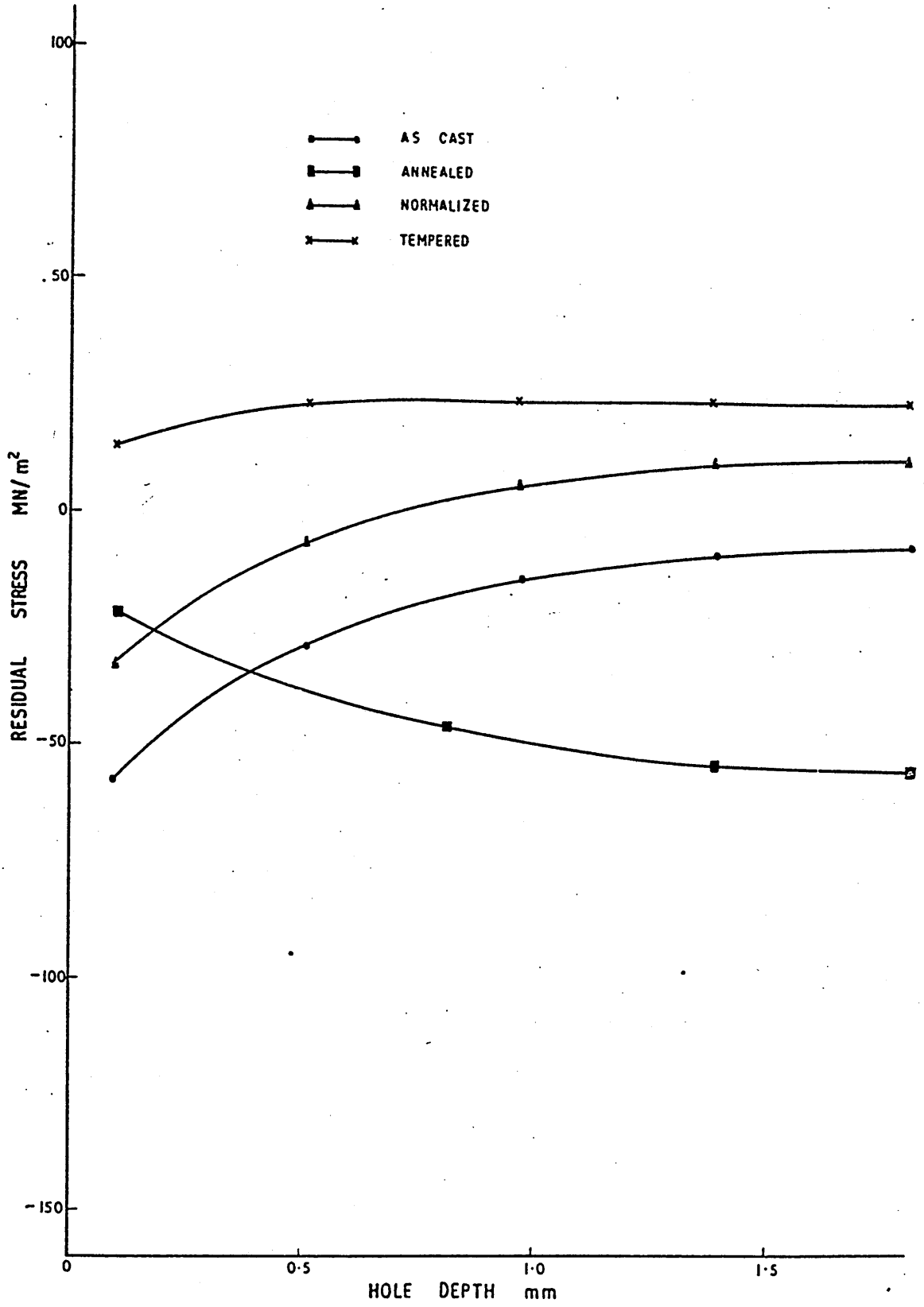
AS CAST
ANNEALED
NORMALIZED
TEMPERED
100
50
0
-50
-100
-150
RESIDUAL STRESS MN/m²
0
0·5
1·0
1·5
HOLE DEPTH mm

FIGURE 98: Residual stresses at position 1 of 30 and 10mm tie bar theta rings in as cast (C), annealed (A) normalized (N) and tempered (T) conditions (Location of position is shown in Figure 21 and 23)

Note: Line drawn does not represent best fit line or trend.

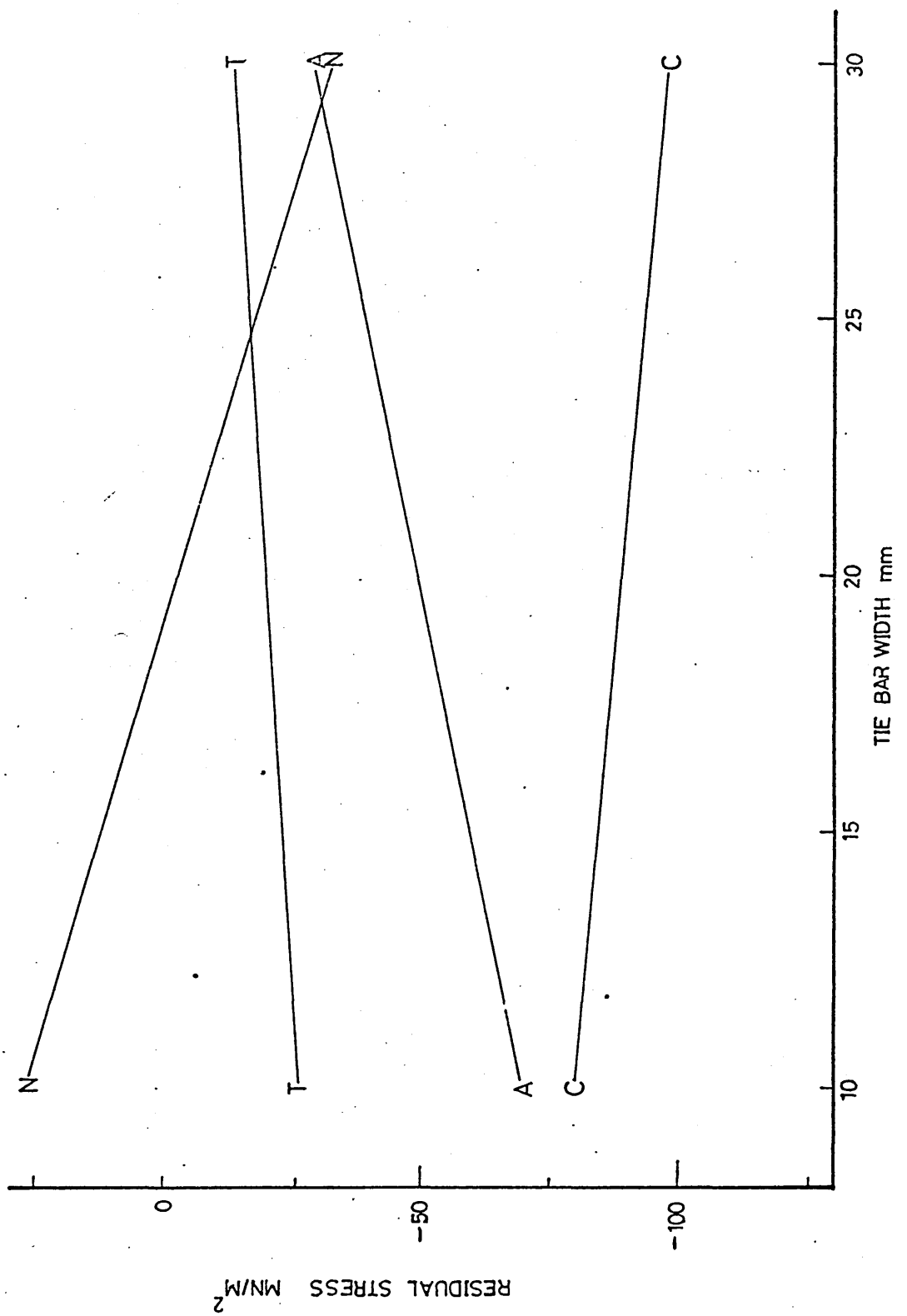
N
T
A
C
0
-50
-100
10
15
20
25
30
TIE BAR WIDTH mm
RESIDUAL STRESS MN/M²

FIGURE 99: Residual stresses at position 5 of 30 and 10mm tie bar theta rings in as cast (C), annealed (A), normalized (N) and tempered (T) conditions (location of position is shown in Figure 21 and 23).

Note: Line drawn does not represent best fit line or trend.

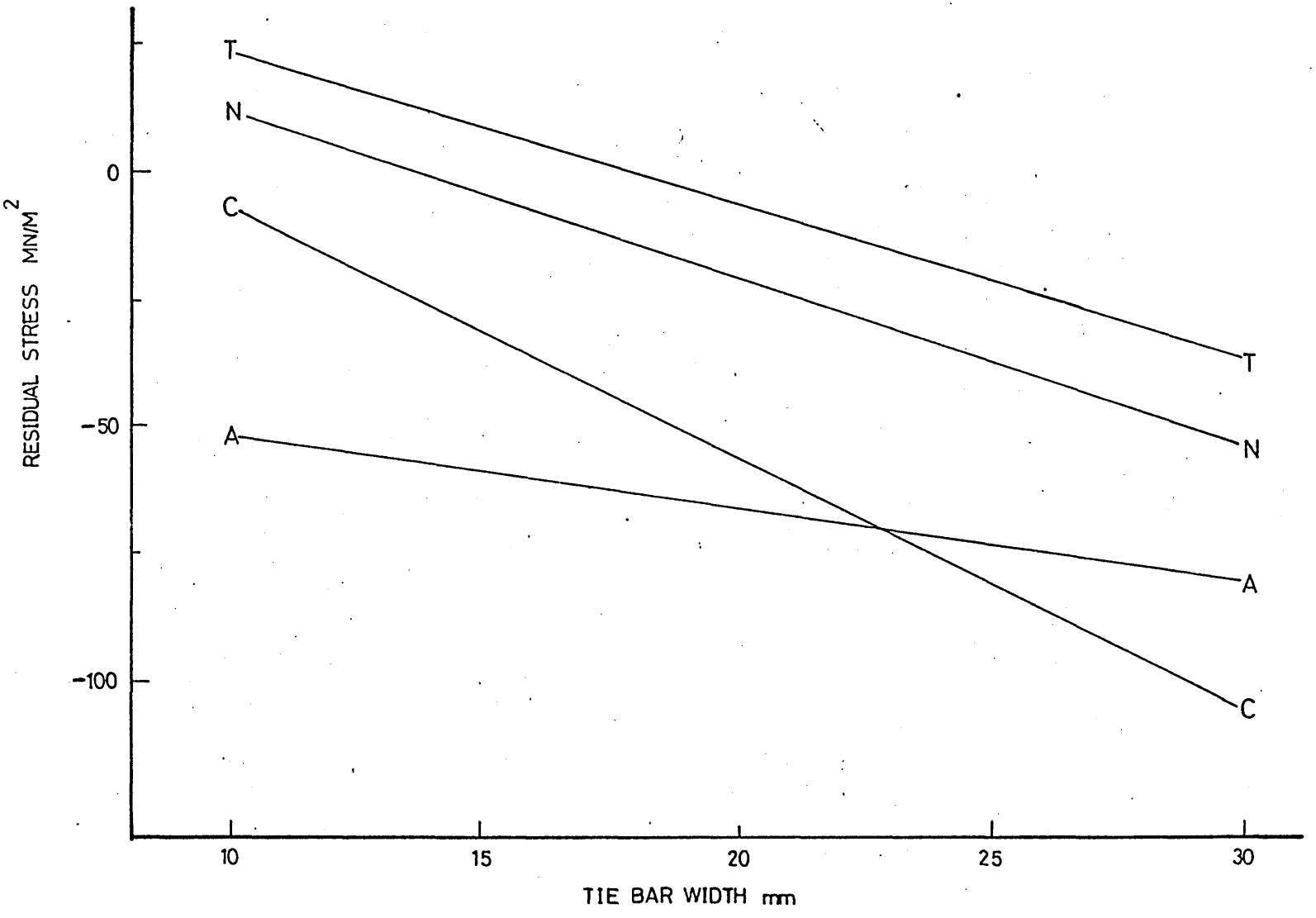
T
N
C
A
0
-50
-100
RESIDUAL STRESS MN/M^2
10
15
20
25
30
TIE BAR WIDTH mm

FIGURE 100: Residual stresses at various positions of 30 and 10mm tie bar theta rings in as cast (C), annealed (A), normalized (N) and tempered (T) conditions (Locations of positions are shown in Figure 21 and 23).

Note: Line drawn does not represent best fit line or trend.

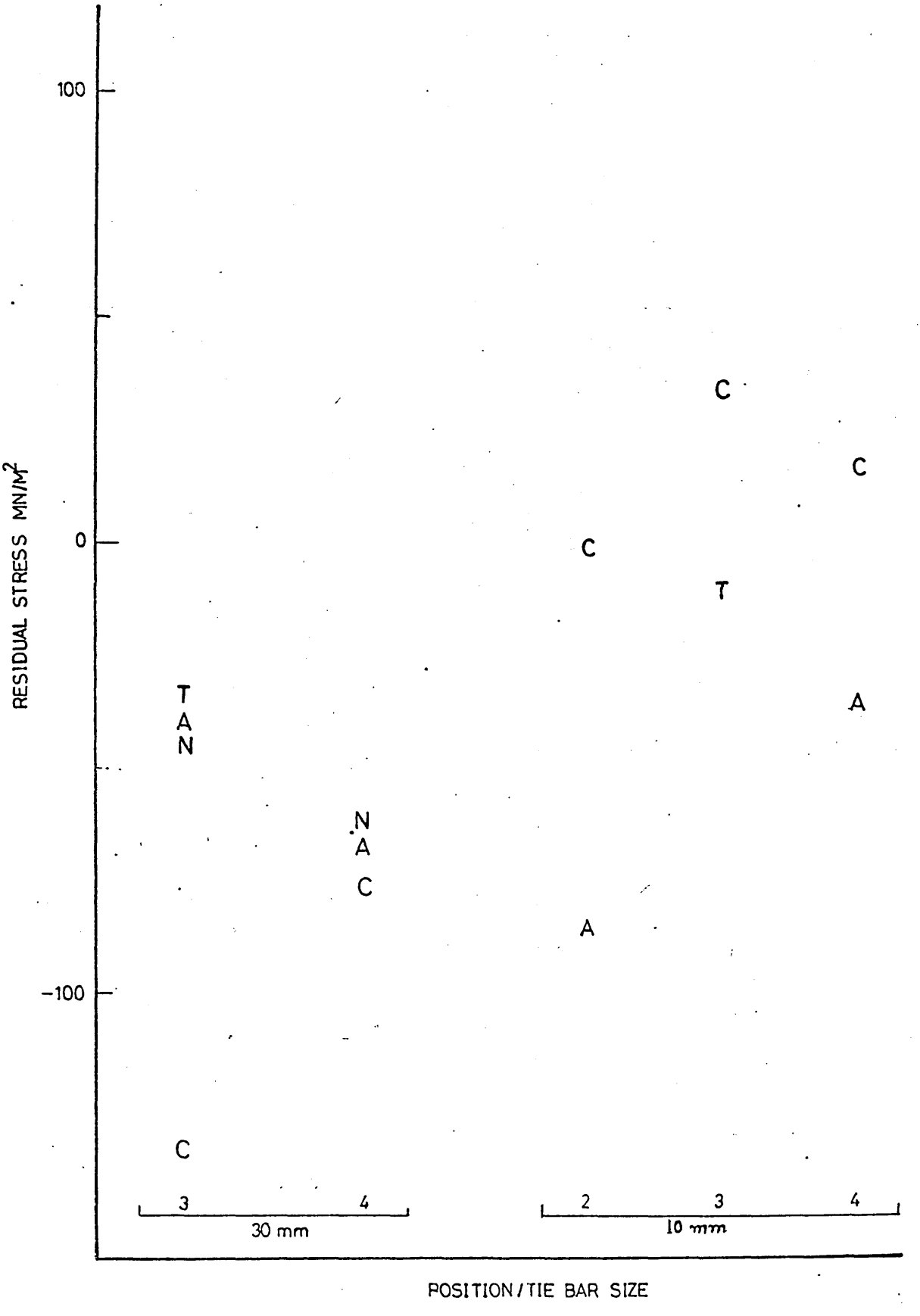
100
0
-100
RESIDUAL STRESS MN/M²
C
C
C
T
T
A
N
A
N
A
C
A
C
3
4
30 mm
2
3
4
10 mm
POSITION / TIE BAR SIZE

FIGURE 101: Computed Best fit lines for the as cast residual stress (according to numerically greatest criteria) at hole depth equal to its diameter at all positions in theta rings with different tie bar widths (Locations of positions are shown in figure 21).

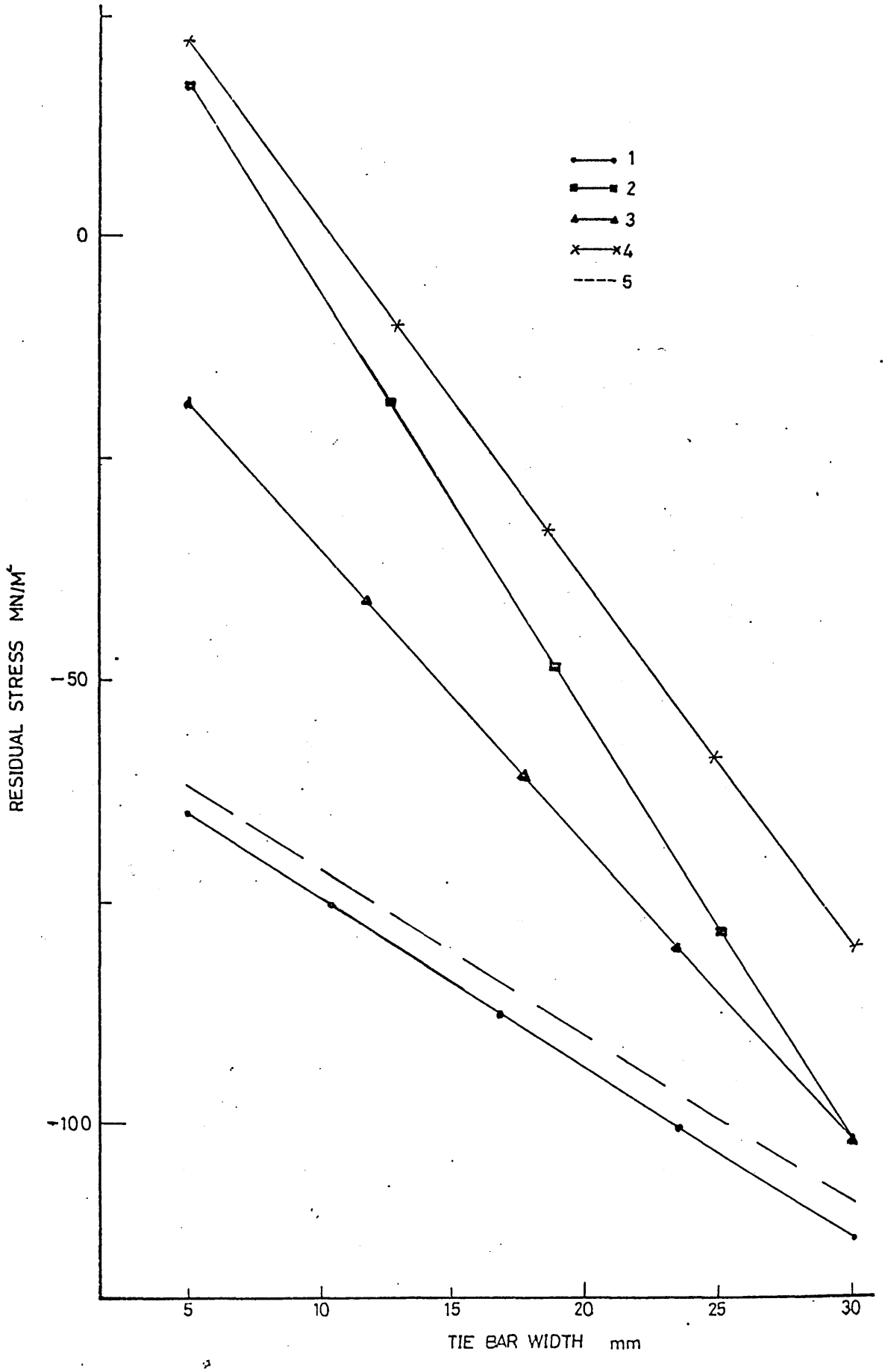
1
2
3
4
5
0
-50
-100
RESIDUAL STRESS MN/M²
5
10
15
20
25
30
TIE BAR WIDTH mm

FIGURE 102: Computed Best fit lines for the Von mises equivalent computed for as cast condition at hole depth equal to its diameter at all positions in theta rings with different tie bar widths (Locations of positions are shown in figure 21).

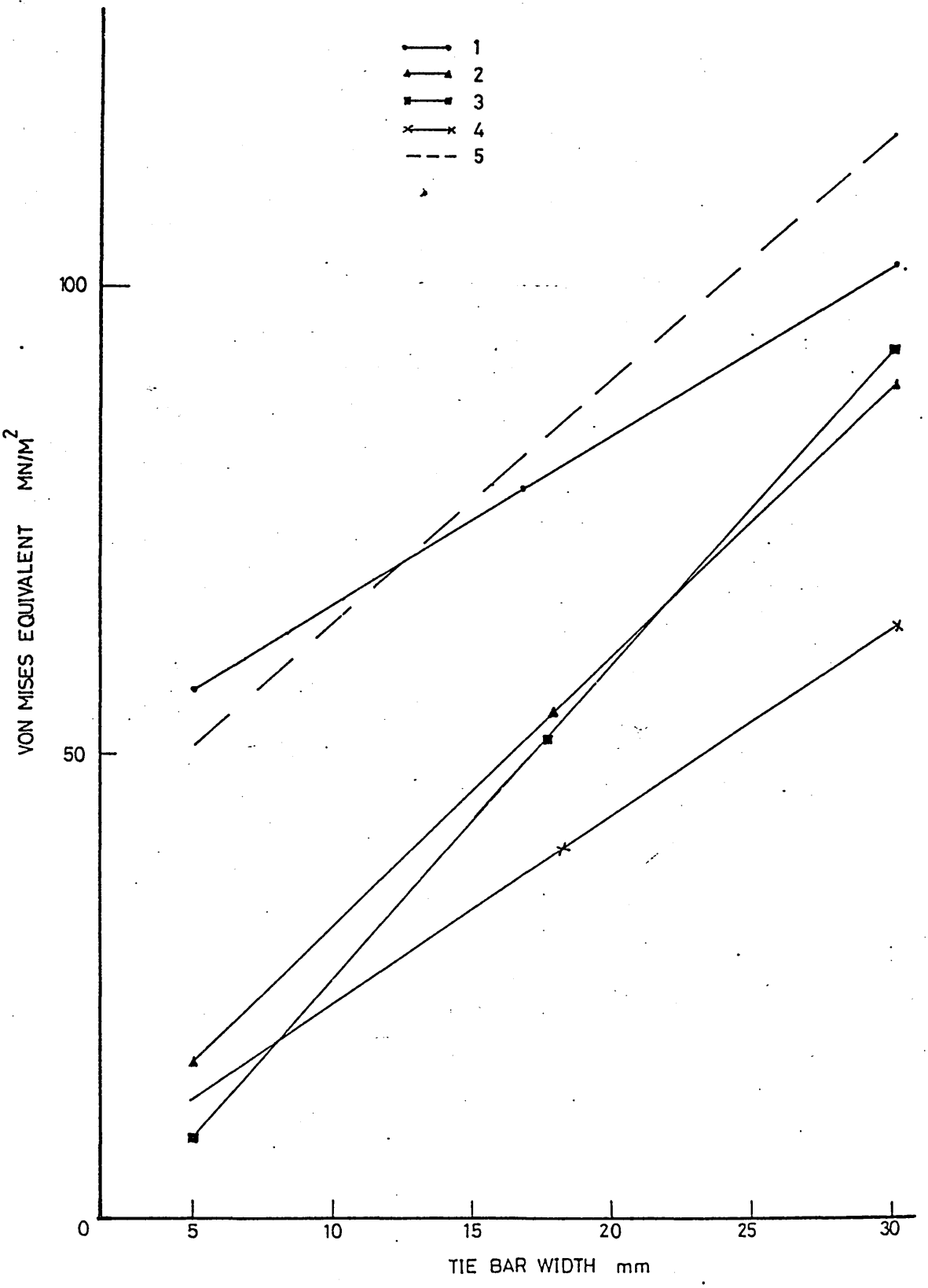
1
2
3
4
5
100
50
0
VON MISES EQUIVALENT MN/M2
5
10
15
20
25
30
TIE BAR WIDTH mm

FIGURE 103: Variation of Hardness with different tie bar widths, best fit line is also superimposed. H refers to hardness after heat treatment.

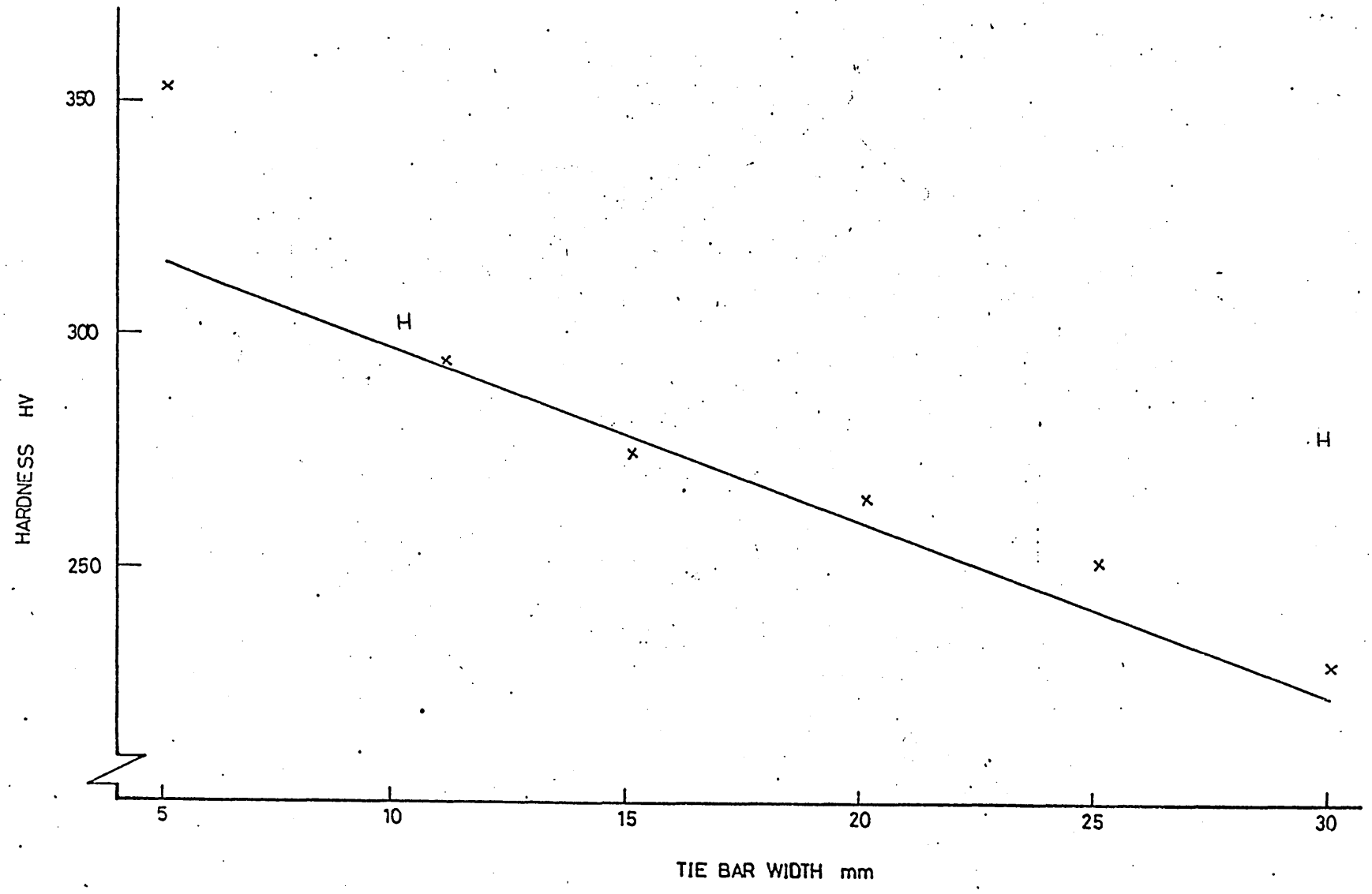
350
300
250
HARDNESS HV
5
10
15
20
25
30
TIE BAR WIDTH mm

FIGURE 104: Variation of Micro hardness in the decarburized layer and centre of the tie bar with different widths; best fit lines are also superimposed.

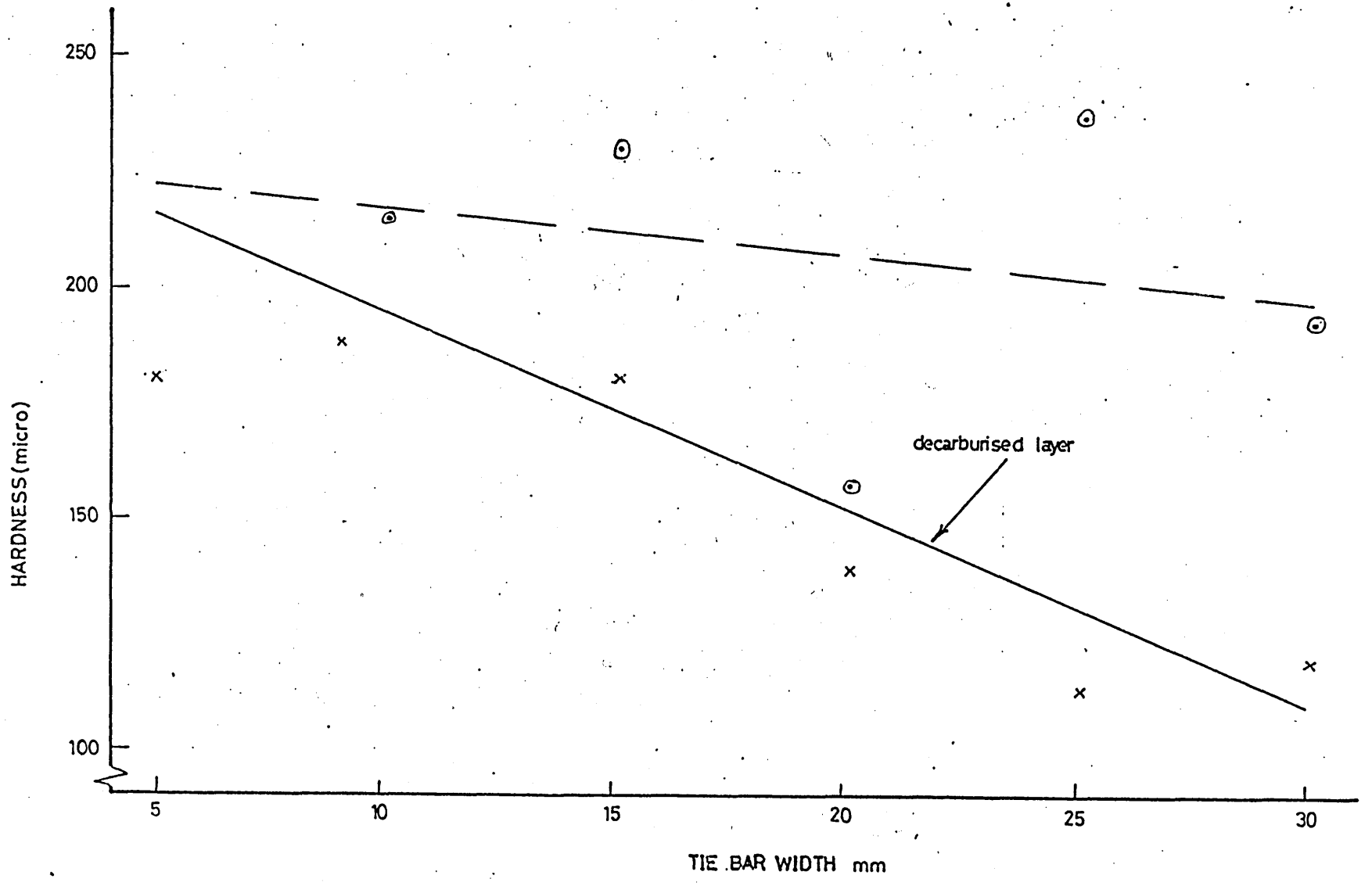
250
200
150
100
HARDNESS(micro)
decarburised layer
5
10
15
20
25
30
TIE BAR WIDTH mm

FIGURE 105: Computed temperature gradient in half tie bar thickness elements after time intervals when tie bar centre crosses liquidus.

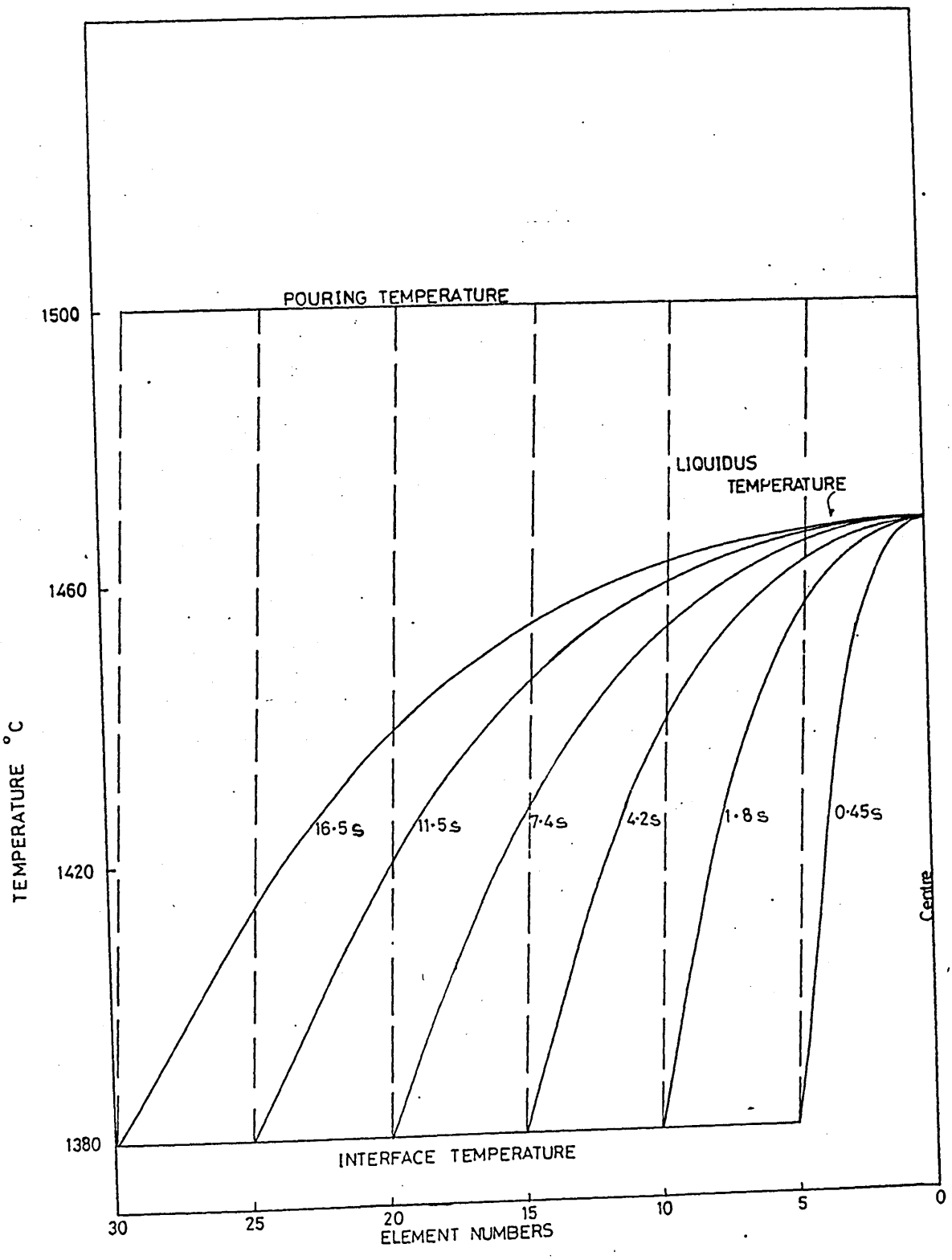
POURING TEMPERATURE
1500
LIQUIDUS
TEMPERATURE
1460
16·5 s
11·5 s
7·4 s
4·2 s
1·8 s
0·45 s
1420
TEMPERATURE °C
Centre
1380
INTERFACE TEMPERATURE
30
25
20
15
10
5
0
ELEMENT NUMBERS

FIGURE 106: Variations in computed times when the tie bar centre crosses liquidus and solidus temperature with different tie bar widths.

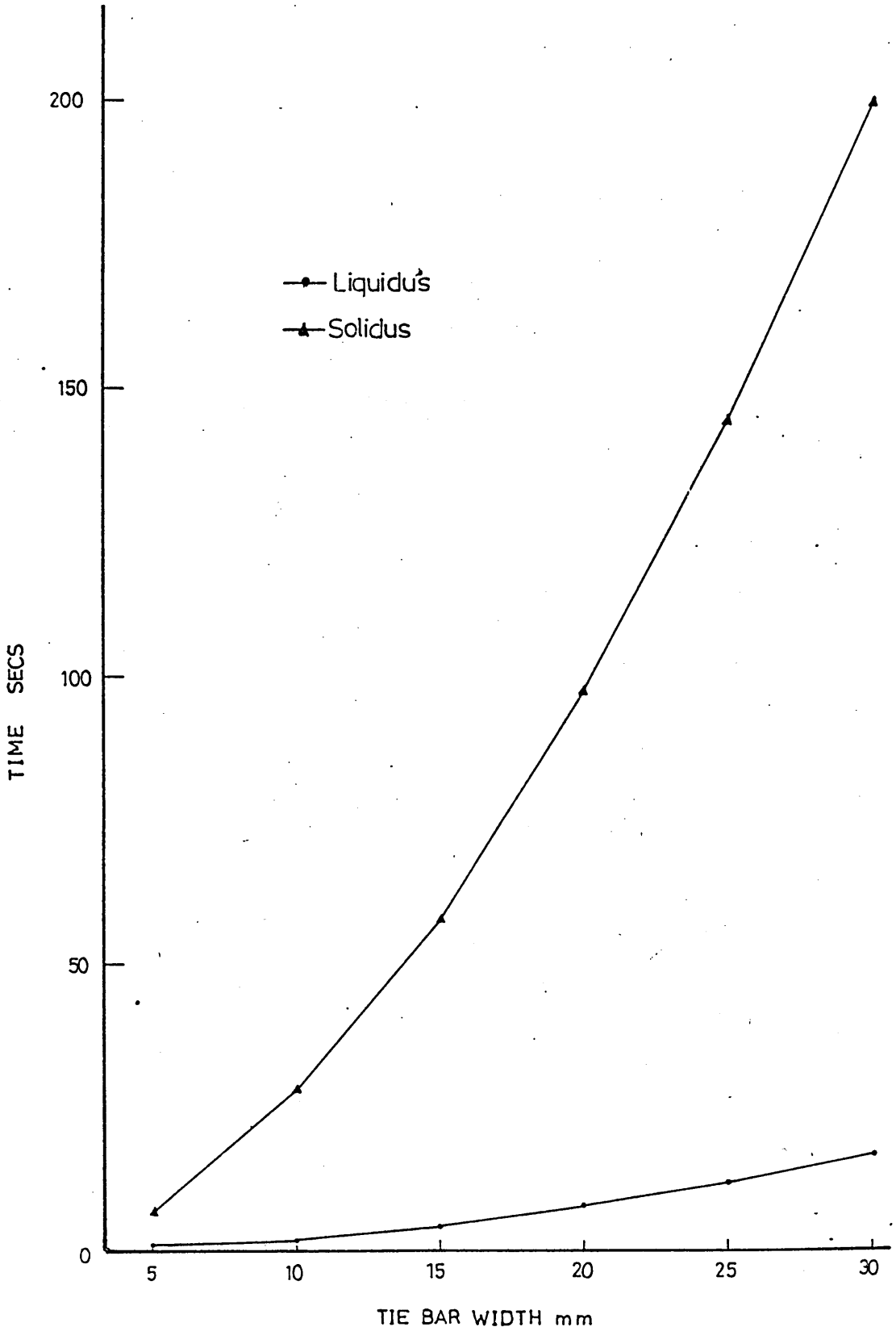
200
150
100
50
0
TIME SECS
Liquidus
Solidus
5
10
15
20
25
30
TIE BAR WIDTH mm

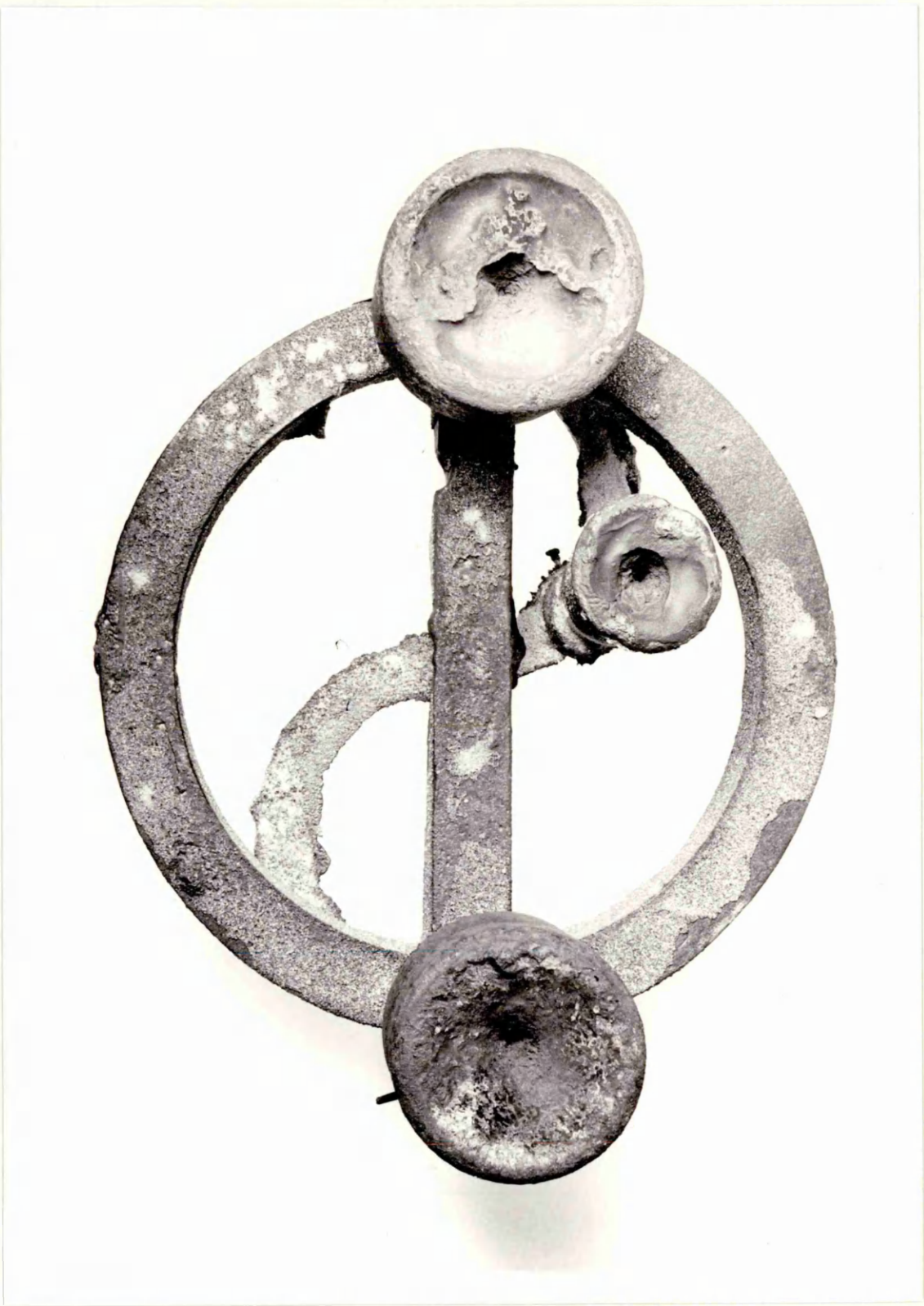

PLATE 2 Microstructure of 30mm tie bar for the theta ring in as cast condition (160X)

PLATE 3 Microstructure of 10mm tie bar for the theta ring in as cast condition (160X)

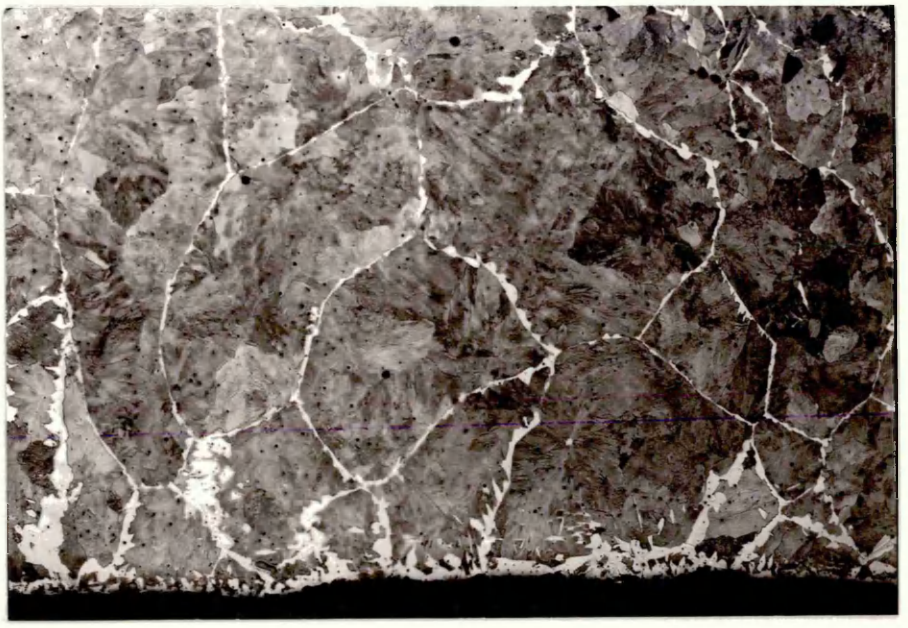

PLATE 4 Microstructure of the hot spot (junction of the ring and tie bar) of a 30mm tie bar theta ring in as cast condition (160X)

PLATE 5 Microstructure of the ring section for a 30mm tie bar theta ring in as cast condition (160X)

PLATE 6 Microstructure of 30mm tie bar for the theta ring, cast, annealed, normalised and tempered (160X)

PLATE 7 Microstructure of 10mm tie bar for the theta ring, cast, annealed, normalised and tempered (160X)

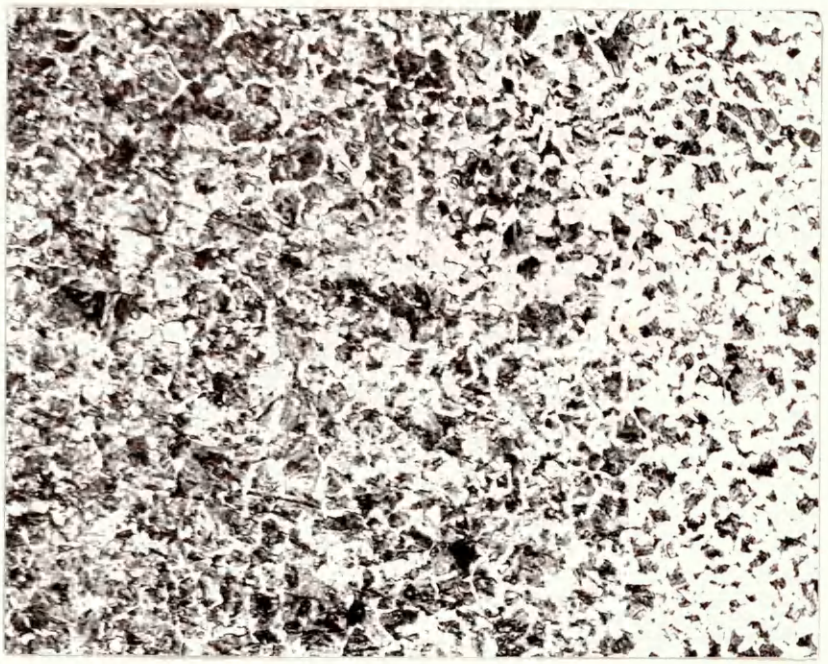

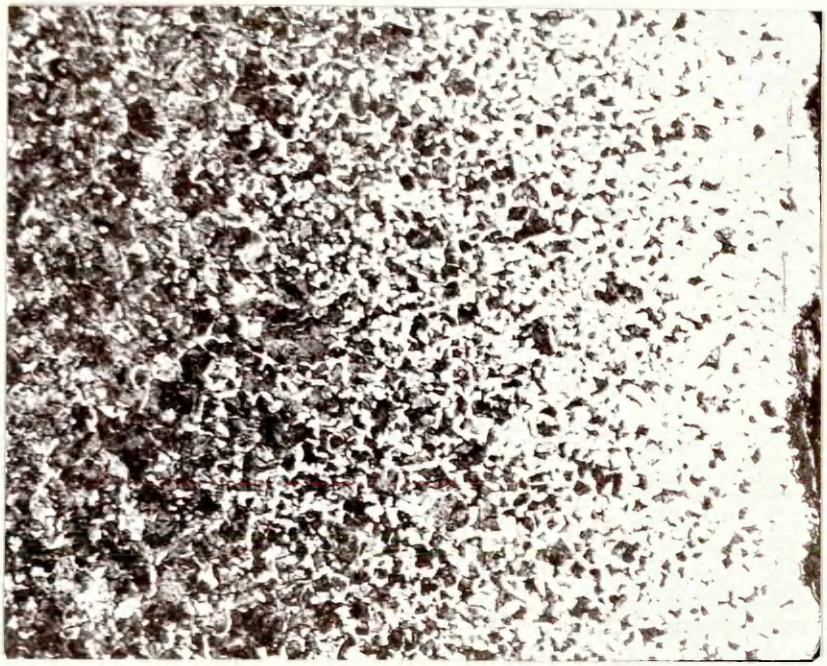

APPENDIX

CASE STUDY: A techno-economic evaluation of surface hardening processes and induced residual stress systems in a Spur gear.

SUMMARY

This case study evaluates the heat treatment processes for surface hardening a spur gear of 29cm pitch diameter. The processes have been evaluated and compared from cost and technical viewpoints.

The heat treatment processes considered for surface hardening were gas carburising and induction hardening.

Technical aspects include the evaluation of the residual stress systems introduced by the two heat treatments. Residual stress measurement techniques have also been evaluated from both cost and technical points of view.

NOMENCLATURE:-

B - a parameter

h - surface heat transfer coefficient $W/m^{2o}C$

A - surface area of gear m^2

t - time in secs.

m - mass of gear. kg.

Cp - Specific heat capacity of steel. J/kg^oC

C - Required carbon concentration at a depth X below surface

X - Required depth of case after carburising

Cs - Carbon content maintained at surface of gear during carburising

Co - Initial carbon content of gear

D - Diffusion coefficient of carbon in gear at carburising temperature $mm^2/sec.$

P - Power density kW/cm^2

1.0 INTRODUCTION

Gear teeth normally fail by either of two following modes:

a) Contact fatigue (pitting)

b) Bending fatigue (tooth breakage)

The resistance to failure, however, can be increased by increasing the tensile strength of material used. Also results of fatigue tests have shown that resistance to contact fatigue increases as the square of the tensile strength over a wide range of hardness, but the resistance to bending fatigue increases linearly with an increase of tensile strength up to optimum value of about 1080 MN/m^2. Above this level there is a progressive fall due to increasing notch sensitivity of higher grades of steel[1].

The objective of heat treating a gear is to improve contact fatigue resistance by increasing surface hardness, and also to neutralize the weakening effect of notch sensitivity by the introduction of a favourable residual-stress system in the surface layers. This residual stress system will favour resistance to high bending fatigue failure.

The residual stress systems that are beneficial to both bending fatigue and surface fatigue are best induced by employing surface hardening processes. These treatments are usually either a thermo-chemical process or a thermal treatment. With small gears of relatively

simple geometrical shape, the choice of process is dependant on a large number of factors, i.e. cost of blank, capital outlay for processing plant, process time and load level of gears concerned. In the case of large gears of above 1.8m diameter, the main factor becomes that of distortion and it is often necessary in such instances to consider the relative importance of the increase in load capacity against cost or difficulty of manufacture.

In this case study, two surface hardening processes, - gas carburizing and induction hardening - will be reviewed and evaluated on the basis of costs and the residual stress system for a gear 29cm diameter. Residual stress measuring technique will also be reviewed and evaluated on the basis of costs.

1.1 GAS CARBURIZING

The surface hardness of plain carbon and low alloy steels containing less than about 0.3% carbon may be effectively increased, without altering the carbon content of the core material, by diffusing carbon into the steel surface. The higher carbon content permits the formation of a very hard martensitic structure during quenching.

Gas carburizing is a process in which steel parts are placed in gaseous environment containing carbon at a suitable temperature near or above the Ac_3 temperature. The process depends upon the hardening agent,

carbon content and its diffusion into steel to attain hardening quality capability, the part being subsequently quenched to attain desired surface hardness.

Carburizing produces surface cases on steel parts; the case containing more hardening agent than the base material, and the gradient in hardening agent causing variations in the response to quench and temper treatment. The surface region becomes a very hard martensite after quenching; the core material being either pearlitic, bainitic, martensitic, or even ferritic depending on its carbon content and hardenability. Thus surface alloying with carbon produces a material whose response to single heat treatment can provide a hard wear resistant surface over a tough ductile core (in case of Ni Carb steel.) Carburized parts have high resistance to wear, seizure, fatigue and contact stresses.

Carburizing is generally done at a closely controlled temperature in the range 850° to 950°C. The rate of carburizing increases with increasing temperature, but so does furnace maintainance expense and likelihood of grain growth of steel. The atmosphere normally used is an endothermic type gas produced by a generator, the control of the carbon potential being maintained over a wide range by control of the ratio of hydrocarbon gas to air at the generator. This gas is called a carrier gas, and by checking the furnace atmosphere and making controlled additions of raw gas, the correct potential

of gas is exposed to the work which carburizes.

Surface carbon contents of near eutectoid composition[8] are generally specified in carburized steels because these carbon contents provide, in addition to high hardness, the highest compressive strength and fatigue resistance that can be obtained from hardened steels. The low carbon core regions of carburized parts serve two important functions, the core must provide toughness and impact resistance to the part, and it must support loads applied to the case without yielding.

Carburized products may be hardened by one of two methods:

a) Direct quenching from the carburizing furance

b) by reaustenizing the product in subsequent operations and then quenching.

Products hardened by direct quenching from carburizing, or cooled to a lower temperature (typically 800°C) and then quenched. Direct quenching produces lower distortion than reheat treatment after carburizing. Quenching is commonly followed by tempering at 120 to 180°C to improve case toughness and prevent possible dimensional changes in service.

1.2 INDUCTION HARDENING

Heat for hardening a steel component is generated within the part by electromagnetic induction. As alternating current flows through the inductor or work coil,

a highly concentrated, rapidly alternating magnetic field is established within the coil. The strength of this field depends primarily on the magnitude of current flowing through the coil. The magentic field thus established induces an electrical potential in the part to be heated, and since this part represents a closed circuit, the induced voltage causes the flow of current. The resistance of the part to flow of induced current causes heating by I^2R, flow of eddy current. In a ferromagnetic steel, additional heat is generated by magnetic hysterisis losses within the material.

The surface is heated into the austenitic range and the heating stage is immediately followed by rapid cooling for transformation to martensite to occur. Because of the'skin effect', heating is concentrated in the outer layers, and since the rate of energy input is high, there is little time for conduction towards the centre to occur so that the body of the component is not hardened. Thus, as with thermo-chemical treatments such as carburizing, the result of the process is a hard 'case' and tough 'core'.

Depth of hardening depends on frequency of power supply, the power input and duration of heating cycle. A high power input and short heating time give a relatively thin hardened layer, whilst the same power supply can be used for deeper hardening by using a lower power level and longer heating time.

employed, single shot hardening and scan hardening. In single shot hardening component is brought within the field of a fixed induction coil whereas in scan hardening a coil is traversed along the component length.

For quenching, in case of shot hardening, the component needs to be immersed in quenching medium. With scan hardening, quenching liquid spray can follow the heating coil as it passes along the length of component. Type of quenching medium depending on composition of steel, for plain carbon steels with poor hardenability, water being recommended.

Induction hardening is a thermal treatment and hence it requires the steel work piece employed to be suitable for direct hardening, steels containing 0.35% - 0.45% Carbon having been found to be most suitable.

1.3 SPUR GEAR DIMENSIONS

Diametral pitch = Dp = 8

Number of teeth = N_G = 92

Pitch diameter = $p = \frac{N_G}{Dp} = \frac{92}{8}$ = 11.5in = 292mm

Whole depth = 7.46mm

Circular pitch = $Cp = \frac{\pi}{Dp}$ = 0.392in = 9.97mm

Arc tooth thickness = $\frac{Cp - 0.006}{2}$ = 0.193in
= 4.9mm

Hole for shaft = 50mm dia.

Face width = 25mm Mass of Gear = 11.94 Kg.

Assume that the heating or cooling process is completed when the parameter B reaches the relevant value given in the table below.

$$B = \frac{\Delta\theta_{final}}{\Delta\theta_{initial}} \times 100,$$

Operation	Surface heat transfer coefficient (h) $W/m^2.^oC$.	B%
Heating to carburising temperature from ambient temperature.	60 (h)	2
Cooling from carburising temperature to that at which quenching is carried out.	120 (h)	4
Heating to tempering temperature from ambient temperature.	30 (h)	4

where $\Delta\theta$ = difference in temperature between the gear and surroundings. Assume that there is no temperature gradient in the gear during furnace heating or cooling.

1.4 CASE DEPTH

Table 3A and 4A show the recommended case depth for different diametral pitches using carburizing and induction hardening heat treatments[3].

For a gear of diametral pitch of 8, the maximum recommended case depth by gas carburizing heat treatment is 0.04" (or 1.016mm). For the gear of same diametral pitch, maximum recommended case depth induction hardening is 0.125" (or 3.175mm).

2.0 CALCULATIONS

2.1 CALCULATIONS OF CARBURIZING TIMES

a) Heating to Carburizing temperature:

$$\text{Ln}\left(\frac{B}{100}\right)^{-1} = \frac{h.A.t}{m.Cp}$$

$$\text{Ln}(0.02)^{-1} = \frac{60\ ^{W}/_{m^2}.C \times 0.293 m^2 \times t}{11.94kg \times 450\ ^{W}/_{sec\ kg^{o}C}}$$

$$t = 1187sec = 0.329\ hrs.$$

b) Carburizing time:

$$\frac{C - Co}{Cs - Co} = 1 - \text{erf}\ (\lambda)$$

Required concentration at a depth **X** below surface (0.1% in excess of core C content) = 0.25%.

Surface carbon content maintained during carburizing = 0.9% = Cs.

Initial Carbon content = 0.15% = Co

$$\frac{0.25 - 0.15}{0.9 - 0.15} = \frac{0.1}{0.75} = 0.133$$

$$\text{erf } (\lambda) = 0.8666$$

from Table 5A(b)

1.0	0.8427
X	
1.1	0.8802

$$\frac{1.1 - 1.0}{0.8802 - 0.8427} = \frac{0.1}{0.0375} = \frac{1.1 - X}{0.0136}$$

$$X = 1.1 - 0.1 \times 0.0136 = 1.09864$$

$$\lambda = \frac{X}{\sqrt{4Dt}} \qquad \lambda^2 = \frac{X^2}{4Dt}$$

$$t = \frac{(1.016)^2}{4x\ 1.4 \times 10^{-5} \times (1.09864)^2}$$

$$t = 15271.74 \text{ sec}$$

$$t = 4.24 \text{ hrs.}$$

c) Cooling to quenching temperature:

$$\text{Ln } \frac{B}{100}^{-1} = \frac{h.A.t.}{m.Cp}$$

$$\text{Ln}(0.04)^{-1} = \frac{120 \times 0.293xt}{11.94 \times 450}$$

$$t = \frac{3.218 \times 11.94 \times 450}{120 \times 0.293}$$

$$t = 492 \text{ sec}$$

$$t = 0.136 \text{ hr.}$$

Assuming a time of 900 sec for loading and purging.

d) Heating time to tempering temperature:

$$\text{Ln}\left(\frac{B}{100}\right)^{-1} = \frac{h.A.t.}{m.Cp.}$$

$$\text{Ln}(0.04)^{-1} = \frac{30 \times 0.293 \times t}{11.94 \times 450}$$

$$t = \frac{3.218 \times 11.94 \times 450}{30 \times 0.293} = 1967 \text{ sec.}$$

$$t = 0.546 \text{ hrs.}$$

Time for loading and purging assumed to be 900 sec or 0.25 hrs.

Time at tempering temperature assumed to be 3600 sec or 1.0 hrs.

2.2 PRODUCTION RATE:

Assuming a 120 hr week and an 80% efficiency to account for any unscheduled stoppages.

Available hours for working = 96 hrs/wk

Assuming a 48 week year

Number of available hours per annum = 4608 hrs.

Time taken for one batch to be processed

	HRS.
Handling time	0.25
Heating time to carburizing	0.329
Carburizing time	4.24
Cooling to quench	0.136
Total time for carburizing	4.955
Loading time	0.25
Heating time for tempering	0.546
Tempering time	1.00
Total time for tempering	1.796

Total time = 6.751 hrs.

Hence total time for the carburizing process is 6.751 hrs. However, the time for carburizing itself is 4.955 hrs, which means that one batch can be carburized at the same time as the other batch can be processed i.e. tempered . Two batches can be tempered whilst a batch is being carburized and therefore for every two carburizing furnace, one tempering furnace will be needed.

Idle time for tempering furnaces will be

$4.955 - 2 \times 1.796 = 1.363$ hrs.

It can be concluded that one batch takes 4.955 hrs.

$$\text{Number of batches/yr} = \frac{\text{Total working time in yr.}}{\text{Carburizing time}}$$

Prodn. rate/yr for carburizing

$$= \frac{4608}{4.955} = 929 \text{ batches/yr.}$$

A furnace of 1.22m length, 1.22m width and 0.915mm height will hold 91 gears.

Number of gears per batch = 91 gears

Number of furnace to be employed to more or less equal the output of induction hardening = 2

Number of gears carburized/yr/furnace = 84539

Number of gear carburized/yr = 169078

Prodn. rate = 169078 gears/yr.

Equipment required. £

Furnaces for carburizing	146000
Jigs & Fixture	28000
Washing Machine	17000
Tempering Furnace	13000
Charging machines	11000
Gas generator	10500
Total	225500

Operational Costs:

Maintenance costs per annum are 10% of Capital costs

Included in these costs are the oil renewal costs.

$\therefore$ Maintenance costs/hr = $\frac{225,500 \times 0.1}{4608}$

= £4.89/hr.

Carburizing:

Gas consumption = 1620 ft^3/hr

Cost of gas = £1.30 ft^3/hr.

Cost of carburizing gas = £2.10/hr.

Mostly for topping up, cost of quenching oil = £1000/yr.

Oil cost/hr = £0.217/hr.

Electricity consumption for furnace, washing machine and generator = 1440 kw/24 hrs.

Annual electricity consumption = 345600 kw

Annual electricity cost at 2.5p/kw = £8640

Electricity cost/hr = £1.875

Labour costs:

2 semi skilled persons will be required to operate the equipment

Labour cost/man = £2.50/hr.
Annual Labour cost/man = £11,520
Total Labour costs = £23,040

Total Annual operating costs compromise of:

a) Maintainance costs

b) Gas costs

c) Electricity costs

d) Oil costs

e) Labour costs

∴ Total annual operating cost

= 22550 + 9676.8 + 1000 + 8640 + 23040

= £64906.8

These operating costs are for two carburizing furnaces and one tempering furnace.

This heat treatment is economically assessed over a period of 10 years. For tax purposes capital equipment will be written off at a rate of 50% in the first year and 25% of the residual capital outstanding in each subsequent year.

Corporation tax is charged at a rate of 52% and allowances due on capital invested will be treated as incoming cash flows in the year after the tax liability has been incurred.

Table 6A shows the income year wise compromising of taxed profits and tax saved because of depreciation allowance. Profits and allowances were taxed in subsequent year.

For this heat treatment to be economically viable the total income should at least equal investment.

$$225{,}500 = 83274 + 2.412P$$

$$P = £58966$$

P is the minimum profit required to make heat treatment economically viable.

Carburizing cost is made of Operating cost and profit.

$$\text{Heat treatment cost} = 64906.8 + 58966$$
$$= 123872.8$$
$$= £123873$$

This cost is for 169078 gears heat treated per annum.

Heat treatment cost/gear = £0.73

2.4 CALCULATION OF INDUCTION HARDENING TIMES

The size of tooth is very small, so the gear has to be single shot hardened.

Area to be hardened will be that of face width. Complexities of tooth configuration are ignored and a disk, cylinderical, is assumed.

$\therefore$ Area to be hardened

$= \pi \times$ Diameter x thickness

$= \pi \times 292 \times 25$

$= 23300 mm^2$

$= 233 cm^2$

For a gear having a diametral pitch of 8, the Gear Handbook recommends a frequency of 300-500 kcycles/sec, table 7A.

Graph in figure 3A, shows for the recommended frequency range and a depth of 3.175mm, a heating time of 35 seconds and a power density of $0.3 kW/cm^2$ is required.

$\therefore$ t = 35sec $\quad \Delta P = 0.3\ kW/cm^2$

$\therefore$ Power reqd. = ΔP x Area to be hardened

= 0.3 x 233

= 69.99 kW.

Since the power required will be intermittent, a generator of output power of 60 kW will be employed.

An induction heating cycle consists of Loading time, Heating period, Quenching time and unloading time. Since heating period may be less than 50% of total induction heating cycle. To fully utilize an induction heating generator a two station switching has to be employed which allows one component to be heated whilst other one is being quenched/loaded.

Production cycle of Induction heating.

35 sec HEAT

60sec QUENCH 15sec LOAD

HEAT 35sec

QUENCH 60sec LOAD 15sec

Total 170sec for two compts.

∴ Actual time of induction heating cycle
= 95sec
Idle time = 15 sec.

∴ Cycle time/gear = 170/2 = 85sec/gear.

Heating time to tempering temperature:

$$\text{Ln} \left(\frac{B}{100}\right)^{-1} = \frac{h A.t.}{m.Cp.}$$

$$\text{Ln } (0.04)^{-1} = \frac{30 \times 0.293 \times t}{11.94 \times 450}$$

$$t = \frac{3.218 \times 11.94 \times 450}{30 \times 0.293}$$

$$t = 0.546 \text{ hrs.}$$

Time for loading assumed to be 1110 sec or 0.308 hrs.

Time at tempering temperature assumed to be 3600 sec or 1.0 hrs.

Total time for tempering is 1.854 hrs.

Tempering furance of dimensions of 660mm diameter and 914mm deep will hold 34 gears.

Time required to induction harden 34 gears

= 34 x 85 = 2890 secs = 0.802 hrs.

Time required to induction harden twice the number of gears = 2 x 0.802 = 1.604 hrs.

Excess time for tempering furnace = 1.854-1.604
= 0.25 hrs.

It can be concluded that two tempering furnaces will be needed to cope with the output of generator.

Since tempering cycle is greater, this time will be used to calculate the production rate:

∴ one batch takes 1.854 hrs because time for tempering exceeds the time for induction hardening.

Production Rate:

Assuming a 120 hr week and an 80% efficiency to account for any unscheduled stoppages.

Available hrs for working = 96 hrs/wk

Assuming a 48 week year
Number of available hours per annum = 4608 hrs.

Production rate/yr for induction hardening

$$= \frac{4608}{1.854} = 2485 \text{ batches/yr.}$$

No. of gears per batch per furnace = 34 gears

Since we are employing two tempering furnaces

∴ No. of gears per batch = 68 gears for one generator

∴ No. of gears induction hardened/generator/yr
= 2485 x 68
= 168980 gears/yr.

This is 98 less than number of gear carburized, and output can be increased by reducing handling time to equal that of carburizing heat treatment.

Costs for Induction hardened gears.

Prodn. rate = 168980 gears/yr.

Equipment required:

	Cost £
60 kW Generator	15400
Water Recirculation valve	3300
2 Transformer & Coil	3000
Quench Tank Fixture	8000
Fixture	6000
Tempering furnaces	14000
2 Station Switching	1100
Total	£50,800

Operational costs:

Maintainance costs per annum is 10% Capital costs

*Maintainance costs = $\frac{50800 \times 0.1}{4608}$ = £1.1/hr.

*includes quenching oil renewal costs.

Total time for which power is supplied.

= 168980 x 35 = 1642.86 hrs/yr.

Electricity consumption = 1642.86 x 95

= 156071.7 kVA hr.

At the rate 2.5p/kW hr.

Total Electricity cost = £3901.79

Electricity cost/hr = £0.85

Water consumption = 8 gpm

Hourly consumption = 480 gal/hr.

Rate = £0.7/1000 gals.

Cost of Water = £0.34/hr

Annual Water cost = £1567

Cost of topping up quenching oil = £1000/yr.

Labour costs:

Assuming requirement of one semi-skilled working at 80% efficiency built into number of hrs/yr, for operating induction heating equipment.

Semi-skilled labour rate = £2.5/hr.

∴ Annual Labour cost of operating induction heating equipment = £2.5 x 4608 = £11520

One additional man is required to operate tempering furnace, semi-skilled also

∴ Annual Labour cost of operating tempering furnace
= 2.5 x 4608 = £11520

Total Labour cost = £11520 + £11520
= £23040

Total Annual operating costs comprise of:

a) maintainance cost and
b) electricity cost
c) water cost
d) labour cost
e) oil cost

∴ Total annual operating cost = £5080 + 3902 + 1567 + 23040 + 1000
= £34589

These operating costs are for one induction heating equipment and two tempering furnace.

This heat treatment will be economically assessed over a period of 10 years. For tax purposes, capital equipment will be written off at rate of 50% in the

first year and 25% of the residual capital outstanding in each subsequent year.

Corporation tax is charged at a rate of 52% and allowance due on capital invested will be treated as incoming cash flows in the year after the tax liability has been incurred.

Table 8A shows the income year wise comprising of taxed profits and tax saved because of depreciation allowance. Profits and allowances were taxed in subsequent year.

For this heat treatment to be economically viable the total income should at least equal investment.

$$18759 + 2.412P = 50,800$$

$$\therefore P = 13283.99 = £13284$$

P is the minimum profit required to make heat treatment economically viable.

Induction hardening cost is made of Operating costs and Profit.

Heat treatment cost = 34589 + 13284

= £47873

This cost is for 168980 gears heat treated per annum.

Heat treatment cost/gear = £0.29

3.0 COMPARISON OF GAS CARBURIZING AND INDUCTION HARDENING

The main object of surface hardening gear is to produce a hardened contour of sufficient depth to carry contact loads and to leave a residual stress system in that layer which favours high resistance to bending fatigue. This surface hardening can be achieved by case hardening, induction hardening and other processes. These processes producing different types of hardened contour and residual stress system.

Figure 1A and 2A show the comparison of Gas carburizing and Induction hardening on basis of characteristics and typical hardness patterns. It can be observed that, in an induction hardened tooth which requires high beam strength, an adequate depth of hardened layer in centre of root fillet will be required.

3.1 REVIEW OF RESIDUAL STRESS SYSTEMS PRODUCED BY:

a) Gas carburizing:

Case hardening processes produce compressive residual stresses in hardened surface regions of part. These residual stresses exist because the high carbon martensite in the case is less dense than the low carbon martensite (or bainite or pearlite) beneath the case.

The differential in density is increased by increasing the tetragonality of the martensite for decreasing the amount of retained austenite in the case for retained austensite, when it coexists with martensite,

results in a decrease of hardness compared with when only martensite exists. The residual stresses developed in carburized and hardened surfaces are related to amount of austenite not transformed as shown in Fig. 4A. Resistance to fatigue failure at a case hardened surface is related mainly to the inherent strength of material and residual stress prevailing there. High values of compressive residual stresses are favoured to negate tensile stresses, but if the presence of retained austenite reduces both compressive residual stresses then resistance to fatigue failure will be lowered.

The retained austenite content is influenced by alloy content of steel, the surface carbon content and quenching temperature; as each variable increases in value so too will the quantity of austenite[5]. An effective control over these variables is therefore required from a residual stress point of view.

The core strength also influences the residual stress distribution within the case and particularly at the surface. Fig. 5A shows that as carbon content of core material increases with increases in hardness and presumably martensite percentage, the value of surface compressive stress decreases. The pattern followed by the residual stresses shown in Fig. 5A is related to the differences in volume expansion between the high carbon martensite of case and the low carbon martensite (or bainite and ferrite) of the core. The greater is this

volume expansion difference, the greater the likelihood of producing high magnitudes of residual stress, provided that the softer core materials do not yield and sequence of transformation is correct. This suggests that, above a certain core strength, the surface residual stresses can become tensile with the consequence that bending fatigue is impaired. However, Arkhipov[7] concluded that core strength had little bearing on fatigue strength but his conclusions are based only on three tests which does not necessarily invalidate the previous statement that core strength can influence the bending fatigue strength.

Induction hardening:

Residual stresses are obtained by induction hardening, these stresses usually being considered to be compressive in the surface layers which favours fatigue resistance. When the surface of component is heated rapidly by induction heating, the outer layer expands, yielding occurring in this outer zone because of its reduced strength. This layer, when quenched, is subjected to opposing forces. The quenching produces transformation of austenite to martensite accompanied by volume increase, this producing tensile residual stresses due to transformation. The quenching also causes contraction in the outer layers producing thermal originiated residual stresses which are compressive. An intermediate layer just below surface, which is not heated

above the critical temperature, will only give thermal or compressive stresses.

The compressive stresses have their greatest value at the surface. Within the limits of the hardened layer, the sign of stresses varies, layer adjacent to hardened layer being under the influence of tensile forces. The core of the work piece is affected by compressive stresses

The tensile stresses which lower the fatigue strength of steel are concentrated in the zone where hardened layer ends. This not only makes the work piece susceptible to cracking in process of cooling when quenching but can also cause the component to fail in operation as a result of the fatigue limit being lowered under action of the tensile stresses. Figure 6A shows the formation of residual stresses during induction hardening process.

Tempering:

Tempering after hardening promotes a reduction in residual stresses, although a sharp decrease in their magnitude only takes place with high temperature tempering.

At tempering temperatures up to 300°C tempering retains a considerable part of the residual stresses in work pieces. At tempering temperatures above 450°C the residual stresses may be partially removed. Tempering

is most effective during the first one and a half to two hours, further increase in duration of tempering having little effect on the amount of residual stress. Figure 7A shows the effect of tempering temperature on residual stresses.

4.0 MEASUREMENT OF RESIDUAL STRESSES IN GEARS:

There are a number of methods for determining the magnitude and distribution of residual stresses in steel articles, the main ones being;

a) Mechanical methods. These are based on cutting, boring or etching a specimen and measuring changes in geometric dimensions. By necessity, all mechanical methods involve some degree of destruction and herein lies their major disadvantage. Another problem with mechanical methods is that there is, at all times, risk of additional residual stresses being created by the relaxation technique used. However, as long as this is understood, the experimental procedure can be adjusted to avoid and minimise these effects.

Two relevant mechanical methods can be applied for measuring residual stresses in gears.

i) Benson's technique. This is a destructive method of measuring residual stresses in gears. To measure residual thermal stresses, rings are machined from the gear rim as shown in Fig. 8A and differences in ring diameter are measured before and after cutting

from the gear. The stresses can be computed from diameter changes. These rings can be split to allow calculation of stress gradient through the ring to be made. In view of three dimensional nature of residual stress system the method gives an under estimation of circumferential stresses. Distortion due to machining, which releases residual stresses, demands an elaborate machining sequence.

ii) Centre hole drilling technique. This is becoming a well established technique. The method is relatively non-destructive owing to nature of 1.6mm diameter hole required, it has a high degree of portability and residual stress can be measured at either the face or root of gear tooth.

For heat treated gears, i.e. carburized or induction hardened, the drilling stresses due to hardened surface are minimised by employing the air abrasive method of drilling hole. This method required drilling a hole through three 45^{o} rectangular rossettes and monitoring strain changes. The changes in strain allow the computation of principal maximum and minimum residual stresses. Care has to be taken, whilst preparing the surface for strain gauge installation, to minimise the introduction of any new stresses before the measurement has been undertaken.

b) X-ray method. This method utilizes the change in parameters of the crystal lattice which vary when internal stresses are present. It is a non-destructive for the measurement of surface stress, but becomes destructive if stress is measured at some point below the surface, material being removed down to that point to expose a new surface for X-ray examination. It also imposes a limit on size of gear whose residual stress can be measured, being limited to smaller end of the scale. This method measures stresses at the surface which makes it relevant since one is interested in stress at the surface where applied stress is highest and hence failure susceptible. The X-ray method, being non-destructive, has the great advantage that it makes possible repeated measurement on the same specimen. It does however, measure the existing stress, whether it be only residual or the sum of residual and applied[12].

The technique is based on principle that the lattice spacing of a particular plane is proportional to the angle of refraction of X-rays, this being determined either by a back reflection camera as shown in Figure 9A or by a suitable diffractometer. In stressed conditions, these lattice spacings change from their stress free value to some new value corresponding to magnitude of stress.

For steel which has been hardened by quenching and

tempering the diffractometer method is to be preferred compared with the photographic method, because broad diffraction lines produced are difficult to measure on photographic records.

Assumptions made in the derivation of the stress by this method are that the material is elastic, homogeneous and isotropic.

5.0 COST OF RESIDUAL STRESS MEASUREMENT

Two methods, X-ray and Centre hole drilling can be compared on basis of cost, composed of direct materials used and labour hours involved. The basic assumption to be made is that capital equipment to carry out measurement using these two different methods already exists within premises, although it must be realised that capital investment required for the X-ray method is much greater than that required by centre hole drilling technique. Another point to be made about centre hole drilling technique is that with a single set up, residual stress can be measured up to a depth equal to hole diameter at a number of various depths, and only one surface preparation is needed for this single set up. In X-ray method for the surface has to be prepared for the stress measurement at each depth.

Centre hole drilling technique:

a) Direct material cost

	£
Emery sleeves for surface preparation	0.50
Strain gauge	12.60
High speed drill	3.90

b) Direct Labour cost: £

Skilled Labour at £6.0/hr reqd.

0.5 hr for surface preparation	3.00
0.5 hr for strain gauge installation	3.00
0.5 hr for drilling the hole and computation of results	3.00
Total	£26

Total cost of carrying out residual stress measurement using centre hole drilling technique is £26. This cost allows the measurement stress values at various depths up to a depth equal to hole diameter.

A typical number of stress values which can be obtained at a single location is 18, this allowing a profile of stress versus depth to be drawn to ensure that the full value of residual stress is obtained.

X-ray technique:

This technique measures residual stress at the depth where the surface is prepared. To compare the two techniques realistically, the cost of measuring residual stress at a single location and 18 various depths using X-ray technique will be calculated. This procedure will allow a similar profile of stress versus depth to be drawn in order to ensure the full determination value of residual stress.

a) Direct material costs £

Energy costs, 1000 watts for 0.5 hr per measurement at 2.5p/kWhr	
For 18 measurements	0.23

	£
Consumables i.e. Film and Chart £0.5/measurement For 18 measurements	9.0

b) Direct Labour costs:

1 hr for surface preparation/measurement. A semi-skilled person can be employed at £2.50/hr. For 18 measurements	45.0
1 hr for setting up and analysing/ measurement. A skilled person to be employed at £6.0/hr. For 18 measurements	108.0
Total	£162.23

Costs clearly make Centre hole drilling technique a clear choice for measuring residual stress.

6.0 CONCLUSION

Cost of hardening a spur gear by gas carburizing has been found to be 2.5 times that by induction hardening. This makes the selection of induction hardening much more favourable on economical grounds. But, these gears, being of relatively small size, are single shot hardened (induction hardening) and this process leaves them with a case which is susceptible to failure under impact loading. In the case of large gears, the tooth size is adequate to allow for tooth by tooth hardening so that this problem can be overcome.

Depending on the use of the gear, it would be technical requirements during service, i.e. loads, that would decide the merits of the particular heat treatment.

Importance of favourable residual stress system to improve fatigue life of gears has been discussed. It has been pointed out that induction hardening has an inferior residual stress system compared with carburizing for improvement of fatigue life as shown in figure 10A.

A quality control system can be installed to monitor residual stress levels and to observe that they are of the kind conducive to the improvement of service life of gears.

Two residual stress measurement techniques have been discussed with regards to their relative merits and disadvantages. The Centre hole drilling technique has been found to be economical and more appropriate because of its portability. However, because of small face width size (for 29cm dia. gear in this case) it is not practical to put strain gauge on the face width, although the gauge can be put on gear side to check stress levels in the case.

Finally it is suggested that an appropriate residual stress level be yet another quality attribute detailed in specifications.

REFERENCES:

1. W. T. Chesters, 'Surface hardening of large Gears', Heat treatment of components, Ist. publication, 17-18, Dec. 69, London
2. K. E. Thelning, 'Steel and its Heat treatment, Bofors Handbook, Butterworths, London.
3. 'Gear Handbook', D. W. Dudley, 1962, McGraw Hill.
4. M. G. Loxinskiu, 'Industrial application of Industrial heating', Pergamon press 1969
5. G. Parrish, 'The influence of microstructure on properties of case carburized components' Heat treatment of Metals, 1976, 4, p101-109.
6. G. Parrish, 'The influence of microstructure on properties of case carburized components' Heat treatment of Metals, 1977, 2, p45-54.
7. Arkhipov I. Ya and Polotski M.S. 'Tooth bending life of case hardened gears with cores of different hardness. Russian Engineering Journal, 1972, Vol. L11, No. 10, 28-30.
8. American Society for Metals. Metals Hdbk. Vol. 1 Properties & Selection, Iron and Steel 9th Ed.
9. 'Why Carbon case harden', Heat treatment of Metals, Report, 1975, 3, p93.
10. M. Hetenyc, Handbook of Experimental Stress analysis, John Wiley & Sons.
11. A. J. A. Parlane, 'The determination of residual stress, a review of contemporary measurement techniques,' Residual stress in welded construction and their effects. Int.Conf. London, 15-17, Nov. 1977

12. B. D. Cullity, 'Elements of X-ray diffraction; 2nd Ed., Addison Wesley Pub.

13. Fulmer Materials Optimizer, Vol. 1, Comparison of Materials, Fulmer Research Institute, 1974.

Table 1.[A] Chemical Composition of Case-Hardening Steels

AISI	BS	EN	SIS	Bofors	Chemical composition % C	Si	Mn	P	S	Cr	Ni	Mo
1015	-	3	1730[2]	B 4 V	0.12	0.10	0.60	-	0.020	-	-	-
					0.18	0.40	0.90	0.035	0.035	-	-	-
8620	805M20	362	2506[3]	CRO 42	0.17	0.15	0.60	-	0.030	0.35	0.35	0.15
					0.23	0.40	0.95	0.035	0.050	0.65	0.75	0.25
A 3115	637M17[1]	352	2511	DR 34	0.13	0.15	0.70	-	0.030	0.60	0.80	-
					0.18	0.40	1.10	0.035	0.050	1.00	1.20	0.10
A 3-20	637M17[1]	352	2512	DR 44	0.18	0.15	0.70	-	0.030	0.60	0.80	-
					0.23	0.40	1.10	0.035	0.050	1.00	1.20	0.10
4720	815M17	353	2523	CRO 53	0.17	0.15	0.70	-	0.030	0.80	1.00	0.08
					0.23	0.40	1.10	0.035	0.050	1.20	1.40	0.16
		33			0.10	0.10	0.3			0.3	2.75	*
					0.15	0.35	0.6			max	3.50	

1. C 0.14-0.20
2. SIS 1370 corresponds to steel 3a in ISO/R 683/XI-1970.
3. SIS 2506 corresponds to steel 12a in ISO/R 683/XI-1970.

Table 2.A Steels for flame and induction hardening ISO 683/X11-1972

Type of steel	C%	Si%	Mn%	P% max	S% max	Cr%	Mo%	Ni%
1	0.33-0.39	0.15-0.40	0.50-0.80	0.035	0.035	-	-	-
2	0.38-0.44	0.15-0.40	0.50-0.80	0.035	0.035	-	-	-
3	0.43-0.49	0.15-0.40	0.50-0.80	0.035	0.035	-	-	-
4	0.48-0.55	0.15-0.40	0.60-0.90	0.035	0.035	-	-	-
5	0.50-0.57	0.15-0.40	0.40-0.70	0.035	0.035	-	-	-
6	0.42-0.48	0.15-0.40	0.50-0.80	0.035	0.035	0.40-0.60	-	-
7	0.34-0.40	0.15-0.40	0.60-0.90	0.035	0.035	0.90-1,20	-	-
8	0.38-0.44	0.15-0.40	0.60-0.90	0.035	0.035	0.90-1.20		
9	0.38-0.44	0.15-0.40	0.50-0.80	0.035	0.035	0.90-1.20	0.15-0.30	
10	0.38-0.44	0.15-0.40	0.70-1.00	0.035	0.035	0.40-0.60	0.15-0.30	0.40-0.70
11	0.37-0.43	0.15-0.40	0.50-0.80	0.035	0.035	0.60-0.90	0.15-0.30	0.70-1.00

Table 3 A Recommended Case Depths for Case Hardening

Normal diametral pitch	Case-depth specification, in.
20	0.010-0.18
16	0.012-0.023
10	0.020-0.035
8	0.025-0.040
6	0.030-0.050
4	0.040-0.060
2	0.070-0.100

Table 4 A Recommended Depth* of Hardness in Root Region for Induction-hardened Teeth

Normal diametral pitch	Recommended hardness depth, in.
20	0.010-0.040
16	0.015-0.060
10	0.020-0.100
8	0.030-0.125
6	0.045-0.150
4	0.060-0.175

* Depth reading taken in centre of root fillet. Depth should be greater at sides of root fillet.

Table 5A(a)

Technical Data:

$M = 11.94$ kg

$A = 0.293\ m^2$

$C_s = 0.9$ mass %

$Co = 0.15$ mass %

$C = 0.25$ mass %

$D = 1.4 \times 10^{-5}\ mm^2/s$

$Cp = 450\ /kg^oC$

Table 5A(b)

Table of Error Function

0	1.0000	0.50	0.4795	1.6	0.0236
0.05	0.9436	0.60	0.3961	1.7	0.0162
0.10	0.8875	0.70	0.3222	1.8	0.0109
0.15	0.8320	0.80	0.2579	1.9	0.0072
0.20	0.7773	0.90	0.2301	2.0	0.0047
0.25	0.7237	1.0	0.1573	2.2	0.0019
0.30	0.6714	1.1	0.1198	2.4	0.0007
0.35	0.6206	1.2	0.0897	2.6	0.0002
0.40	0.5716	1.3	0.0660	2.8	0.0001
0.45	0.5245	1.4	0.0477	3.0	0.0000
		1.5	0.0399		

Interpolate for intermediate values of .

TABLE 6A

Yr. (1)	Investment (2)	Depreciation Allowance (3)	Depreciation Allowance for Year (4)	Tax saved by depreciation allowance Tax at 52% (5)	Present value factor at 15% (6)	Tax saved discounted (5)x(6)= (7)	Profit P discounted at 15% (8)	Tax on profit (9)	Income (7)+(8)-(9)
0	(225,500)								
1		112750	112750	58630	0.870	51008	0.87P		51008 + 0.87P
2		84562	28187	14657	0.756	11080	0.756P	0.452P	11080 + 0.304P
3		63422	21140	10992	0.658	7232	0.658P	0.393P	7232 + 0.265P
4		47567	15855	8244	0.572	4715	0.572P	0.342P	4175 + 0.23P
5		35676	11891	6183	0.497	3073	0.497P	0.297P	3073 + 0.2P
6		26757	8919	4637	0.432	2003	0.432P	0.258P	2003 + 0.174P
7		20068	6689	3478	0.376	1307	0.376P	0.224P	1307 + 0.152P
8		15051	5017	2608	0.327	852	0.327P	0.196P	852 + 0.131P
9		11289	3762	1956	0.284	555	0.284	0.170P	555 + 0.114P
10		0	11289	5870	0.247	1449	0.247P	0.147P	1449 + 0.1P
								-0.128P	0 - 0.128P
									83274 + 2.412P

Table 7 A Frequencies Generally Recommended for Induction Hardening.

Normal diametral pitch	Frequency, cycles per sec.
20	500,000-1,000,000
10	300,000- 500,000
8	300,000- 500,000
6	10,000- 500,000
4	6,000- 10,000
2	6,000- 10,000

TABLE 8 A

Yr. (1)	Investment (2)	Depreciation Allowance (3)	Depreciation Allowance for year (4)	Tax saved by depreciation allowance Tax @ 52% (5)	Present value factor @ 15% (6)	Tax saved discounted (5)x(6) =(7)	Profit P discounted @ 15% (8)	Tax on Profit (9)	Income (7)+(8)-(9)
	(50,800)								
		25400	25400	13208	0.870	11491	0.87P	-	11491 + 0.87P
		19050	6350	3302	0.756	2496	0.756P	0.452P	2496 + 0.304P
		14288	4762	2476	0.658	1629	0.658P	0.393P	1629 + 0.265P
		10717	3571	1857	0.572	1062	0.572P	0.342P	1062 + 0.23P
		8039	2678	1392	0.497	692	0.497P	0.297P	692 + 0.2P
		6030	2009	1044	0.432	451	0.432P	0.258P	451 + 0.174P
		4523	1507	783	0.376	294	0.376P	0.224P	294 + 0.152P
		3393	1130	587	0.327	192	0.327P	0.196P	192 + 0.131P
		2546	847	440	0.284	125	0.284P	0.170P	125 + 0.114P
		0	2546	1324	0.247	327	0.247P	0.147P	327 + 0.1P
								-0.128P	0 - 0.128P
									18759 + 2.412P

FIGURE 1A: Comparison of Induction and Gas carburizing Heat treatments

FIGURE 2A: Typical hardness patterns

(a) Carburized or nitrided
(b) Induction-hardened or shallow hardened
(c) Induction-hardened or shallow-hardened
(d) Flame-hardened

(from Dudley[3])

Characteristics	Heat Treatment	
	Induction	" Gas carburizing
	Hard	Hard
Wear resistance	High	High
Capacity for contact load	Good	Excellent
Bending fatigue strength	Good	Good
Resistance to seizure	Fair	Good
Freedom from quench cracks	Fair	Excellent
Steel cost	Low	Low to medium
Capital investment	Medium	High

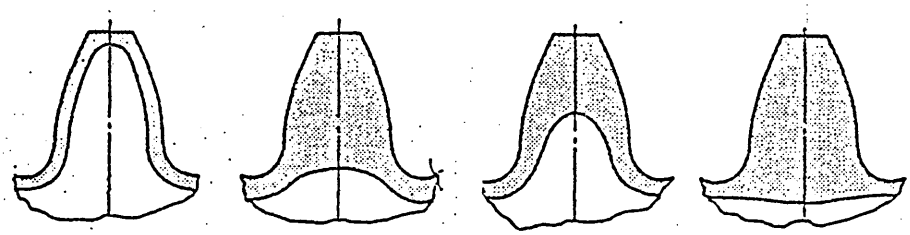

FIGURE 3A: Graph for determining approximately the conditions for induction heating a surface layer of steel to a thickness up to 10mm at different supply current frequencies

(a) values of power density
(b) heating time

(from Lozinskiu[4])

FIGURE 4A: Retained austenite and residual stress distribution in case hardened test pieces

(from Parish[5])

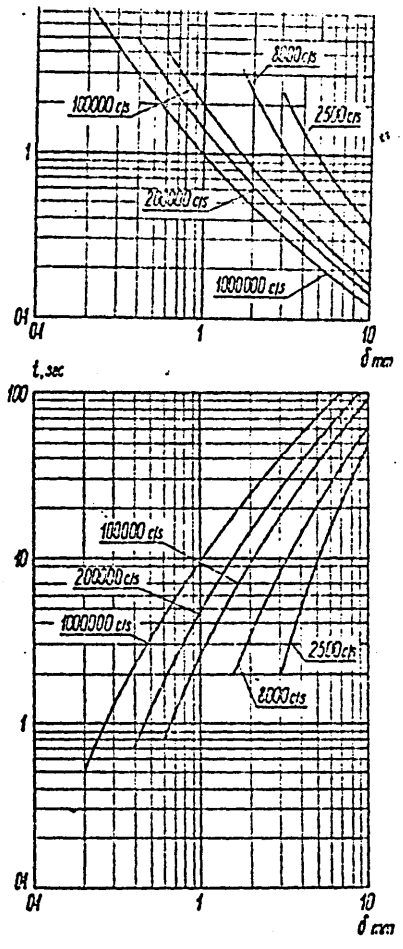
100000 cps
2500 cps
1000000 cps
t, sec
100
10
1
0.1
0.1
1
10
δ mm
100000 cps
200000 cps
1000000 cps
2500 cps
2000 cps
δ mm

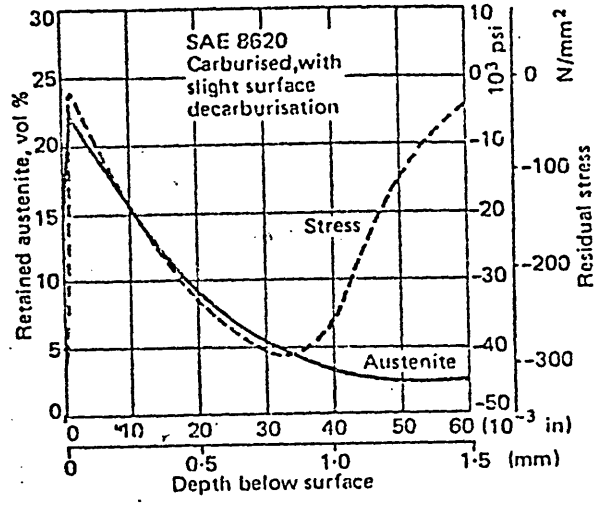
SAE 8620
Carburised, with
slight surface
decarburisation
Stress
Austenite
Retained austenite, vol %
30
25
20
15
10
5
0
10
0
-10
-20
-30
-40
-50
10³ psi
0
-100
-200
-300
N/mm²
Residual stress
0
10
20
30
40
50
60 (10⁻³ in)
0
0·5
1·0
1·5 (mm)
Depth below surface

FIGURE 5A: The dependence of residual stress in carburized and hardened cases on core carbon level:
(a) Residual stress distribution in samples of Cr-Mn-Ti steel of varying core carbon contents. Case depth 1.2mm; quenched from 810°C. (b) The relationship between surface residual stress and core carbon in (a). (c) The relationship between peak compressive stress and core carbon; (A) for the Cr-Mn-Ti steel in (a) and (B) for the SAE 8600 steels.
(from Parish[6])

FIGURE 6A: Diagram showing formation of residual stresses when surface hardening a heated layer, and the curve of residual stresses (radial and shearing)

(from Lozinskiu[4])

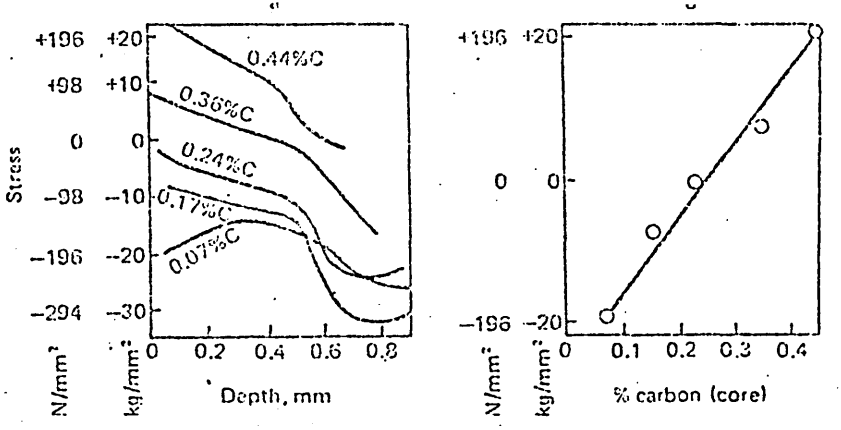
+196
+98
0
−98
−196
−294
+20
+10
0
−10
−20
−30
Stress
N/mm²
kg/mm²
0.44%C
0.36%C
0.24%C
0.17%C
0.07%C
0
0.2
0.4
0.6
0.8
Depth, mm
+196
0
−196
+20
0
−20
0
0.1
0.2
0.3
0.4
% carbon (core)

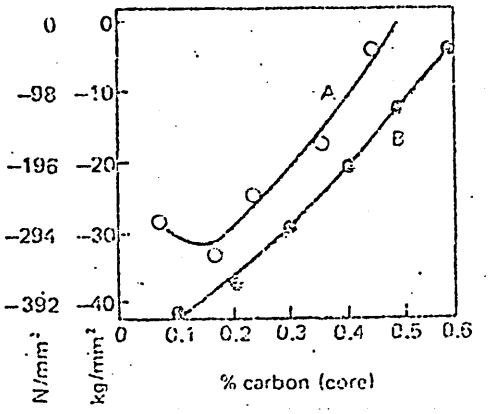
0
−98
−196
−294
−392
−10
−20
−30
−40
A
B
0
0.1
0.2
0.3
0.4
0.5
0.6
N/mm²
kg/mm²
% carbon (core)

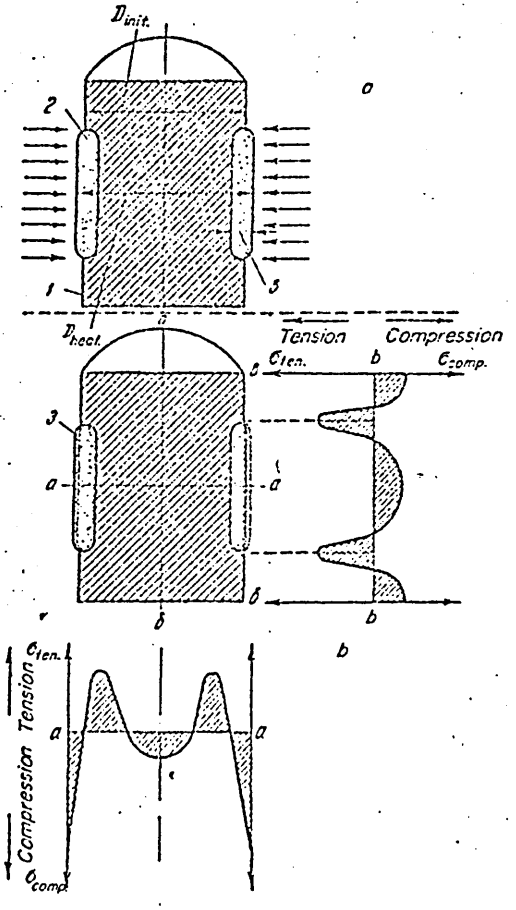
$D_{init.}$
2
1
3
$D_{heat.}$
Tension
Compression
$\sigma_{ten.}$
$\epsilon_{comp.}$
a
b
$\sigma_{comp.}$

FIGURE 7A: Effect of tempering temperature on residual stress in carburized bars of 8617 steel, 19mm (0.75in) in diameter. Bars were carburized, direct oil quenched, and tempered for 1hr at the indicated temperature.

(from Metals Hdbk[8])

FIGURE 8A: Gear Tooth failure from Residual Tensile Stress.

(from Hetenye[10])

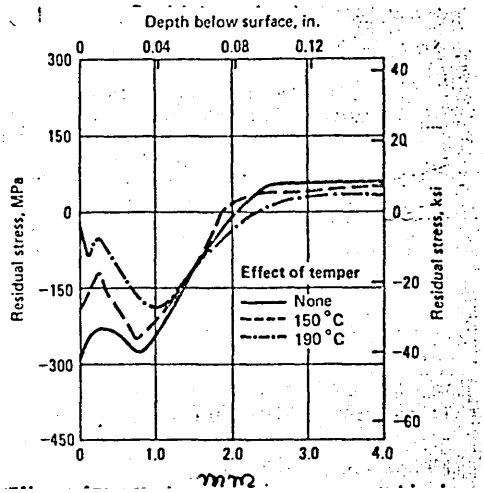
Depth below surface, in.
0
0.04
0.08
0.12
300
150
0
−150
−300
−450
40
20
0
−20
−40
−60
Residual stress, MPa
Residual stress, ksi
Effect of temper
None
150 °C
190 °C
0
1.0
2.0
3.0
4.0
mm

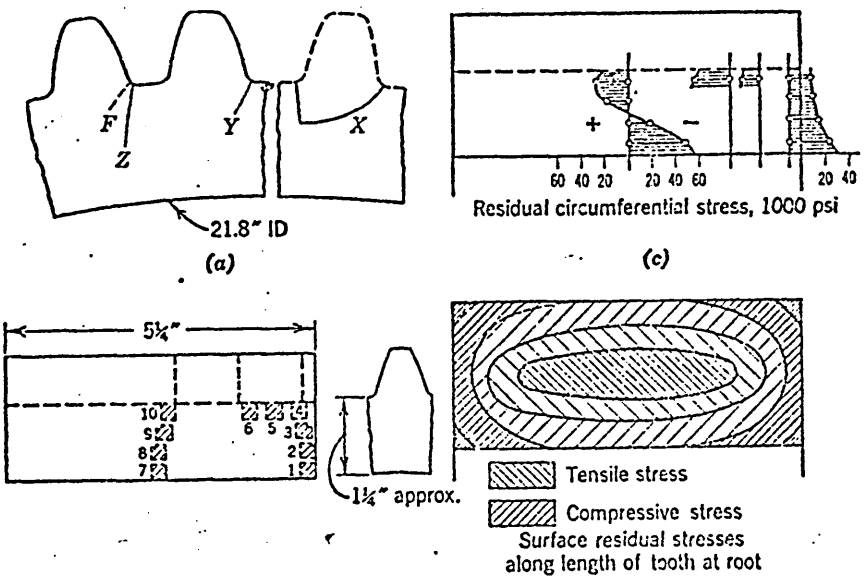
F
Z
Y
X
21.8" ID
(a)
+
−
60 40 20
20 40 60
20 40
Residual circumferential stress, 1000 psi
(c)
5¼"
10
9
8
7
6
5
3
2
1
1¼" approx.
Tensile stress
Compressive stress
Surface residual stresses
along length of tooth at root

FIGURE 9A: Principle of back reflection technique for stress-strain measurements using X-ray diffraction. Angle 2θ is function of lattice strain. 1 - film (or diffractometer): 2 - diffracted ray: 3 - reflecting planes of atoms

(from Parlane[11])

FIGURE 10A: Diagrammatic representation of the distribution of residual heat treatment stresses and applied bending stresses in a simple specimen.
(a) In induction or flame hardening there is a risk of producing high tensile stresses at the case/core junction which can combine with the applied stresses to precipitate failure.
(b) Hardening by nitriding or carburizing results in lower tensile stresses at the case/core junction. The wider range of case depths attainable by carburizing allows more flexibility in selecting a treatment which ensures that maximum applied sub-surface stresses are well removed from the maximum tensile residual stresses.

(From Heat treatment of Metals, Report[9])

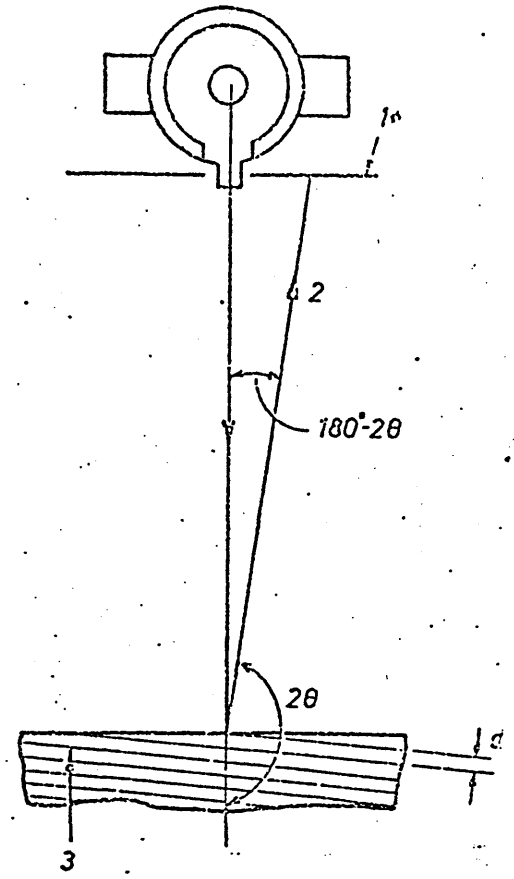

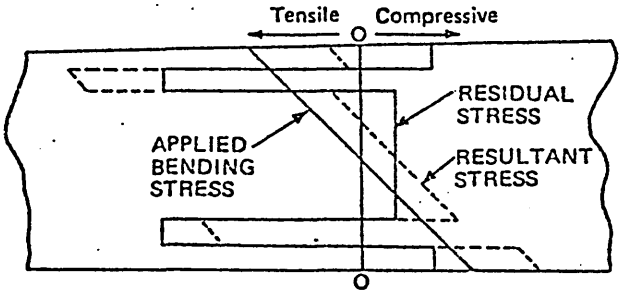

a. Induction or flame - hardened

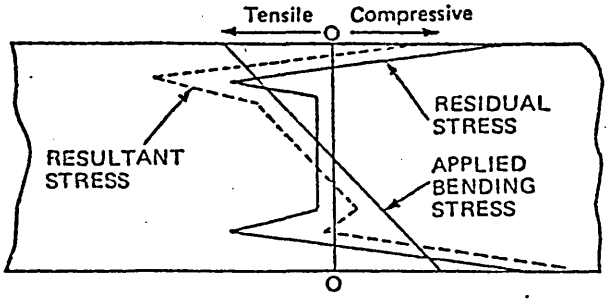

b. Nitrided or carburised and hardened

APPENDIX:

Heat transfer from surroundings at θf to gear at θ can be represented as

$$\frac{\partial Q}{dt} = k.A.(\theta f - \theta)$$

$$d = k.A.(\theta f - \theta)dt = m.Cp.d\theta$$

$$\frac{k.A.dt}{m.Cp} = \frac{-d(\theta f - \theta)}{\theta f - \theta}$$

$$\frac{k.A.t}{m.Cp} = -\int_{\theta i}^{\theta} Ln(\theta f - \theta)$$

$$\frac{k.A.t}{m.Cp} = Ln\left(\frac{\theta f - \theta i}{\theta f - \theta}\right) \quad -1$$

Now $B = \frac{\Delta\theta \text{ final}}{\Delta\theta \text{ initial}} \times 100 = \frac{\theta f - \theta}{\theta f - \theta i} \times 100$

$$Ln\ \frac{\theta f - \theta}{\theta f - \theta i} = Ln\ \frac{B}{100} \quad -2$$

Equating 1 and 2 we get

$$Ln\ \frac{\theta f - \theta i}{\theta f - \theta} = Ln\ \frac{B}{100}^{-1} = \frac{k.A.t.}{m.Cp.}$$

$$Ln\ \frac{B}{100}^{-1} = \frac{k.A.t.}{m.Cp.}$$

A STUDY OF RESIDUAL STRESSES IN LOW ALLOY STEEL THETA RING CASTINGS

R. A. AKHTAR

ABSTRACT

Residual stresses generated during the casting and heat treatment of a low alloy steel, BW2 have been studied using a theta ring so that temperature differentials could be varied using different tie bar sizes. Residual stresses have been measured using centre hole drilling and tie bar sectioning techniques. Centre hole drilling was shown to be sensitive to surface preparation methods. Stresses induced by drilling were accounted for in measured stresses and drilling stresses were found to be greater in cast than annealed samples.

Cast theta rings have been shown to have compressive residual stresses, becoming less compressive or tensile as the tie bar width was reduced. Tie bar sectioning produced expansion which increased with increasing tie bar width, although there was no direct correlation between tie bar stress and width. Results from both techniques have been explained using factors contributing to residual stress formation. The S-shaped runner contained residual stresses and its removal altered residual stress levels.

Heat treatments have been found to produce different amounts of stress relief according to the geometry and thermal cycle imposed. In a uniform section theta ring normalising and tempering relieved stresses in the tie bar but not in the outer ring, and the tie bar contained no stresses after sectioning. For the non-uniform section theta ring annealing made stresses more compressive whilst normalising and tempering generated stresses due to differential cooling, and the tie bar contained compressive stresses after sectioning. Maximum Von Mises equivalent in the cast theta ring was shown to be 25% of the yield strength and reduced further after heat treatment.

A computational model based on finite difference has been used to simulate solidification of a tie bar across the width. Temperature gradients computed along this bar axis were shown to be small and are believed not to significantly contribute to residual stresses.